SURFACE AND MOLECULAR MODIFICATION OF POLYIMIDES *VIA* GRAFT COPOLYMERIZATION AND FUNCTIONALIZATION

WANG WENCAI

NATIONAL UNIVERSITY OF SINGAPORE

2003

SURFACE AND MOLECULAR MODIFICATION OF POLYIMIDES *VIA* GRAFT COPOLYMERIZATION AND FUNCTIONALIZATION

WANG WENCAI
(M.Eng., BUCT)

A THESIS SUBMITTED

FOR THE DEGREE OF DOCTOR OF PHILOSOPHY

DEPARTMENT OF CHEMICAL & BIOMOLECULAR ENGINEERING

NATIONAL UNIVERSITY OF SINGAPORE

2003

ACKNOWLEDGEMENTS

I wish to express my deepest gratitude to my supervisors, Professor Kang En-Tang and Professor Neoh Koon-Gee, for their guidance, advice, support and encouragement throughout the period of this research work. I have gained invaluable knowledge from them on how to do research work and how to enjoy doing research. Their enthusiasm, sincerity and dedication to scientific research have greatly impressed me and will benefit me in my future career.

I would like to thank all my colleagues and lab technologists of the Department of Chemical and Biomolecular Engineering, for their help and support. In particular, thanks are due to Dr. Li Sheng, Dr. Zhang Yan, Mr. Ying Lei and Mr. Yu Weihong for sharing the research experience with me. It is my great pleasure to work with all of them. Special thanks go to Madam Liu Suxia, Madam Chow Pek and Madam Samantha for their kind assistance. I am also indebted to Dr. R.H. Vora for providing the polyimide materials and Dr. Chen Linfeng for the material characterization.

The financial support provided by the National University of Singapore (NUS) in the form of research scholarship is greatly appreciated.

Finally, but not least, I would like to express my deepest gratitude and indebtedness to my parents, my sisters and brothers for their constant concern and support. Special thanks to my wife, Zhou Jingyu, for her persist love and encouragement.

TABLE OF CONTENTS

SUMMARY

Adhesion of polymeric dielectrics to metals is one of the major concerns in the microelectronics industry. To improve the surface properties of polyimide (PI) and fluorinated polyimide (FPI), molecular redesign and functionalization *via* graft polymerization have been carried out. Surface modification of PI and FPI by UV- or plasma-induced graft copolymerization with 1-vinylimidazole (VIDz) and 4-vinylpyrindine (4VP) was first performed. Chemical composition and surface topography of the copolymer were studied by X-ray photoelectron spectroscopy (XPS) and atomic force microscopy (AFM), respectively. Electroless plating of copper on these surface modified PI and FPI were carried out by a Sn-free process. The T-peel adhesion strength of the electrolessly deposited copper with the PI and FPI films was depended on the nature of the monomer used and the graft concentration, as well as the glow discharge conditions. The T-peel adhesion strength of the electrolessly deposited copper with the PI and FPI films were much higher than that of the electrolessly deposited copper with the pristine or the Ar plasma-treated PI and FPI films. The high adhesion strength between the electrolessly deposited copper and the surface-modified PI and FPI films was attributed to the fact that the plasma-polymerized and the UV graft-copolymerized chains were covalently tethered on the PI and FPI surfaces, as well as the fact that these grafted polymer chains were spatially and reactively distributed into the copper matrix.

The technique of molecular modification by grafting of thermally labile side chains was developed for the preparation of nanoporous PI and FPI films with low dielectric constants and preserved polyimide backbones. Thermally-induced molecular graft copolymerization of AAc or methoxy poly(ethylene glycol) monomethacrylate (PEGMA) with the ozone-pretreated poly(amic acid) precursor (PAmA) or FPI in

NMP solution was carried out. The resulting PAmA or FPI copolymers with grafted AAc and PEG side chains were characterized by elemental analysis, XPS, thermogravimetric (TG) analysis and differential scanning calorimetry (DSC). Nanoporous low dielectric constant (low-κ) PI films were obtained after thermal imidization of the PAmA backbones under reduced argon pressure and the subsequent thermal decomposition of the side chains in air. The nanoporous PI and FPI films were characterized by density measurements, scanning electron microscopy (SEM) and dielectric constant measurements. SEM images revealed that the pore size was in the range of 30-100 nm. Dielectric constants as low as 2.1 and 1.9 were obtained for the resulting nanoporous PI and FPI films, respectively.

Finally, molecular graft polymerization is also an effective approach for the synthesis of stimuli-responsive polymeric materials. New graft copolymers were successfully synthesized through molecular graft copolymerization of AAc, 4VP and *N*-isopropylacrylamide (NIPAAm) with the ozone-preactivated FPI backbone. The membranes prepared from these stimuli-responsive polymeric materials by phase inversion exhibited distinctive pH- or temperature-sensitive properties. The flux of aqueous solution through the MF membranes prepared from the PAAc-*g*-FPI or P4VP-*g*-FPI copolymers by phase inversion in aqueous media exhibited a pH-dependent behavior, but in an opposite manner. The most drastic change in permeation rate was observed at solution pH between 1 and 4. For the temperature-sensitive PNIPAAm-*g*-FPI MF membranes cast below the lower critical solution temperature (LCST) of the NIPAAm polymer (~32°C), the rate of water permeation increased substantially at a permeate temperature above 32°C. A reverse permeate temperature dependence was observed for the flux of isopropanol through the membrane cast above the LCST of the NIPAAm polymer.

NOMENCLATURE

α	XPS photoelectron take-off angle
AAc	acrylic acid
AFM	atomic force microscopy
BCB	benzocyclobutene
BE	binding energy
DPPH	2, 2-diphenyl-1-picrylhydrazyl
DSC	differential scanning calorimetry
6FDA	2, 2'-bis(3,4-dicarboxyphenyl) hexafluoropropane dianhydride
FPAmA	fluorinated poly(amic acid)
FPI	fluorinated polyimide
FTIR	Fourier transform infrared
FWHM	full width at half maximum
-*g*-	graft
GMA	glycidyl methacrylate
GPC	gel permeation chromatography
GSI	giga-scale integration
IC	integrat circuit
κ	dielectric constant
LCST	lower critical solution temperature
MF	microfiltration
NIPAAm	*N*-isopropylacrylamide
NMP	*N*-methyl-2-pyrrolidone
PAmA	poly(amic acid)

Pd	palladium
PEG	poly(ethylene glycol)
PEGMA	poly(ethylene glycol) methyl ether methacrylate
PI	polyimide
pp	plasma polymerization
PTFE	poly(tetrafluoroethylene)
PVDF	poly(vinylidene fluoride)
R_a	average surface root-mean-square roughness
RF	radio-frequency
p-SED	4, 4'-bis(4-aminophenoxy)diphenyl sulfone
SEM	scanning electron microscopy
T_g	glass transition temperatures
TG	thermogravimetric
THF	tetrahydrofuran
TOS	thermo-oxidative stability
VIDz	vinylimidazole
VLSI	very large-scale integration
4VP	4-vinylpyridine
XPS	X-ray phtoelectron spectroscopy

LIST OF FIGURES

LIST OF TABLES

CHAPTER 1

INTRODUCTION

With the development of the microelectronics industry, the feature size of the semiconductor devices has become from 1 μm in very large-scale integration (VLSI) devices to submicron (~0.18 μm) in giga-scale integration (GSI) devices (Morgen et al., 2000). The miniaturizing in device size and the advances in integrated circuit (IC) technology have resulted in reduction of the interconnect size and the propagation delay, as well as the improvement in the density of the chip circuitry. Since the early 1950s, polymers have been a key element in the growth of the semiconductor industry (Alvino, 1995). These materials range from radiation-sensitive resists used to pattern the circuit on chips and boards, to the polymers used both as insulators on chip carriers themselves, and as encapsulants for mechanical and corrosion protection of these chips.

In the microelectronics industry, the use of interlayer materials with very low dielectric parameters can greatly reduce the resistance-capacitance (RC) time delays, cross-talks, and power dissipation in the new generation of high density integrated circuits. In addition to exhibiting low dielectric constants, the next generation of interlayer dielectrics for sub-micron and nano-level electronics must also satisfy a variety of requirements, such as good thermal stability, low moisture absorption, good adhesion to semiconductor and metal substrates, and chemical inertness. Historically, ceramic materials, such as silicon oxide and silicon nitride, have been used as interlayer dielectrics. The major drawback of the ceramic dielectrics is their high dielectric constants, which limit the miniaturization of the IC devices. Recently, the use of organic polymers increase continuously, such as polyimides (PIs), poly(tetrafluoroethylene) (PTFE), benzocyclobutene (BCB), and parylene, as interlayer dielectric due to their low dielectric constants. Among the polymeric

dielectric materials, PIs have attracted a great deal of attention due to their combined physicochemical, mechanical and electrical properties. The first successful interconnect structure of PIs was developed in 1973 by Hitachi Co. (Sato et al., 1973). Since then, a large number of studies on PIs in microelectronics have been carried out. Besides being used as an interlayer dielectric, PIs have also been used as passivation layer, die adhesive, buffer coating, as well as alpha-partical barrier (Bolger, 1984; Makino and Works, 1994). On the other hand, however, the conventional PIs with dielectric constants (κ) of about 3.1-3.5, are insufficient in meeting the requirement of κ<2.5 for the dielectrics of the near future. Attempts have been made to prepare PIs with lower dielectric constants (see Chapter 2 below).

In addition, adhesion of polymeric materials to other substrates, including silicon, metal and other polymer layers, plays a very important role in the building of multi-layer microelectronics device (Morgen et al., 2000). Good adhesion of polymer to other substrates is necessary to prevent the moisture by capillary action through the interfaces. The interfacial moisture gives rise to the degradation of the adhesion strength of polymers to the substrates and, finally, the delamination of polymers from the substrates, leading to structural disintegration and immediate device failure. The conducting materials most often used in the IC devices are aluminium and copper. Copper has a relatively high electric conductivity and other advantages, such as low cost, and high thermal conductivity. A serious drawback of copper, however, is its poor adhesion to the primary dielectric materials, such as PI. Since adhesion is fundamentally a surface phenomenon, often governed by an interphase of molecular dimensions, it is possible to modify this near-surface region without affecting the desirable bulk properties of the materials to achieve enhanced adhesive properties.

Various methods have been developed or proposed to improve the adhesion of PIs with copper, as described in detail in Chapter 2.

Because of their unique physicochemical properties, PIs have also been widely investigated as membrane materials during the past decades for proton conducting, fouling resistance, gas removal and gas separation applications (Ohya et al., 1996). Recently, extensive efforts have been focused on the development of "smart" membranes that can regulate the permeability in response to environmental changes, such as changes in temperature, pH, ionic strength, etc. Membranes with stimuli-sensitive properties have been applied in controlled drug delivery, chemical separation and bioreactors. Environmental stimuli-sensitive membranes can be prepared by grafting of functional polymers or graft copolymerization of functional monomers directly onto the existing porous membranes. These approaches, however, may be accompanied by changes in membrane pore size and pore size distribution, leading to reduced permeability. Furthermore, the extents of grafting on the membrane surface and the surfaces of the pores may differ substantially. Accordingly, the strategy of molecular or bulk graft copolymerization, followed by phase inversion, to membrane fabrication may prove to be particularly useful in certain cases.

The excellent physicochemical and mechanical properties of PIs make these polymers most desirable in application studies. In this dissertation, surface graft polymerization, such as UV-induced graft copolymerization and plasma-induced graft copolymerization, is explored to improve the adhesion of PI and fluorinated polyimide (FPI) with electrolessly deposited copper. The results of implementation of this new technique in adhesion enhancement of the PIs and FPIs with copper are evaluated. On the other hand, a new method, molecular graft copolymerization was first utilized for

the preparation of nanoporous low-k polyimide films and to the preparation of polyimide membranes with “smart surface”. Thus, the application of polyimides has been further extended.

Chapter 2 gives an overview of the related literature. In Chapter 3, electroless plating of copper *via* a tin-free activation process was carried out effectively on two types of FPI films modified by UV-induced surface graft copolymerization with N-containing monomers, such as 1-vinylimidazole (VIDz) and 4-vinyl pyridine (4VP). The UV-induced surface graft copolymerization of VIDz and 4VP was carried out on the argon (Ar) plasma-pretreated FPI films *via* a solvent-free process under atmospheric conditions. The surface compositions of the modified FPI films were studied by X-ray photoelectron spectroscopy (XPS). The adhesion strength of the electrolessly deposited copper to the graft-modified FPI films was evaluated by measuring the T-peel adhesion strength. The factors that affected the adhesion of the PI/Cu laminate were discussed.

In Chapter 4, surface modification of Ar plasma-pretreated PI (Kapton® HN) and FPI films by plasma graft copolymerization with 4VP was carried out. The effects of glow discharge conditions on the chemical composition and structure of the plasma-polymerized 4VP (pp-4VP) films were analyzed by XPS and Fourier transform infrared (FTIR) spectroscopy, respectively. The XPS and FTIR results revealed that the pyridine groups in the pp-4VP layer could be preserved to a large extent under proper glow discharge conditions. The topography of the modified PI and FPI surfaces were investigated by atomic force microscopy (AFM). The pp-4VP film with well-preserved pyridine groups was used not only as the chemisorption sites for the palladium complexes (without the need for prior sensitization by $SnCl_2$) during the

electroless plating of copper, but also as an adhesion promotion layer to enhance the adhesion of the electrolessly deposited copper with the PI and FPI film.

Chapter 5 outlines the preparation of low dielectric constant nanoporous PI and FPI films. In the first part, thermally-induced molecular graft copolymerization of acrylic acid (AAc) or methoxy poly(ethylene glycol) monomethacrylate (PEGMA) with the ozone-pretreated poly(amic acid) precursor, poly[*N,N'*-(1,4-phenylene)-3,3'4,4'-benzophenonetetra-carboxylic amic acid] or PAmA, in *N*-methyl-2-pyrrolidone (NMP) solution was carried out. The resulting PAmA copolymers with grafted AAc and PEG side chains (the PAAc-*g*-PAmA and PEGMA-*g*-PAmA copolymers, respectively) were characterized by elemental analysis, XPS, thermogravimetric (TG) analysis and differential scanning calorimetry (DSC). Nanoporous low-κ PI films were obtained after thermal imidization of the PAmA backbones under reduced argon pressure and the subsequent thermal decomposition of the side chains in air. The nanoporous PI films were characterized by density measurements, scanning electron microscopy (SEM) and dielectric constant measurements. The densities of the nanoporous films were 3-14% lower than the pristine PI films. SEM images revealed that the pore size was in the range of 30-100 nm. The nanoporous PI films with dielectric constants as low as 2.1 and 2.4, were obtained from the PAAc-*g*-PAmA and P(PEGMA)-*g*-PAmA copolymer, respectively. In the second part, molecular modification of the ozone-pretreated FPI *via* thermally-induced graft copolymerization with AAc was carried out. Films of the copolymers were subjected to thermal treatment to decompose the AAc polymer (PAAc) side chains, leaving behind nano-sized pores and gaps in a matrix of preserved FPI backbones. The nanoporous FPI films were characterized by density, SEM and dielectric constant measurements. The nanoporous FPI film having dielectric

constant as low as 1.9 was prepared from the PAAc-g-FPI copolymer with an initial bulk graft concentration of about 1.67 and a final porosity of about 8%.

Chapter 6 illustrates that molecular modification is an effective method to prepare "smart" polyimide membranes. In the first part, molecular modification of the ozone-pretreated FPI *via* thermally-induced graft copolymerization with either AAc or 4VP in NMP solution was carried out. The resulting FPI copolymers with grafted AAc and 4VP side chains (the PAAc-*g*-FPI and P4VP-*g*-FPI copolymers, respectively) were characterized by FTIR spectroscopy, elemental analysis, TG analysis and DSC. In general, the graft concentration increased with the monomer concentration. Microfiltration (MF) membranes were prepared from the PAAc-*g*-FPI or P4VP-*g*-FPI copolymers by phase inversion in aqueous media with pH values ranging from 1.0 to 6.4. The surface composition of the membranes was characterized by XPS. A substantial surface enrichment of the grafted AAc and 4VP polymer was observed for the copolymer membranes. The morphology of the MF membranes was studied by SEM. The pore sizes of the MF membranes were measured using a Coulter® Porometer. The flux of aqueous solutions through the PAAc-*g*-FPI and P4VP-*g*-FPI MF membranes exhibited a pH-dependent behavior, but in an opposite manner，with the most drastic change in permeation rate being observed at solution pH values between 1 and 4.

In the second part of Chapter 6, molecular modification of a FPI *via* ozone-pretreatment and thermally-induced graft copolymerization with *N*-isopropylacrylamide (NIPAAm) in NMP solution was carried out. The resulting FPI with grafted NIPAAm polymer side chains (P(NIPAAm)-*g*-FPI) were characterized by

FT-IR spectroscopy, elemental analysis, TG analysis and DSC. In general, the graft concentration increased with the monomer concentration. Microfiltration (MF) membranes were prepared from the P(NIPAAm)-*g*-FPI copolymers by phase inversion in water at temperatures ranging from 4°C to 55°C. The surface composition of the membranes was characterized by XPS. A substantial surface enrichment of the grafted NIPAAm polymer was observed for the copolymer membranes. The surface composition, mean pore size and morphology of the membrane varied with the temperature of the aqueous coagulation bath. For the copolymer membrane cast below the lower critical solution temperature (LCST) of the NIPAAm polymer (~32°C), the rate of water permeation increased substantially at a permeate temperature above 32°C. For the flux of 2-propanol through the membrane cast above 32°C, a reversed permeate temperature dependence was observed.

CHAPTER 2

LITERATURE SURVEY

Aromatic polyimides were first produced in 1908 by Marston Bogert (Bogert and Renshaw, 1908) through polycondensation of ethers or anhydride of 4-aminophthalic acid. In the late 1950's, high molecular weight products were synthesized by two-stage polycondensation of pyromellitic dianhydride with diamines (Andrey, 1965). Since then, the interest of researchers in this class of polymers has been growing steadily because it possesses a number of valuable physico-mechanical and chemical properties, such as excellent thermal stability, low dielectric constant, good mechanical strength, etc. (Wilson et al., 1990; Sroog, 1996).

2.1 Surface Modification of PI Films and Their Relevance to Adhesion

After first commercialized by Dupont Co. (with a trade name of Kapton® HN) in early 1960s (Sroog et al., 1965), polyimide (PI) has been an important polymer for the packaging of microelectronics because of its combined good physicochemical and electrical properties. PI has been used extensively as interlayer dielectrics, protective overlayers, and alpha-particle barriers in microelectronics devices. The most widely used and studied polyimide is poly(pyromellitic dianhydride-*co*-4,4'-oxydianiline) (PMDA-ODA)-derived PI. In an IC device, two interfaces exist between PI interlayer dielectric and the metal conductors. PI on metal interface is typically formed by depositing the PI precursors, such as poly(amic acid), onto the solid metal surface. On the other hand, metal on PI interface is formed by depositing metal thin films onto the surface of a fully cured PI substrate. The deposition of metal thin film has been achieved by vacuum deposition, plasma deposition, sputtering, electroplating and electroless plating from solution (Matienzo and Unertl, 1996). High interaction for the two interfaces is necessary for the purpose of the device integration and performance

reliability. Compare with other polymeric dielectrics, such as fluoropolymers, the adhesion of PI to metals is good, especially in the case of using silane coupling agents as adhesion promoter on the metal surface. On the other hand, however, the adhesion of metal to PI surfaces has been a constant challenge in the microelectronics industry. Copper is the most preferred conductor for high-speed IC devices due to its high conductivity. The poor interaction between Cu and the pristine PI surface dictates the adhesion promoters between Cu and PI films.

The formation of chemical bond is the most important way to achieve high interfacial adhesion. The first systematic spectroscopic study of interaction of the metal to PI surface was reported by Chou and Tang in 1984 (Chou and Tang, 1984). Since then, there has been a large number of studies to investigate the interfacial chemistry between metal and PI surface. A comprehensive review on this topic has been written by Matienzo and Unertl (Matienzo et al., 1996). It was found that the interaction of Cu with pristine PMDA-ODA polyimide is very weak (Chou and Tang, 1984). Infrared (IR) absorption studies showed that absorption bands associated with the PMDA part of the PI are preferentially attenuated but no new or shifted bands were observed (Dunn and Grant, 1989), indicating no chemical components formed and, thus, no charge transfer interaction happened between Cu and the PI surface. The presence of some Cu^{+} species, though at the level of a few percent of the carbonyl sites, was also observed in the interface region (Mack et al., 1990; Pertisin and Pashunin, 1991). Unertl and Mack (Unertl and Mack, 1992) have hypothesized that the Cu^{+} species may originate from the interaction with the end groups of the PI molecules, defects, or impurities, rather than from the interaction with the PI molecules. The lack of Cu interaction with the PI surface has caused a lot of technical problems in the microelectronics industry. One example is that Cu atoms and small Cu clusters easily

diffuse below the PI surface even at room temperature. The diffusion of Cu atoms into the PI films will, thus, increase the dielectric constant of the PI film (Silverman and Platt, 1994).

A variety of different methods have been applied to activate polyimide surfaces and to enhance adhesion. In general, these methods can be classified into chemical treatment, irradiation treatment, plasma treatment, and graft copolymerization, which have shown to be the effective technique for adhesion enhancement of Cu to PI film. Chemical treatment of PI is usually accomplished by immersing PI film into a reactive acid or base solution. Chemical treatment of PI film *via* a base solution was first published in 1971 (Dine-Hart et al., 1971). Dine-Hart et al. successfully used potassium hydroxide (KOH) to remove the PI coating. Since then, surface modification of PI surface using a strong base solution to improve the adhesion property has attracted extensive research interests. A fine review on this topic has been given by Lee and Viehbeck (Lee and Viehbeck, 1996). Generally, surface modification of PI film in a base solution is *via* a hydrolysis reaction. The chemical nature of PI surface treated by strong base has been investigated by XPS (Lee and Kowalczyk , 1991; Lee and Viehbeck, 1994) and sum-frequency vibrational spectroscopy (Kim and Shen, 1999). Strong bases, such as NaOH, KOH, can be used to open the imide ring. The ring-opening reaction gives rise to the formation of carboxylate salt (Lee et al., 1990a; Lee et al., 1990b). The subsequent acidification of the base-treated PI film gives rise to the presence of a poly(amic acid) layer on the surface. The base treatment of the PI surface has greatly improved the adhesion strength of PI to the deposited metals. The adhesion of sodium hydroxide-treated PI film to Cu is affected by a lot of factors, including the temperature of the etching solution and the etching time of the PI surface. In Vorobyova's work (Vorobyova, 1997), the highest adhesion strength of about 9 N/cm

of the electrolessly-deposited Cu to the NaOH-treated PMDA-ODA PI surface was obtained at a lower etching temperature (20°C) and a medium etching time (6 min). The high adhesion strength of Cu to the chemically treated PI surface is attributed to the formation of C-O-M and M-N bonds (M=metal) *via* the ion-exchange or donor-acceptor interaction. Apart from using strong base solution to treat the PI surface, Baumgartner and Scott (Baumgartner and Scott, 1995) have improved the adhesion strength of the electrolessly deposited copper and nickel to a fluorinated PI surface modified by CrO_3, $Ce(SO_4)_2$, $(NH_4)_2Cr_2O_7$, or $K_2Cr_2O_7$ salts in the sulfuric solutions.

Irradiation treatments, including the use of ion-beam and excimer laser, have been employed to treat the PI surface. The effects of ion-beam treatment on the surface chemistry of PI film have been summarized by Lee (Lee, 1996). Generally, irradiation treatments result in crosslinking, chain scission, and element ablation. Crosslinking effect has caused a significant improvement in electrical conductivity, chemical resistant, surface hardness, and wear resistant of the PI film. The surface hardness of PI film increased almost 30 times after 1 MeV Ar^+ bombardment with a fluence of 4.7×10^{19} ions/m^2 (Lee et al., 1993). The surface chemistry of PI film was greatly influenced by the ion bombardment. Depletion of O and N elements by Ar^+ ion-beam from the PI surface was confirmed by the XPS results (Karpuzov et al., 1989). The loss of oxygen was attributed to the predominant damage of imide rings and the ablation of carbonyl groups in the case of Ar^+ ion bombardment (Marletta et al., 1989). At low doses and energies, carbonyl groups were preferentially sputtered, keeping the rest of the molecule intact. Loss of nitrogen was insignificant compared to losses of carbon and oxygen. At higher energies and doses, the PI underwent extensive bond scission, restructuring of various functional groups and species, together with radical and anion

formation (Sengupta and Birnbaum, 1991). Ion-beam irradiation can also give rise to the formation of new chemical bonds on the PI surface, including C-C-C, C-O-C and C-N-C (Ektessabi and Hakamata, 2000). The effects of ion bombardment on adhesion improvement of copper film to PI film were investigated by Ebe et al. (Ebe et al., 1997). In their work, copper thin films were evaporated onto polyimide surfaces with simultaneous irradiation of Ar^+ ions, having energies in the range of 0.5 to 10.0 keV. Transmission electron microscopy (TEM) analysis showed that the ion bombardment generated the mixed layer which consisted of the PI elements and copper atoms at the interface. The thickness of the mixed layers increased with an increase in ion dose and ion energy. The peel adhesion tests showed that the Cu film adhesion to PI film was dependent on the conditions of the ion bombardment. At low ion energy, the adhesion was improved by the formation of the intermixed layer. However, high energy ions, which increased the thickness of the intermixed layers, decreased the film adhesion. It is revealed that the high energy ions caused the carbonization at the polyimide surfaces, which, in turn, decreased the adhesion strength. It was also found by Pappas and coworkers (Pappas et al., 1991) that for PMDA-ODA PI films, exposure to low energy Ar^+ and/or O^{2+} ions improved adhesion to the metal overlayer, while for BPDA-PDA polyimide, the role of O^{2+} was more effective. The 90°-peel adhesion strength of Cu to the both PI films increased about 2-3 times after ion-beam irradiation.

Laser technique has been practically used in the microelectronics industry for surface ablation of PI films (Pappas, 1989; Lankard and Wolbold, 1992). The principle and the effect of laser on the surface properties of the PI film have been reviewed by Pettit (Pettit, 1996). Laser treatments give rise to photochemical degradation of the PI molecules to generate free radicals (Qin et al., 2000). Atmospheric oxygen sequentially

reacts with the produced radicals to form a highly oxidized layer. The formation of carbonyl group on the PI surface is enhanced by the heat remaining on the irradiated PI surfaces. Adhesion enhancement of Cu to laser-treated surfaces has been reported in the literature (Weichenhain et al., 1997; Frerichs et al., 1995). Laser ablation of PI film results in the formation of a glassy carbon layer on its surface, especially at near-threshold fluence (Shafeev and Hoffmann, 1999). Glassy carbon can mediate the electroless metal deposition, thus, resulting in a local metallization of the surface. The ability of this layer to promote the electroless Cu deposition from the corresponding plating solution is a function of laser processing parameters and conditions of deposition.

Plasma treatment is commonly used in the microelectronics industry for cleaning and etching purposes. This technique has also been an effective method for the surface modification of polymer substrate for adhesion promotion purpose (Chan et al., 1996). The effect of plasma treatment on the surface properties of the PI substrate has been described by Egitto and Matienzo (Egitto and Matienzo, 1996). Generally, plasma treatment of PI film can give rise to the changes in surface hydrophilicity (Katnani et al., 1989; Inagaki, et al., 1992) and adhesion property (Inagaki et al., 1994). Plasma treatment also gives rise to new functional groups, such as oxygen, nitrogen, and fluorine-containing groups, on the PI surface, depending on the gas used (Inagaki, 1992). The easy and fast operating process makes this technique a very attractive method for surface modification of the PI substrates. Rozovskis et al. (Rozovskis et al., 1994) reported that O_2 plasma treatment of PI surface greatly improved the adhesion to the electrolessly deposited copper. Adhesion strength of copper to O_2 plasma-treated PI film is affected by the plasma treatment time. Maximum adhesion strength was obtained for polyimide thin films etched in oxygen plasma for 3 min (Nakamura et al.,

1996). Inagaki et al. (Inagaki et al., 1994) also indicated that the Ar, NO, and NO_2 plasma treatments improved the adhesion of the thermally evaporated copper to the PI (Kapton® HN) film. The improvement in adhesion strength was attributable to the formation of coordinate bonds between carboxyl groups and copper atoms, and the mechanical interlocking by penetration of the copper layer into the deep valleys between the protuberances.

Recently, surface modification *via* graft copolymerization has shown to be a more effective method for adhesion enhancement of copper to PI films (Inagaki, 1995; Inagaki, 1996; Ang et al., 1999; Ang et al., 2000) than other traditional surface modification approaches. Surface graft copolymerization can be carried out under relatively mild conditions. The technique requires only the generation of active species, such as peroxides and hydroperoxides, on the substrate to initiate the subsequent surface copolymerization. Thus, surface graft copolymerization commonly proceeds *via* the free radical reaction of vinyl or acrylic monomers, although it may also proceed *via* the cationic or anionic mechanism. Through the intelligent choice of monomers with appropriate functional groups, new molecular functionalities can be incorporated onto the activated PI surfaces. Inagaki et al. (Inagaki et al., 1995) have shown that high adhesion strength can be obtained between thermally evaporated copper and vinylimidazole graft-modified PMDA-ODA PI film. The high adhesion strength was attributed to the formation of N-Cu complexes between the imidazole ring and the Cu atoms. The presence of N-Cu complexes was verified by the changes in the N 1s core-level spectra of XPS results. Ang et al. (Ang et al., 1999; Ang et al., 2000) also improved the adhesion of Cu foil to Ar plasma-pretreated PI surface by simultaneous lamination and graft copolymerization with vinylimidazole.

Plasma polymerization is a unique technique for modifying polymer and other substrate surfaces. It allows the direct deposition of a thin polymer film on almost any substrate surface, without affecting the bulk properties of the substrate. Most important of all, the process is solvent free. For these reasons, plasma polymerization and deposition have attracted considerable attention in recent years (Silverstein et al., 1996; Ward and short, 1995). Tarducci et al. (Tarducci et al., 2000) deposited glycidyl methacrylate (GMA) to the fluoropolymer surface *via* plasma polymerization and deposition technique. The epoxide functional groups in the plasma-deposited GMA polymer were nearly fully preserved by using proper deposition conditions. The preservation of the epoxide groups was verified by the XPS, TOF-SIMS and FTIR results. In a parallel research, GMA is plasma-polymerized and deposited on the Si(100) surface with the preservation of a high percentage of the epoxide groups(Zhang et al., 2000; Zhang et al., 2001). The plasma-deposited film acts as an adhesion promoter to improve the adhesion of thermally-imidized PI and FPI films on the silicon substrate.

2.2 Surface Metallization of Polymer Dielectrics

Metallization of polymer films has always been of great interest to the microelectronics industry. The deposition of metal thin film has been achieved by vacuum deposition, plasma deposition, sputtering, electroplating and electroless plating from solution (Rye and Ricco, 1998; Mittal, 2001). Electroless plating process are used mainly for functional coatings of metals and non-conductors in major industries, such as in the fabrication of electronic circuits and interconnections, magnetic memory disks and electromagnetic interference shielding. Electroless technologies yield alloy deposits with unique mechanical characteristics for wear and

corrosion protection in automotive and aerospace applications, as well as for the protection of equipment used in chemical manufacturing, and in oil and gas production (Mallory and Hajdu, 1990).

Electroless metal plating is a non-electrolytic deposition from solution. The basic components of an electroless plating solution include a metal salt and a reducing agent. An additional requirement is that the solution, although thermodynamically unstable, is stable in practice until a suitable catalyzed surface is introduced. Plating is then initiated upon the catalyzed surface, and the plating reaction is sustained by the catalytic nature of the plated metal surface itself. The history of electroless plating began with the discovery by Brenner and Riddell during a series of nickel electroplating experiments in 1946 (Brenner and Riddell, 1946). Electroless copper plating chemistry was first reported in 1947 by Narcus (Narcus, 1947). The evolution of electroless plating during the last 30 years are remarkable. The advantage of electroless plating include uniformity of coverage, the possibility of metallizing non-conductors, and the ability to plate selectively especially when compared with electroplating.

Palladium chemisorption is a determinant step in metallization by the electroless plating process. The step establishes strong chemical bonds between the substrate and the metallic film. Different methods have been proposed to perform the surface activation of polymer substrates for electroless plating (Paunovic and Schlesinger, 1999). Historically, the most widely used methods for the surface sensitization and activation of substrates were the “two-step” process (Pearlstein, 1955) and the “one-step” activation process (Meek, 1975). In the ‘two-step’ method, the polymer surface was first sensitised by $SnCl_2$ and then activated in the $PdCl_2$ solution (Muller and

Baudrand, 1971). The ‘one-step’ process, on the other hand, used a mixed $SnCl_2/PdCl_2$ colloidal solution. The mixed $SnCl_2/PdCl_2$ solutions are of a great complexity and their aging plays a significant effect on the metallization efficiency. It was indicated that the complexes formed at the very beginning of the solution mixture are rapidly transformed into colloidal particles whose core consists of a metallic alloy (Sn/Pd) surrounded by a $SnCl_2$ shell (Jackson, 1990). On the other hand, however, $SnCl_2$ is not an active catalyst for electroless plating (Muller and Baudrand, 1971). As a result, the growth of the copper deposit was inhibited.

To avoid the side-effect of the tin atom in the subsequent electroless plating process, a tin-free process is preferred. Viehbeck et al. (Viehbeck et al., 1990) described a seeding process for activating the surface of polyimide and other electroactive polymers. The process consists of reducing electrochemically the outer region of such materials when these materials are brought into contact with an electrolyte containing a strong organic reducing agent. In this way, the electroactive surface is used to provoke electron transfer to metal ions in solution, which caused metals to be deposited at the surface. The deposition of such metals renders the polymer surface active towards further metal deposition from conventional electroless plating bath. Baum et al. (Baum et al., 1991) described a selective process based on the photoreduction in the formation of an active palladium catalyst. This process worked well on a variety of dielectric materials including PI films when the iron-palladium treated dielectric films are irradiated with deep UV lamp (500 W Hg-Xe). On the other hand, Charbonnier et al. (Charbonnier et al., 1996) have reported that palladium can be adsorbed directly on the nitrogen functional groups of the polymer surfaces generated from N_2 or NH_3 plasma treatment. More recently, several N-containing polymers have been grafted on plasma-pretreated fluoropolymer surfaces by UV-induced graft copolymerization to the

chemisorption of Pd^{2+}, in the absence of prior surface sensitizaition by $SnCl_2$, for the electroless plating of copper (Yang et al., 2001). The "Sn-free" process involved initially the chemsorption of Pd, in complex form, on the nitrogen sites of the grafted polymer. The Pd complex underwent a reduction to Pd metal in the electroless copper plating bath prior to the initiation of electroless deposition of copper.

2.3 Nanoporous Low-*k* Materials for Microelectronic Applications

In the past few decades, the increasing demands of miniaturization in the microelectronics industry has forced continual improvement in the materials that are used in the fabrication of semiconductor devices. The use of interlayer materials with very low dielectric parameters can greatly reduce the RC time delays, cross-talks, and power dissipation in the new generation of high density integrated circuits (Lee et al., 1995; Maier, 2001). In addition to exhibiting low dielectric constants, the next generation of interlayer dielectrics for sub-micron and nano-level electronics must also satisfy a variety of requirements, such as good thermal stability, low moisture absorption, good adhesion to semiconductor and metal substrates, and chemical inertness. Polyimides (PIs) have been widely used as dielectric and packaging materials in the microelectronics industry because of their good mechanical, thermal and dielectric properties (De Souza-Machado et al., 1996; Auman, 1993). However, with dielectric constants (κ) of about 3.1-3.5, the conventional PIs are insufficient in meeting the requirement of $\kappa<2.5$ for the dielectrics of the near future (Morgan et al., 1995).

Various attempts have been made to prepare PIs with lower dielectric constants. It is well known that the incorporation of fluorinated substitutents into polymers decreased

the dielectric constant due to the small dipole and the low polarizability of the CF bond as well as the increase in free volume, which accompanies the replacement of methyl groups by trifluoromethyl groups (Van Krevelen, 1990). An additional positive effect of fluorinated substitutes is reduced moisture aborption due to the non-polar character of fluorocarbon groups, which further reduces the dielectric constant. A large number of fluorinated polyimides have been prepared (Brink et al., 1994; Vora et al., 2001; Misra et al., 1992). The modified PIs have dielectric constants in the order of 2.4-3.0 (Sasaki and Nishi, 1996). However, it is well known that the lowest dielectric constant available for fluorinated dense materials is around k~2.1 for PTFE (Teflon) and none of the current approaches using dense materials is expected to achieve k values lower than that. Furthermore, the preparation of fluorinated polyimide may be limited by high cost, reduced mechanical properties, and difficulties in synthesis. There are also serious concerns about the effect of fluorinated dielectrics on the interconnect metals and metal liners at elevated temperatures.

An alternative approach toward lowering a polymer's dielectric constant is to introduce nanoscopic porosity into the polymer film. The incorporation of air，which has a dielectric constant of about 1, can greatly reduce the dielectric constant of the resulting porous structure/material. Porous materials may have dielectric constants in the ultra-low-k region. Porosity may be classified as either closed or open cell, the latter characterized by interconnected pores. Ideally, the pores of on-chip insulators should be closed cell, uniformly distributed and controlled to the nanoscopic level.

At present, most porous low-k materials are produced using either surfactant-templated or sol-gel processes. In the templated approach, the precusor contains a composite of thermally labile and stable materials. After film deposition, the thermally liable

materials are removed by thermal heating, leaving pores in the dielectric film. Polyamide nanofoams are examples which were obtained by this approach (Hedrick et al., 1998a). In the sol-gel process, the porous films are formed using hydrolysis and polycondensation of alkoxide, such as tetraethoxysilane (TEOS). During the aging process, porous network is formed and strengthened while liquid solvent is still present in the pores. The solvent is then removed in a subsequent drying process. Aerogels or xerogels with SiO_2 as matrix with porosities above 90% and dielectric constant close to 1 have been reported (Hrubesh et al., 1993; Ramos et al., 1997). However, a large volume of solvent must be removed to obtain such extremely porous structures. Since the pores must not be interconnected, the diffusion of the solvent has to proceed through the matrix material. Control of the process without shrinkage and formation of macroscopic cracks is quite difficult. Moreover, high porosity also has adversely effects on other important film properties, such as thermal conductivity and stability.

The approaches to the preparation of porous polyimide (PI) films include microwave processing (Gagliani and Supkish, 1979), incorporation of foaming agents (Krutchen and Wu,1985) and hollow microspheres (Narkis et al., 1982). However, most of the materials prepared by these methods may have large pore sizes and open pore structures, which make it unsuitable for microelectronic applications. Therefore, control over the pore size, shape, and distribution is critical to obtain porous materials with suitable mechanical and electrical properties to withstand the rigorous requirement for the production of integrated circuits, especially when the device feature size is approaching 100 nm and the film is thin (less than 1 um). Materials with homogeneous, nanometer-scaled, closed pores are preferred to preserve electrical and mechanical properties. In addition, these nanopores should be randomly distributed to ensure that the thin film properties are isotropic.

Fine works on the preparation of porous PI films, with pore sizes in the nanometer range, by utilizing the block copolymer approach have been reported. To this end, block copolymers of PI with poly(methylmethacrylate) (Hedrick et al., 1995b), polystyrene (Hedrick et al., 1995a), poly(lactones) (Hedrick et al., 1998b) and poly(propylene oxide) (Hedrick et al., 1995a, 1995b) have been prepared. Thermal degradation of the labile components in the block copolymers gives rise to the nanoporous PI films with low dielectric constants. The exact process for the decomposition depends on the nature of the labile blocks. Porosities up to 30% could be achieved. The dielectric constant of a PMDA-3FDAm film with 18% porosity was reduced to 2.35 from 2.85 for the pristine polyimide film (Hedrick et al., 1998). One of the major problems of this procedure is the potential collapse of the pores. This may due to the high surface tension of the small pores, and during pore formation because of the polar products from the decomposition of the labile blocks, which can plasticize the polyimide and hence increase the chain mobility required for collapse. In addition, when the temperature used to generate the pores or any processing temperature during the interconnect fabrication using such nanoporous films is too close to the glass transition temperature of the polyimide phase, softening of the matrix will result in collapse due to the surface tension. Hence, further increase of the porosity by the block copolymer method is rather difficult. The morphology will change from spherical domains to cylinders in a matrix and then to lamellar structure, when the content of the minor component is increased. Thus, isolated, non-interconnected pores can no longer be expected, as the porosity approaches or exceeds 30%. The exact composition for the morphology transition depends on the degree of immiscibility of the two phases, the block lengths and block length distributions, as well as the film casting process.

2.4 Preparation and Modification of Polymeric Microfiltration Membranes

PIs have also been widely investigated as membrane materials during the past three decades for proton conducting, fouling resistance, gas removal and gas separation applications (Semenova, 1996; Yamamoto et al., 1990; Eastmond et al., 2002; Shimizu et al., 2002), due to their unique physicochemical properties, such as good thermal stability, low dielectric constants, excellent mechanical strength, and surface inertness (Wilson et al., 1990; Auman, 1993; Ferge, 1993). It was shown that polyimides have excellent mass exchange characteristics, which together with their other valuable physicochemical properties make them extraordinary materials for separation and purification technologies.

The physical structure and the physical properties of a membrane are directly related to the preparation procedures. Various methods have been utilized to prepare polymeric microporous membranes such as sintering, stretching, track-etching, and phase inversion. Among them, the phase inversion techniques is most widely used, especially in the preparation of commercial microfiltration (MF) membranes. Phase inversion is a process whereby a homogeneous polymer solution is converted into a three-dimensional net structrue or gel containing solid polymer areas and voids located in between (Kesting, 1985; Strathmann, 1985). A detailed description of the phase inversion process can be found in “Basic Priciples of Membrane Technology” (Mulder, 1991). The technology for the preparation of PI membrane by phase inversion method is complicated. It includes several stages, and changing process conditions at these stages can significantly affect the structure and properties of resultant membranes. In the most general way, a typical process for preparation of PI

membranes by phase inversion involves the following steps: (1) preparation of solution of polyimide or poly(amic acid); (2) spreading the polymer solution on a solid surface, porous support surface (in this case composite membranes are to be prepared), or forming hollow fiber in the form of a stream through a spinneret; (3) solvent evaporation; (4) immersion precipitation: choice of the precipitation bath composition and temperature, residence time in the bath; (5) eventual post-treatment of the membranes, such as drying or annealing. Depending on the rate of polymer precipitation, three types of membranes can be obtained: (a) symmetric, with an almost even porosity across the membrane cross-section; (b) asymmetric, with a selective thin microporous upper layer (skin) on a thicker macroporous globular or spongy sub-layer; (c) asymmetric, with large voids and/or finger-like cavities beneath the microporous upper layer (Strathmann and Kock, 1977).

Recently, much attention has been directed to the development of more sophisticated membranes that can regulate the permeability in response to environmental changes. Porous membranes with signal-responsive “polymer brushes” are advantageous over the hydrogel membrane in terms of mechanical strength and quick response to external stimuli. Certain polymeric materials are known to change reversibly their conformation and phase structures in response to the external chemical or physical stimuli, such as changes in pH (Chung et al., 1996; Iwata et al., 1998), ionic strength (Nonaka et al., 2003), temperature (Park et al., 1998; Peng and Cheng, 1998), or electrical potential (Jaworek et al., 1998). These materials are termed as “smart polymers”. Different kinds of changes can be induced by the responses of the smart polymers, such as phase, shape, surface energies, permeation rate, reaction rate and molecule recognition. For example, Poly(*N*-isopropylacrylamide) (PNIPAAM) is the most widely studied thermo-sensitive polymer (Hirotsu et al., 1987; Ebara et al.,

2000). It exhibits a lower critical solution temperature (LCST) at around 32°C in aqueous solution (Heskins et al., 1968). Below the LCST, it adopts an extended random coil conformation. As the temperature is increased, the hydrogen bonds weaken, with the concomitant release of water of hydration. The hydrophobic interaction tend to overcome the hydrophilic interaction, leading to a coil-to-globule transition and finally to phase separation.

Various types of smart polymeric systems, such as signal-responsive interpenetrating polymer network (IPN), polymer gels, and membranes have been devoloped (Ju et al., 2001; Alvarez-Lorenzo and Concheiro, 2002; Chu et al., 2001). Among them, porous membranes with 'smart polymer brush' are of particular interest due to their excellent mechanical strength and quick response to external stimulus. On the other hand, however, permeation of commercial porous membranes are often independent on the environment. Therefore, surface or bulk modification of current membranes was often used to render them with environmental-responsive properties.

The well-known surface modification methods include physical adsorption (Brink et al., 1993), surface coating (Nunes et al., 1995), and surface grafting (Uchida et al., 1994; Gancarz et al., 1999). During these processes, stimuli-responsive polymer brushes can be chemically-grafted or physically-adsorbed onto solid polymer substrates, and the surface film thickness, wettability, or surface charge can then change rapidly in response to small changes in stimuli such as solution temperature, pH or specific ionic concentrations. These responses is much faster than for solids such as hydrogels since the surface coating is very thin. Permeation "switches" can be prepared by coating or grafting "smart" polymers onto the surfaces of pores in a porous membrane, and stimulating their swelling (to block the pore flow) or collapse

(to open the pore to flow). Surface grafting has several advantages over other methods, including easy and controllable introduction of graft chains with a high density and exact localization of graft chains on the surface with the bulk properties unchanged.

On the other hand, however, both the surface coating and grafting methods may have their own drawbacks. For the coating method, the coated surface layers may be easily removed, especially by changes in pH of the solution. Furthermore, surface modification of existing membranes by grafting is likely to be accompanied by changes in membrane pore size and pore size distribution, leading to reduced permeability. In addition, the extents of grafting on the membrane surface and the surfaces of the pores may differ substantially. In order to overcome these problems, bulk-modified or chain-modified polymer may be used as membrane materials. Contrary to surface modification techniques, where the surface composition was modified and adapted to a given application by some external treatment such as grafting, the preparation of membranes from bulk modified polymers can greatly facilitate the control of the pore size, the pore size distribution and the composition of the pore surfaces through the control of the copolymer structure and composition.

Ozone treatment has been widely utilized to generate peroxide and hydroperoxide species on polymer chains and surfaces (Fargere et al., 1994; Boutvein et al., 1992; Fujimoto et al.,1993; Boutvein et al., 2002). Under thermal induction, these labile functional groups undergo decomposition to initiate the free radical graft copolymerization of vinyl monomers. Landler and Lebel (Landler and Lebel, 1960) used an ozone flow on polystyrene (PS) and succeeded in grafting vinylic monomers. Sarraf et al. focused their research on polyethylene (PE) (Sarraf et al., 1984), which also gave grafted products with various monomers such as styrene,

methylmethacrylate vinyl-chloride, or glycidylmethacrylate. In 1991, poly(vinylidene fluoride) (PVDF) was pretreated with ozone to make PVDF/MMA and PVDF/S copolymers (Boutevin et al., 1991). After ozonization, the polymer is somewhat degraded and the molecular weight is reduced. Infrared spectroscopy shows that the presence of carbonyl and ketone groups. In the case of ozonized polymers used for grafting, the presence of peroxides and hydroperoxides is controlled. The different methods of determining these groups *via* titration are described in the literature use ferrous ion, iodine, or free radicals such as 2,2-diphenyl-1-picrylhydrazil (DPPH) (Boutevin et al., 1992; Elmidaoui et al., 1991; Fargere et al., 1994).

CHAPTER 3

ELECTROLESS PLATING OF COPPER ON FPI FILMS MODIFIED BY UV-INDUCED GRAFT COPOLYMERIZATION WITH *N*-CONTAINING MONOMERS

3.1 Experimental

3.1.1 Materials

2,2'-bis(3,4-dicarboxyphenyl) hexafluoropropane dianhydride (6FDA) was obtained from Chriskev, KS, USA. 4,4'-bis(4-aminophenoxy)diphenyl sulfone (*p*-SED), was received from Wakayama Seika Kogyo Co. Ltd., Japan. 2,2'-bis(4-aminophenyl) hexafluoro propane (4,4'-6F-Diamine), 1-vinylimidazole (VIDz), 4-vinyl pyridine (4VP), N-methyl 2-pyrolidinone (NMP) and methanol were received from Sigma–Aldrich, Milwaukee, WI, USA. All monomers and solvents were used as received. The chemical structures of the VIDz and 4VP are shown below:

VIDz:

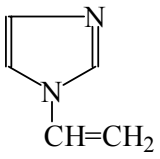

4VP:

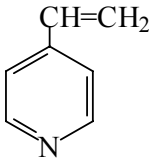

3.1.2 Polymer Synthesis

The fluorinated polyimides (FPIs) used in this study were synthesized by solution condensation polymerization method, utilizing a simplified two-step polymerization (Vora et al., 2001; Vora et al., 1990). For example, in the case of synthesis of [6FDA + *p*-SED], a fluoro-polyetherimide based on 2,2'-bis (3,4-dicarboxyphenyl) hexafluropropane dianhydride (6FDA) and 4,4'-bis(4-aminophenoxy) diphenyl sulfone (*p*-SED), accurately weighed 0.02 mole of solid 6FDA was added to an equimolar

amount of diamine pre-dissolved in NMP to make 20% solid concentration. The mixture was stirred under nitrogen at room temperature for over 12 h to make fluorinated poly(amic acid) (FPAmA) solution, which was then imidized to form fluorinated polyimide (FPI). The cyclization can be achieved by either thermal or chemical means. In this work, the chemical imidization were carried out by adding of stoichiometric amounts of β-picoline (catalyst) base (pKa=5.6) and acetic anhydride (dehydrating agent). Under a nitrogen atmosphere at room temperature, 0.04 mol of β-picoline was added to the polymeric acid and stirred for 15 min. Then, 0.02 mol of acetic anhydride was added drop-wise to the mixture over a period of 10 min. The reaction mixture was stirred under nitrogen at room temperature for another 8 h to obtain the polyetherimide polymer solution. The polymer was precipitated with methanol and dried overnight in an air circulating oven at 100^{o}C. The polymer and a small sample of the poly(amic acid) were retained for viscosity measurement. The structures of the two FPIs referred in this work as FPI–1, i.e. (6FDA + 4,4-6F Diamine) and FPI-2, i.e. (6FDA + *p*SED), are shown as follows:

FPI-1:

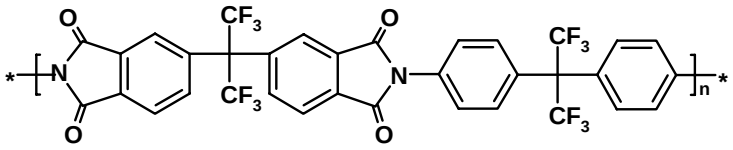

FPI-2:

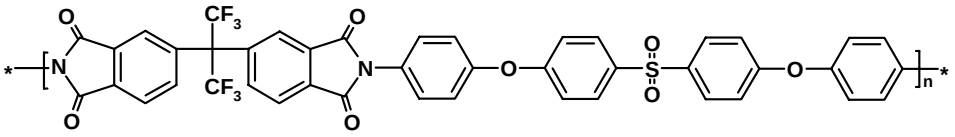

3.1.3 FPI Film Preparation

The FPI film was obtained by casting the 15 wt% NMP solution on a glass plate. The films were first dried under atmospheric condition at room temperature. They were then heated gradually over a period of 4 h in a vacuum oven up to 250°C and then kept at 300°C for 1 h. The film was allowed to cool down gradually to room temperature over a period of 6 h. The surface of the FPI films was then cleaned with ethanol in an ultrasonic water bath for 20 min, followed by drying at 80°C for 6 h under reduced pressure.

3.1.4 Plasma Pretreatment and UV-induced Surface Graft Copolymerization

The FPI films were cut into strips of about 2 × 4 cm^2 in size. Argon (Ar) plasma pretreatment of the FPI films was carried out in a cylindrical quartz glow discharge chamber of about 1,400 cm^3 in volume, model SP 100, manufactured by Anatech Inc. of Springfield, VA, USA. The glow discharge was produced at an applied frequency of 40 kHz, a power of 32 W, an Ar pressure of 0.5 Torr and an Ar flow rate of 50 standard cubic centimeter per min (sccm). The film was placed between two parallel plate electrodes of 12 × 8 cm^2 in area and 3 cm in separation. It was subjected to the glow discharge for a pre-determined period of time. The Ar plasma-pretreated FPI films were then exposed to the atmosphere for about 30 min to effect the formation of surface peroxides and hydroperoxides (Zhang et al., 2001b) for the subsequent graft copolymerization with VIDz or 4VP.

The UV-induced graft copolymerization was performed *via* a "solvent-free" process under atmospheric conditions. About 0.2 ml of pure VIDz or 4VP monomer was

introduced onto the surface of the plasma-pretreated FPI film. The film was then sandwiched between two quartz plates. The assembly was subjected to UV irradiation for 60 min in a Riko RH 400-10W rotary photochemical reactor, manufactured by Riko Denki Kogyo of Chiba, Japan. The reactor was equipped with a 1000 W high-pressure Hg lamp and a constant temperature bath. All UV-induced graft copolymerizations were carried out at a constant temperature of 28°C under atmospheric condition. After the surface graft copolymerization, the FPI films were washed thoroughly with doubly distilled water for 24 h to remove the residual VIDz or 4VP homopolymer physically adsorbed in the graft layer.

3.1.5 Surface Activation and Electroless Plating of Copper on FPI Films

The graft-modified FPI films were activated *via* immobilization of the Pd catalyst, in the absence of prior sensitization by $SnCl_2$ (the Sn-free process), for the electroless deposition of copper. The film was immersed in an aqueous solution containing 0.1 wt% $PdCl_2$ and 1.0 wt% HCl (12M) for 10 min, followed by rinsing thoroughly with doubly distilled water. The $PdCl_2$-activated FPI film was then placed in an electroless copper plating bath for 15-20 min. The thickness of the deposited copper was determined gravimetrically. Typically, a copper layer of about 1 μm was deposited. The composition of the solution in the plating bath was as follows: 0.7 wt% $CuSO_4 \cdot 5H_2O$, 2.5 wt% potassium sodium tartrate, 0.4 wt% sodium hydroxide, and 0.4 wt% formaldehyde (Ebneth, 1993). Copper-plated FPI film was rinsed thoroughly with copious amounts of doubly distilled water. It was then subjected to thermal post-treatment in a vacuum oven at 140°C for about 2 h. Post thermal treatment has been known to promote the further interaction of the deposited copper with the graft chain, resulting in improved adhesion (Wu et al., 2000). Thermally-treated sample was

allowed to cool slowly to room temperature in the vacuum oven over a period of about 4 h to minimize the thermal stress at the metal-polymer interface. The metallized sample was then adhered to a copper sheet backing (0.1 mm in thickness) using a commercial epoxy adhesive (Araldite Stand®, from Ciba Specialty Chemicals (UK) Ltd., Duxford, England.), subsequently the assembly was thermally cured at 140°C for 3 h in a vacuum oven prior to the T-peel adhesion strength measurement.

For comparison purposes, electroless plating of copper was also carried out on the pristine FPI and the plasma-pretreated FPI films *via* the conventional "two-step" process (Ebneth, 1993). In this method, the FPI films were first sensitized by immersing in an aqueous solution containing 0.3 wt% $SnCl_2$ and 2.5 wt% HCl (12 M) for 2 min, followed by rinsing with doubly distilled water. The subsequent processes of activation in the $PdCl_2$ solution, electroless copper plating and thermal post-treatment were similar to those described above for the Sn-free process

3.1.6 Viscosity Measurements

The viscosities of both FPAmAs and FPIs were determined according to ASTM 2515/D446 using a Schott-Gerate AVS360 Viscometer, DIN Ubbelohde, at 25°C in NMP. The viscosities of both FPAmAs were determined at fixed shear rate and temperature using a Brookfield Programmable Rheometer Model DV-III (with Rheocalc software and Brookfield water bath TC-200/500) at 5 rpm using CP42 spindle. About 1 mL of bubble free sample was used. Prior to analysis, sample was allowed to reach equilibrium for 1 min before taking reading. An average of 6 readings was taken.

3.1.7 Thermal Analyses

Decomposition temperatures (5 wt% loss) of the polymer films were determined using a Perkin Elmer TGA-7 system at a heating rate of 10°C/min under a dry nitrogen or air atmosphere (10 cc/min). The glass transition temperatures (T_g) of both FPI films were determined at a heating rate of 10°C/min and under a flowing nitrogen atmosphere (10 cc/min), by using a Perkin Elmer DSC-7 Differential Scanning Calorimeter with Pyris software. Long-term isothermal, thermo-oxidative stability (TOS) studies of both FPI films samples were performed in air for 300 h at 315ºC in a Lenton programmable forced air oven with Eurotherm 2408 Temperature controller programmer from Lenton Thermal Design, UK.

3.1.8 Dielectric Constant Measurement

The dielectric constant (ε) of both FPI films was measured between two-parallel plate of the dielectric analyzer (model DEA-2970) from TA Instruments at a frequency of 10 MHz and at 50 % relative humidity at temperature of 25°C in a flowing nitrogen atmosphere condition.

3.1.9 X-Ray Photoelectron Spectroscopy (XPS)

XPS measurements were carried out on a Kratos Analytical AXIS HSi spectrometer (Kratos Analytical Ltd, Manchester, England) with a monochromatized Al Kα X-ray source (1486.6 eV photons). The X-ray source was run at a reduced power of 150 W (15 kV and 10 mA). The surface-modified FPI samples were mounted on the standard sample studs by means of double-sided adhesive tapes. The core-level spectra were obtained at the photoelectron take-off angle (α, with respect to the sample surface) of

90°. The pressure in the analysis chamber was maintained at 10^{-8} Torr or lower during each measurement. To compensate for surface charging effects, all binding energies (BE's) were referenced to the C 1s hydrocarbon peak at 284.6 eV. In peak synthesis, the line width (full width at half maximum or FWHM) of Gaussian peaks was maintained constant for all components in a particular spectrum. Surface elemental stoichiometries were determined from the peak area ratios and were accurate to within ±10 %.

3.1.10 Atomic Force Microscopy (AFM)

The topography of the VIDz-g-FPI and 4VP-g-FPI film surfaces were characterized using a Nanoscope IIIa atomic force microscope (AFM), manufactured by the Digital Instruments Inc., Santa Barbara, CA. In each case, an area of 50 μm × 50 μm was scanned using the tapping mode. The drive frequency was 330 ± 50 kHz. The applied voltage was between 3.0 ~ 4.0 V, and the drive amplitude was about 300 mV. The scan rate was 1.0 Hz. An arithmetic mean of the surface roughness (R_a) was calculated from the roughness profile determined by AFM.

3.1.11 Adhesion Strength Measurements

The adhesion strength of the electrolessly deposited copper with the various FPI substrates was determined by measuring the T-peel adhesion strength. The T-peel adhesion strength was measured at 25°C on an Instron model 5544 tensile tester from Instron Corp., Canton, MA. All measurements were carried out at a crosshead speed of 10 mm/min. For each T-peel adhesion strength reported, at least three sample measurements were averaged. The values of adhesion strength among these measurements usually did not vary by more than ±0.3 N/cm.

3.2 Results and Discussion

The FPI polymers have high glass trasition temperature, excellent thermal properties and thermo-oxidative stability (TOS) along with lower dielectric constant ($\varepsilon<2.8$), as shown in Table 3.1. The processes of surface modification of FPI film *via* plasma pretreatment and UV-induced graft copolymerization with VIDz or 4VP monomer, the surface activation by $PdCl_2$, and the subsequent electroless plating of copper on the modified FPI surfaces are illustrated schematically in Figure 3.1. Details of the surface modification and electroless deposition processes are described below.

3.2.1 Surface Composition of the Pristine and Surface-modified FPI Films

Figure 3.2 shows the respective wide scan and C 1s core-level spectra of the pristine FPI-1 and FPI-2 film surfaces (part (a) and part (b), respectively), and the 60-s argon plasma pre-treated FPI-1 and FPI-2 films after air exposure (part (c) and part (d), respectively). The C 1s core-level spectra of both types of pristine FPI films can be curved-fitted with five peak components, having binding energies (BE's) at 284.6 eV for the C-H species, at 285.8 eV for the C-O and C-N species, at 288.4 eV for the $N(C=O)_2$ species, at 291.1 eV for the π-π^* shakeup satellite, and at 292.8 eV for the CF_3 species (Moulder et al., 1992; Zhang et al., 2000). Due to the difference in the chemical structure of the two types of FPI films, as shown in Section 3.1.1, the FPI-1 film has a higher fluorine concentration than the FPI-2 film. It can be verified from Figure 3.2 that the peak intensity of the CF_3 species in the pristine FPI-1 C 1s spectrum is higher than that in the pristine FPI-2 spectrum. An additional peak component with a

Table 3.1 Properties of the Fluorinated Polyimides

Polymers	Bulk Visc. (cPs)	FPAmA Inh.[η] (dl/g)	FPI Inh.[η] (dl/g)	DSC T_g (^oC)	TGA (^oC) (5% Weight Loss)		Char Yield (%)	TOS (% Weight Loss)	Film Thickness (mm)	Dielectric Constant [a] (10 MHz)
					In Air	In N_2				
FPI-1	5167	0.80	0.78	293	520	555	54.5	2.1	1.1	3.10
FPI-2	11200	1.40	1.07	244	544	561	51.6	2.3	1.0	2.74

[a.] Measured as per ASTM D-150-81 method.

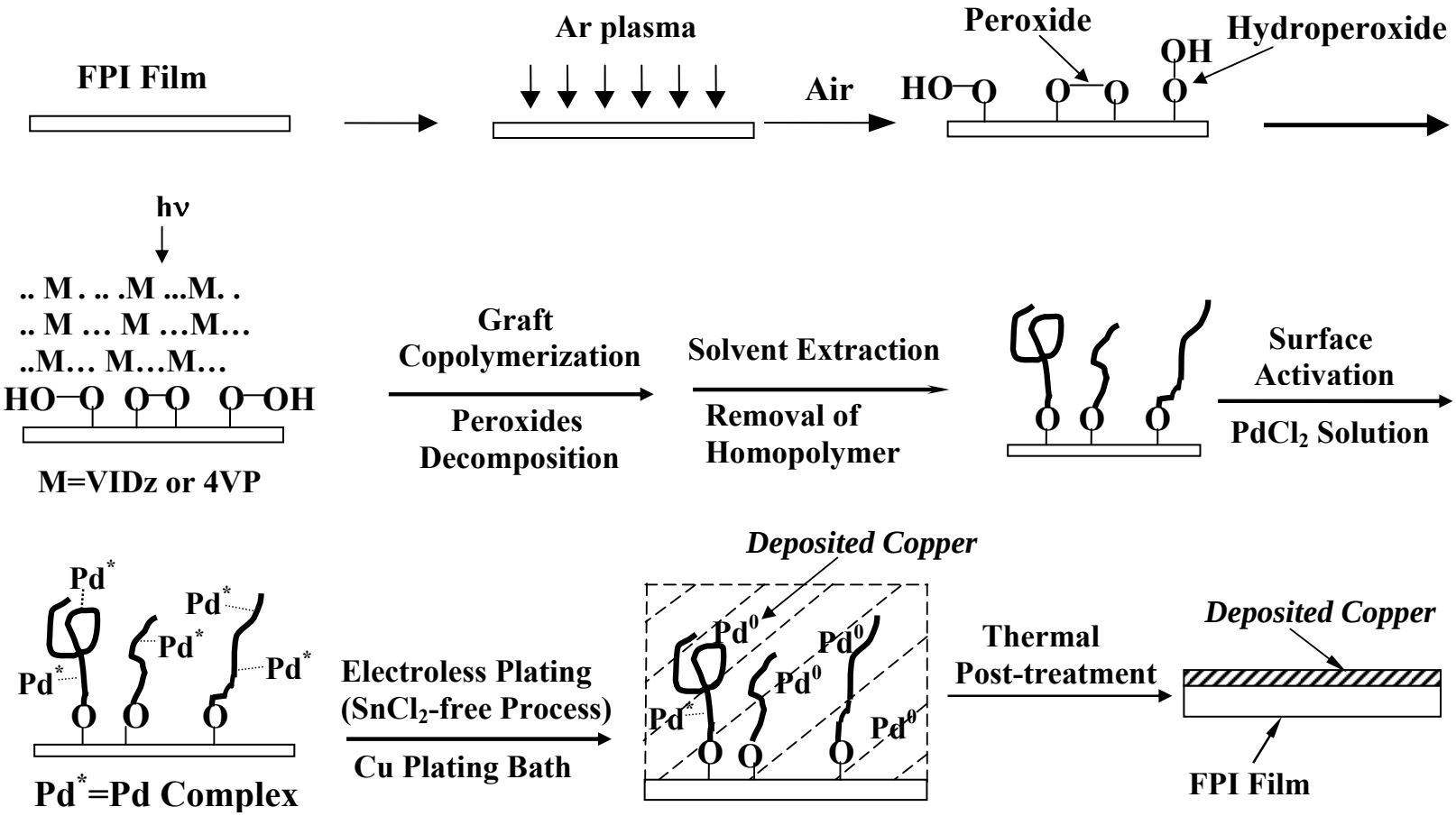

Figure 3.1 Schematic diagram illustrating the processes of Ar plasma pretreatment and UV-induced graft copolymerization of FPI with VIDz to form the VIDz-g-FPI surface and 4VP to form a 4VP-g-FPI surface, and the activation of the modified FPI surface *via* the Sn-free process for the subsequent electroless deposition of copper to form a copper/FPI assembly.

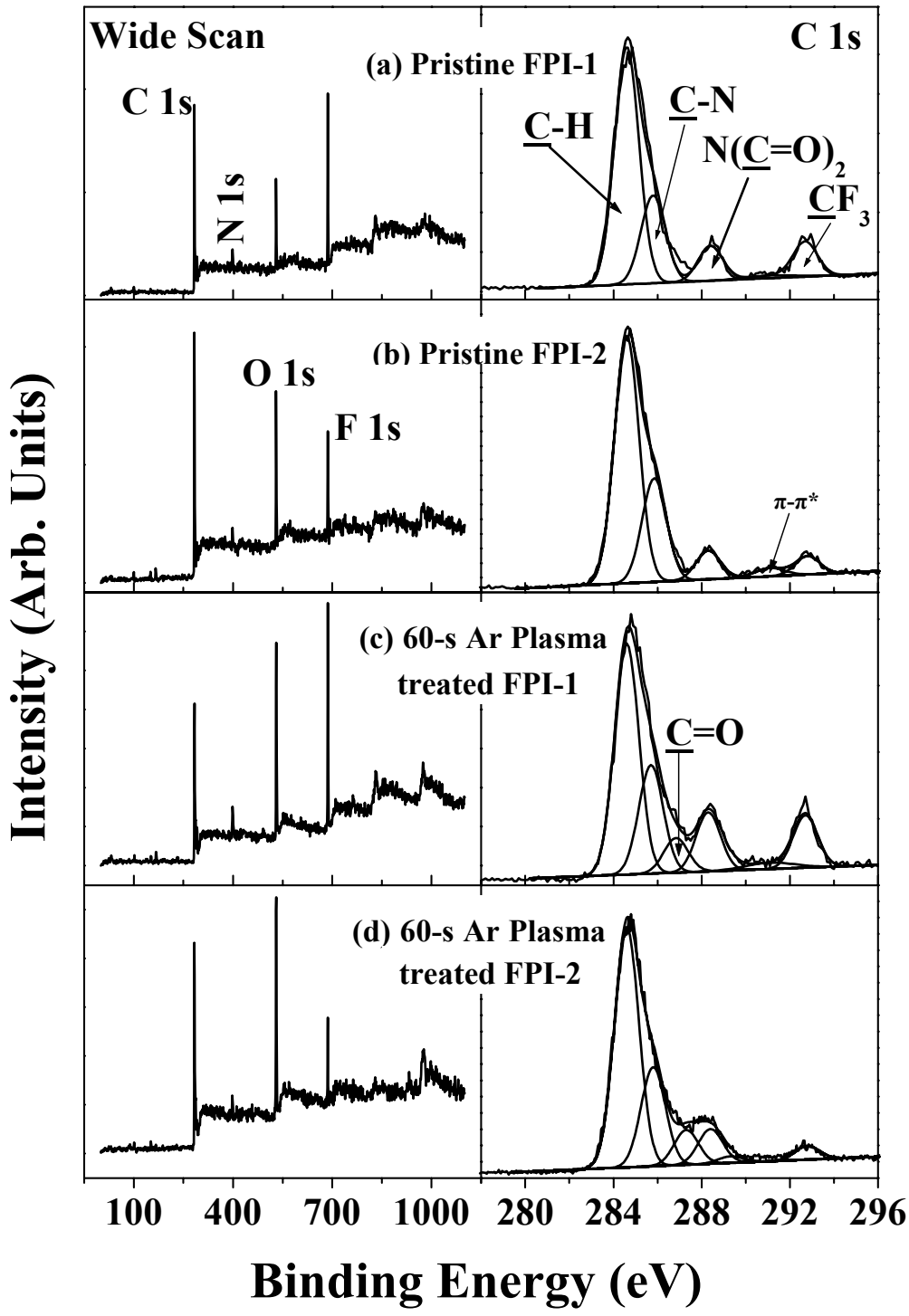

Figure 3.2 XPS wide scan and C 1s core-level spectra of (a) the pristine FPI-1 surface, (b) the pristine FPI-2 surface, (c) the FPI-1 surface subjected to 60 s of Ar plasma pretreatment. (d) the FPI-2 surface subjected to 60 s of Ar plasma pretreatment.

BE at 287.4 eV and attributable to the C=O species is found in the Ar plasma pretreated FPI surfaces. The peak component is different from the carbonyl structure of the imide group in the dianhydride structure. The presence of the C=O species in the plasma pretreated FPI surfaces is attributable to the oxidation in air of the active species on the FPI surface induced by the plasma pretreatment, as is also the case of peroxide and hydroperoxide formation shown in Figure 3.2. Furthermore, in comparison with the wide scan spectra of the pristine FPI surfaces, an increase in intensity of the O 1s peak component is observed in the wide scan spectra of the Ar plasma pretreated FPI films. The above results suggest that plasma pretreatment, followed by air exposure, gives rise to an oxidized surface.

The effects of Ar plasma pretreatment and subsequent air exposure on the surface [O]/[C] and [F]/[C] ratios of the FPI films, as determined from the O 1s, C 1s and F 1s core-level spectral area ratios, are shown in Figure 3.3. It can be observed that the [O]/[C] ratios of the two types of FPI surfaces increase sharply with the Ar plasma pretreatment time during the first 30 s of plasma pretreatment. The increase in the oxygen concentration on the FPI surfaces with the plasma pretreatment time is consistent with the fact that a longer plasma pretreatment time will lead to the formation of more active species on the FPI surface. The observations are in agreement with the results reported in the literature for the Ar plasma pretreatment of other fluoropolymer surfaces (Wu et al., 1999; Da et al., 1991). The [O]/[C] ratio for each FPI films approaches an asymptotic value at Ar plasma pretreatment times above 30 s. This observation suggests that prolonged Ar plasma pretreatment does not introduce more oxygen species on the FPI surfaces, probably due to the onset of the etching effect of the plasma. On the other hand, however, the [F]/[C] ratio of both types of the

FPI surface does not change after the Ar plasma pretreatment. Ar plasma pretreatment of the FPI surfaces, followed by air exposure, results in the formation of oxidized carbon species. These results suggest that oxidation of the FPI surface from Ar plasma pretreatment involves mainly the scission of the C-H bonds. The formation of the peroxide and hydroperoxide species on the FPIs have been quantitatively determined by reaction with 2,2-diphenyl-1-picrylhydrazyl (DPPH). They can be utilized to initiate the subsequent UV-induced surface free radical graft copolymerization.

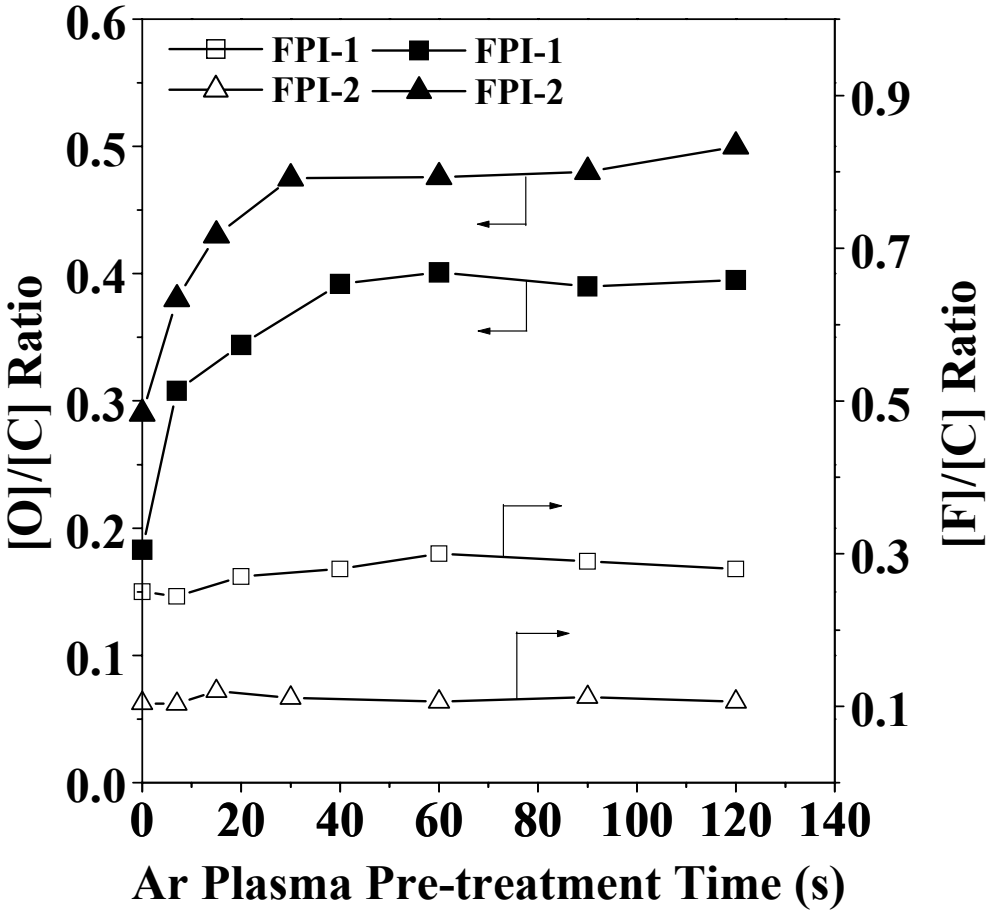

Figure 3.3 Effect of Ar plasma pretreatment time on the [O]/[C] and [F]/[C] ratios of the FPI film surfaces.

3.2.2 Electroless Deposition of Copper on FPI Films Modified by Surface Graft Copolymerization with VIDz: the Cu/VIDz-*g*-FPI Assemblies

Figure 3.4 shows the wide scan and N 1s core-level spectra of the pristine FPI-1 and FPI-2 film (Part (a) and Part (b), respectively), and the 60-s Ar plasma pretreated and air-exposed FPI-1 and FPI-2 surfaces after having been subjected to UV-induced graft copolymerization with VIDz for 60 min (the VIDz-*g*-FPI-1 and VIDz-*g*-FPI-2 surfaces, Part (c) and Part (d), respectively). The N 1s core-level spectrum of the pristine FPI film has only one peak component with the BE at about 400.5 eV, which is associated with the imide or -$\underline{N}(C=O)_2$ species (Zhang et al., 2001b). However, the N 1s core-level spectra of the VIDz-*g*-FPI-1 and VIDz-*g*-FPI-2 films consist of three species. The peak component with the lower BE of 398.5 eV is associated with the imino species (=$\underline{N}$-), and that at the higher BE of 400.3 eV with the amino species (-$\underline{N}$<), of the imidazole ring (Han et al., 1998). The latter component overlaps with that of the imide nitrogen at the BE of 400.5 eV. Due to the small difference (~0.2 eV) in BE, the -$\underline{N}$< and -$\underline{N}(C=O)_2$ species cannot be resolved unambiguously. The two species are represented by a single peak component at the BE of about 400.4 eV. The presence of the grafted VIDz polymer on the FPI surface can thus be deduced from the new imino component which has appeared in the N 1s core-level spectrum of the VIDz graft-copolymerized FPI film. Based on the chemical structure of the VIDz, the theoretical ratio of the imino and amino species should be 1:1. The apparently higher concentration of the amino species in Figures 3.4(c) and 3.4(d) is attributable to the contribution of the -$\underline{N}(C=O)_2$ from the underlying FPI substrate. The relative low intensity of the -N($\underline{C}$=O)$_2$ species on the VIDz-*g*-FPI surface suggests that the thickness of the grafted VIDz polymer layer is approaching the probing depth of the XPS technique (~7.5 nm in an organic polymer matrix (Tan et al., 1993)).

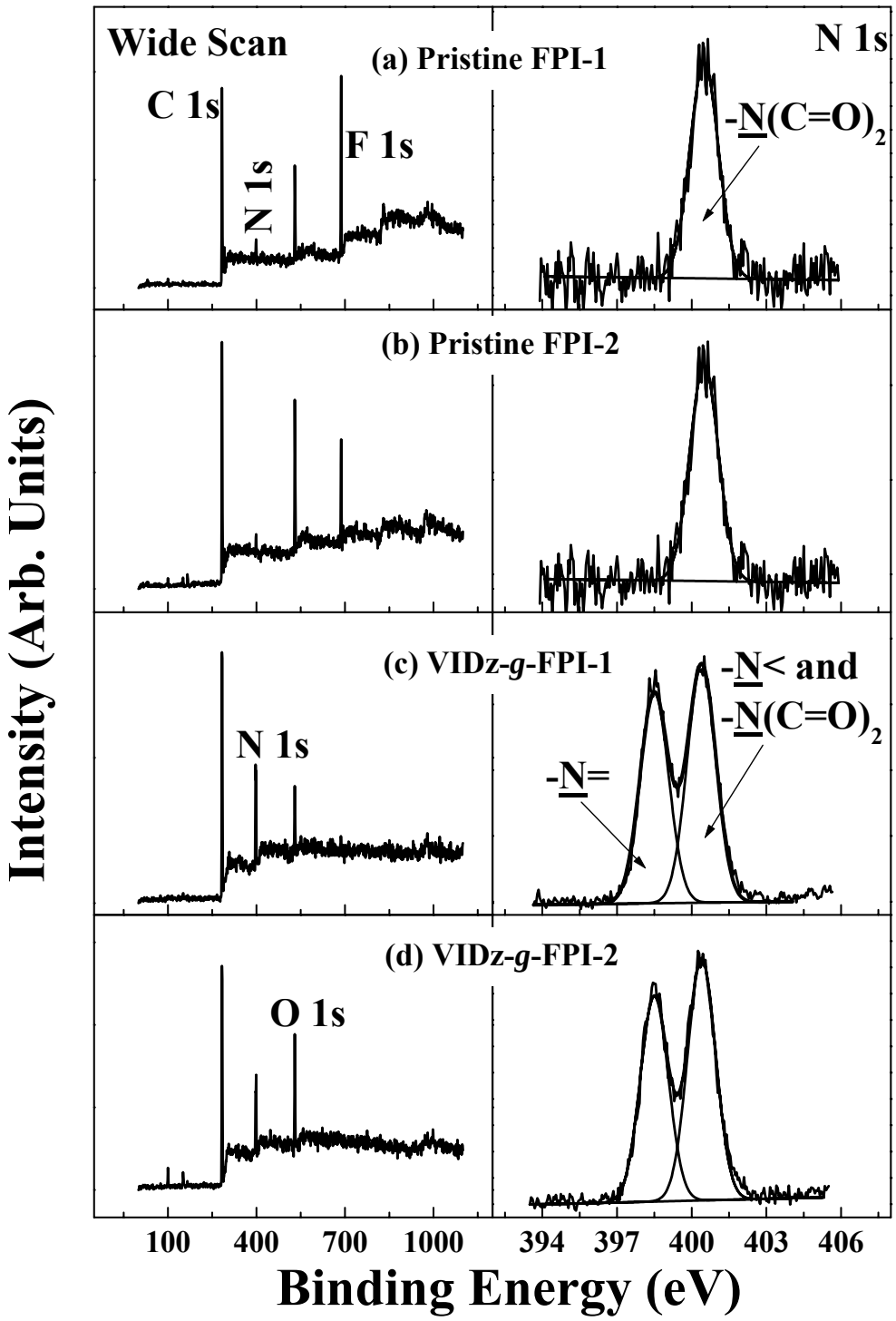

Figure 3.4 XPS wide scan and N 1s core-level spectra of (a) the pristine FPI-1 surface, (b) the pristine FPI-2 surface, (c) the 60 s Ar plasma-pretreated FPI-1 films after UV-induced graft copolymerization with VIDz for 60 min, and (d) the 60 s Ar plasma-pretreated FPI-2 films after UV-induced graft copolymerization with VIDz for 60 min.

The Ar plasma pretreatment time of the FPI surface affects the graft concentration, and thus the adhesion strength of the resulting Cu/FPI assemblies, as shown in Figure 3.5. The surface graft concentration is defined as the number of repeat units of the graft chain per repeat unit of the substrate chain. Thus, the surface graft concentrations are determined from the curve-fitted N 1s peak area ratios of the imine (-N=) and imide (-$\underline{N}(C=O)_2$) components, associated, respectively with the graft and the substrate polymers. The graft concentration is thus expressed as the $2[\text{-N=}]/[\text{-}\underline{N}(C=O)_2]_{PI}$ ratio. The factor 2 in the numerator is introduced to account for the fact that there are two functional –$\underline{N}(C=O)_2$ groups in every repeat unit of the PI molecule. The number of the –$\underline{N}(C=O)_2$ species contributed by the PI substrate is deduced from the N 1s spectrum by subtracting the peak area of the imine species –N= of the grafted VIDz polymer from the area of the peak component arising from the combined contribution of the -$\underline{N}(C=O)_2$ and –N< species, as each VIDz unit contains equal numbers of –N= and –N< species. Taking into account of the fact that the [O]/[C] ratio increases with the Ar plasma pretreatment time of the FPI film, the graft concentrations of the VIDz-*g*-FPI surfaces exhibit a similar dependence on the Ar plasma pretreatment time of the FPI films. The adhesion of the electrolessly deposited copper on the FPI substrate reaches about 9.5 N/cm at an Ar plasma pretreatment time of about 60 s and a fixed UV graft-copolymerization time of 60 min. This T-peel adhesion strength is much higher than that obtained for the electrolessly deposited copper on the pristine FPI film or the 60-s Ar plasma pretreated FPI film, which have T-peel adhesion strengths of only about 0.5 N/cm and 2 N/cm, respectively. Thus, the effective contribution of the grafted VIDz polymer to the adhesion enhancement of the electroless deposited copper onto the FPI films is ascertained. The electrolessly deposition of copper to the surface-

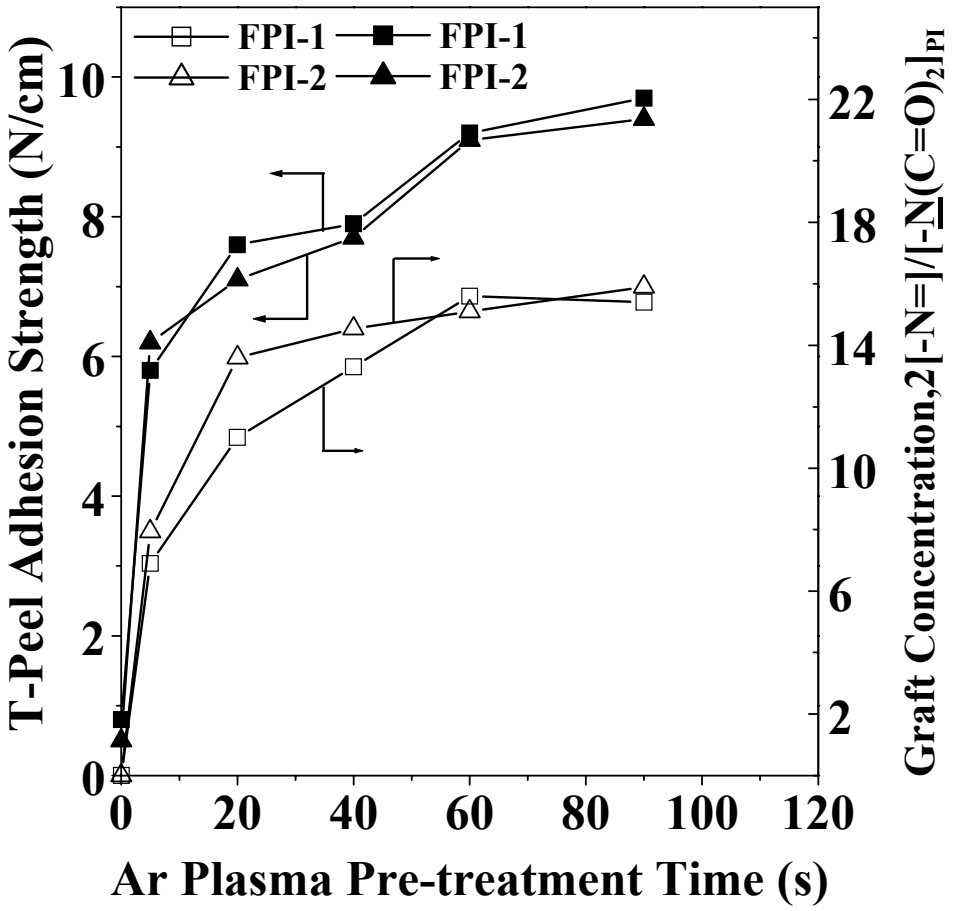

Figure 3.5 Effect of Ar plasma pretreatment time of the FPI film on the T-peel adhesion strength of the Cu/VIDz-*g*-FPI assemblies, and on the surface graft concentration of the VIDz polymer.

modified FPI surface can be carried out by the one-step, Sn-free process. On the other hand, however, electroless deposition of copper on the pristine or plasma pretreated FPI surface can only be carried out by the conventional "two-step" method. The tin chloride used in the two-step method is not an active catalyst for electroless plating (Da et al., 1991; Tan et al., 1993). It can also be observed in Figure 3.5 that the increase in adhesion strength coincides approximately with the increase in graft concentration for both types of the VIDz-*g*-FPI surfaces. The fact suggests that a graft chain-induced adhesion mechanism is operative. The adhesion of the electrolessly deposited copper to the graft-modified FPI surface can be described in terms of the microscopic interactions at the metal/graft polymer interface or interphase, and is related to the sum of all the intermolecular interactions (Pritchart, 1983). The imidazole rings of the grafted VIDz chains on the PI film undergo charge transfer and the formation of the coordinate complexes with the electrolessly deposited copper (Inagaki et al., 1996; Xue et al., 1988). The spatial distribution of the graft chains, and thus the imidazole rings, on the FPI film surface dictates the formation of an interphase consisting of an interpenetrating network of the graft chains in the metal matrix.

3.2.3 Electroless Deposition of Copper on FPI Films Modified by Surface Graft Copolymerization with 4VP: the Cu/4VP-*g*-FPI Assemblies

The respective wide scan and N 1s core-level spectra of the 60-s Ar plasma pretreated FPI-1 and FPI-2 films after having been subjected to UV-induced graft copolymerization with 4VP for 60 min (the 4VP-*g*-FPI surfaces) are shown in Figure 3.6. The presence of the grafted 4VP polymer on the FPI surface can be deduced from the N 1s peak component at the BE of 398.5 eV, attributed to the imino species (=<u>N</u>-) of the 4VP polymer (Zhang et al., 2001b). The highest BE peak component at about 400.5 eV is assigned to the $-\underline{N}(C=O)_2$ species of the FPI substrate (Zhang et al.,

2001b; Yang et al., 2001). An additional peak component appears at the BE of about 399.5 eV, which may be due to the partially protonation or the hydrogen bonding of the nitrogen in the 4VP polymer. The formation of hydrogen bonding between the pyridine ring and other polymers has been reported (Zhou et al., 1997; Ruokolainen et al., 1998; Huang et al., 2000). The presence of only a weak –N-$(C=O)_2$ component in the N 1s core-level spectra suggests that the thickness of the grafted 4VP polymer on both FPI films is approaching the probing depth of the XPS technique (about 7.5 nm for an organic matrix (Tan et al., 1993).

The dependence of the graft concentration and the T-peel adhesion strength of the electrolessly deposited copper with the corresponding 4VP-*g*-FPI film on the Ar-plasma pretreatment time of the FPI surface is shown in Figure 3.7. The concentration of the surface-grafted pp-4VP is expressed as the $2[(\text{-N=})+(\text{-N<})]/[\text{–N-(C=O)}_2\ ]_{PI}$ ratio, as each 4VP unit contains one –N= group. The increases in graft concentration and T-peel adhesion strength with the Ar-plasma pretreatment time is also observed in the present work. T-peel adhesion strength above 9 N/cm can be achieved for the electrolessly deposited copper with the 4VP-*g*-FPI substrate involving the 60-s Ar plasma pretreated FPI and 60 min of UV graft copolymerization time. The adhesion strengths are much higher than those of the assemblies involving the pristine FPI film and the FPI film with 60-s of Ar plasma pretreated alone, obtained from the two-step activation method. Thus, the effective contribution of the grafted 4VP polymer in improving the adhesion of FPI with electrolessly deposited copper is ascertained. In the case of the Cu/4VP-*g*-FPI assembly, the nitrogen atoms in the pyridine rings of the grafted 4VP polymer can interact with the electrolessly deposited copper to form the Cu-N bonds (Lyons et al., 1988), which accounts for the strong adhesion of the metal to the polymer substrate.

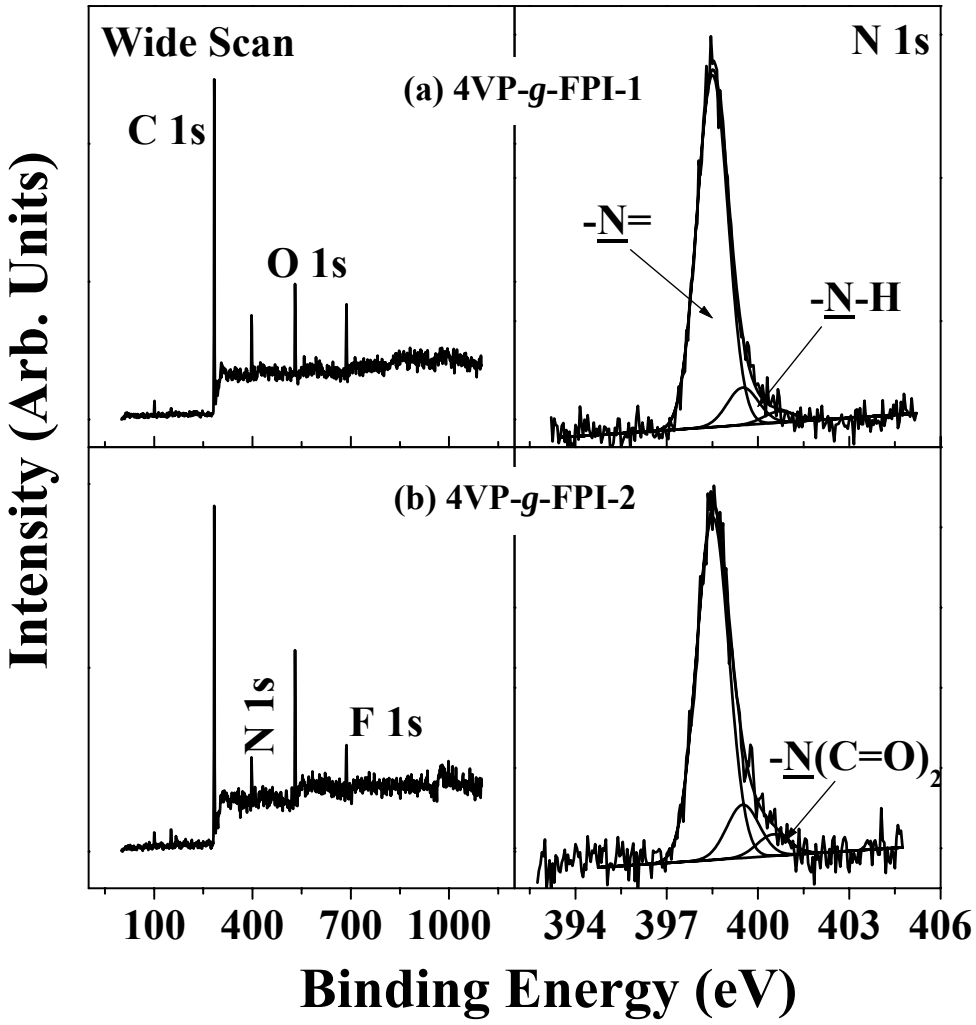

Figure 3.6 XPS wide scan and N 1s core-level spectra of (a) the 60 s Ar plasma pretreated FPI-1 films after UV-induced graft copolymerization with 4VP for 60 min, and (b) the 60 s Ar plasma pretreated FPI-2 films after UV-induced graft copolymerization with 4VP for 60 min.

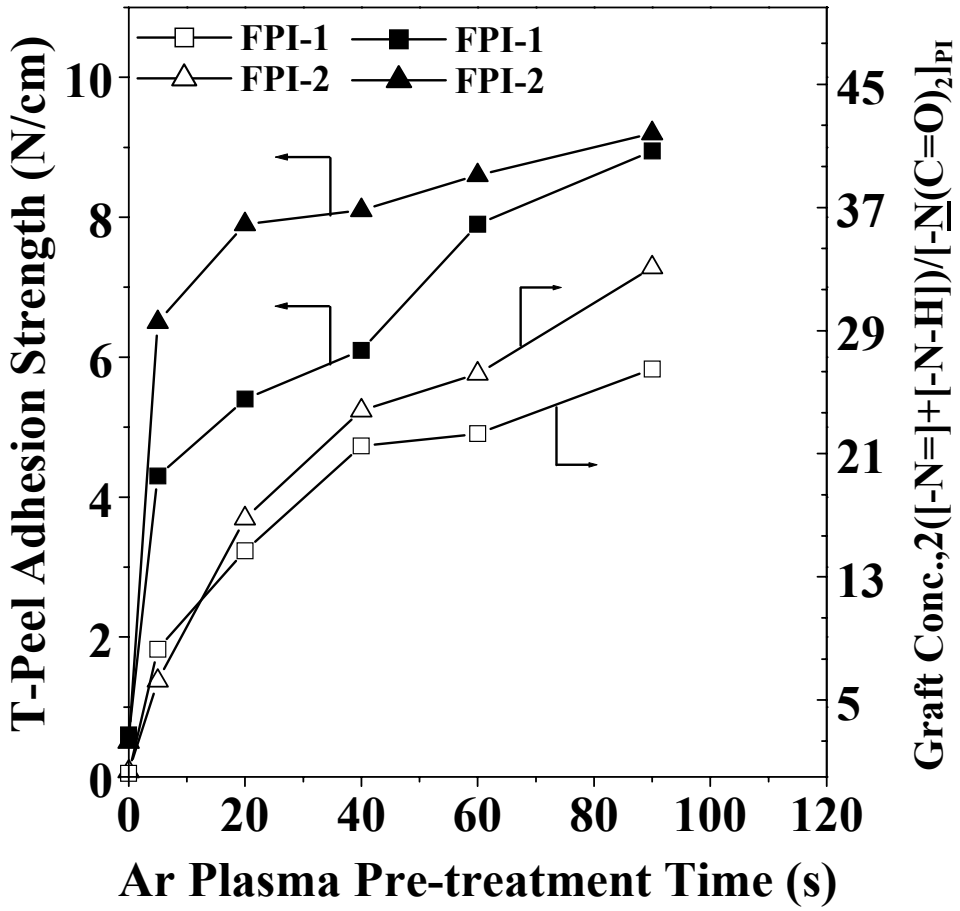

Figure 3.7 Effect of Ar plasma pretreatment time of the FPI film on the T-peel adhesion strength of the Cu/4VP-*g*-FPI assemblies, and on the surface graft concentration of the 4VP polymer.

3.2.4 Surface Topography of the Modified FPI Films

The changes in surface topography of the FPI films after modification by plasma pretreatment and by UV-induced graft copolymerization with VIDz and 4VP are studied by atomic force microscope (AFM). The AFM images of a pristine FPI-1 film surface, a 60 s Ar plasma pretreated FPI-1 surface, a VIDz-*g*-FPI-1 surface (graft concentration=15.6) and a 4VP-*g*-FPI-1 surface (graft concentration=22.3) are shown in Figures 3.8(a) to 3.8(d), respectively. The root mean square surface roughness value, R_a, of the pristine FPI-1 film surface is about 1.18 nm. Under the mild glow discharge conditions used for surface activation, the R_a value did not change appreciably after the Ar plasma pretreatment. The roughness of the 60-s Ar plasma pretreated FPI-1 surface is about 1.02 nm. However, the R_a values of the VIDz-*g*-FPI-1 and 4VP-*g*-FPI-1 film surfaces increase to about 2.7 nm and 7.1 nm, respectively. As shown in Figures 3.8(c) and 3.8(d), the graft-copolymerized VIDz or 4VP on the FPI-1 film surface exists as a distinctive overlayer. The rougher surface topography of the VIDz-*g*-FPI-1 and 4VP-*g*-FPI-1 films presumably will also facilitate the spatial interactions of the grafted VIDz or 4VP chains with the incoming metal atoms during the subsequent surface activation and electroless plating processes.

3.2.5 Failure Mode of the Electrolessly Deposited Copper on the Graft-modified FPI Films

In the investigation of metal/polymer adhesion, a study of the locus of failure is expected to be informative. In the present work, the failure mode of the Cu/FPI interfaces obtained from the electroless deposition of Cu onto the graft-modified FPI surfaces was investigated by analyzing the composition of the delaminated surfaces using XPS. Figure 3.9 shows the respective wide scan and C 1s core-level spectra of

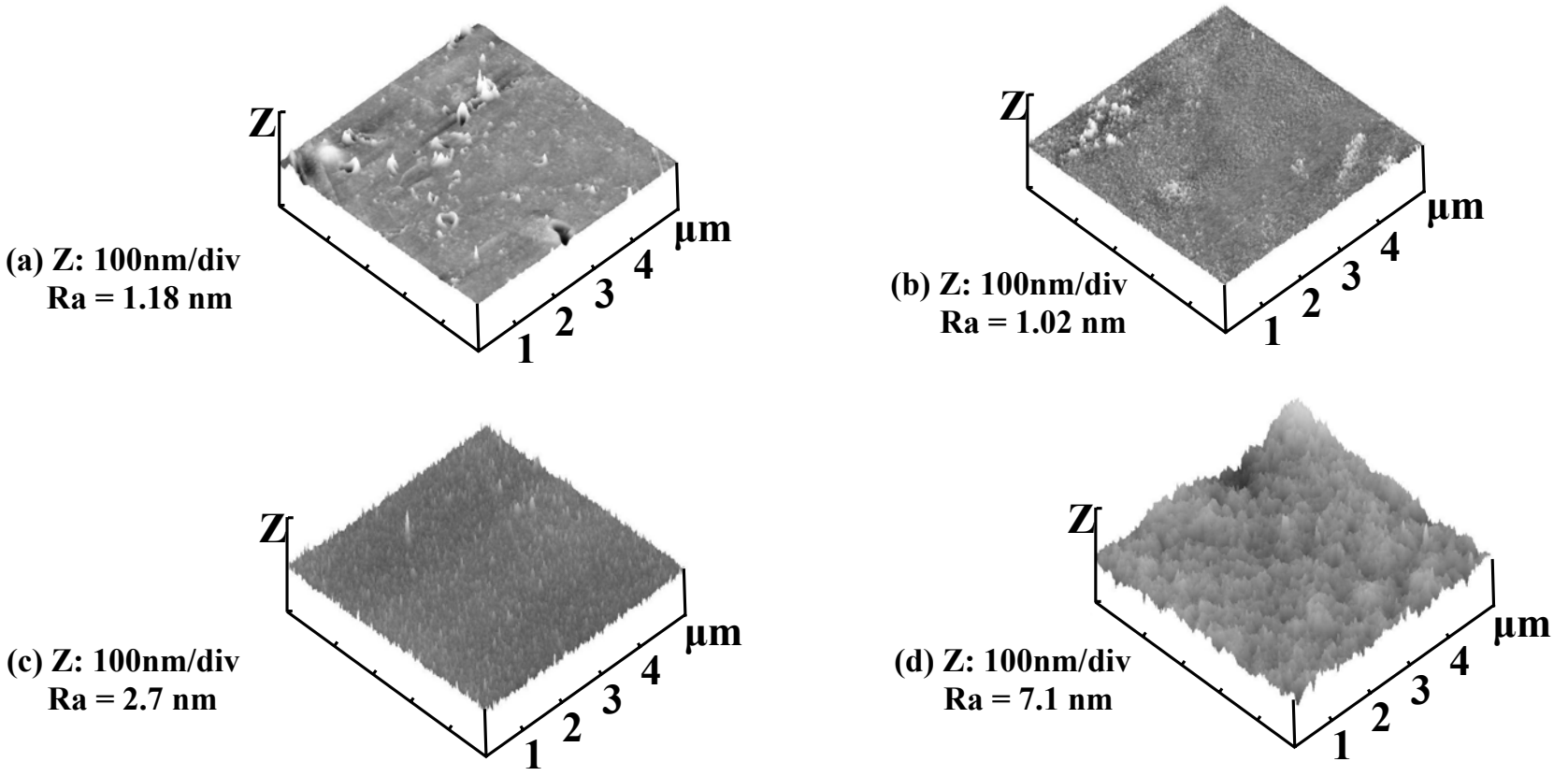

Figure 3.8 Atomic force microscope (AFM) images of (a) the pristine FPI-1 surface, (b) the 60 s Ar plasma pretreated FPI-1 surface, (c) the VIDz-*g*-FPI-1 surface(Ar plasma pretreatment time was 60 s, UV graft copolymerization time was 60 min), and (d) the 4VP-*g*-FPI-1 surface (Ar plasma pretreatment time was 60 s, UV graft copolymerization time was 60 min).

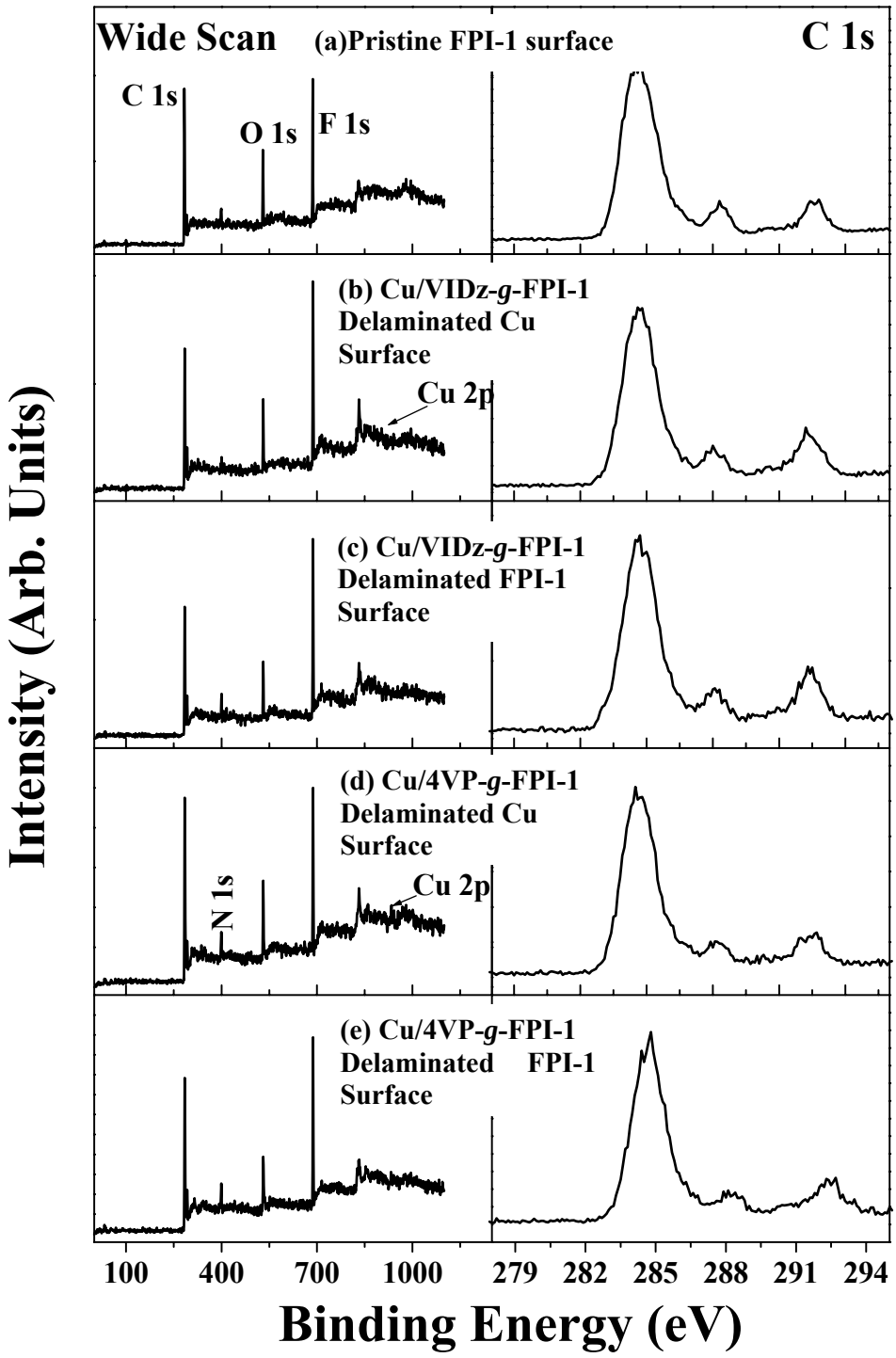

Figure 3.9 XPS wide scan and C 1s core-level spectra of (a) the pristine FPI-1 surface, the delaminated (b) Cu surface and (c) FPI-1 surface from a Cu/VIDz-*g*-FPI-1 assembly; the delaminated (d) Cu surface and (e) FPI-1 surface from a Cu/4VP-*g*-FPI-1 assembly. (The T-peel adhesion strengths for the two assemblies were 9.5 and 9.1 N/cm, respectively).

the pristine FPI-1 film (Figure 3.9(a)), and the delaminated FPI-1 film and Cu surface from a Cu/VIDz-*g*-FPI-1 assembly having a T-peel adhesion strength of 9.5 N/cm (Figures 3.9(b) and 3.9(c)). The wide scan spectra of the delaminated FPI-1 surface and Cu surface are grossly similar to that of the pristine FPI-1 film (Figure 3.9(a)). No Cu or Pd signal is detected in the wide scan spectrum of the delaminated FPI-1 surface, while a strong fluorine and nitrogen signal is observed in the delaminated copper surface. Furthermore, the respective C 1s core-level line shapes of the delaminated Cu and FPI-1 surfaces closely resemble that of the pristine FPI-1 film. These facts readily suggest that the assembly has delaminated by cohesive failure inside the FPI-1 substrate. On the other hand, a weak Cu 2p signal is discernible in the wide scan spectrum of the delaminated copper surface, suggesting that the failure locus in the FPI-1 film is slightly less than the probing depth of the XPS technique (~7.5 nm in an organic matrix (Tan et al., 1993).

The failure mode of the Cu/4VP-*g*-FPI-1 assembly having a T-peel adhesion strength of about 9.1 N/cm was also investigated by examining the chemical compositions of the delaminated FPI-1 and copper surfaces. Similar to the delamination results of the Cu/VIDz-*g*-FPI-1 assembly, the wide scan and C 1s core-level spectra of both delaminated surfaces (Figures 3.9(d) and 3.9(e)) are again grossly similar to that of the pristine FPI-1 surface. No Cu signal is discernible in the wide scan spectrum of the delaminated FPI-1 surface, while strong F 1s and N 1s signals are present in the wide scan spectrum of the delaminated Cu surface. Again, a weak Cu 2p peak component is also discernible in the wide scan spectrum of the delaminated copper surface. These results suggest that the Cu/4VP-*g*-FPI-1 assembly has failed cohesively inside the FPI-1 film, within a depth comparable to the probing depth of the XPS technique. A similar failure mode has been reported for the adhesion of the electrolessly deposited copper

onto the surface of the modified fluoropolymer film from remote hydrogen plasma treatment (Inagaki et al.,1999). The surface topography of the 4VP-*g*-FPI film (graft concentration=22.3) before and after electroless plating of copper, as well as that of the delaminated FPI and copper surface from the corresponding assembly, are shown in Figure 3.10. The R_a of the 4VP-*g*-FPI film surface is about 7.1 nm. The roughness of the surface after copper plating is about 25.6 nm. The result suggests that the electroless plated copper forms a uniform layer on the FPI surface. However, the R_a value of the delaminated FPI film and copper surface increases to about 280 nm and 250 nm, respectively, as shown in Figures 3.10(c) and 3.10(d). This result is consistent with the mechanism of cohesive failure inside the FPI substrate to result in the highly rough delaminated surfaces.

The distinct cohesive failure inside the FPI substrate testifies to the presence of strong interactions of the Pd catalyst and the electrolessly deposited copper atoms with the nitrogen moieties of the grafted VIDz or 4VP chains. The extents of these interactions are further augmented by the spatial distribution of the graft chains on the FPI surface and inside the copper matrix.

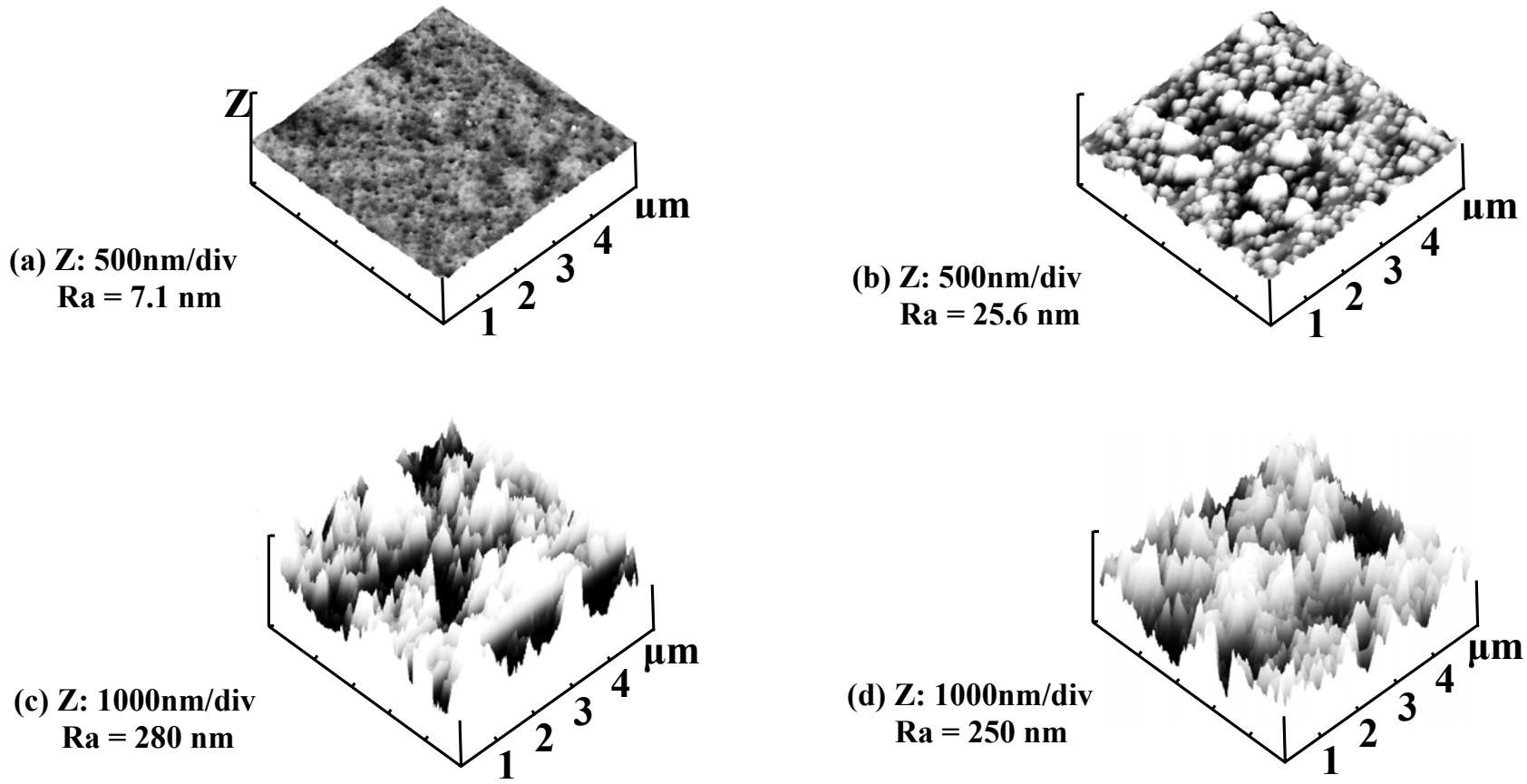

Figure 3.10 AFM images of the 4VP-g-FPI-1 (graft concentration=22.3) (a) before and (b) after the electroless plating of copper . The AFM images of the delaminated FPI-1 and copper surface are shown in (c) and (d) , respectively.

3.3 Conclusion

Surface modification of Ar plasma-pretreated FPI films was carried out *via* UV-induced graft copolymerization with 1-vinylimidazole (the VIDz-*g*-FPI surface) and 4-vinylpyridine (the 4VP-*g*-FPI surface) under atmospheric conditions and in the absence of an organic solvent. The VIDz-*g*-FPI and 4VP-*g*-FPI surfaces could be activated by $PdCl_2$ in a simple one-step, Sn-free process for the electroless deposition of copper. The surface composition of the graft-copolymerized FPI film was analyzed by XPS. In all cases, the adhesion strength between the electrolessly deposited copper and the surface-modified FPI film increased with the graft concentration. T-peel adhesion strength above 9 N/cm was obtained for the electrolessly deposited copper on the surface-modified FPI films. The adhesion strengths were much higher than that of the electrolessly deposited copper on the pristine, or the Ar plasma-pretreated FPI surfaces using the conventional "two-step" activation method. The mode of adhesion failure of the electrolessly deposited copper on the graft-modified FPI film was cohesive in nature. The good adhesion strength of the electrolessly deposited copper could be attributed to the synergistic effect of strong interaction between the grafted VIDz and 4VP polymer with the metal atoms, the spatial distribution of the graft chains into the metal matrix, and the fact that the graft chains were covalently tethered on the PI surface.

CHAPTER 4

ELECTROLESS PLATING OF COPPER ON PI AND FPI FILMS MODIFIED BY PLASMA GRAFT COPOLYMERIZATION OF 4-VINYLPYRIDINE

4.1 Electroless Plating of Copper on PI Films Modified by Plasma Graft Copolymerization with 4-Vinylpyridine

4.1.1 Experimental

4.1.1.1 Materials

The polyimide (PI) film used in this study was purchased from the Du Pont Chemical Co. as Kapton® HN in rolls of 40 mm in width and 75 μm in thickness. The surface of the PI films was cleaned with acetone immersing in an ultrasonic water bath for 20 min and then dried at 80°C under reduced pressure. The monomer, 4-vinylpyridine (4VP), used for surface graft copolymerization was obtained from the Aldrich Chemical Co. of Milwaukee, WI, USA. The chemical structure of PI (Kapton® HN) is as follows:

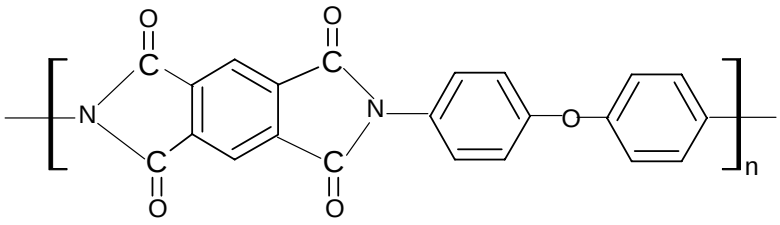

4.1.1.2 Plasma Graft Copolymerization of 4VP on PI Films: the pp-4VP-PI Films

The plasma polymerization system was manufactured by Samco International of Kyoto, Japan (Model Samco BP-1). The physical geometry of the system has been described previously (Yang et al., 2000). The radio-frequency (RF) generator supplied power from 0 to 200 W and was operated at a frequency of 13.56 MHz. The plasma deposition was performed between two circular parallel plate electrodes of 10 cm in diameter in a Pyrex® bell-jar chamber of about 6,000 cm^3 in volume. The PI samples were placed on the ground electrode, which was about 2.8 cm away from the biased

electrode. The 4VP monomer at 5ºC was introduced into the deposition chamber by the argon carrier gas flowing through a thermostated monomer reservoir. All the gas lines were thermally insulated. The monomer-carrier gas mixture was then allowed to flow evenly into the reactor from a distributor in the upper electrode. In all cases, the carrier gas stream was assumed to be saturated with the 4VP monomer, as dictated by the partial pressure of the latter. The system pressure was varied between 25 Pa and 200 Pa, while the gas flow rate was fixed at 20 standard cubic centimeter per min (sccm). For deposition on all the PI film surfaces, the plasma polymerization time was fixed at 60 s. Prior to the plasma polymerization and deposition, the PI substrates were pretreated or pre-activated by Ar plasma for 30 s at a RF power of 70 W, a system pressure of 100 Pa and an Ar flow rate of 20 sccm. The graft-modified surfaces were referred to as the pp-4VP-PI surfaces. Each pp-4VP-PI film was immersed in a large volume of ethanol at 40^{o}C with continuous stirring for at least 12 h to remove the residual monomer and homopolymer.

4.1.1.3 X-Ray Photoelectron Spectroscopy (XPS)

The surface composition of the samples was determined by XPS, the procedures were the same as those described in Section 3.1.9.

4.1.1.4 Fourier Transform Infrared (FTIR) Spectroscopy

Samples for FTIR spectroscopic measurements were obtained by direct plasma polymerization and deposition of 4VP on the surface of a freshly pressed KBr disc for about 5 min. The spectra were recorded on a Bio-Rad FTIR spectrophotometer (Model FTS135) under ambient conditions. Typically, 16 scans with a resolution of 8 cm^{-1} were accumulated to obtain one spectrum.

4.1.1.5 Atomic Force Microscopy (AFM)

The topography of the pp-4VP-PI surfaces were characterized on a Nanoscope IIIa atomic force microscope (AFM), as described in Section 3.1.10.

4.1.1.6 Electroless Deposition of Copper on the pp-4VP-PI Films

The graft-modified PI films were activated *via* immobilization of the Pd catalyst, in the absence of prior sensitization by $SnCl_2$ (the Sn-free process), for the electroless deposition of copper. The film was immersed in an aqueous solution containing 0.1 wt% $PdCl_2$ and 1.0 wt% HCl (12M) for 10 min, followed by rinsing thoroughly with doubly distilled water. The surface-activated PI film was then placed in an electroless copper plating bath for 15-30 min. The electroless deposition of copper usually commenced after about 10 min. The composition of the solution in the plating bath was the same as in Section 3.1.5. The copper-plated PI films were then rinsed thoroughly with copious amounts of doubly distilled water. The thickness of the electrolessly deposited copper was determined gravimetrically. Typically, a copper layer of about 1 μm was deposited.

4.1.1.7 Adhesion Strength Measurements

The adhesion strength of the electrolessly deposited copper with the PI substrates was determined by measuring the T-peel adhesion strength. The procedures of T-peel adhesion strength measurements were the same as those described in Section 3.1.11.

4.1.2 Results and Discussion

The processes of surface pretreatment, plasma graft copolymerization of 4VP on the PI surface (the pp-4VP-PI surface), and the subsequent electroless deposition of copper on the pp-4VP-PI surface are illustrated schematically in Figure 4.1. The details of each process are discussed below.

4.1.2.1 Effect of Ar Plasma Treatment on the Surface Composition of the PI Films

Figure 4.2 shows the respective wide scan and C 1s core-level spectra of the pristine PI film surface (Figure 4.2(a)) and the 20-s Ar plasma-treated PI films at the RF powers of 5 W (Figure 4.2(b)) and 120 W (Figure 4.2(c)), after air exposure. The C 1s core-level spectrum of the pristine PI film can be curved-fitted with four peak components, having binding energies (BE's) at 284.6 eV for the C-H species, at 285.6 eV for the CH-N and CH-C(O) species, at 286.4 eV for the C-O species, and at 288.5 eV for the $N(C{=}O)_2$ species (Zhang et al., 2001b; Moulder, 1992). Ar plasma treatment of PI film, followed by air exposure, resulted in the formation of two additional carbon species at the BEs of 287.5 eV and 289.3 eV. These two peak components are attributable, respectively, to the C=O species, which is different from the carbonyl structure of the imide group in the pyromellitic dianhydride chain, and to the carboxyl species, as shown in Figures 4.2(b) and 4.2(c). The presence of the carbonyl and carboxyl species on the plasma-treated PI surface is attributable to the oxidation in air of the active species on the PI surface induced by the argon plasma treatment. In agreement with the results reported in the literature (Zhang et al., 2001b; Yang et al., 2001), an increase in the [O]/[C] ratio is observed upon increasing the input RF power used for the treatment of the PI surface.

Step 1: Plasma Polymerization of 4VP on PI Substrate

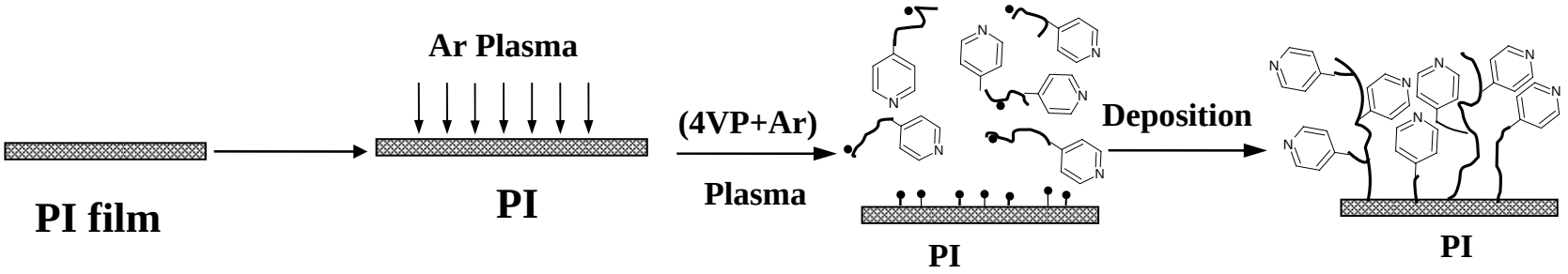

Step 2: Electroless Copper Plating onto 4VP Plasma-Polymerized PI Surface

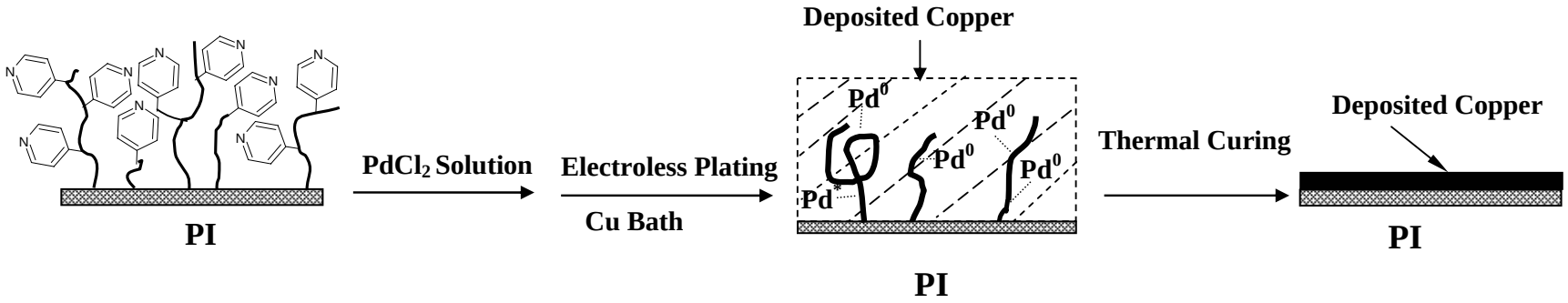

Figure 4.1 Schematic diagrams illustrating the processes of Ar plasma pretreatment, plasma polymerization and deposition of 4VP, and the electroless deposition of copper onto the 4VP plasma graft-copolymerized PI surface.

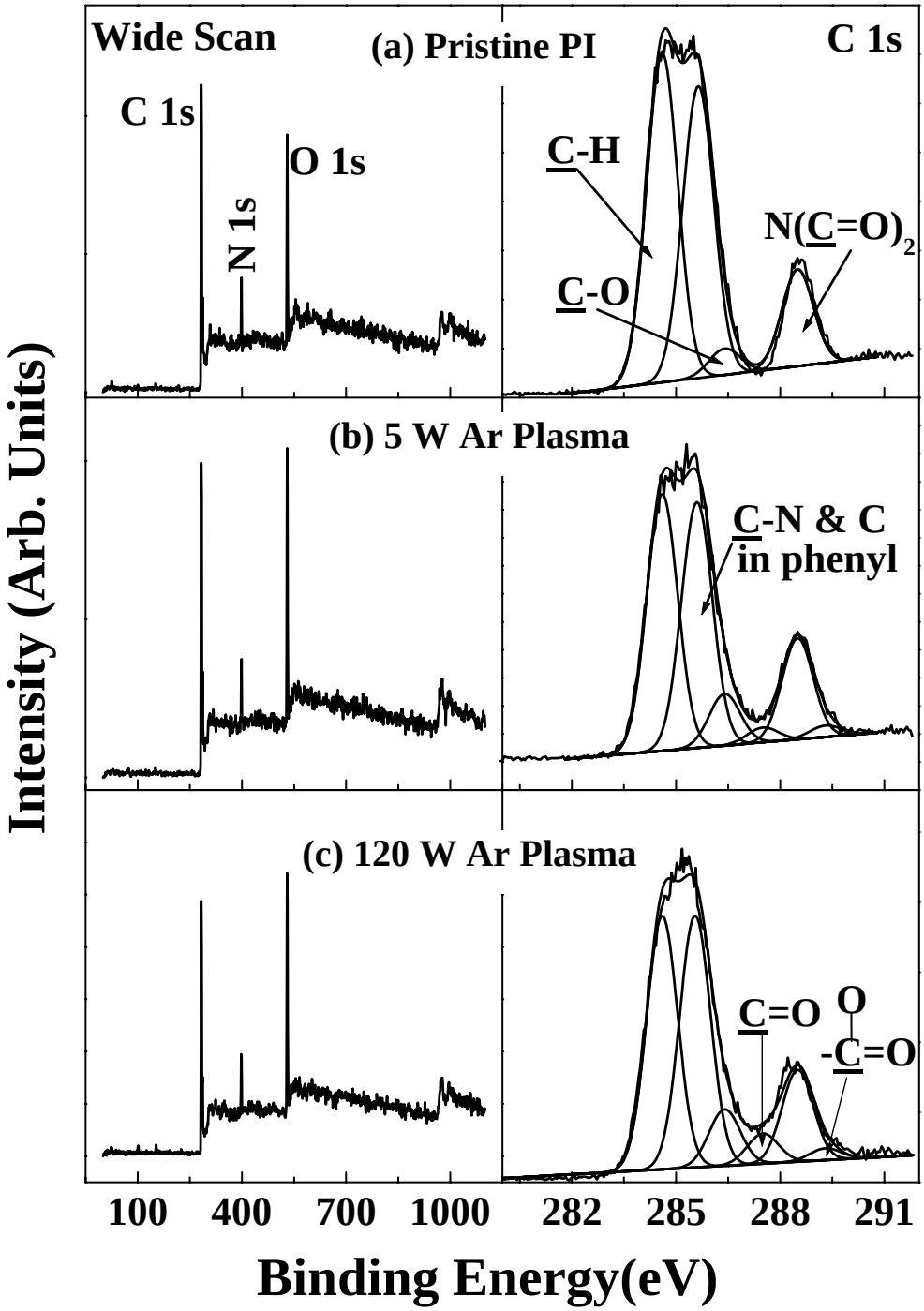

Figure 4.2 XPS wide scan and C 1s core-level spectra of (a) the pristine PI surface, and the PI surfaces after (b) 5 W and (c) 120 W of Ar plasma treatment for 30 s, followed by air exposure.

The increase in the oxygen concentration on the PI surface with the input RF power is consistent with the fact that a higher RF power will lead to the formation of more active species on the PI surface. This result is also in agreement with those commonly observed for other polymer surfaces after Ar plasma treatment and air exposure (Wu et al., 1999). For the plasma system used in this work and at a fixed treatment time of 30 s, the [O]/[C] ratio increases with the input RF power and reaches an asymptotic value at the input RF power of 70 W. Further increase in the RF power, however, does not result in the introduction of more oxygen-containing species, as the etching effect of the plasma treatment becomes predominant. Thus, the Ar plasma pretreatment of the PI films is fixed at 70 W for 30 s in the present study.

4.1.2.2 Structure and Composition of the 4VP Plasma Graft-Copolymerized PI Surfaces (the pp-4VP-PI Surfaces)

Figure 4.3 shows the respective FTIR spectra of the 4VP monomer (Figure 4.3(a)), and the plasma-polymerized 4VP on KBr discs at the RF powers of 5 W (Figure 4.3(b)) and 180 W (Figure 4.3(c)). For comparison purpose, the FTIR spectrum of the 4VP homopolymer is also shown in Figure 4.3(d). The 4VP monomer displays characteristic vibration absorption bands of the pyridine ring at the wavenumbers of 1410 cm^{-1} and 1597 cm^{-1} (Fochler et al.,1985). Thus, the pp-4VP layers deposited under the low and high RF powers (Figures 4.3(b) and 4.3(c), respectively) contain the same pyridine functional groups as that of the 4VP monomer, albeit the relative absorbance of the two adsorption bands varies somewhat with the RF power. For the FTIR spectra of the two pp-4VP samples, the absence of the $CH=CH_2$ out-of-plane bending absorptions at 1857 cm^{-1} and 927 cm^{-1}, the substantial decrease in the $CH=CH_2$ out-of-plane twisting absorption at 993 cm^{-1} and stretching

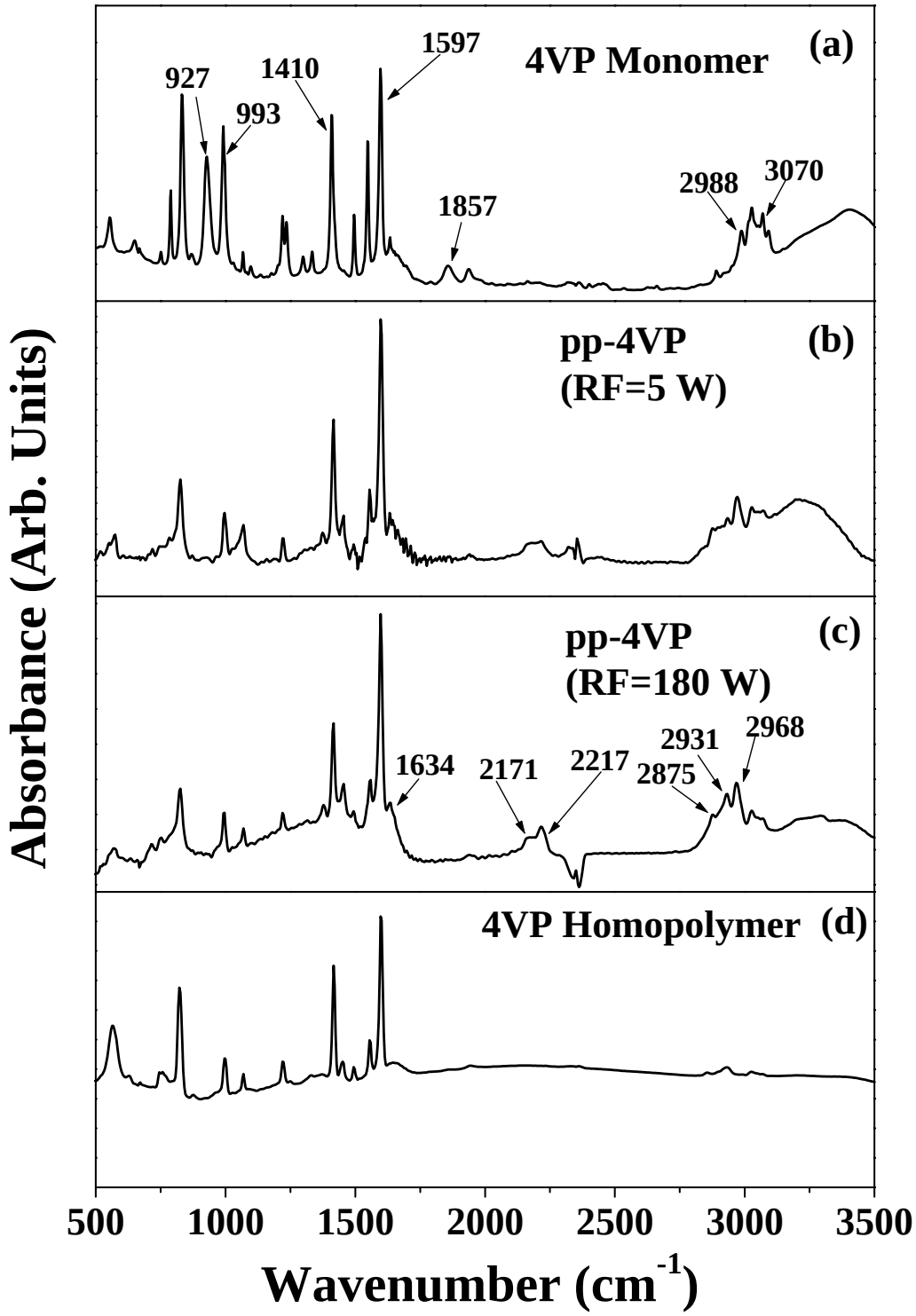

Figure 4.3 FTIR spectra of (a) the 4VP monomer, the pp-4VP films on KBr disc deposited at the input RF powers of (b) 5 W and (c) 180 W, and (d) the 4VP homopolymer.

absorptions at 3070 cm^{-1} and 2988 cm^{-1}, and the increase in $–CH_2$ stretching absorptions at 2931 cm^{-1} indicate that the plasma polymerization of 4VP has proceeded mainly through the vinyl group of the main chain (Lin et al., 1991). For the pp-4VP layer deposited at the high RF power of 180 W, the $–CH_3$ stretching absorption bands in the 2968 cm^{-1} and 2875 cm^{-1} region are also enhanced. The appearance of these absorption bands suggests that free methyl groups are formed in the plasma polymerization and are incorporated into the pp-4VP film. In addition, new minor bands at 2217 cm^{-1} (-C≡N group) and 2171 cm^{-1} (–N-C≡N group) (Ellaboud et al., 1996) are discernible, as shown in Figure 4.3(c). The appearance of these two species suggests that the pyridine groups of the pp-4VP film have partially undergone ring-opening reactions under the high RF power. The opening of the pyridine rings is further indicated by the reduction in 1410 cm^{-1} to 1597 cm^{-1} absorption band intensity ratio. It is also useful to compare the FTIR spectra of pp-4VP to that of the 4VP homopolymer. The FTIR spectrum of poly(4-vinylpyridine) (P4VP) (a commercial product of Polyscience Inc., Warrington, PA) is shown in Figure 4.3(d). The absorption bands at 2217 cm^{-1} (-C≡N group), 2171 cm^{-1} (–N-C≡N group) and 1634 cm^{-1} (non-ring -C=N groups) are not discernable, indicating that the polymerization of 4VP has proceeded mainly through the vinyl groups.

The pp-4VP-PI surfaces were also analyzed by XPS. As a reference, the wide scan and N 1s core-level spectrum of the pristine PI and the 4VP homopolymer are shown in Figure 4.4(a) and Figure 4.4(b), respectively. For the pristine PI surface, the N 1s core-level spectrum consists of a main peak component at the BE of about 400.5 eV, attributable to the-<u>N</u>-$(C=O)_2$ species. On the other hand, however, the N 1s core-level spectrum of the 4VP homopolymer consists of a main peak component at the BE of

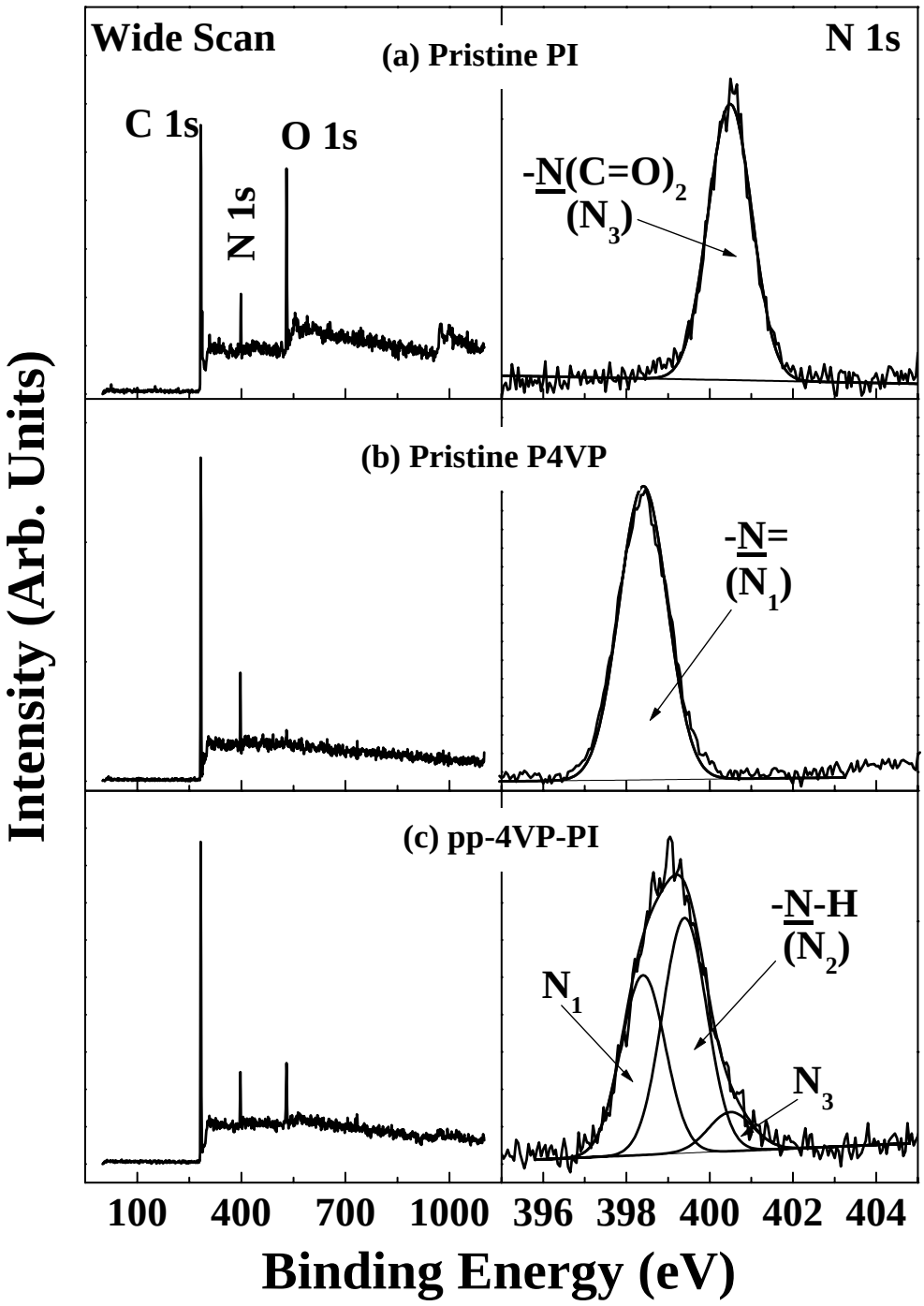

Figure 4.4 XPS wide scan and N 1s core-level spectra of (a) the pristine PI surfaces, (b) the pristine P4VP surface, and (c) the pp-4VP-PI surface prepared at the input RF power of 70 W.

398.4 eV, attributed to the –N= species. Figure 4.4(c) shows the wide scan and N 1s core-level spectra of the pp-4VP-PI film prepared at the input RF power of 70 W. Before plasma polymerization and deposition, the PI surface was pretreated by Ar plasma at 70 W for 30 s to introduce the active sites on the PI surface to enhance the interaction with the pp-4VP layer. The presence of the pp-4VP on the PI surface can be deduced from the appearance of the new peak components with the BE at about 398.4 eV and 399.4 eV, associated with the imine species (-N=) and the hydrogen-bonded imine species, respectively. The formation of hydrogen bonding between the pyridine ring and other polymers has been reported (Zhou et al., 1997; Ruokolainen et al., 1998). The presence of only a weak $–N-(C=O)_2$ component in the N 1s core-level spectrum and a weak O 1s signal in the wide scan of Figure 4.4(c) suggests that the thickness of the pp-4VP polymer is approaching the probing depth of the XPS technique (about 7.5 nm for an organic matrix (Tan et al., 1993)).

4.1.2.3 The Process of 4VP Plasma Polymerization and Deposition

The process of plasma polymerization is relatively complicated. The atomic polymerization mechanism appears to be a reasonable concept for plasma polymerization (Iriyama and Yasuda, 1992). Thus, plasma polymerization differs significantly from the conventional ionic or radical polymerization. To achieve the plasma state of atoms and molecules, appropriate ionization energy at a low pressure is required. The process of plasma polymerization includes the fragmentation of monomer molecules, the formation of active species (radicals or ions), the recombination of the active fragments between themselves and with the activated sites of the substrates to result in polymer grafting and deposition. The deposition process, nevertheless, is accompanied by other non-desirable side reactions, such as crosslinking and substrate ablation. For the application of the deposited film as an

adhesion promoter, for example, in microelectronics packaging, the retention of the functional group during the plasma polymerization process is the most important issue.

To preserve the pyridine functional groups in the plasma polymerized 4VP (pp-4VP) films, the polymerization should proceed *via* the activation of the carbon-carbon double bonds instead of the pyridine rings. Based on the FTIR and XPS results, a plausible mechanism of activation for the 4VP monomer during the deposition of pp-4VP films is illustrated schematically in Figure 4.5. The bond dissociation energies for the various linkages in organic molecules are listed in Table 4.1. Among them, the π bond of the C=C double bond has the lowest activation energy of about 267 kJ/mol (rough estimate from the difference between the dissociation energies of the C=C and C-C bonds). The two plausible reaction schemes, arising from different bond scission mechanisms, will give rise to the pp-4VP films of different chemical composition and structure. The bond scission mechanisms, in turn, are governed by the glow discharge conditions. At the low RF power, activation occurs mainly at the π bond of the vinyl group, as the π bond has the lowest bond energy. Under this condition molecular arrangement of the activated species results predominantly in a plasma polymer, which has similar chain structure as that of the 4VP homopolymer (Reaction Scheme I, Figure 4.5). With the increase in RF power, the 4VP plasma contains more active species and radicals, which come from the excitation of the carbon-carbon π-bonds, as well as the C-H bond scission and the pyridine ring-opening (Reaction Scheme II, Figure 4.5). Reactions involving the various active species and excited states result in a deposited pp-4VP film which is structurally more disordered. Thus, it is possible to achieve an optimum processing condition, by controlling the energy and concentration of the radical species and activated gaseous molecules, for the preparation of pp-4VP film that retains a high proportion of the pyridine functional group.

Reaction Scheme I - Under Low Input RF Power:

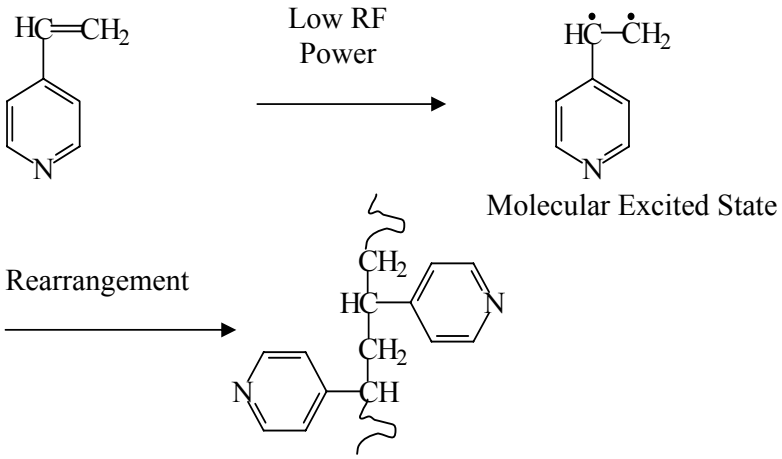

Reaction Scheme II - Under High Input RF Power:

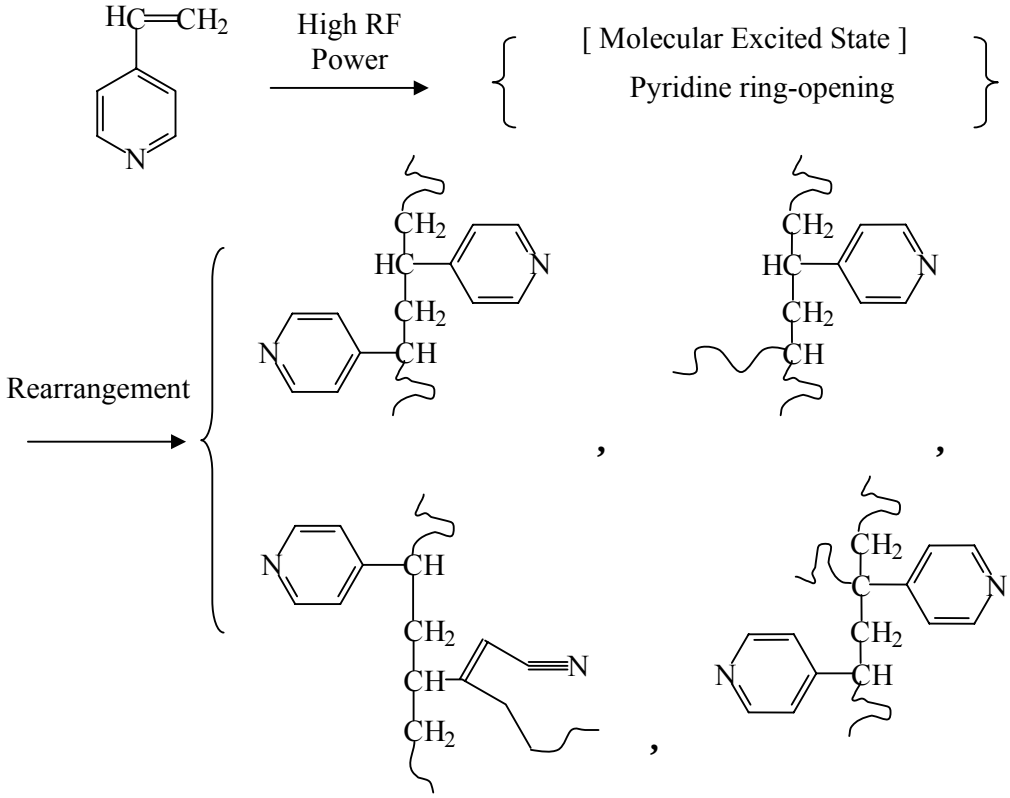

Figure 4.5 The plausible processes of molecular rearrangement of the activated 4VP molecules and radicals during the 4VP plasma polymerization process.

Table 4.1 Bond Dissociation Energies for Some Covalent Bonds

Bond	π bond of C=C	C-C	C-H	C-N	C=N
Bond Energy (kJ/mol)	267	351	414	305	614

4.1.2.4 Effect of Plasma Parameters on the Chemical Composition of the pp-4VP-PI Surfaces

It is well known that the operating conditions, such as the type of monomer, flow rate, system pressure, and RF power, affect the nature of plasma and the plasma-deposited polymer (Yasuda and Hirotsu, 1978; Yang et al,2000). Figure 4.6 shows the concentration of the grafted pp-4VP on PI surface as a function of two plasma variables. The concentration of the grafted pp-4VP is defined as the number of repeat units of the graft chain per repeat unit of the substrate chain. Thus, the surface concentration of the grafted material is determined from the N 1s peak component area ratios of the imine (-N=), the hydrogen-bonded imine, and the [-N-$(C=O)_2$] species. The first two components are associated with the pp-4VP layer, while the last component with the PI substrate. The three N 1s peak components are denoted as N_1, N_2 and N_3, respectively. The concentration of the surface-grafted pp-4VP is thus expressed as the $2[N_1+N_2]/[N_3]$ ratio. The factor 2 in the numerator is introduced to account for the fact that there are two functional [-N-$(C=O)_2$] groups in every repeat unit of the PI molecule.

Figure 4.6(a) shows the dependence of the 4VP polymer graft concentration of the pp-4VP-PI surface on the input RF power. The 4VP plasma polymerization and deposition were carried out on the 70 W Ar-plasma pretreated PI surfaces at a fixed Ar carrier gas flow rate of 20 sccm, a system pressure of 100 Pa, and a monomer

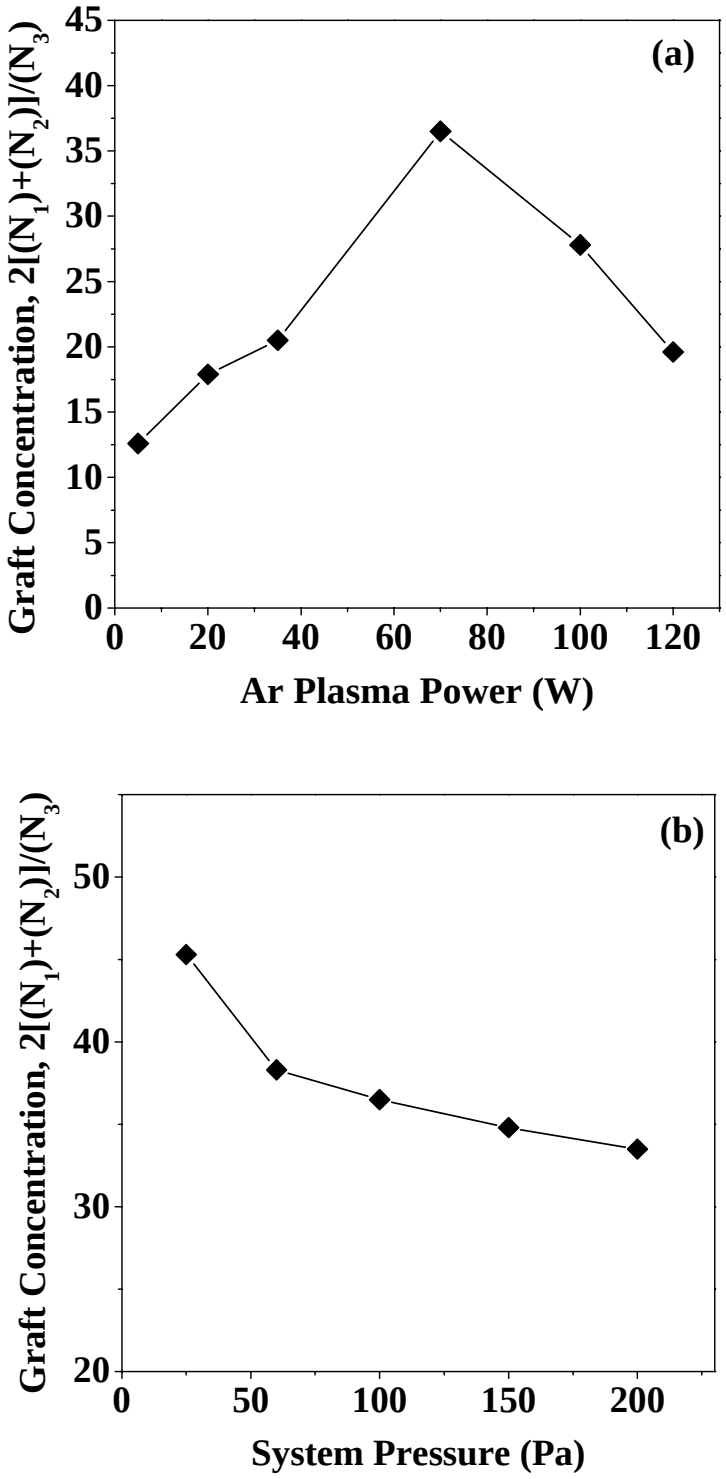

Figure 4.6 The dependence of the graft concentration of the pp-4VP-PI films on the plasma (a) input RF power; and (b) system pressure.

temperature of 5 ºC. The graft concentration of the pp-4VP-PI surfaces increases with the input RF power up to the RF power of about 70 W, above which the graft yield tends to decrease gradually. The variations in graft concentration of the pp-4VP-PI surface with the plasma power are attributable to the difference in bond scission mechanism in the plasma polymerization process. A popular controlling parameter, or the W/FM ratio, where W, F, and M are the input RF power, the monomer molar flow rate, and the molecular weight of the monomer, respectively, proposed by Yasuda and Hirotsu (Yasuda and Hirotsu, 1978), has been widely used to correlate the characteristics of the plasma and the deposited films. Taking into account the W/FM parameter, different input RF power will give rise to different energy per 4VP unit. As the input RF power is increased, the plasma polymerization is transformed from an energy-deficient state to a more energetic state. More energy per unit mass of the monomer is available at the high RF power, leading to the generation of more active species and to an increase in the deposition rate of the pp-4VP layer. As a result, the graft concentration increases with the increasing of the input RF power. On the other hand, however, further increase in the input RF power will result in the more extensive fragmentation of the 4VP molecules, as well as in the more extensive etching of the PI surface. Under these conditions, the efficiency of the pp-4VP deposition on the PI substrate is reduced.

The dependence of the 4VP polymer graft concentration of the pp-4VP-PI surface on the system pressure is shown in Figure 4.6(b). The 4VP plasma polymerizations were carried out on an Ar-plasma pretreated PI surface at an input RF power of 70 W, an Ar carrier gas flow rate of 20 sccm, and a monomer temperature of 5 ºC. The graft concentration of the 4VP polymer on the pp-4VP-PI surface decreases with the increase in system pressure. The increase in system pressure, as regulated by the

throttle valve, results in an increase in monomer concentration (partial vapor pressure) in the plasma chamber, and is equivalent to an increase in flow rate (F) of the monomer. Taking into account of the W/FM ratio, the energy per unit mass of the monomer molecules decreases with the increase in system pressure. The decrease in energy per unit mass of the 4VP molecules results in a decrease in the polymerization and deposition rate, leading to a decrease in the surface graft concentration of the 4VP polymer.

4.1.2.5 Surface Topography of the pp-4VP-PI Film

The surface topography of the plasma deposited polymer films is strongly dependent on the glow discharge conditions. The changes in surface topography of the PI substrates after modification by plasma graft copolymerization with 4VP are studied by atomic force microscopy (AFM). Figure 4.7 shows the AFM images of the pristine PI (Figure 4.7(a)) and the pp-4VP-PI surfaces prepared under the RF power of 5 W (Figure 4.7(b)) and 70 W (Figure 4.7(c)). The pp-4VP is deposited as a uniform layer over the entire PI surface, confirming the advantage of surface modification by plasma polymerization. The root mean square surface roughness (R_a) of the pristine PI surface is about 1.5 nm [Figure 4.7(a)]. The deposited pp-4VP layer gives rise to a rougher PI surface. For the pp-4VP-PI surface prepared at a lower RF power, the R_a value increases slightly to about 1.9 nm [Figure 4.7(b)]. However, for the pp-4VP-PI surface prepared at high RF power, the roughness is increased substantially to about 7.2 nm [Figure 4.7(c)]. The increase in surface roughness probably arises from the aggregation of the grafted 4VP polymer chains on the PI surface due to the limited miscibility of the graft and the substrate chains at the surface. The rougher surface topography of the modified PI surface facilitates the interlocking with the eletrolessly deposited copper.

(a) Pristine PI
Z: 50nm/div
Ra = 1.5 nm

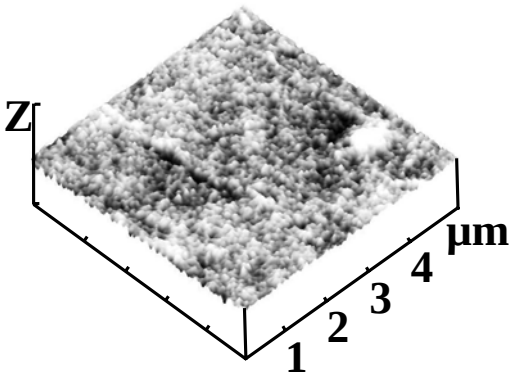

(b) pp-4VP-PI
Z: 50nm/div
Ra = 1.9 nm

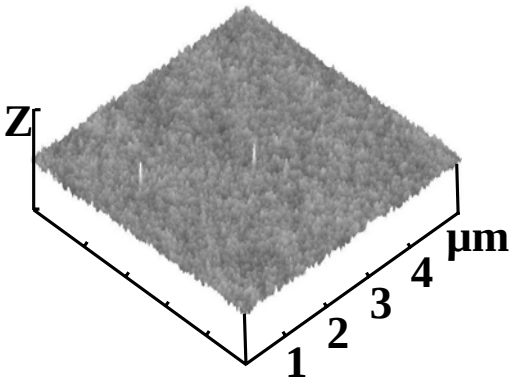

(c) pp-4VP-PI
Z: 100nm/div
Ra = 7.2 nm

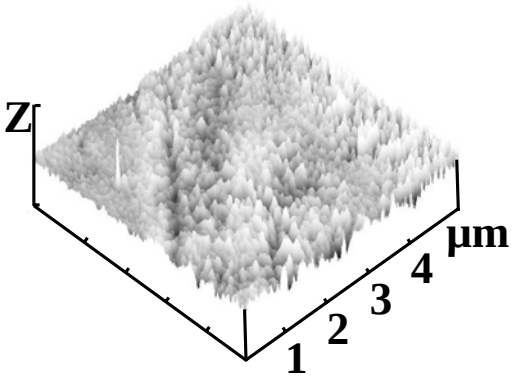

Figure 4.7 AFM images of (a) the pristine PI surface, and the pp-4VP-PI surfaces prepared at the RF powers of (b) 5 W and (c) 70 W.

4.1.2.6 Adhesion Strength of the Electrolessly Deposited Copper with the pp-4VP-PI Films

The adhesion of the electrolessly deposited copper to the PI surface is the primary concern in the preparation of the Cu/PI systems. The adhesion of the electrolessly deposited copper to the various PI substrates was evaluated by measuring the T-peel adhesion strength. The Pd in the Pd^{o} state has been considered as the catalyst for the electroless metal deposition process. In this study, the pp-4VP-PI surfaces were activated either *via* the Sn-free process or *via* the conventional two-step process. In the "two-step" method, the polymer surface was first sensitized by $SnCl_2$, then activated in the $PdCl_2$ solution. $SnCl_2$ is the reducing agent that supplies electrons for the reduction of Pd^{2+} to Pd metal. On the other hand, however, during the Sn-free activation process, the palladium catalyst is attached on the pp-4VP-PI surface as a Pd-N complex (Pd* in Figure 4.1). The formation of the Pd-N complex has been described earlier (Zhang et al., 2001b; Charbonnier et al., 1996). A [Pd]/[N] ratio in the range of 0.25 to 0.4 is obtained for the pp-4VP-PI surface. The results of adhesion strength are shown in Table 4.2. For comparison purpose, the electroless copper deposition was also carried out, *via* the "two-step" activation process, on the pristine, as well as on the 5 W and 70 W Ar plasma-treated PI surfaces. Electroless copper deposition cannot be carried out *via* the Sn-free process on these surfaces. It can be observed from Table 4.2 that, regardless of the activation method used, the adhesion strength of the electrolessly deposited copper to the graft-modified PI surface is always much higher than that of the electrolessly deposited copper to the pristine PI film or the Ar plasma-treated PI film. An adhesion strength as high as 6.8 N/cm can be achieved for the electrolessly deposited copper to the pp-4VP-PI surface using the Sn-free activation method. This adhesion strength represents about 13.4-fold, 3.2-fold and 2.6-fold increases, respectively, over those of the assemblies involving the pristine, the 5 W and the 70 W

Ar plasma-treated PI surfaces obtained from the two-step activation method. Thus, the effective contribution of the deposited pp-4VP polymer in simplifying the electroless deposition and in improving the adhesion of the electrolessly deposited copper to the PI film is ascertained.

Table 4.2 Effect of Surface Modification of PI Film on the Adhesion of the Electrolessly Deposited Copper

Surface Treatment of PI Film	Activation Method	T-Peel Adhesion Strength (N/cm)
Pristine PI Film	Two-step Process[a]	0.5
Ar Plasma treatment at 5 W[c]	Two-step Process	2.1
Ar Plasma treatment at 70 W[c]	Two-step Process	2.6
pp-4VP-PI deposited at the RF power of 70W[d]	Two-step Process	7.8
pp-4VP-PI deposited at the RF power of 70W[d]	Sn-free Process[b]	6.8

[a.] Sensitization in $SnCl_2$ solution for 2 min, followed by activation in $PdCl_2$ for 10 min.
[b.] Direct activation in $PdCl_2$ solution for 10 min.
[c.] Ar plasma treatment time = 30 s.
[d.] Plasma pretreatment of the PI film at 70 W for 30 s, monomer temperature = 5°C.

The adhesion strength of the electrolessly deposited copper with the pp-4VP-PI surface activated by the one-step process is somewhat lower than that of the electrolessly deposited copper with the corresponding pp-4VP-PI surface activated by the two-step process. This phenomenon can be attributed to the difference in the electroless metal deposition time required to achieve the same metal thickness in both processes. The electroless metallization on the pp-4VP-PI surface activated by the Sn-free process was carried out in the copper plating bath for about 30 min to obtain the desirable

thickness of the metal film (about 100 nm in thickness, as determined gravimetrically). However, only about 5 min are required to achieve the similar film thickness on the pp-4VP-PI surface activated by the two-step process. The difference in deposition times could be explained by the long incubation period required for the initiating of the copper deposition in the one-step process. Longer immersion time in the alkaline plating bath probably will give rise to the formation of a weak boundary layer in the PI film (Vorobyoba et al., 1997), which, in turn, will lower the adhesion strength with the electrolessly deposited copper. Nevertheless, the two-step activation process involving $SnCl_2$ is comparatively more complicated.

The adhesion strength of the electrolessly deposited copper with the graft-modified PI surface can be described in terms of the microscopic interactions between the copper atoms and the pp-4VP chains at the metal/pp-4VP interface and in the metal matrix. The spatial distribution of the graft chains, and thus the pyridine rings, on the PI film surface, as well as the formation of the Pd-N complex, dictate the formation of an interphase consisting of an interpenetrating network of the grafted chains in the copper matrix or layer. For the copper metallized pp-4VP-PI surface, the nitrogen atom in the pyridine rings of the pp-4VP-PI surface can interact directly with the copper atoms to form the Cu-N bonds (Charbonnier et al., 1996), which accounts in part for the enhanced adhesion of the metal to the PI surface.

The input RF power during the plasma polymerization affects the thickness of the 4VP polymer deposit on the PI surface (see Figure 4.6(a)). The graft concentration, in turn, affects the adhesion strength of the electrolessly deposited copper to the graft-modified PI surface. Figure 4.8 shows this dependence versus the input RF power used for the graft copolymerization. It can be observed that both the adhesion strength and the graft

concentration (see Figure 4.6(a)) of the 4VP polymer increase with the RF power up to about 70 W and then decrease gradually. The variation in adhesion strength coincides approximately with the variation in graft concentration of the pp-4VP-PI film. The phenomenon further testifies to the fact that a graft chain-induced adhesion mechanism is operative.

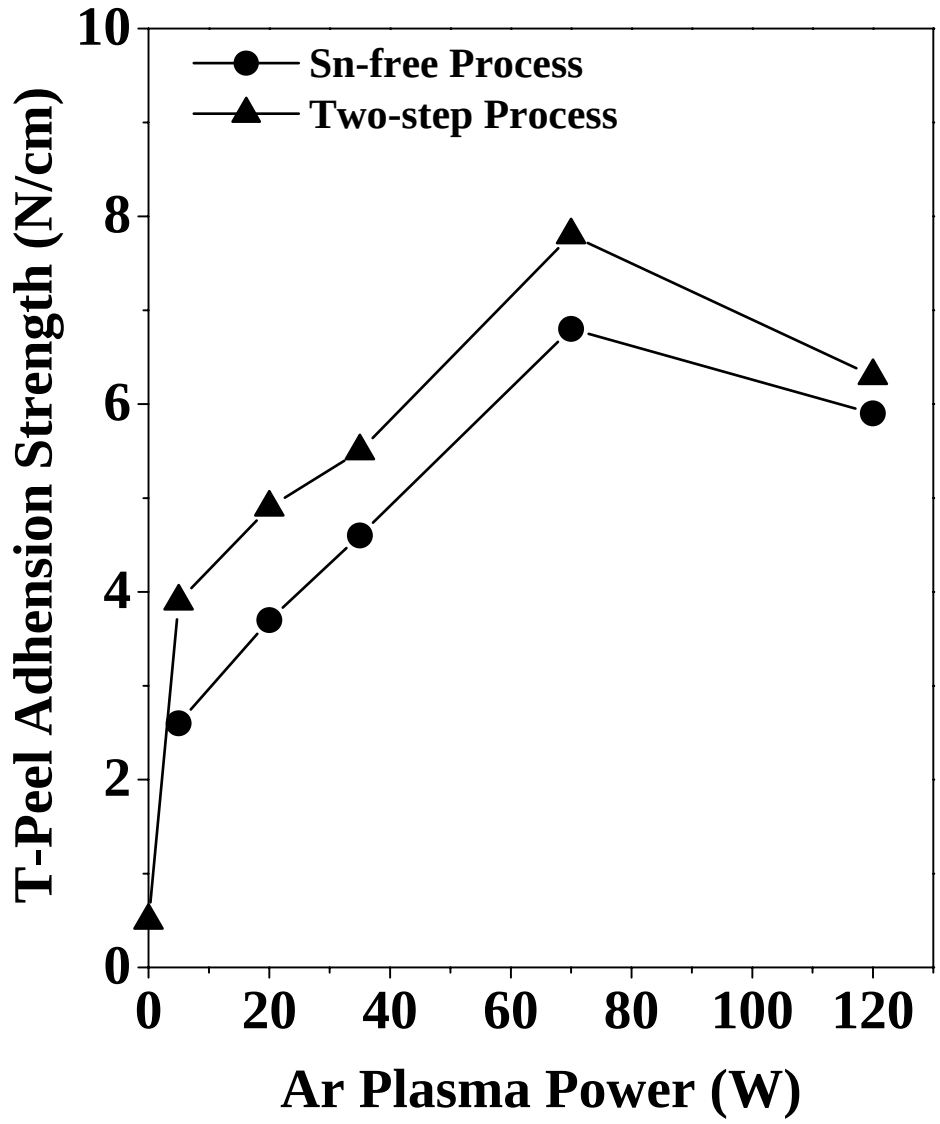

Figure 4.8 Effect of the input RF power on the T-peel adhesion strength of the electrolessly deposited copper with the pp-4VP-PI surface.

4.1.2.6 Adhesion Failure Mode of the Electrolessly Deposited Copper with the pp-4VP-PI Films

In the investigation of metal/polymer adhesion, a study of the locus of failure is expected to be informative. In the present work, the locus of the adhesion failure of the electroless deposited copper with the pp-4VP-PI films was investigated by analyzing the composition of the delaminated surfaces using XPS. As a reference, the wide scan, C 1s and N 1s core-level spectra of the pristine P4VP homopolymer surface are shown in Figure 4.9 (a). Figure 4.9 also shows the wide scan, C 1s and N 1s core-level spectra of the delaminated PI film side (part(b)) and the Cu surface side (part(c)) from an assembly involving the electrolessly deposited copper on the pp-4VP-PI film and having a T-peel adhesion strength of about 7 N/cm. The compositions of the opposite part of the Cu/pp-4VP-PI assembly differ from one another. The N 1s core-level spectrum of the delaminated PI and Cu surfaces can be curved-fitted with three peak components, having BEs at 398.4 eV for the –N= species, at 399.4 eV for the hydrogen-bonded imine species, and at 400.5 eV for the –N-$(C=O)_2$ species. The –N-$(C=O)_2$ species is the dominant component in the N 1s core-level spectrum of the delaminated PI surface. On the other hand, however, the –N= species and the hydrogen-bonded imine species are the major components in the N 1s core-level spectrum of the delaminated Cu surface. No Cu or Pd signal is discernible in the wide scan spectrum of the delaminated PI surface. Furthermore, the –N-$(C=O)_2$ peak component is rather prominent in the C 1s core-level spectrum of the delaminated PI surface. The peak intensity of the -N-$(C=O)_2$ component, however, is substantially reduced in the C 1s core-level spectrum of the delaminated Cu surface. These observations readily suggest that the Cu/pp-4VP-PI assembly has failed in a mixed mode at the pp-4VP and the PI interface. In addition, the presence of copper signals in

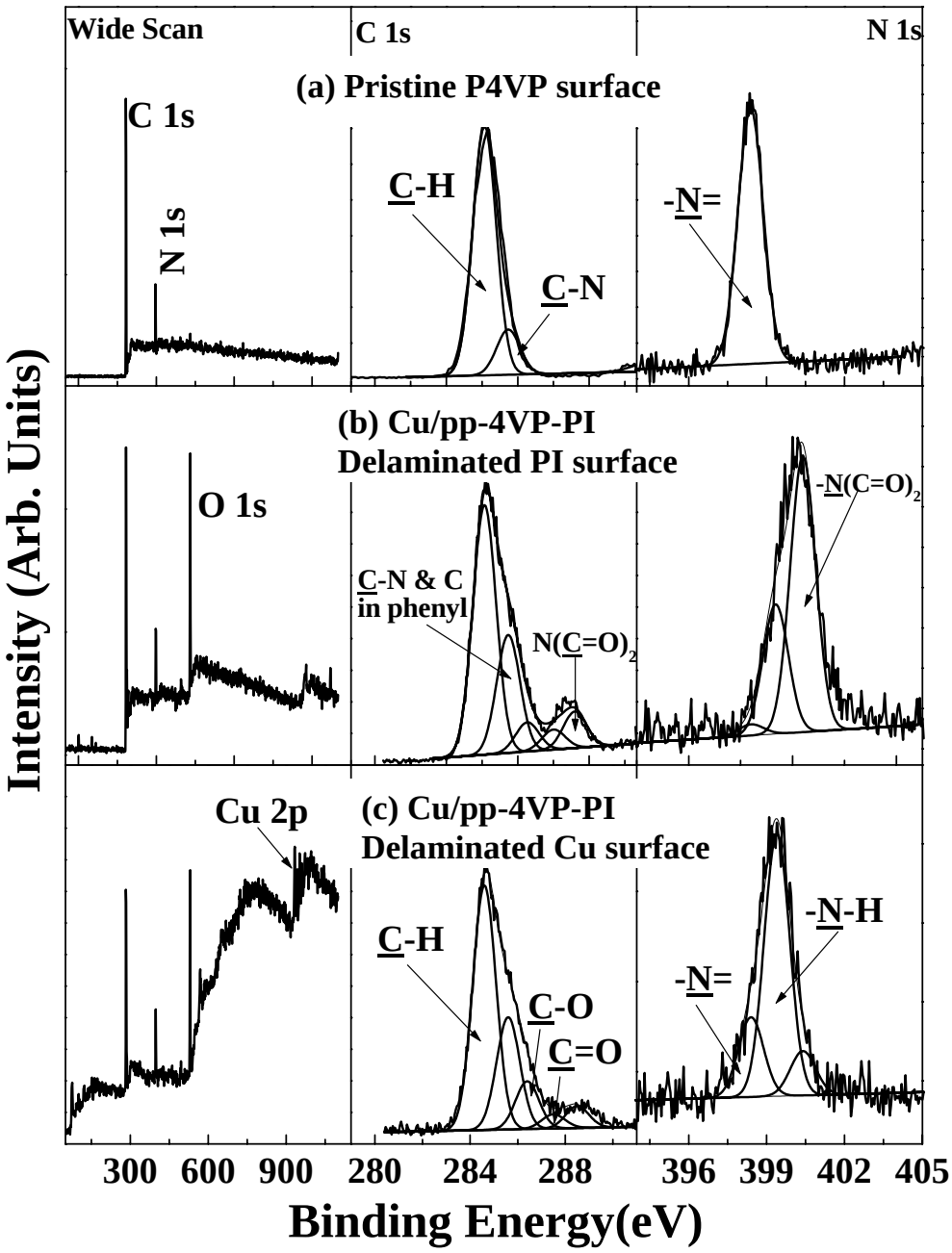

Figure 4.9 XPS wide scan, C 1s and N 1s core-level spectra of (a) the pristine P4VP surface, and the delaminated (b) PI and (c) Cu surfaces from a Cu/pp-4VP-PI assembly having a T-peel adhesion strength of about 7 N/cm.

the wide scan spectrum of the delaminated Cu surface suggests that the failure locus above the copper surface is slightly less than the probing depth of the XPS technique (~7.5 nm in an organic matrix).

4.1.3 Conclusion

Thin 4-vinylpyridine (4VP) polymer films were deposited, *via* plasma graft polymerization of 4VP, on the Ar plasma pretreated PI film surfaces. XPS and FTIR results revealed that the pyridine functional groups of the plasma-polymerized 4VP (pp-4VP) could be retained to a large extent under proper glow discharge conditions. The grafted pp-4VP layer on the PI surface was used not only as chemisorption sites for the palladium complex during the Sn-free activation process, but also as an adhesion promotion layer for the electrolessly deposited copper on the PI surface (the Cu/pp-4VP-PI assembly). The T-peel adhesion strength between the electrolessly deposited copper and the pp-4VP-PI surface could reach about 7 N/cm. This adhesion strength was much higher than that of the electrolessly deposited copper on the pristine and the Ar plasma-treated PI surfaces using the conventional "two-step" activation method. The strong adhesion of the electrolessly deposited copper could be attributed to the strong interaction of the pyridine functional groups of the plasma polymerized 4VP with palladium and copper, and to the spatial distribution of the grafted 4VP polymer chains on the PI surface and into the metal layer. XPS results suggested that the adhesion failure of the electrolessly deposited copper with the pp-4VP-PI films occurred near the pp-4VP/PI interface.

4.2 Electroless Plating of Copper on FPI Films Modified by Plasma Graft Copolymerization of 4-Vinylpyridine

4.2.1 Experimental

4.2.1.1 Materials

The fluorinated polyimides (FPIs) used in this study were (6FDA+4,4-6F Diamine) and (6FDA+p-SED), the former was based on 2,2'-bis(3,4-dicarboxyphenyl) hexafluoropropane dianhydride and 2,2'-bis(4-aminophenyl) hexafluoropropane, and the latter was based on 2,2-bis(3,4-dicarboxyphenyl) hexafluoropropane dianhydride and 4,4'-bis(4-aminophenoxy) diphenyl sulfone. The structures of the two FPI samples are shown in Section 3.1.2. The two FPIs are referred to as FPI-1 and FPI-2, respectively, in this work. The 4-vinyl pyridine (4VP) monomer used for surface graft copolymerization were obtained from the Aldrich Chemical Co. of Milwaukee, WI, USA.

4.2.1.2 Plasma Graft Copolymerization of 4VP on FPI Films: the pp-4VP-FPI Films

Plasma graft copolymerization of 4VP on FPI films was carried out in the system manufactured by Samco International of Kyoto, Japan (Model Samco BP-1). The plasma polymerization precedures were the same as those described in Section 4.1.1.2.

4.2.1.3 Electroless Deposition of Copper on the Surface Modified FPI Films

The graft-modified FPI films were activated *via* immobilization of the Pd catalyst, in the absence of prior sensitization by $SnCl_2$ (the Sn-free process), for the electroless deposition of copper. The processes of the electroless plating of copper for pp-4VP-FPI films were the same as those described in Section 4.1.1.6.

4.2.1.8 Surface Characterization by XPS

The surface composition of the samples was determined by X-ray photoelectron spectroscopy (XPS). The procedures were the same as those described in Section 3.1.9.

4.2.1.7 Adhesion Strength Measurements

The adhesion strength of the electrolessly deposited copper with the various FPI substrates was determined by measuring the T-peel adhesion strength. The procedures of T-peel adhesion strength measurements were the same as those described in Section 3.1.11.

4.2.2 Results and Discussion

The processes of surface pretreatment, plasma graft copolymerization of 4VP on the FPI surface (the pp-4VP-FPI surface) and the subsequent electroless deposition of copper on the FPI surface were the same as those described in Figure 4.1. The details of each process are discussed below.

4.2.2.1 Effect of Ar Plasma Treatment on the Surface Composition of the FPI Films

The C 1s core-level spectrum for both types of pristine FPI films can be curved-fitted with five peak components, having binding energies (BE's) at 284.6 eV for the C-H species, at 285.8 eV for the C-O and C-N species, at 288.4 eV for the $N(C=O)_2$ species, at 291.1 eV for the π-π^* shake-up satellite, and at 292.8 eV for the CF_3 species (Moulder et al., 1992; Zhang et al., 2000). Due to the difference in chemical structure for the two types of the FPI films (see Section 3.1.2), the FPI-1 film have a higher fluorine concentration than the FPI-2 film. The relative peak intensity of the CF_3 species in the C 1s spectrum of the pristine FPI-1 film is higher than that of the pristine FPI-2. An additional peak component with a BE at 287.4 eV, attributable to the C=O species, is found in the Ar plasma treated FPI surfaces. The peak component is different from the carbonyl structure of the imide group in the dianhydride structure. The appearance of the C=O species in the plasma-treated FPI surfaces is attributable to the oxidation in air of the active species on the FPI surface induced by the plasma treatment, as is also the case of peroxide and hydroperoxide formation shown in Step 1 of Figure 4.1. Furthermore, in comparison with the wide scan spectra of the pristine FPI surfaces, an increase in intensity of the O 1s peak component is observed in the wide scan spectra of the Ar plasma-treated FPI films. The above results suggest that the radicals induced by Ar plasma treatment can react with oxygen and moisture in air

to give rise to an oxidized surface. As will be shown later, these active species generated by the Ar plasma pretreatment can also help to enhance the interaction of the subsequently plasma-polymerized 4VP film with the FPI surface.

4.2.2.2 Composition of the 4VP Plasma Graft-Copolymerized FPI Surfaces (the pp-4VP-FPI Surfaces)

The composition of the pp-4VP-FPI surfaces was investigated first by XPS. As a reference, the wide scan and N 1s core-level spectrum of the pristine FPI-1 and FPI-2 are shown in Figure 4.10 (a) and Figure 4.10 (b), respectively. For the pristine FPI surface, the N 1s core-level spectrum consists of a main peak component at the BE of about 400.5 eV, attributable to the-N-$(C=O)_2$ species (Zhang et al., 2001b). On the other hand, however, the N 1s core-level spectrum of the 4VP homopolymer consists of a main peak component at the BE of 398.4 eV, attributed to the –N= species (Yang et al., 2001). Figures 4.10 (c) and 4.10(d) show the wide scan and N 1s core-level spectra of the pp-4VP-FPI-1 and pp-4VP-FPI-2 films prepared at the input RF power of 70 W. Prior to plasma polymerization and deposition, the FPI surface was pretreated by Ar plasma at 70 W for 60 s to introduce the active species on the FPI surface to enhance the interaction with the pp-4VP layer. The presence of the pp-4VP on the FPI surfaces can be deduced from the appearance of the new peak components with the BEs at about 398.4 eV and 399.4 eV, associated with the imine species (-N=) and the hydrogen-bonded imine species, respectively, of the 4VP polymer. The formation of hydrogen bonding between the pyridine ring and other polymers has been reported (Zhou et al., 1997; Ruokolainen et al., 1998). The presence of only a weak –N-$(C=O)_2$ component in the N 1s core-level spectrum and a weak O 1s signal in the wide scan of Figure 3(c) suggests that the thickness of the pp-4VP polymer is approaching the probing depth of the XPS technique (about 7.5 nm for an organic matrix).

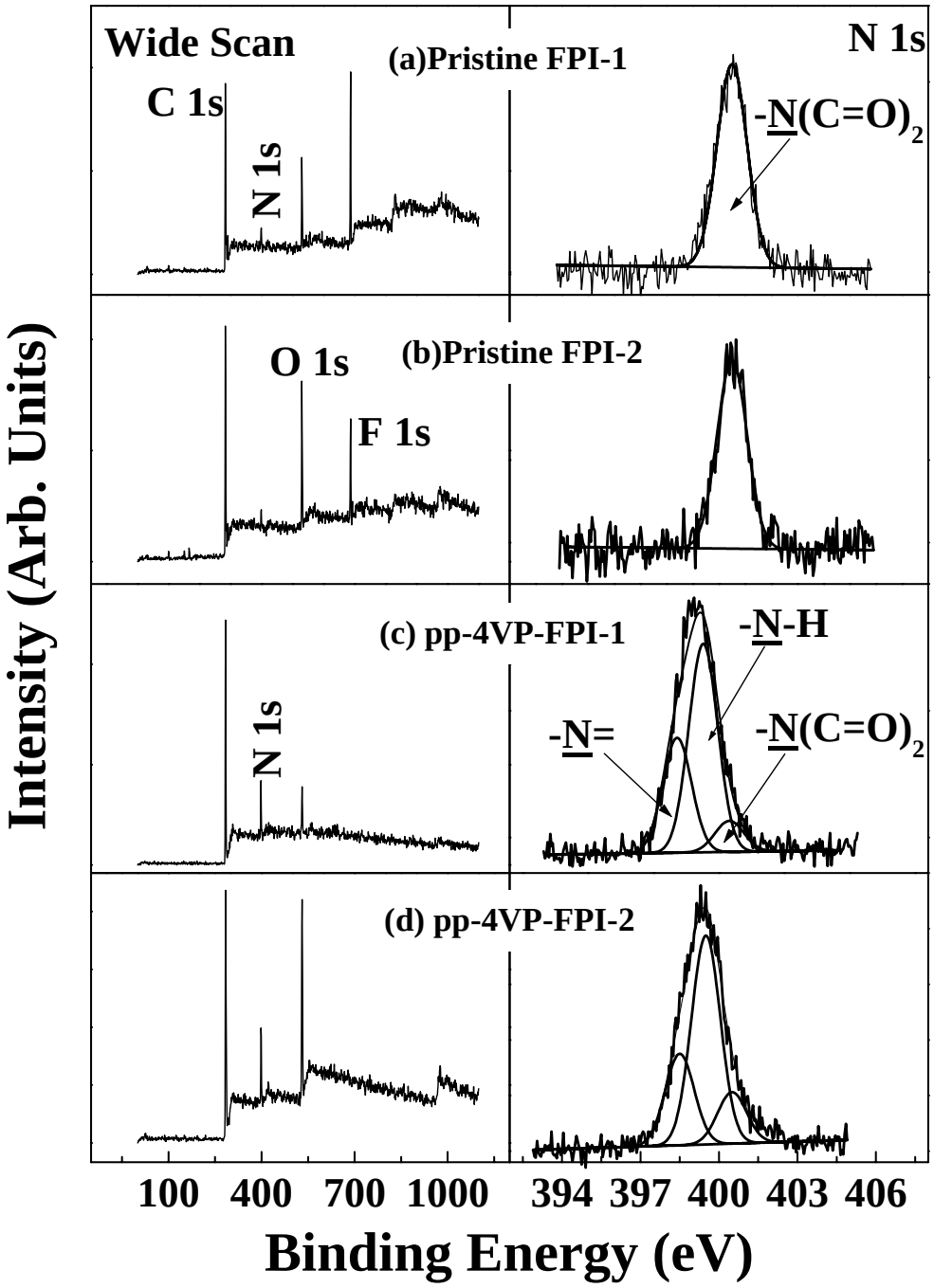

Figure 4.10 XPS wide scan and N 1s core-level spectra of (a) the pristine FPI-1 surface, (b) the pristine FPI-2 surface, (c) the pp-4VP-FPI-1 surface and (d) the pp-4VP-FPI-2 surface prepared at the input RF power of 70 W.

4.2.2.3 Effect of Input RF Power on the Chemical Composition of the pp-4VP-FPI Surfaces

Figure 4.11 shows the dependence of the 4VP polymer graft concentration of the pp-4VP-FPI surface on the input RF power. The 4VP plasma polymerization and deposition were carried out on the 70 W Ar-plasma pretreated FPI-1 and FPI-2 surfaces at a fixed Ar carrier gas flow rate of 20 sccm, a system pressure of 100 Pa, and a monomer temperature of 5ºC. The concentration of the grafted pp-4VP is defined as the number of repeat units of the graft chain per repeat unit of the substrate chain. Thus, the surface graft concentration are determined from the N 1s peak component area ratios of the imine (-N=), the hydrogen-bonded imine, and the [-N-$(C=O)_2$] species. The first two components are associated with the pp-4VP layer, while the last component with the FPI substrate. The concentration of the surface-grafted pp-4VP is thus expressed as the $2[(-N=)+(-N<)]/[-N-(C=O)_2]_{PI}$ ratio. The factor 2 in the numerator is introduced to account for the fact that there are two functional [-N-$(C=O)_2$] groups in every repeat unit of the FPI molecule. It can be observed from Figure 4.11 that the graft concentration of the pp-4VP-FPI-1 and pp-4VP-FPI-2 surfaces increases with the input RF power up to the RF power of about 70 W, above which the graft yield tends to decrease gradually. The variations in graft concentration of the pp-4VP-FPI-1 and pp-4VP-FPI-2 surfaces with the plasma power are attributable to the difference in bond scission mechanism in the plasma polymerization, which have been illustrated in Section 4.1.2.4.

4.2.2.4 Adhesion Strength of the Electrolessly Deposited Copper on the pp-4VP-FPI Films: the Cu/pp-4VP-FPI Assemblies

The adhesion of the electrolessly deposited copper to the FPI surface is the primary concern in the preparation of the Cu/FPI systems. The adhesion of the electrolessly deposited copper to the various FPI substrates was evaluated by measuring the T-peel

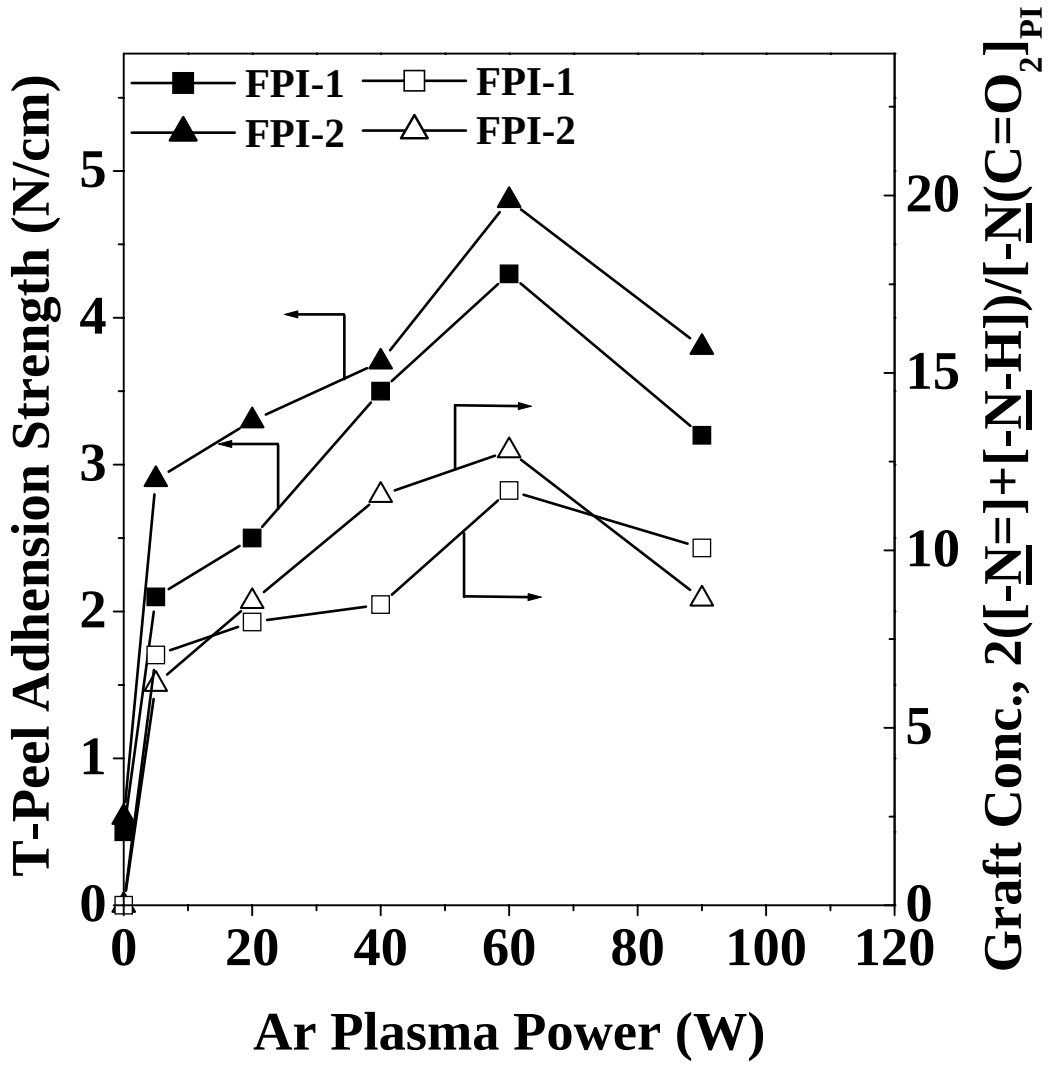

Figure 4.11 Effect of input RF power on the T-peel adhesion strength of the Cu/pp-4VP-FPI assemblies, and on the surface graft concentration of the 4VP polymer.

adhesion strength. The Pd metal has been known to serve as a catalyst for the electroless metal deposition process. In this study, the pp-4VP-FPI surfaces were activated *via* the Sn-free process (in the absence of prior sensitization by $SnCl_2$). For comparison purpose, the electroless copper deposition was also carried out, *via* the "two-step" activation process, on the pristine, as well as the 70 W Ar plasma-treated FPI-1 and FPI-2 surfaces. Electroless copper deposition cannot be carried out *via* the Sn-free process on these surfaces. Adhesion strength of about 4.8 N/cm and 4.3 N/cm are achieved with an input power of 70 W for the electrolessly deposited copper to the pp-4VP-FPI-1 and pp-4VP-FPI-2 surfaces, respectively, using the Sn-free activation method (Figure 4.11). These adhesion strength values are much higher than that of the electrolessly deposited copper with the pristine or Ar plasma-treated FPI-1 and FPI-2 films. Thus, the effective contribution of the deposited pp-4VP polymer in simplifying the electroless deposition process and in improving the adhesion of the electrolessly deposited copper to the FPI film is ascertained.

The variation in adhesion strength coincides approximately with the variation in graft concentration of the pp-4VP-FPI-1 and pp-4VP-FPI-2 films. The phenomenon further testifies to the fact that a graft chain-induced adhesion mechanism is operative. Furthermore, the adhesion results also indicate that the electrolessly deposited copper with both types of the pp-4VP-FPI surfaces show similar adhesion characteristics. This fact suggests that the difference in molecular structure of the FPI substrates, such as the number of $-CF_3$ groups, has almost no effect on the adhesion strength of the resulting Cu/pp-4VP-FPI assemblies prepared from the FPI substrates modified by the present surface functionalization technique.

4.2.2.5 Failure Modes of the Electrolessly Deposited Copper with the pp-4VP-FPI Films

In the present work, the locus of the adhesion failure of the electrolessly deposited copper with the surface modified FPI films is also investigated by analyzing the composition of the delaminated surfaces using XPS. As a reference, the wide scan, C 1s and N 1s core-level spectra of the pristine P4VP homopolymer are shown in Figure 12(a). Figure 12 also shows the wide scan, C 1s and N 1s core-level spectra of the delaminated Cu surface (part (b)) and the delaminated FPI-1 film (part(c)) from an assembly involving the electrolessly deposited copper on the pp-4VP-FPI-1 film and having a T-peel adhesion strength of about 4.5 N/cm. The composition of the delaminated FPI surface and Cu surface from the Cu/pp-4VP-FPI -1 assembly are grossly similar with each other. The N 1s core-level spectrum of the delaminated FPI-1 surface and Cu surface can be curved-fitted with three peak components, having BEs at 398.5 eV for the –N= species, at 399.5 eV for the hydrogen-bonded imine species, and at 400.5 eV for the –N-$(C=O)_2$ species. The hydrogen-bonded imine species is the dominant component in the N 1s core-level spectra of the delaminated FPI-1 and Cu surfaces. No Cu or Pd signal is discernible in the wide scan spectrum of the delaminated FPI-1 surface. Furthermore, the –CF_3 peak component is rather prominent in the C 1s core-level spectrum of the delaminated FPI-1 surface. The peak intensity of the –CF_3 component, however, is substantially reduced in the C 1s core-level spectrum of the delaminated Cu surface. These observations readily suggest that the Cu/pp-4VP-FPI-1 assembly has failed in a mixed mode at the pp-4VP and the FPI-1 interface. In addition, the presence of copper signals in the wide scan spectrum of the delaminated Cu surface suggests that the failure locus above the copper surface is slightly less than the probing depth of the XPS technique (~7.5 nm in an organic matrix). The distinctive

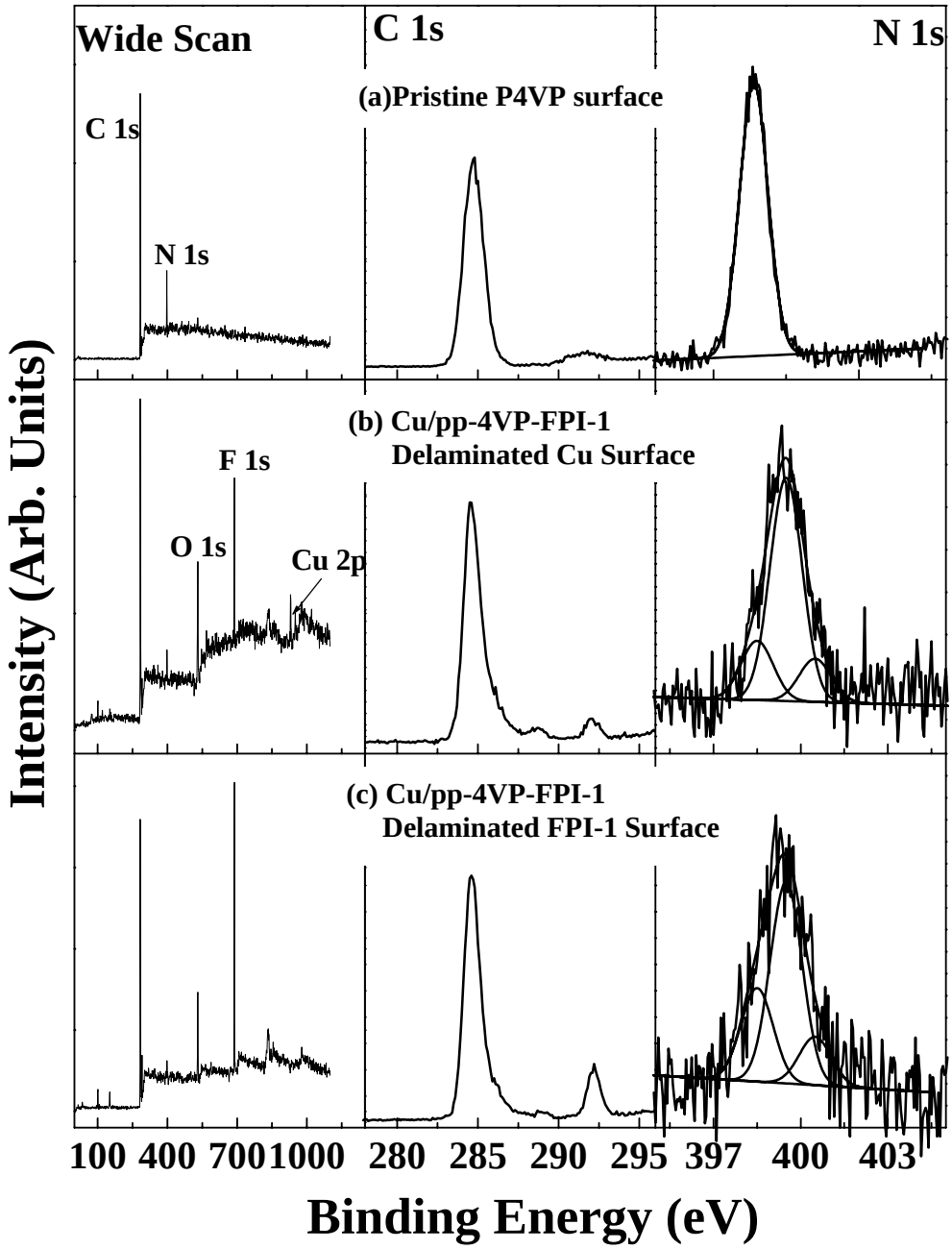

Figure 4.12 XPS wide scan, C 1s and N 1s core-level spectra of (a) the pristine 4VP homopolymer surface, the delaminated (b) Cu and (c) FPI-1 surfaces from a Cu/pp-4VP-FPI-1 assembly having a T-peel adhesion strength of about 4.5 N/cm.

cohesive failure inside the FPI substrate testifies to the presence of strong interactions of the Pd catalyst and the electrolessly deposited copper atoms with the nitrogen moieties of the grafted 4VP chains. The extents of these interactions are further augmented by the spatial distribution of the graft chains on the FPI surface and into the copper matrix.

4.2.3 Conclusion

Thin 4-vinylpyridine (4VP) polymer films could be reactively deposited, *via* plasma graft polymerization of 4VP, on two types of the Ar plasma-pretreated FPI film surfaces. XPS and FTIR results revealed that the pyridine functional groups of the plasma-polymerized 4VP (pp-4VP) could be retained to a large extent under proper glow discharge conditions. The grafted pp-4VP layer on the FPI surface was used not only as chemisorption sites for the palladium complex during the Sn-free activation process, but also as an adhesion promotion layer for the electrolessly deposited copper on the FPI surfaces (the Cu/pp-4VP-FPI assembly). The T-peel adhesion strength of the electrolessly deposited copper with the pp-4VP-FPI-1 and pp-4VP-FPI-2 surfaces reached about 4.5 N/cm. These adhesion strength values were much higher than those of the electrolessly deposited copper with the pristine and the Ar plasma-treated FPI surfaces. The high adhesion strength of the electrolessly deposited copper was attributed to the strong interaction of the pyridine functional groups of the plasma polymerized 4VP with palladium and copper, and the spatial distribution of the grafted 4VP polymer chains on the FPI surfaces and into the metal matrix.

CHAPTER 5

NANOPOROUS LOW-*K* FILMS PREPARED FROM FLUORINATED POLYIMIDE AND POLY(AMIC ACID)S WITH GRAFTED SIDE CHAINS

5.1 Nanoporous Low-κ Polyimide Films Prepared from Poly(amic acid)s with Grafted Poly(acrylic acid)/Poly(ethylene glycol) Side Chains

5.1.1 Experimental

5.1.1.1 Materials

The poly(amic acid) precursor, poly[*N,N'*-(1,4-phenylene)-3,3'4,4'-benzophenonetetra-carboxylic amic acid] (PAmA), was obtained from Aldrich Chemical Co. in powder form and was used as received. Ethanol, *N*-methyl-2-pyrrolidone (NMP), acrylic acid (AAc) and methoxy poly(ethylene glycol) monomethacrylate (PEGMA) (MW=300) were obtained from Sigma-Aldrich Chemical Co. The AAc monomer was purified by vacuum distillation before use. The chemical structures of PAmA, AAc and PEGMA are shown as follows:

PAmA:

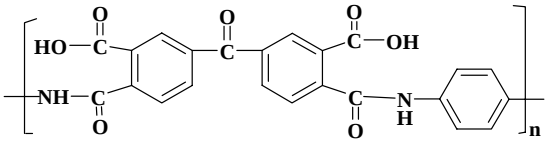

AAc:

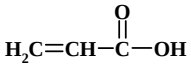

PEGMA:

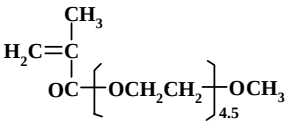

5.1.1.2 Preparation of Nanoporous PI Films

The graft copolymers were performed by thermally-induced molecular graft copolymerization of AAc or PEGMA, with the ozone pre-activated PAmA in NMP solution at 60°C for 3 h and under an argon atmosphere. The monomer and about 50 ml of the 2 wt% NMP solution of the pre-activated PAmA were introduced into a 3-

necked round bottom flask equipped with a thermometer, a condenser, and a gas line. The AAc and PEGMA monomer concentrations were varied from 0.01 g/ml to 0.06 g/ml. The reaction mixture was saturated with purified argon for 30 min under stirring. The reactor flask was then placed in a thermostated water bath at 60°C to initiate the graft copolymerization. A constant flow of argon was maintained during the thermal graft copolymerization. After the reaction time for 3 h, the reactor flask was cooled in an ice bath. The AAc graft-copolymerized PAmA (PAAc-*g*-PAmA), or the PEGMA graft-copolymerized PAmA (P(PEGMA)-*g*-PAmA), was precipitated in excess ethanol. After filtration, the copolymer was further purified by stirring for 48 h in copious amounts of ethanol at room temperature to remove the residual AAc or PEGMA homopolymer. The copolymers were then dried by pumping under reduced pressure for subsequent characterization and processing.

Nanoporous PI films were prepared by a two-step process. Initially, a thin film was obtained by casting a 20 wt% NMP solution of the respective copolymer on a polished silicon substrate (Si(100) wafer). Each film was heated initially in a vacuum oven at 90°C for 1 h under atmospheric pressure. It was then heated, sequentially, at 150°C for 1 h, at 200°C for 1 h, at 250°C for 0.5 h and final at 300°C for 10 min, in a vacuum oven pre-purged with argon. The film was allowed to cool down gradually to room temperature over a period of 6 h. The second step involved the thermolysis and removal of the grafted side chains (AAc or PEGMA polymer chains), by heating the copolymer film at 250°C for 12 h in air, yielding the nanoporous PI film. The processes of ozone pre-activation, thermal-induced grafting, and nanoporous film preparation are illustrated schematically in Figure 5.1.

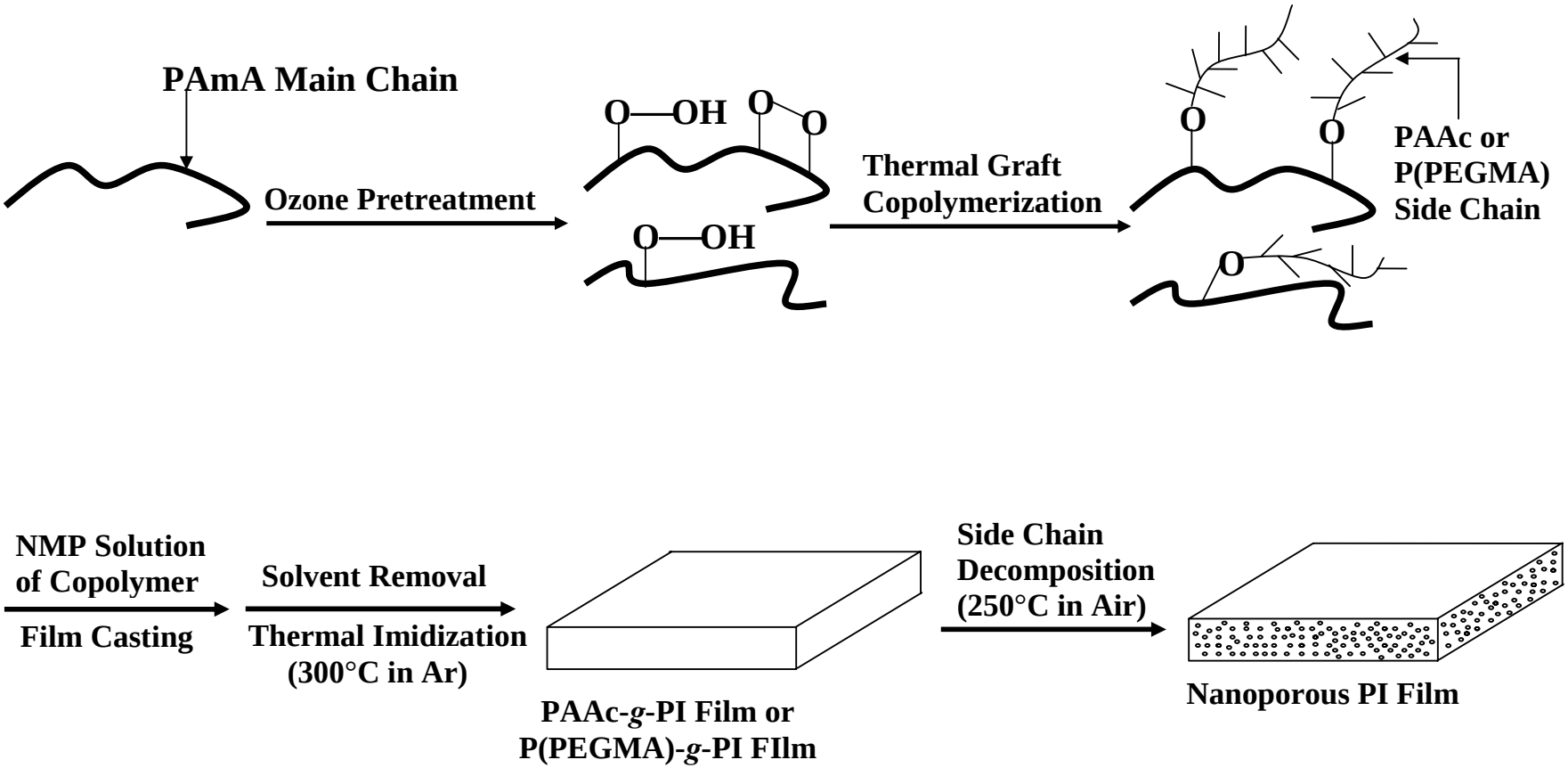

Figure 5.1 Schematic illustration of the processes of thermally-induced graft copolymerization of AAc and PEGMA with the ozone-preactivated PAmA backbone and the preparation of a nanoporous PI film.

5.1.1.3 Elemental Analysis

The carbon, nitrogen and hydrogen elemental contents of the pristine PAmA and the copolymer samples were determined using a Perkin-Elmer 2400 elemental analyzer.

5.1.1.4 Density Measurement

Film density was measured using a top-loading electronic Mettler Toledo balance equipped with a density kit and according to the Archimedean principle. The sample was weighed in air and in doubly distilled water at room temperature.

5.1.1.5 Surface Characterization by XPS

The surface composition of the samples was determined by X-ray photoelectron spectroscopy (XPS). The procedures were the same as those described in Section 3.1.9.

5.1.1.6 Thermal Analyses

The thermal properties of the homopolymer and copolymer samples were measured by both thermogravimetric (TG) analysis and differential scanning calorimetry (DSC). For the TG analysis, the polymer samples were heated up to 900°C at a heating rate of 10°C/min under a dry nitrogen atmosphere in a Du Pont Thermal Analyst 2100 system, equipped with a TGA 2050 thermogravimetric thermal analyzer. For the DSC analysis, the spectra were recorded on a DSC 822e (Mettler Toledo Co., Switzerland) at a heating rate of 10°C/min and under a nitrogen atmosphere. The software for data processing allowed the automatic subtraction of the baseline and the normalization of the thermogram for sample weight.

5.1.1.7 Scanning Electron Microscopy (SEM)

The morphology of the cross-section of the nanoporous PI films was studied by scanning electron microscopy (SEM), using a JEOL 6320 electron microscope. The cross-section of the film was mounted on the sample stud by means of a double-sided adhesive tape. A thin layer of palladium was sputtered onto the cross-sectional surface prior to the SEM measurement. The SEM measurements were performed at an accelerating voltage of 15 kV.

5.1.1.8 Dielectric Constant Measurements

The dielectric constant (κ) of the PI films was measured on a RF impedance/capacitance material analyzer (Hewlett Packard Model 4291B) at the frequency of 1 MHz under ambient conditions. The consistency of the κ values obtained was constantly checked by making reference measurements on dielectric polymer films with well-characterized low dielectric constants, such as the poly(tetrafluoroethylene) (PTFE) films, under similar conditions.

5.1.2 Results and Discussion

5.1.2.1 Characterization of PAmA with PAAc and P(PEGMA) Side Chains

Direct oxidation of polymers by ozone is a well-known method for introducing peroxide and hydroperoxide species onto polymer chains and surfaces for the subsequent functionalization, such as graft polymerization (Kang and Zhang, 2000; Fargere et al., 1994). Under thermal induction, the peroxide functional groups undergo decomposition to initiate the free radical graft copolymerization of vinyl monomers. The amount of peroxides introduced by ozone treatment can be regulated by the polymer concentration, ozone treatment temperature, ozone concentration and ozone treatment time. In this study, the ozone concentration was fixed at 0.027 g/L under an O_3/O_2 mixture flow rate of 300 L/h and a temperature of 25°C for every 50 ml of 2 wt% PAmA solution. Previous study (Wang et al., 2003) performed under similar conditions had shown that the increase in peroxide concentration of PI leveled off at an ozone treatment time of about 15 min. Thus, the ozone pretreatment time was fixed at 15 min in the present study.

For the graft copolymerization of AAc and PEGMA with PAmA in NMP solution, the monomer feed ratio can be used to regulate the graft concentration of the resulting graft copolymer. The bulk graft concentration of the copolymers is defined as the number of AAc or PEGMA repeat units in the graft chains per repeat unit of the PAmA main chain. It can be calculated from the $([C]/[N])_{bulk}$ molar ratio by taking into account of the carbon stoichiometries of the graft and the main chains, and the carbon to nitrogen ratio of the PAmA main chain. Thus, the bulk graft concentrations, or the $([PAAc]/[PAmA])_{bulk}$ and $([P(PEGMA)]/[PAmA])_{bulk}$ molar ratios, can be calculated, respectively, from the following relationships:

$$([PAAc]/[PAmA])_{bulk} = 2([C]- (23/2)[N])_{bulk}/3[N]_{bulk}$$

$$([P(PEGMA)]/[PAmA])_{bulk} = 2([C]- (23/2)[N])_{bulk}/14[N]_{bulk}$$

in which the factor 23/2 accounts for the fact that there are 23 carbon atoms and 2 nitrogen atoms per repeat unit of the PAmA chains, while the factors 3 and 14 account for the fact that there are 3 carbon atoms in each AAc unit and 14 carbon atoms in each PEGMA unit. The dependence of the bulk graft concentration of the PAAc-*g*-PAmA and P(PEGMA)-*g*-PAmA copolymers on the respective monomer to PAmA molar feed ratio used for graft copolymerization is summarized in Table 5.1. It can be seen from Table 5.1 that, for both copolymers, the graft concentration increases with the increase in monomer feed ratio.

5.1.2.2 Thermal Properties of the PAAc-*g*-PAmA or P(PEGMA)-*g*-PAmA Copolymers

Thermal stability is one of the unique properties of PIs. The thermal properties of the graft copolymers were studied by thermogravimetric(TG) analysis in nitrogen and in air, and by differential scanning calorimetry (DSC) in nitrogen. Figure 5.2 shows the respective TGA curves (in nitrogen) of the pristine PAmA (Curve 1), the PAAc-*g*-PAmA copolymer with bulk graft concentration of 0.62 (Curve 2), the P(PEGMA)-*g*-PAmA copolymer with bulk graft concentration of 0.90 (Curves 3), the AAc homopolymer (Curve 4) and the PEGMA homopolymer (Curve 5). The corresponding TGA curves in air for the AAc homopolymer (Curve 6) and PEGMA homopolymer (Curve 7) are also shown for comparison purpose. The temperature for the onset of decomposition of the AAc homopolymer decrease from about 280°C in nitrogen to only about 200°C in air. A similar decrease in the decomposition temperature is observed for the PEGMA homopolymer in air. In comparison with the pristine PAmA, PAAc and P(PEGMA) homopolymers, the copolymer samples exhibit an intermediate

weight loss behavior and undergo a two-step degradation. The onset of the first major weight loss occurs in the temperature range of 300°C-310°C, which corresponds to the decomposition of the AAc or the PEGMA side chains of the copolymer in nitrogen. The second major weight loss begins at about 510°C, which coincides with the decomposition temperature of the PAmA main chain. For TGA carried out in air, the temperature for the onset of the first major weight loss decrease to the range of 250°C-270°C for the two graft copolymers. The TGA curves also indicate that the extent of weight loss in the copolymer during the first stage of thermal decomposition is approximately equal to the AAc or PEGMA polymer content in the copolymer. The glass transition temperatures (T_g's), obtained from DSC analysis, of the pristine PAmA and the PAAc-*g*-PAmA and P(PEGMA)-*g*-PAmA copolymers of different graft concentrations are also shown in Table 5.1. Polyimides are well-known for their good thermal stability and high T_g's. The pristine PAmA has a T_g of about 317°C. The T_g of the graft copolymer decreases with the increase in graft concentration. Graft copolymerization with AAc or PEGMA reduces the structural rigidity of PAmA and increases the molar free volume of the polymer, resulting in the lowering of T_g.

Table 5.1 Characteristics of the PAAc-*g*-PAmA and P(PEGMA)-*g*-PAmA Copolymers and the Resulting Nanoprous PI Films

PAmA Samples	PAAc-*g*-PAmA and P(PEGMA)-*g*-PAmA			PI and Nanoporous PI Films						
	Monomer Molar Feed Ratio [AAc]/[PAmA] or [PEGMA]/[PAmA]	Bulk Graft Concentration[a] [PAAc]/[PAmA] or [P(PEGMA)]/[PAmA]	Glass Trans. Temp. (°C)	Element Composition Before Thermal Decomposition (wt%)		Element Composition After Thermal Decomposition (wt%)		Weight Loss After Thermal Decomp. (%)	Density (g/cm^3)	Porosity
				C	N	C	N			
Pristine PAmA	---	---	317	70.05	7.11	--	--	--	1.43	---
PAAc-*g*-PAmA	3	0.32	315	68.18	6.52	67.62	7.16	2.9	1.39	3%
PAAc-*g*-PAmA	6	0.54	313	67.82	6.40	67.48	7.11	3.7	1.37	4%
PAAc-*g*-PAmA	12	0.62	311	67.73	6.39	66.78	7.01	6.5	1.33	7%
PAAc-*g*-PAmA	18	0.70	310	67.59	6.31	67.43	7.10	7.2	1.31	9%
P(PEGMA)-*g*-PAmA	0.8	0.91	312	67.37	6.28	67.17	6.80	2.8	1.34	6%
P(PEGMA)-*g*-PAmA	1.5	1.09	309	65.69	5.72	67.22	6.65	4.2	1.31	8%
P(PEGMA)-*g*-PAmA	3	1.32	307	65.32	5.08	66.99	5.98	6.3	1.28	10%
P(PEGMA)-*g*-PAmA	4.5	1.35	305	64.72	5.01	67.04	5.87	7.6	1.23	14%

[a] Defined as the number of repeat units of the graft chain per repeat unit of the PAmA main chain.

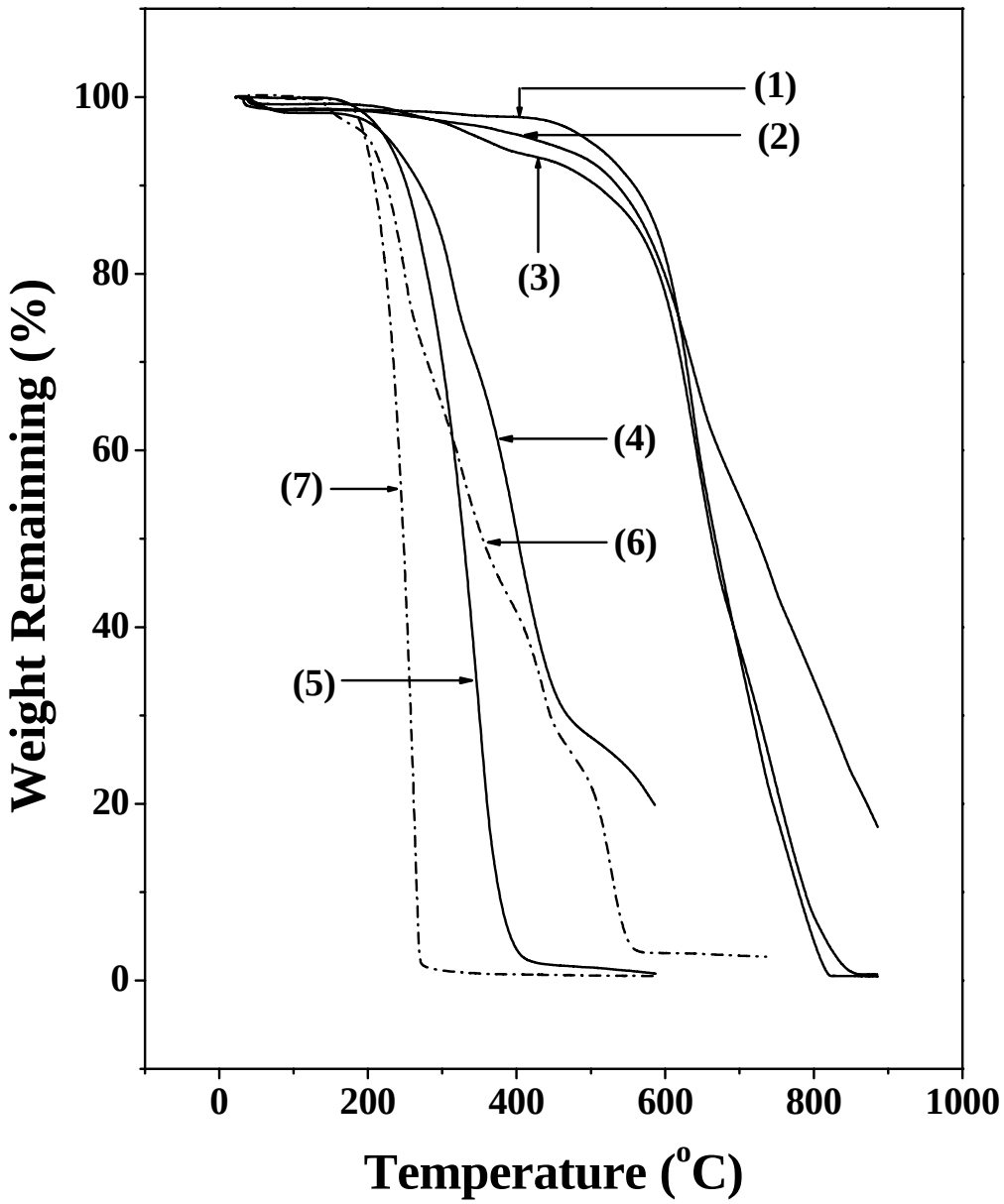

Figure 5.2 TGA curves of (1) the PAmA homopolymer, (2) the PAAc-*g*-PAmA copolymer (bulk graft concentrations=0.62), (3) the P(PEGMA)-*g*-PAmA copolymer (bulk graft concentration=0.90), (4) the AAc homopolymer, and (5) the PEGMA homopolymer in nitrogen. The weight loss behavior of the AAc and PEGMA homopolymer in air is shown by Curve 6 and Curve 7, respectively.

5.1.2.3 Characterization of the Nanoporous PI films

After solvent removal and imidization, the nanoporous PI film was generated by subjecting the copolymer film to the subsequent thermal treatment in air to decompose the labile side chain. The basic requirement for the grafted side chains is that they must undergo a controllable and quantitative degradation into low molecular weight products, which can diffuse readily through the PI matrix. On the other hand, the grafted side chains must also possess sufficient thermal stability during the solvent removal and the thermal imidization. In the present study, the copolymers films were cured at 300°C for 10 min under reduced argon pressure to complete the imidization. Under an inert atmosphere, PAAc and P(PEGMA) are thermally stable up to about 300°C. This thermal stability allows the imidization of PAmA to PI without any appreciable decomposition of the graft chains. Both FTIR and XPS results show that under these conditions, the imidization is complete without any appreciable loss of the grafted PAAc or P(PEGMA) components. On the other hand, however, in the presence of air or oxygen, the decomposition temperature of PAAc or P(PEGMA) decreases substantially. TGA results indicate that the decomposition of the AAc homopolymer starts at about 180°C, while that of the PEGMA homopolymer at about 200°C, in air. Thus, the formation of the nanoporous PI structure can be accomplished by the subsequent heat treatment of the film at 250°C in air to decompose the PAAc or P(PEGMA) side chains. The selection of the thermal decomposition temperature and conditions is important. The temperature should be sufficiently high to decompose the labile side chains, but below the T_g of the PI to avoid the collapse of the porous structure. After thermal treatment of the imidized PI films at 250°C in air for 12 h, no AAc segments were discernible, while residual PEGMA segments and fragments were

retained in the resulting nanoporous PI films, as indicated by the subsequent TGA, XPS (see Figure 5.3 below) and elemental analyses (see Table 5.1).

Density measurements were used to characterize the formation of the porous structure. As shown in Table 5.1, the density of the nanoporous PI films prepared from the PAAc-*g*-PAmA copolymers decreases from 1.43 to 1.31, as the porosity increases to 9%. In the case of the PI films prepared from the P(PEGMA)-*g*-PAmA copolymers, a density as low as 1.23 was obtained from the thermal decomposition of a copolymer having a molar graft concentration of 1.35. It can also be seen from Table 1 that with the decomposition of the AAc or PEGMA side chains, the nitrogen content of the films is increased. The fact that the nitrogen content of the P(PEGMA)-*g*-PI (imidized P(PEGMA)-*g*-PAmA) samples after thermal decomposition is still substantially below that of the pristine PI suggests that the thermal decomposition of the PEGMA side chains is not complete.

The decomposition of the grafted PAAc or P(PEGMA) side chains is also verified by the XPS results. Figure 5.3 shows the C 1s core-level spectra of the pristine PI film (part (a)), the PAAc-*g*-PI (imidized PAAc-*g*-PAmA, bulk graft concentration=0.62) film before and after side chain decomposition(part (b) and part (c), respectively), and the P(PEGMA)-*g*-PI (imidized P(PEGMA)-*g*-PAmA, bulk graft concentration=0.91) film before and after side chain decomposition(part (d) and part (e), respectively). The C 1s core-level spectrum of the pristine PI film (Figure 5.3(a)) can be curved-fitted with four peak components, having binding energies (BE's) at 284.6 eV for the C-H species, at 285.6 eV for the C-N species, at 287.4 eV for the C=O species, and at 288.4 eV for the N-(C=O)$_2$ species (Zhang et al., 2000). The O-C=O species of the grafted PAAc chains have a C 1s peak component at the BE of about 288.3 eV (Briggs, 1998).

The BE of the O-C=O species and that of the N-(C=O)$_2$ (imide) species of PI cannot be resolved clearly. The two species are represented by a single peak component at the BE of about 288.3 eV. The presence of the grafted AAc polymer on PI is readily indicated by the increase in intensity of the peak component at 288.3 eV (Figure 5.3(b)). The slight increase in intensity of the peak component at 287.4 eV (the C=O species) probably arises from the contribution of the oxidized carbon species produced during the ozone pretreatment and the thermal imidization. On the other hand, the decomposition of the grafted PAAc side chain is indicated by the decrease in intensity of the peak component at 288.3 eV, as shown in Figure 5.3(c). In the case of the (PEGMA)-g-PI copolymer, the presence of the grafted PEGMA polymer on PI can be deduced from the substantially increase in intensity of the C 1s peak component at the BE of 286.2 eV, attributable to the C-O species of the PEGMA side chain (Figure 5.3(d)). Similarly, the decomposition of the PEGMA side chains is indicated by the substantial reduction in intensity of the C-O peak component after the thermal treatment (Figure 5.3(e)). The persistence of a high BE tail in the C 1s core-level spectrum of Figure 5.3(e) suggests the incomplete thermal decomposition of the PEGMA side chains, consistent with the elemental and TG analysis results of the P(PEGMA)-g-PI samples after thermal decomposition.

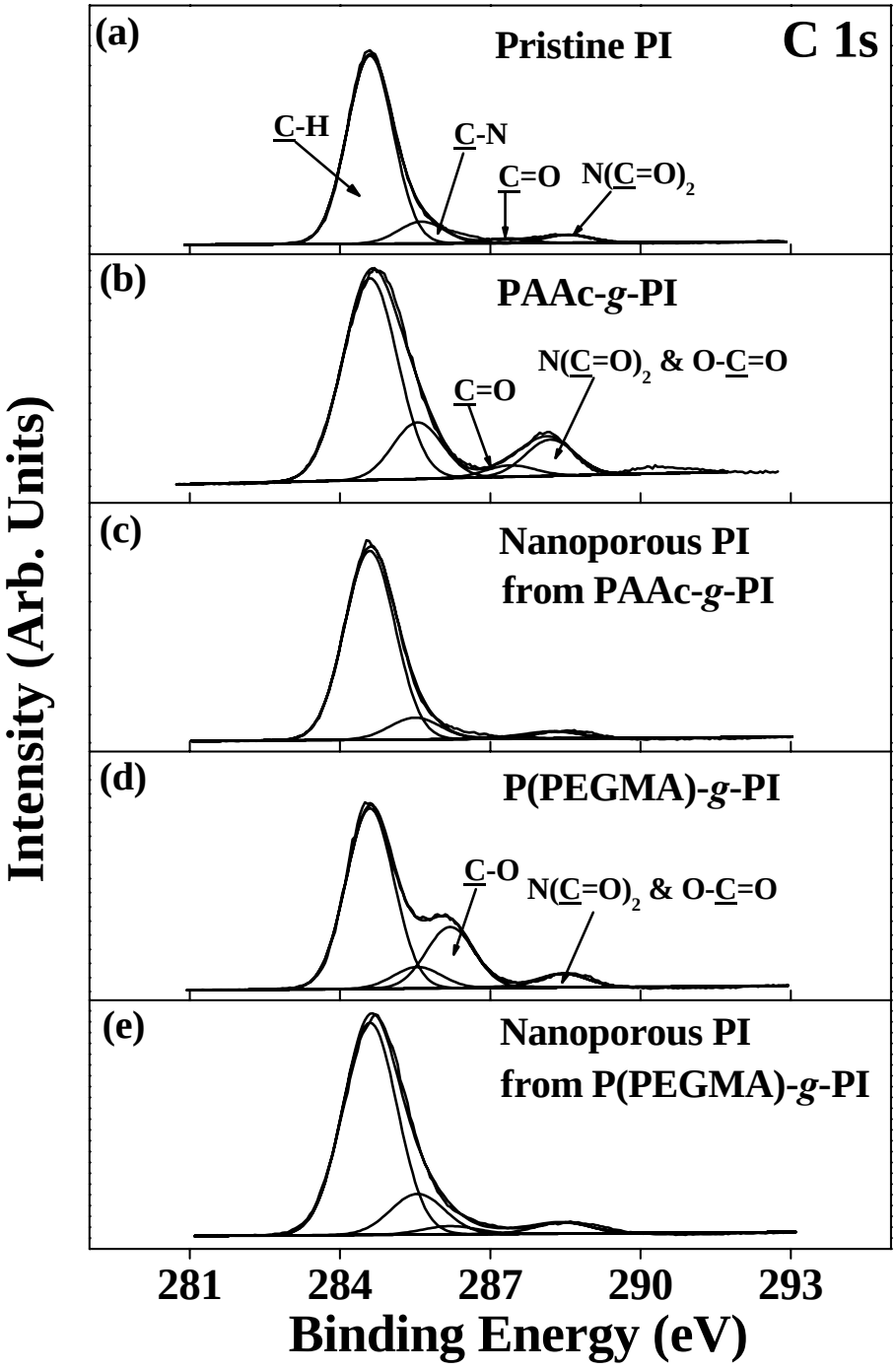

Figure 5.3 XPS C 1s core-level spectra of (a) the pristine PI film, the PAAc-*g*-PI film (imidized PAAc-*g*-PAmA, bulk graft concentration=0.62) (b) before and (c) after side chain decomposition, and the P(PEGMA)-*g*-PI film (imidized P(PEGMA)-*g*-PAmA, bulk graft concentration=0.91) (d) before and (e) after side chain decomposition.

It is important to control the pore size and pore size distribution for preparing porous materials with suitable mechanical and electrical properties. In this study, the nanoporous structure of the PI films was confirmed by SEM at a magnification of 50,000. The SEM images (cross-sectional view) of the pristine PAAc-*g*-PI and the P(PEGMA)-*g*-PI copolymer films are shown in Figures 5.4(a) and 5.4(b), respectively. The nanoporous PI films prepared from the corresponding PAAc-*g*-PI and P(PEGMA)-*g*-PI copolymer films are shown in Figures 5.4(c) and 5.4(d). The nanoporous films were obtained from the samples that had been fully imidized, followed by side-chain decomposition at 250°C in air for 12 h. The SEM images in Figures 5.4(c) and 5.4(d) reveal the formation of the randomly distributed nanopores in the PI matrix. The dark areas are the voids created from degradation and removal of the PAAc or PEGMA side chains. The average size of the pores is in the range of 30 to 100 nm. The pores are irregularly in shape and show a small degree of interconnection. During the imidazation and thermal degradation processes, microphase separation of the degraded side chains and their fragments probably had occurred in the polymer film, resulting in the formation of the nanoporous morphology.

The dielectric constant (κ) of the resulting nanoporous PI film is of the primary concern. For the nanoporous PI film, the ultimate dielectric constant is governed by the intrinsic dielectric constant of the PI matrix and the morphology and porosity of the porous structure. Figure 5.5 shows the dielectric constant (at 1 MHz) of the pristine PI film and the nanoporous PI films, prepared from the PAAc-*g*-PAmA and P(PEGMA)-*g*-PAmA copolymers, as a function of porosity of the films. The κ value of the pristine PI film is 3.5 under ambient conditions. As anticipated, all the nanoporous films exhibit considerable lower dielectric constants. For films prepared from both types of

the copolymers, the κ value decreases with the increase in porosity. A dielectric constant of about 2.1 is obtained for the nanoporous PI film prepared from the PAAc-*g*-PAmA copolymer with a bulk graft concentration of about 0.7 and a porosity (after thermal decomposition) of about 9%. This dielectric constant is comparable to that of the very inert poly(tetrafluoroethylene) (PTFE). Similarly, a κ value of about 2.4 is achieved for the film prepared from the P(PEGMA)-*g*-PAmA copolymer with a bulk graft concentration of about 1.35 and a porosity (after thermal decomposition) of about 14%. The higher dielectric constant, in spite of the increase in porosity, for the PI film from the P(PEGMA)-*g*-PAmA copolymer is probably due to the incomplete decomposition of the PEGMA side chains. Nevertheless, the dielectric constants of the nanoporous films are all substantially lower than that of the PI homopolymer film.

Graft copolymerization with AAc or PEGMA reduces the structural rigidity and the intermolecular packing density of the PI chains and, thus, increases the molar free volume of the polymer. Subsequent thermal decomposition of the grafted AAc or PEGMA side chains introduces the nano-voids. The synergistic effect arising from the increase in molar free volume of the polymer and the formation of nano-voids in the film has given rise to a significant decrease in the dielectric constant of the material. In fact, the observed lowering of the dielectric constant is greater than that predicted by a linear rule-of-mixtures model or the Maxwell-Garnett approximation (Carter et al., 2001). Presumably the dielectric constants for both types of the PI films in Figure 5.5 could be further reduced through the further increase in porosity of the films (or the further increase in graft concentration of the PAmA copolymers). However, further increase in porosity of the film above 15% will result in a marked increase in pore size, as well as a marked deterioration in mechanical properties (for example, a more than 50% decrease in tensile strength), of the film.

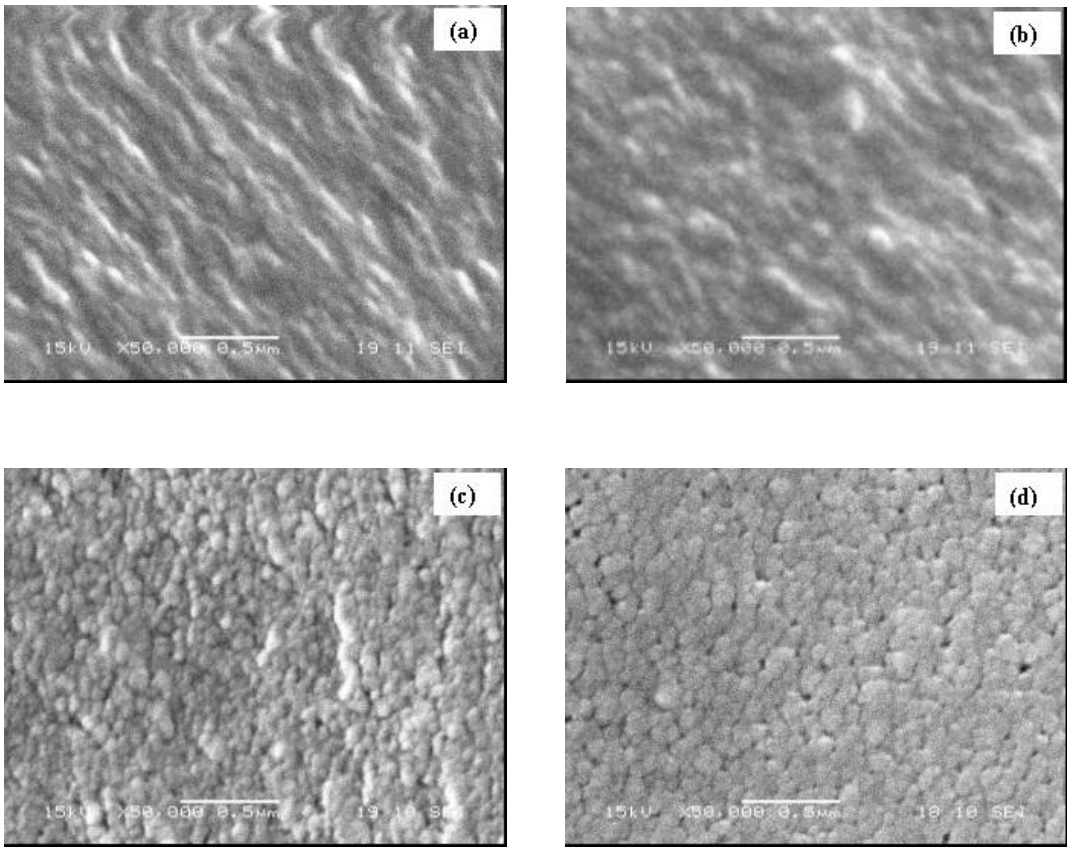

Figure 5.4 SEM cross-sectional images of (a) the PAAc-*g*-PI film (bulk graft concentration=0.32), (b) the P(PEGMA)-*g*-PI film (bulk graft concentration=0.91), and the nanoporous PI film prepared from (c) the PAAc-*g*-PAmA copolymer and from (d) the P(PEGMA)-*g*-PAmA.

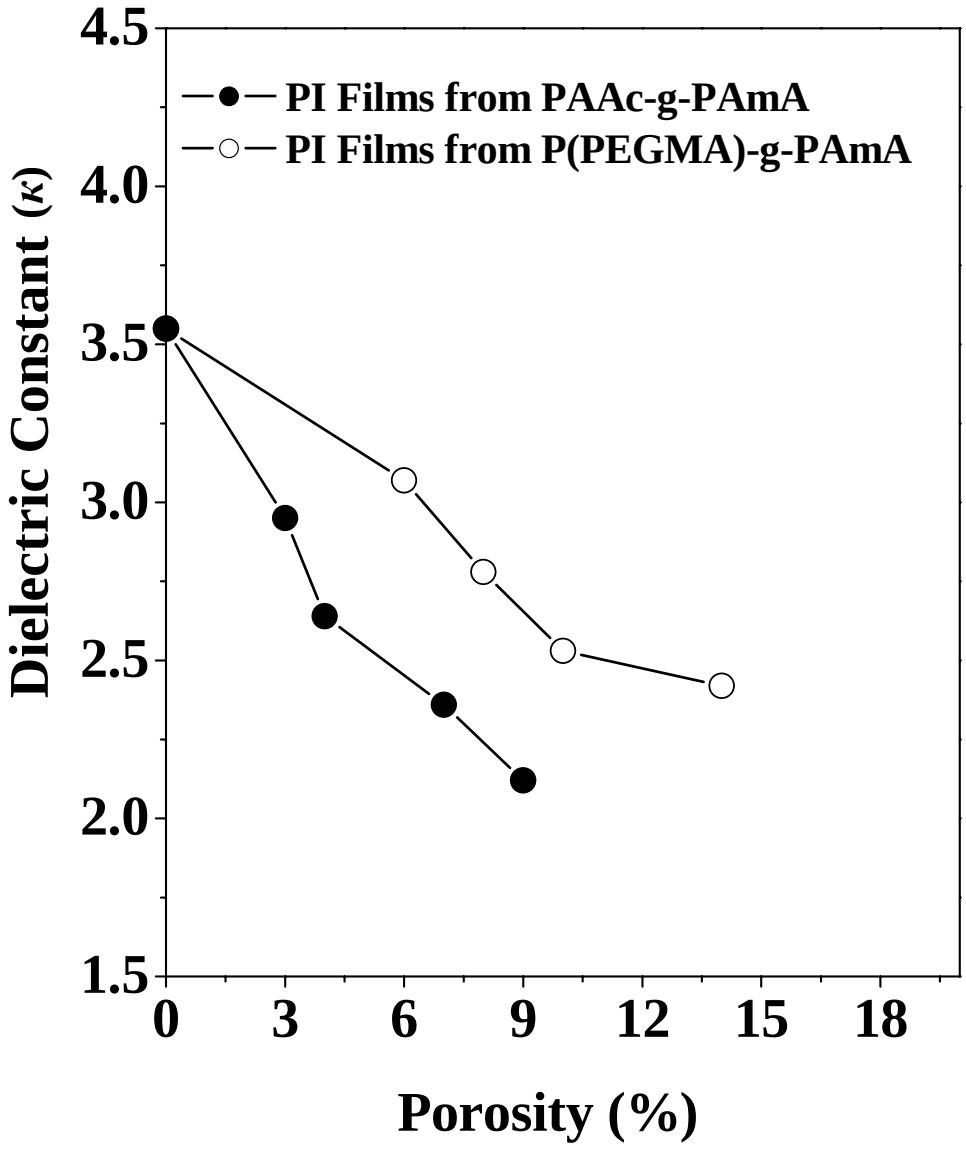

Figure 5.5 Dielectric constant of the nanoporous PI film as a function of porosity.

5.1.3 Conclusion

Poly(amic acid) (PAmA) precursors with grafted AAc or PEGMA side chains have been successfully prepared. Nanoporous low-κ PI films were obtained after thermal imidization of the PAmA backbones in an inert atmosphere and thermal decomposition of the side chains in air. The densities of the nanoporous films so-formed were 3-14% lower than that of the pristine PI film. SEM images revealed that the pore sizes were in the order of 30-100 nm. The dielectric constant of the nanoporous PI films decreased with the increase in graft concentration of the side chains, and thus the porosity of the PI films. Dielectric constant as low as 2.1 and 2.4 were obtained for the nanoporous PI films prepared form the PAAc-*g*-PAmA and P(PEGMA)-*g*-PAmA copolymer, respectively. Thus, molecular modification by grafting of thermally labile side chains is a relatively simple and effective approach for the preparation of nanoporous PI films with low dielectric constants and preserved PI backbones.

5.2 Nanoporous Ultra-Low-κ Films Prepared from Fluorinated Polyimide with Grafted Poly(acrylic acid) Side Chains

5.2.1 Experimental

5.2.1.1 Materials

The fluorinated polyimide (FPI) used in this study was 2,2-bis(3,4-dicarboxyphenyl) hexafluoropropane dianhydride+4,4'-bis(4-aminophenoxy) diphenyl sulfone and was synthesized by step reaction polymerization, as described in Section 3.1.1.2. The chemical structures of FPI were also shown in Section 3.1.1.2 (FPI-2).

5.2.1.2 Ozone Treatment of FPI

The FPI powder was first dissolved in NMP to achieve a concentration of 75 g/L. A continuous stream of O_3/O_2 mixture was bubbled through the solution at 25°C. The O_3/O_2 mixture was generated from an Azcozon RMU16-04EM ozone generator. The gas flow rate was adjusted to 300 L/h to give rise to an ozone concentration of about 0.027 g/L of the gaseous mixture. A treatment time was fixed to about 5 min to achieve the desired content of peroxides (see below). After the ozone treatment, the polymer solution was cooled in an ice bath.

5.2.1.3 Graft Copolymerization of AAc with FPI: The PAAc-*g*-FPI Copolymer

The functional copolymer was prepared by thermally-induced molecular graft copolymerization of AAc with the ozone pre-activated FPI in NMP solution at 60°C for 3 h and under an argon atmosphere. Then the monomer and about 50 ml of the FPI solution were introduced into a 3-necked round bottom flask equipped with a thermometer, a condenser, and a gas line. The AAc monomer concentrations was varied from 0.03 g/ml to 0.21 g/ml. The final volume of each reaction mixture was

adjusted to 50 ml. The solution was saturated with purified argon for 30 min under stirring. The reactor flask was then placed in a thermostated water bath at 60°C to initiate the graft copolymerization reaction. A constant flow of argon was maintained during the thermal graft copolymerization. After reaction time for 3 h, the reactor flask was cooled in an ice bath and the AAc graft-copolymerized FPI (PAAc-*g*-FPI) was precipitated in excess ethanol. After filtration, the copolymer was further purified by stirring for 48 h in copious amounts of ethanol at room temperature. The precipitation and exhaustive washing ensured the complete removal of the residual AAc homopolymer. The copolymer were then dried by pumping under reduced pressure for subsequent characterization.

5.2.1.4 Preparation of Nanoprous FPI films

Nanoporous PI films were prepared by a two-step process. Initially, a thin film was obtained by casting a 20 wt% NMP solution of the respective copolymer on a polished silicon substrate (Si (100) wafer). Each film was heated initially in a vacuum oven at 90°C for 1 h under atmospheric pressure. It was then heated, sequentially, at 150°C for 1 h, at 200°C for 1 h, at 225°C for 5 h, in a vacuum oven pre-purged with argon. The film was allowed to cool down gradually to room temperature over a period of 6 h. The second step involved the thermolysis and removal of the grafted PAAc side chains, by heating the copolymer film at 250°C for 12 h in air, yielding the nanoporous FPI film. The processes of ozone pre-activation, thermal-induced grafting, and nanoporous film preparation are illustrated schematically in Figure 5.6.

5.2.1.5 Elemental Analysis

The carbon, nitrogen and hydrogen elemental contents of the pristine FPI and the copolymer samples were determined same as described in Section 5.1.1.3. The fluorine

contents, on the other hand, were determined by the Schöniger combustion method (Walton, 1964).

5.2.1.6 Density Measurement

The procedures for density measurement of the pristine FPI and the nanoporous FPI films were the same as those described in Section 5.1.1.4.

5.2.1.7 Surface Characterization by XPS

The surface composition of the samples was determined by X-ray photoelectron spectroscopy (XPS). The prodedures were the same as those described in Section 3.1.9.

5.2.1.8 Thermal Analyses

The thermal properties of the homopolymer and copolymer samples were measured by both thermogravimetric analysis (TGA) and differential scanning calorimetry (DSC). The procedures were the same as those described in Section 5.1.1.6.

5.2.1.9 Scanning Electron Microscopy (SEM)

The morphology of the cross-section of the nanoporous FPI films was studied by scanning electron microscopy (SEM). The procedures were the same as those described in Section 5.1.1.7.

5.2.1.10 Dielectric Constant Measurements

The prodedures of dielectric constant (κ) measurement were the same as those described in Section 5.1.1.8.

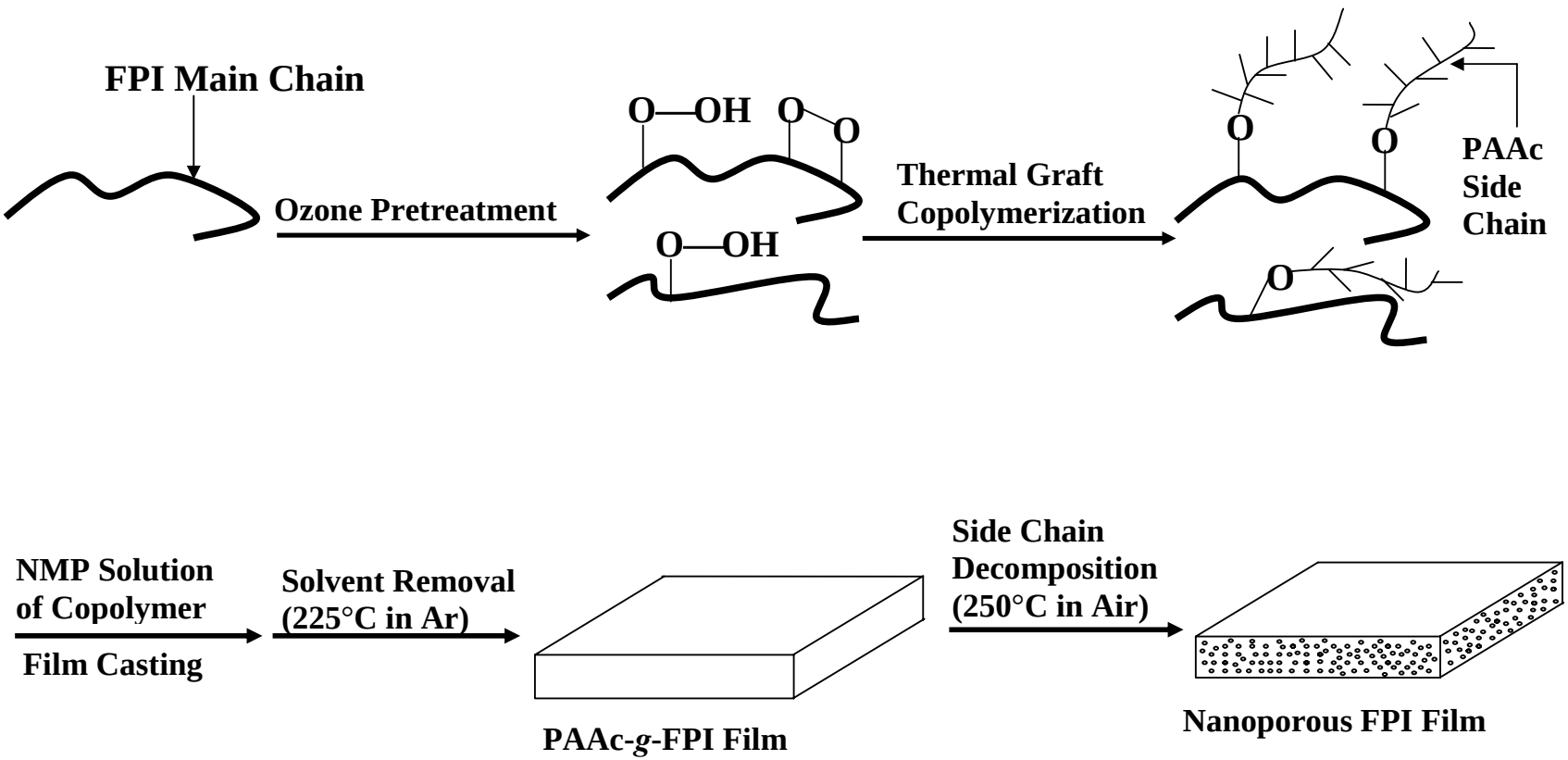

Figure 5.6 Schematic illustration of the process of thermally-induced graft copolymerization of AAc with the ozone-preactivated FPI backbones and the preparation of a nanoporous FPI film.

5.2.2 Results and Discussion

5.2.2.1 Characterization of the PAAc-*g*-FPI Copolymers

Ozone treatment is a well-known method for introducing peroxide and hydroperoxide groups onto polymer chains and surfaces for the subsequent functionalization, such as graft copolymerization. Under thermal induction, the peroxide groups undergo decomposition to initiate the free radical graft copolymerization of vinyl monomers. Since ozone treatment of the FPI is also accompanied by degradation and scission of the polymer chains, the ozone pretreatment time was fixed at 5 min under the conditions (Wang et al., 2003) that give rise to 1.3×10^{-5} moles of peroxides per gram of the FPI. The bulk graft concentration of the PAAc-grafted FPI (PAAc-*g*-FPI) copolymers is defined as the number of the AAc repeat units in the graft (side) chains per repeat unit of the FPI main chain. Thus, the bulk graft concentration, or the $([PAAc]/[FPI])_{bulk}$ molar ratio, can be calculated from the C and N elemental composition and the following relationship:

$$([PAAc]/[FPI])_{bulk} = 2([C]- (43/2)[N])_{bulk}/3[N]_{bulk}$$

in which the factor 43/2 accounts for the fact that there are 43 carbon atoms and 2 nitrogen atoms per repeat unit of the FPI chains, while the factor 3 accounts for the fact that there are 3 carbon atoms in each AAc unit. The data in Table 5.2 show that the bulk graft concentration of the PAAc-*g*-FPI copolymer increases with increasing AAc monomer to FPI molar feed ratio used for graft copolymerization.

Table 5.2 Characteristics of the PAAc-g-FPI Copolymers and the Nanoporous FPI Films

FPI Samples	PAAc-g-FPI Copolymer			FPI and Nanoporous FPI Films		
	Monomer Molar Feed Ratio [AAc]/[FPI]	Bulk Graft Concentration[a] [PAAc]/[FPI]	Glass Transition Temperature (T_g) (°C)	Density (g/cm^3)	Porosity	Dielectric Constant (at 1 MHz)
Pristine FPI	---	---	293	1.47	---	3.1
PAAc-g-FPI Copolymer	12	0.68	290	1.43	3%	2.8
PAAc-g-FPI Copolymer	35	0.99	287	1.40	5%	2.6
PAAc-g-FPI Copolymer	47	1.58	286	1.38	6%	2.2
PAAc-g-FPI Copolymer	58	1.67	284	1.36	8%	1.9

[a] Defined as the number of repeat units of the graft chain per repeat unit of the FPI main chain and determined from the elemental C and N composition.

The thermal properties of the graft copolymers were studied by thermogravimetric (TG) analysis and differential scanning calorimetry (DSC). Figure 5.7 shows the TG analysis curves of the pristine FPI (Curve 1) in nitrogen, the PAAc-*g*-FPI copolymers with graft concentrations of 0.68 and 1.67 (Curves 2 and 3, respectively) in nitrogen, and the AAc homopolymer (PAAc) in nitrogen and in air (Curves 4 and 5, respectively). The PAAc have a thermal decomposition temperature of about 280°C in an inert atmosphere and only about 200°C in air. The pristine FPI homopolymer has a decomposition temperature of about 560°C in nitrogen and 544°C in air (Vora et al., 2001). On the other hand, however, the copolymer samples exhibit intermediate weight loss behavior and undergo a two-step degradation. The onset of the first major weight loss at about 280°C corresponds to the decomposition of the PAAc side chains in the copolymers. The second major weight loss begins at about 560°C, which coincides with the decomposition temperature of the FPI main chain. The TG analysis curves also indicate that the extent of weight loss of the copolymers during the first stage of thermal decomposition is approximately equal to the AAc polymer content in the respective graft copolymer. The relative small weight loss of the copolymers during the first stage of thermal decomposition is consistent with the fact that the molecular weight of the AAc repeat unit is much lower than that of the FPI repeat unit. Table 5.2 also shows the glass transition temperature (T_g), measured by DSC in nitrogen, of the pristine FPI and the PAAc-g-FPI copolymers of different graft concentrations. The pristine FPI has a T_g of about 293°C. Graft copolymerization with AAc reduces the structural rigidity and increases the molar free volume of the FPI. As a result, the T_g of the graft copolymer decreases with the increase in graft concentration.

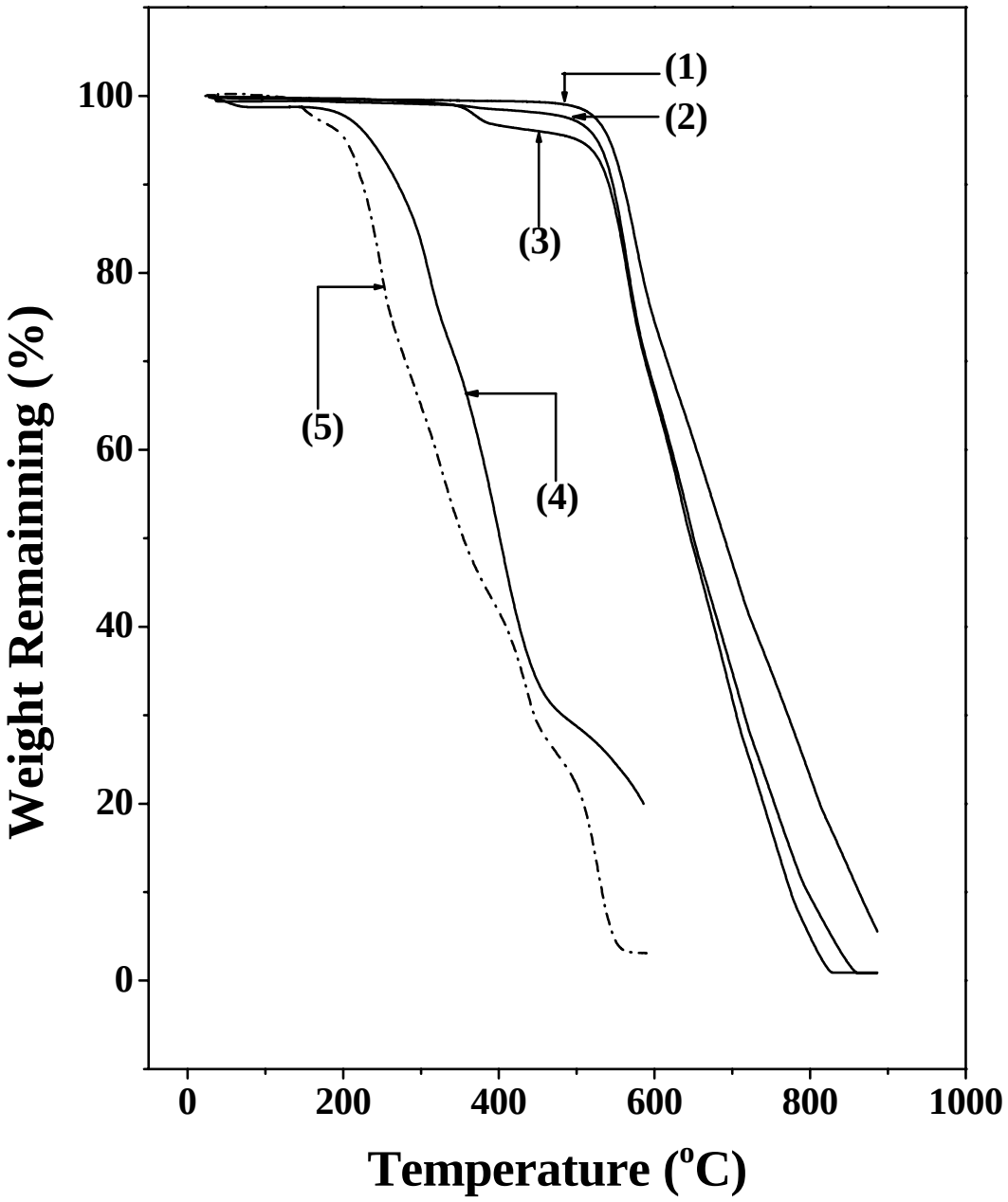

Figure 5.7 TG analysis curves of: (1) the FPI homopolymer, the PAAc-*g*-FPI copolymers with graft concentrations of (2) $([PAAc]/[FPI])_{bulk}$=0.68, (3) $([PAAc]/[FPI])_{bulk}$=1.67, and the AAc homopolymer (4) in nitrogen and (5) in air.

5.2.2.2 Characterization of the Nanoporous Films

The generation of nanoporous FPI film was accomplished by subjecting the copolymer film to thermal treatment in air to decompose the labile PAAc side chains. The copolymers films were heated first at 225°C for 5 h under argon to remove the NMP solvent. Under vacuum or in an inert atmosphere, PAAc are thermally stable up to about 280°C. This thermal stability allows the completely removal of the NMP solvent in an inert atmosphere without any appreciable decomposition of the graft chains. TGA results indicate that the decomposition of PAAc starts at only about 200°C in air. Thus, the formation of the nanoporous FPI structure can be accomplished by the subsequent heat treatment of the film at 250°C in air for 14 h to decompose the PAAc side chains. The selection of the thermal decomposition temperature and conditions is important. The temperature should be sufficiently high to quantitatively decompose the labile side chains, yet below the T_g of the FPI (or the graft copolymer) to avoid the collapse of the porous structure. The FPI has a T_g of 293°C and all the PAAc-*g*-FPI copolymers used in this study have T_g's above 280°C (Table 5.2). Finally, the FT-IR spectra of the nanoporous FPI films are almost identical to that of the pristine FPI film, indicating that the FPI backbones remain intact during the thermal decomposition of the PAAc side chains.

Figures 5.8 show the SEM images (cross-sectional view, magnification=50,000×) of the PAAc-*g*-FPI copolymer film (graft concentration=0.68) before (part 3(a)) and after (part 3(b)) thermal treatment at 250°C in air. The SEM image in Figure 3(b) reveals the formation of randomly distributed nano-pores in the FPI matrix. The dark areas are the voids left behind by the degraded PAAc phase. The irregularly shaped pores have sizes substantially below 100 nm.

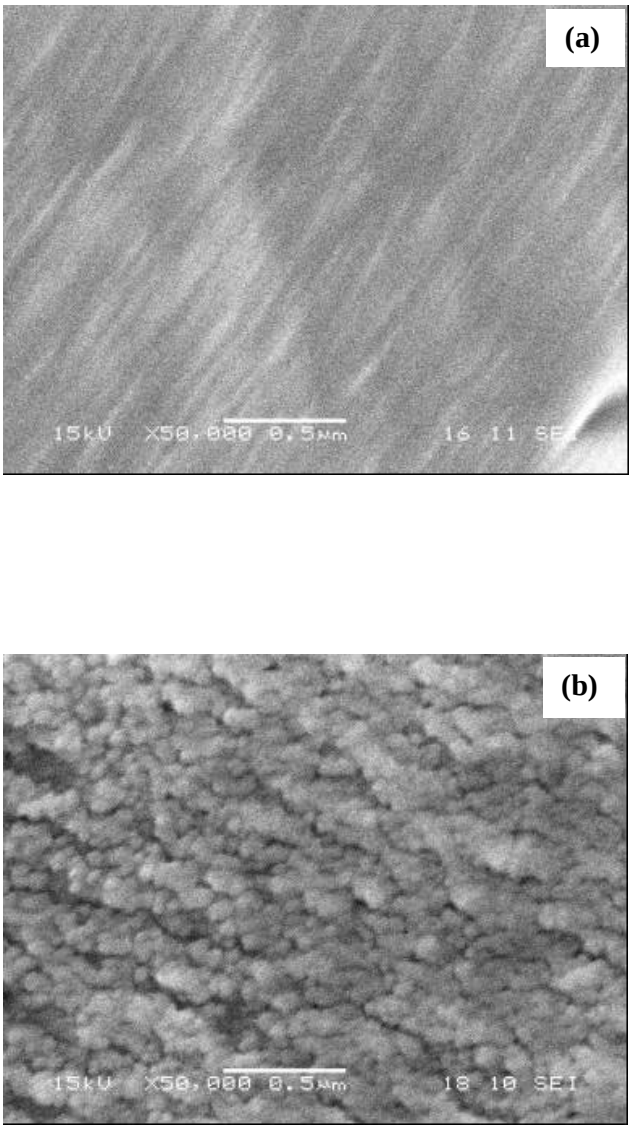

Figure 5.8 SEM cross-sectional images of the PAAc-*g*-FPI copolymer film (bulk graft concentration=0.68), (a) before and (b) after thermal treatment in air at 250°C for 14 h to form the nanoporous structure.

Density measurements were used to characterize the porosity of the films. As shown in Table 5.2, the density of the nanoporous FPI films prepared from the PAAc-*g*-FPI copolymers decreases from 1.47 to 1.36, as the porosity increases to 8%. The porosity of the nanoporous FPI films increase with the increase in the graft concentration of the PAAc-*g*-FPI copolymers. However, further increase in graft concentration to above 2.0, and thus the resulting porosity to above 15%, is accompanied by a marked deterioration in mechanical properties of the film, for example, a more than 50% decrease in tensile strength.

The dielectric constant of the resulting nanoporous FPI film is governed by the intrinsic dielectric constant of the FPI matrix and the morphology (porosity) of the porous structure. Table 5.2 shows the dependence of the dielectric constant (at 1 MHz) of the nanoporous FPI film on the porosity of the film. The dielectric constant of the pristine FPI film is about 3.1 under ambient conditions. As anticipated, all the nanoporous FPI films exhibit considerably lower dielectric constants and the dielectric constant decreases with the increase in porosity. A dielectric constant of about 1.9 is obtained for the nanoporous FPI film prepared from the PAAc-*g*-FPI copolymer with an initial bulk graft concentration of about 1.67 and a final porosity of about 8%. This dielectric constant is even lower than that of the poly(tetrafluoroethylene) film (κ~2.1) (Kang and Zhang, 2000). Graft copolymerization with AAc reduces the structural rigidity and the intermolecular packing density of the FPI chains and, thus, increases the molar free volume of the polymer. As a result, the dielectric constant decreases significantly, especially, after the decomposition of the grafted AAc side chains to form the nano-voids.

5.2.3 Conclusion

Nanoporous low-κ FPI films (with $\kappa < 2$) were obtained by thermal decomposition of the grafted AAc side chains on the FPI backbones in air. SEM images revealed that the pore size was in the range of 30-100 nm. The dielectric constant of the nanoporous FPI film can be varied by varying the graft concentration of the labile side chains. Dielectric constant as low as 1.9 was obtained for the resulting nanoporous FPI films. Thus, molecular modification by grafting of thermally labile side chains is a relatively simple and effective approach to the preparation of nanoporous FPI films with low dielectric constants and a well preserved FPI backbone structure.

CHAPTER 6

STIMULI-SENSITIVE FLUORINATED POLYIMIDE MEMBRANES WITH GRAFTED POLYMER SIDE CHAINS

6.1 pH-Sensitive Fluorinated Polyimides with Grafted Acid and Base Side Chains

6.1.1 Experimental

6.1.1.1 Materials

The fluorinated polyimide (FPIs) used in this study was 2,2-bis(3,4-dicarboxyphenyl) hexafluoropropane dianhydride and 4,4'-bis(4-aminophenoxy) diphenyl sulfone (6FDA+p-SED). The structure of the FPI was shown in Section 3.1.1.2 (FPI-2). Acrylic acid (AAc) and 4-vinylpyridine (4VP) monomers were obtained from Aldrich Chemical Co. and were purified by vacuum distillation before use.

6.1.1.2 Ozone Treatment of FPI

The procedure for ozone treatment of FPI was the same as that described in Section 5.2.1.2. After the ozone treatment, the polymer solution was cooled in an ice bath. The polymer solution was poured into an excess volume of ethanol to obtain the solid polymer precipitate.

6.1.1.3 Determination of Peroxides Concentration by Reaction with DPPH

About 100 mg of the ozone-treated FPI sample was dissolved in 10 ml of NMP, containing 6 mg of 2,2-diphenyl-1-picrylhydrazyl (DPPH). The solution was purged with purified argon for about 45 min. The reaction mixture was then placed in a thermostated oil bath at 110°C for 30 min, followed by cooling in an ice bath. The ozone-activated FPI was precipitated in 90 ml of pure isopropanol. After 30 min, the solution was filtered and the residual DPPH concentration was determined from the absorption intensity at 520 nm by UV-visible absorption spectroscopy. A calibration curve was obtained using DPPH solutions of known concentrations. The peroxide and hydroperoxide content was equal to half of the concentration of the reacted DPPH

radicals since each peroxide and hydroperoxide group gives rise to two free radicals upon decomposition. The number of moles of peroxides (including hydroperoxides) per gram of the ozone-treated FPI can be determined from the following equation (Fargere et al., 1994):

$$[\text{Peroxides}] = [(C_{\circ} - C) \times 100]/(2 \times 1000 \times 394.33 \times m)$$

where $C_{\circ}$ and C are the initial and final DPPH concentrations in g/L, respectively, and m is the weight of the ozone-treated FPI sample in gram. The factor 394.33 arises from the molecular weight of DPPH.

6.1.1.4 Graft Copolymerization of AAc and 4VP with FPI: The PAAc-*g*-FPI and P4VP-*g*-FPI Copolymers

The functional copolymer was prepared by thermally-induced molecular graft copolymerization of AAc or 4VP with the ozone pre-activated FPI in NMP solution at 60°C for 3 h and under an argon atmosphere. The procedures of grafting copolymerization were the same as those described in Section 5.2.1.3.

6.1.1.5 Preparation of Microfiltration (MF) Membranes

MF membranes were prepared by phase inversion in aqueous media. The FPI homopolymer or the copolymer powders were dissolved in NMP at room temperature. The polymer or copolymer solution was cast onto a glass plate. After allowing exposure in air for a brief period of time, the glass plate was immersed in the casting bath. The temperature of the aqueous medium in the casting bath was maintained at 25°C. Each membrane was left in the bath for about 20 min after separation from the glass plate. It was then extracted in a second bath of double-distilled water at 70°C for 30 min. Such a heat treatment was commonly performed during the fabrication of

commercial membranes in order to refine the pore size distribution (Strathmann and Kock, 1977). The purified membranes were dried under reduced pressure for subsequent characterization. The processes of ozone preactivation, thermally induced graft copolymerization, and MF membrane preparation are illustrated schematically in Figure 6.1.

6.1.1.6 Gel Permeation Chromatography (GPC)

The molecular weight of the FPI homopolymer and the ozone-treated FPI samples was measured by gel permeation chromatograph (GPC) on a Hewlett Packard MSD series 1100 high pressure liquid chromatograph (HPLC), equipped with a PL-gel Mixed-C column. Tetrahydrofuran (THF) was used as the eluent at a flow rate of 1.0 ml/min at 25°C. The molecular weight calibration was carried out using the polystyrene (PS) standards.

6.1.1.7 Fourier Transform Infrared Spectroscopy (FTIR) Measurements

FTIR spectra of thin copolymer films cast from tetrahydrofuran (THF) solutions were obtained on a Bio-Rad FTIR spectrophotometer (Model FTS135) under ambient conditions. Typically, 16 scans at a resolution of 8 cm^{-1} were accumulated to obtain one spectrum.

6.1.1.8 Thermal Analyses

The thermal properties of the homopolymer and copolymer samples were measured by both thermogravimetric (TG) analysis and differential scanning calorimetry (DSC). The procedures were the same as those described in Section 5.1.1.6.

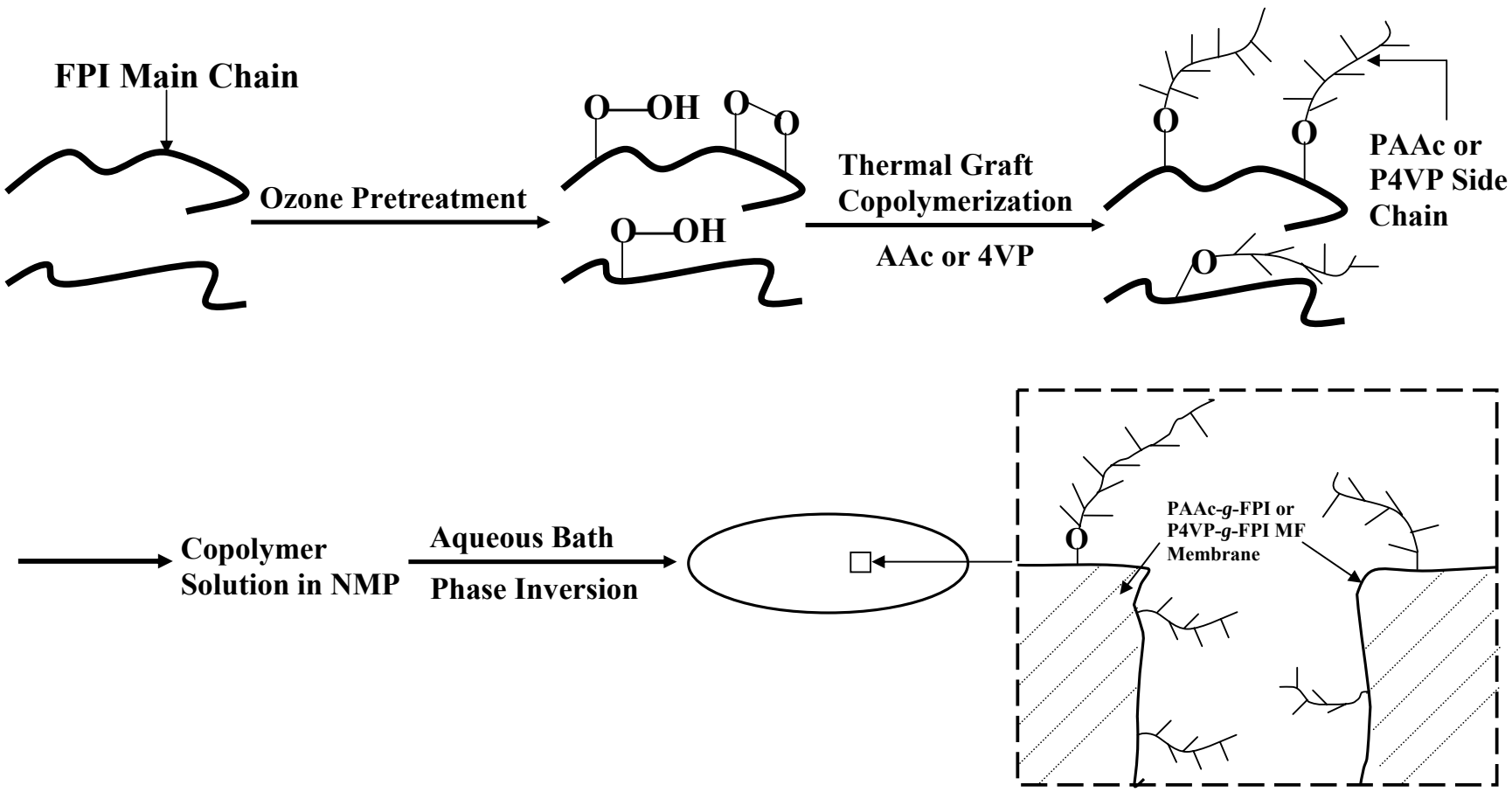

Figure 6.1 Schematic illustration of the processes of thermally-induced graft copolymerization of AAc and 4VP with the ozone-preactivated FPI backbone and the preparation of the PAAc-*g*-FPI and P4VP-*g*-FPI MF membranes by phase inversion.

6.1.1.9 Elemental Analysis

The carbon, nitrogen, hydrogen and fluorine elemental contents of the pristine FPI and the PAAc-*g*-FPI and P4VP-*g*-FPI copolymer samples were determined using the same procedures as those described in Section 5.2.1.5.

6.1.1.10 XPS Measurements

The surface composition of the samples was determined by X-ray photoelectron spectroscopy (XPS), the procedures were the same as those described in Section 3.1.9.

6.1.1.11 Water Contact Angle Measurements

Static water contact angles of the pristine FPI, the ozone-treated FPI, the PAAc-*g*-FPI and the P4VP-*g*-FPI films cast from THF solutions were measured at 25°C and 50% relatively humidity by the sessile drop method, using a 3 μL water droplet in a telescopic goniometer (Model 100-00-230, Rame-Hart, Mountain Lakes, NY, USA). The telescope with a magnification power of 23 was equipped with a protractor of 1 degree graduation. For each sample, at least five measurements on different surface locations were averaged. The angles reported were reliable to ±3°.

6.1.1.12 Morphology and Pore Size of the MF Membranes

The surface morphology of the MF membranes was studied by scanning electron microscopy (SEM), using a JEOL 6320 electron microscope. The procedures were same as described in Section 5.1.1.7. The pore sizes of the PAAc-*g*-FPI and the P4VP-*g*-FPI membranes were measured using a Coulter® Porometer II apparatus, manufactured by Coulter Electronics Ltd., UK. 'POROFIL' (the pore wetting liquid for the Coulter® Porometer instrument) was used as the wetting agent.

6.1.1.13 Measurements of the pH-Dependent Solution Flux Through the MF Membranes

The PAAc-*g*-FPI or P4VP-*g*-FPI MF membrane was preconditioned by immersing in an aqueous solution of a prescribed pH value prior to being mounted on the microfiltration cell (Toyo Roshi UHP-25, Tokyo, Japan). An aqueous solution of the same prescribed pH value and a fixed ionic strength (I =0.2 mol/L) was added to the cell. The ionic strength of the solution was kept constant by the addition of acetic acid and sodium acetate. The flux was calculated from the weight of solution permeated per unit time and per unit area of the membrane surface under a fixed N_2 pressure head of 0.4 kg/cm^2.

6.1.2 Results and Discussion

6.1.2.1 Ozone Pretreatment of the FPI in NMP Solution

Ozone treatment has been widely utilized to generate peroxide and hydroperoxide species on polymer chains and surfaces (Boutevin et al., 2002; Fujimoto et al., 1993). Under thermal induction, these labile functional groups undergo decomposition to initiate the free radical graft copolymerization of vinyl monomers. The amount of peroxides introduced by ozone treatment can be regulated by the polymer concentration, ozone treatment temperature, ozone concentration and ozone treatment time. In this study, the ozone concentration was fixed at 0.027 g/L under an O_3/O_2 mixture flow rate of 300 L/h and a temperature of 25°C. The peroxide contents of the ozone-treated FPI samples, in mol per gram of the activated FPI and determined from the DPPH assay, are shown in Table 6.1. It can be seen that the peroxide concentration increases with the increase in ozone treatment time. A 5 min ozone treatment time under the present experimental conditions could lead to a peroxide content of about 1.3×10^{-5} mol per gram of FPI. The increase in the peroxide concentration is also consistent with the corresponding increase in the elemental [O]/[C] ratio, as determined from the O 1s and C 1s XPS core-level spectral area ratio of the samples. Ozone treatment can also introduce other polar groups, such as carbonyl and hydroxyl groups, into the polymer chains. The water contact angle data suggest that the film cast from the ozone-treated FPI were less hydrophobic than that cast from the pristine FPI. Since ozone treatment of the FPI is also accompanied by degradation and scission of the polymer chains, as indicated by the decrease in molecular weight of the polymer (Table 6.1), the ozone pretreatment time is fixed at 5 min in the present study.

Table 6.1 Peroxide Content, Water Contact Angle and Molecular Weight of the Pristine and Ozone-treated FPI

FPI Samples	Peroxides Content[a)] (mol/g of FPI)	Molecular Weight[b)]	Water Contact Angle[c)] (± 3°)	[O]/[C] Ratio[d)]
Pristine FPI film	----	1.79×10^{5}	88	0.148
2-min Ozone-treated FPI	0.7×10^{-5}	1.70×10^{5}	83	0.151
5-min Ozone-treated FPI	1.30×10^{-5}	1.56×10^{5}	78	0.158
15-min Ozone-treated FPI	1.42×10^{-5}	1.11×10^{5}	71	0.159
30-min Ozone-treated FPI	1.45×10^{-5}	9.75×10^{4}	62	0.160
45-min Ozone-treated FPI	1.72×10^{-5}	8.23×10^{4}	58	0.170
60-min Ozone-treated FPI	1.75×10^{-5}	7.93×10^{4}	51	0.174

[a.] Determined from reaction with DPPH.
[b.] Determined by GPC.
[c.] The films were cast from THF solutions.
[d.] Determined from the corrected O 1s and C 1s XPS core-level spectral area ratio of the respective sample.

6.1.2.2 Bulk Graft Concentrations of the PAAc-*g*-FPI and P4VP-*g*-FPI Copolymers

For the graft copolymerization of AAc and 4VP with FPI in solution, the monomer feed ratio can be used to regulate the graft concentration of the resulting graft copolymer. Elemental analysis was employed to determine the bulk content of elemental carbon and nitrogen. The bulk graft concentration of the copolymers is defined as the number of AAc or 4VP repeat units in the graft chains per repeat unit of the FPI main chain. In the case of the PAAc-*g*-FPI copolymer, the $([C]/[N])_{bulk}$ ratio increases with the AAc monomer feed ratio. The bulk graft concentration can be calculated from the $([C]/[N])_{bulk}$ molar ratio by taking into account of the carbon stoichiometries of the graft and the main chains, and the carbon to nitrogen ratio of the FPI main chain. Thus, the bulk graft concentration or the $([PAAc]/[FPI])_{bulk}$ molar ratio can be calculated from the following relationship:

$$([PAAc]/[FPI])_{bulk} = 2([C]- (43/2)[N])_{bulk}/3[N]_{bulk}$$

in which the factor 43/2 accounts for the fact that there are 43 carbon atoms and 2 nitrogen atoms per repeat unit of the FPI chains, while the factor 3 accounts for the fact that there are 3 carbon atoms in each AAc unit.

In the case of the P4VP-*g*-FPI copolymer, the $([N]/[F])_{bulk}$ ratio increases with the 4VP monomer feed ratio. The bulk graft concentration can be calculated from the $([N]/[F])_{bulk}$ molar ratio by taking into account of the nitrogen stoichiometries of the graft and the main chains, and the nitrogen to fluorine ratio of the FPI main chain. Thus, the graft concentration or the $([P4VP]/[FPI])_{bulk}$ molar ratio can be calculated from the following relationship:

$$([P4VP]/[FPI])_{bulk} = 6([N]-[F]/3)_{bulk}/[F]_{bulk}$$

in which the factor 3 accounts for the fact that there are 2 nitrogen atoms and 6 fluorine atoms per repeat unit of the FPI chains.

For graft copolymerization, the monomer feed ratio is an important parameter that can be used to regulate the graft concentration. Figure 6.2 shows the dependence of the bulk graft concentration of the PAAc-*g*-FPI copolymer (part (a)) and the P4VP-*g*-FPI copolymer (part (b)) on the respective monomer to [FPI] molar feed ratio used for graft copolymerization. For both copolymers, the graft concentration increases with increasing monomer concentration used for graft copolymerization.

6.1.2.3 FTIR Spectroscopy of the PAAc-*g*-FPI and P4VP-*g*-FPI Copolymers

The chemical structures of the FPI and the PAAc-*g*-FPI and P4VP-*g*-FPI copolymers were first studied by FTIR spectroscopy. The absorption bands associated with the imide ring and linkage of FPI at 1730 cm^{-1} (symmetrical C=O stretching), 1376 cm^{-1} (C-N stretching), and 1063 cm^{-1} and 744 cm^{-1} (imide ring stretching) are present in all the copolymer samples (Vora et al., 2001). Comparing the FTIR spectra of the PAAc-g-FPI copolymers with that of the pristine FPI, the absorption band of the copolymer samples at 1718 cm^{-1}, attributable to the O-C=O stretching vibration, must be associated with the grafted AAc chains (Moharram et al., 2002). Since the concentration of a functional group is directly proportional to the absorption band area in the FTIR spectrum, the ratio of the absorption band area at 1718 cm^{-1} to those at 1376 cm^{-1} and 1063 cm^{-1} (the characteristic absorption bands of the FPI) is directly related to the bulk graft concentration of the AAc side chains in the corresponding

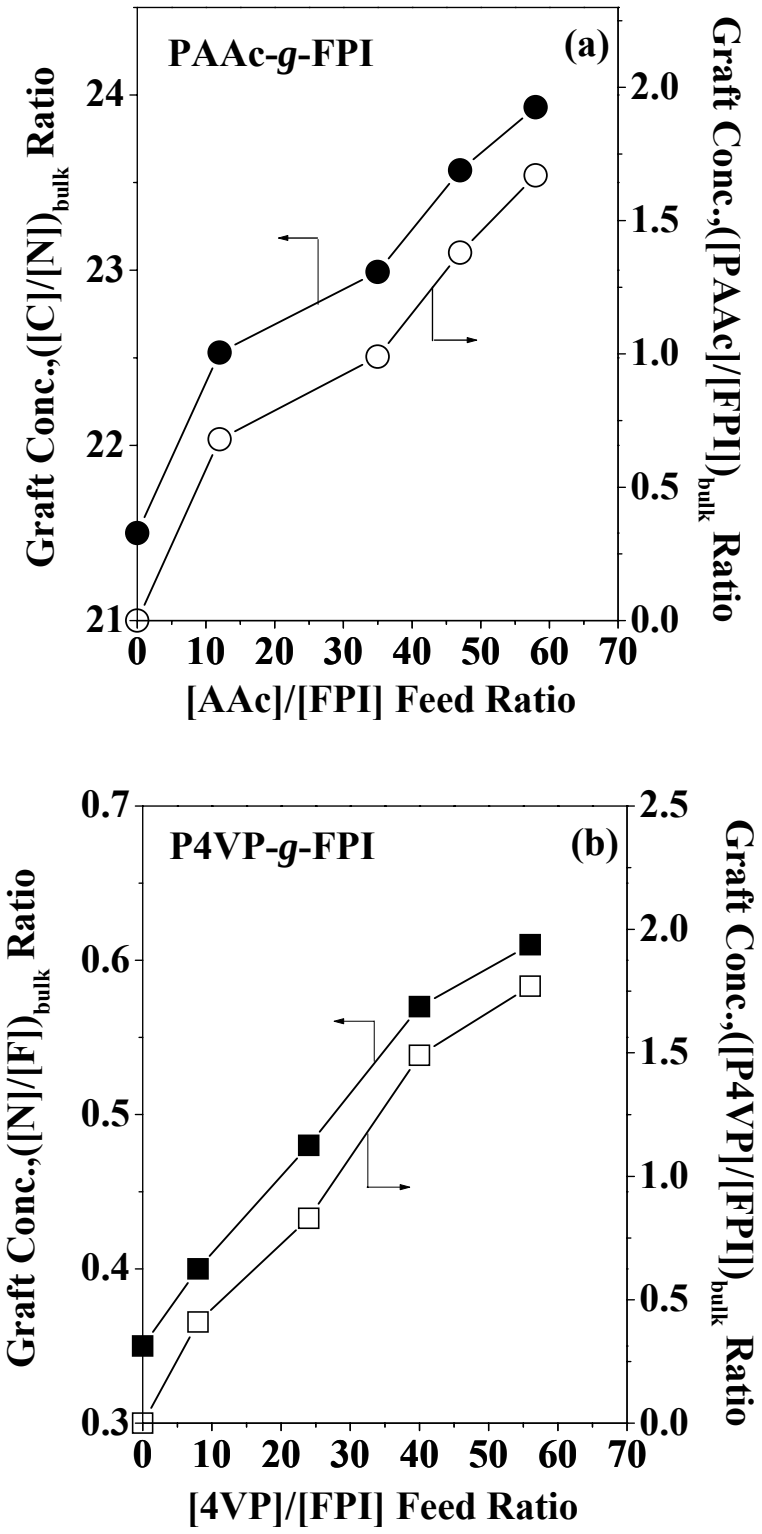

Figure 6.2 Effect of monomer molar feed ratio on the bulk graft concentration of (a) the PAAc-*g*-FPI copolymers and (b) the P4VP-*g*-FPI copolymers.

AAc-*g*-FPI copolymer. In the case of the P4VP-*g*-FPI copolymers, a new absorption band at 1410 cm^{-1}, attributable to the pyridine ring group, is discernable. The intensities of the absorption bands at 1730 and 1410 cm^{-1} increase with the increase in the respective AAc to FPI and 4VP to FPI monomer feed ratio. Therefore, the FTIR data suggest that the graft concentration increases with the increase in the AAc or 4VP monomer to FPI molar feed ratio used for graft copolymerization. This result is in good agreement with that obtained from the elemental analysis.

6.1.2.4 Thermal Stability of the PAAc-*g*-FPI or P4VP-*g*-FPI Copolymers

Figure 6.3 shows the respective TG analysis curves of the pristine FPI (Curve 1), the PAAc-*g*-FPI and P4VP-*g*-FPI copolymers of different graft concentrations (Curves 2 to 5), the AAc homopolymer (Curve 6) and the 4VP homopolymer (Curve 7). In comparison with the pristine FPI, AAc and 4VP homopolymers, the copolymer samples exhibit an intermediate weight loss behavior and undergo a two-step degradation process. The onset of the first major weight loss occurs at the temperature which corresponds to the decomposition of the PAAc or the P4VP segments in the copolymers. The second major weight loss begins at about 560°C, which coincides with the decomposition temperature of the FPI main chain. The TG analysis curves also indicate that the extent of weight loss of copolymers during the first stage of thermal decomposition is approximately equal to the AAc or 4VP polymer content in the respective graft copolymer. The relative smaller weight loss of the copolymers during the first stage of thermal decomposition is consistent with the fact that the molecular weight of the FPI repeat unit is substantially higher than that of the AAc or 4VP repeat unit. Furthermore, the fact that the temperature for the onset of the major weight loss in the copolymer is substantial high than the decomposition temperature of the PAAc or P4VP homopolymer suggests that the graft chains have been stabilized

through covalent bonding to the FPI backbones. They may also have been partially imidized into the FPI structure at elevated temperatures.

Table 6.2 shows the glass transition temperature (T_g), obtained from DSC, of the pristine FPI and the PAAc-*g*-FPI and P4VP-*g*-FPI copolymers of different graft concentrations. In the present study, the pristine FPI has a T_g of about 284°C. Graft copolymerization with AAc or 4VP reduces structural rigidity of the FPI and increases the molar free volume of the polymer, resulting in the lowering of T_g. It can also be seen in Table 6.2 that the T_g of the graft copolymer decreases with the increase in graft concentration. Only the T_g of the FPI backbone is discernible in the DSC curves of the graft copolymers. This phenomenon is probably associated with the fact that FPI is the major phase in each copolymer, arising from the large disparity in molecular sizes between the FPI and the AAc (or 4VP) repeat units.

6.1.2.5 Water Contact Angles of the PAAc-*g*-FPI and P4VP-*g*-FPI Copolymer Films

The pristine FPI film is hydrophobic, with a water contact angle of about 88°. A substantial decrease in water contact angle of the FPI films is achieved through graft copolymerization with AAc or 4VP. The contact angle is reduced to about 60° for copolymer films with $([PAAc]/[FPI])_{bulk}$=1.67 or $([P4VP]/[FPI])_{bulk}$=1.77 (Table 6.2). This phenomenon is attributable to the hydrophilic nature of the grafted AAc or 4VP polymer side chains. Thus, as shown in Table 6.2, the water contact angle of the PAAc-*g*-FPI or P4VP-*g*-FPI films decreases with the increase in the AAc or 4VP polymer graft concentration.

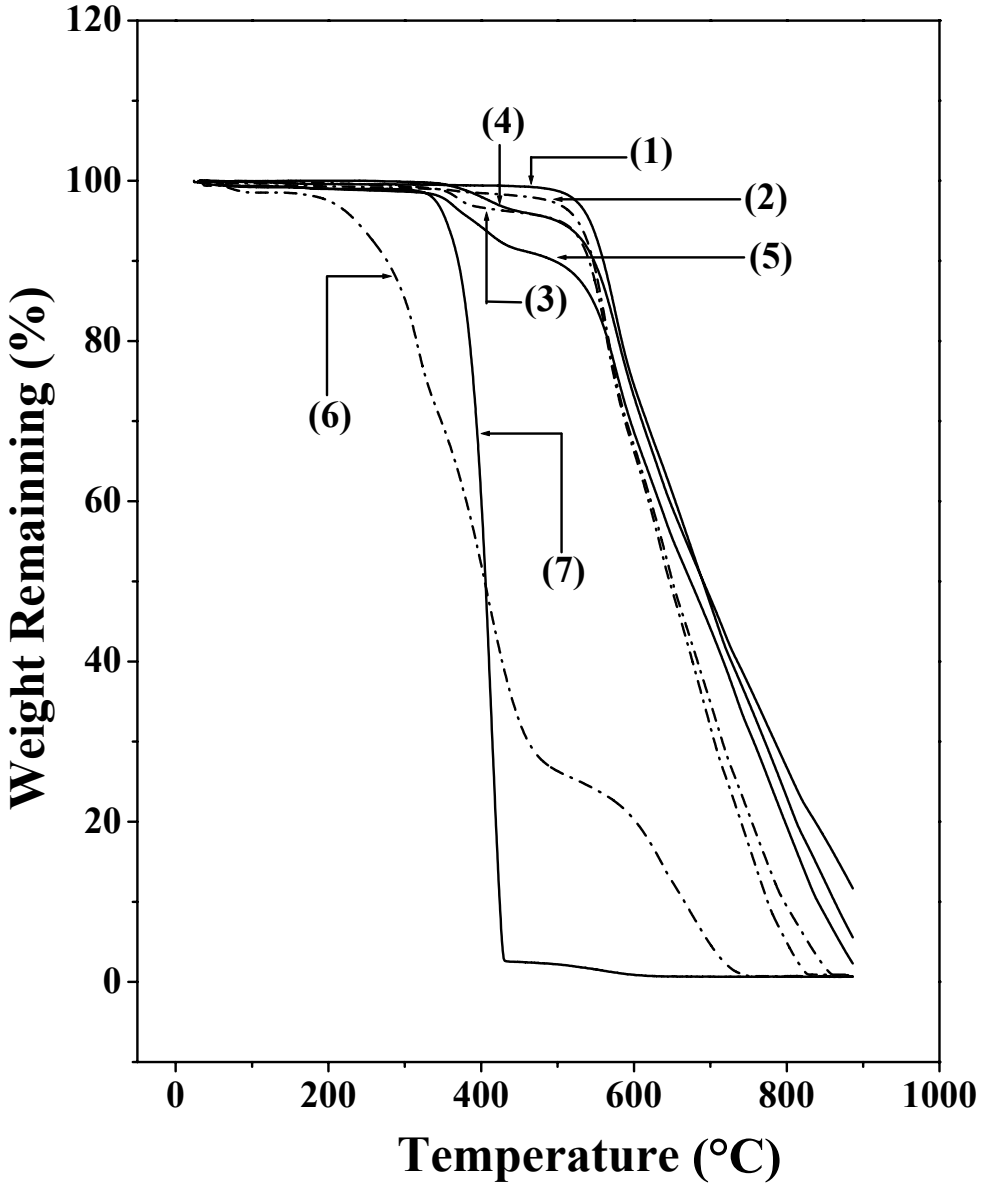

Figure 6.3 TG analysis curves of: (1) the FPI homopolymer, the PAAc-*g*-FPI copolymers with graft concentrations of (2) $([PAAc]/[FPI])_{bulk}$=0.68, (3) $([PAAc]/[FPI])_{bulk}$=1.67, the P4VP-*g*-FPI copolymers with graft concentration of (4) $([P4VP]/[FPI])_{bulk}$=0.41, (5) $([P4VP]/[FPI])_{bulk}$=1.77, (6) the AAc homopolymer and (7) the 4VP homopolymer.

Table 6.2 Physicochemical Properties of the FPI, PAAc-*g*-FPI and P4VP-*g*-FPI Copolymers

FPI Samples	Molar Feed Ratio [AAc]/[FPI] or [4VP]/[FPI]	Graft Concentration $([PAAc]/[FPI])_{bulk}$ or $([P4VP]/[FPI])_{bulk}$	Grafted Chain Length $(\overline{DP})$ [a)]	Molecular Weight of the Grafted Chain	Glass Transition Temperature (T_g)[b)] (°C)	Water Contact Angle[c)] (± 3°)
1. Pristine FPI	---	---	---	---	293	88
2. PAAc-*g*-FPI Copolymer	12	0.68	62	4464	287	79
3. PAAc-*g*-FPI Copolymer	35	0.99	90	6480	282	67
4. PAAc-*g*-FPI Copolymer	47	1.38	126	9072	279	65
5. PAAc-*g*-FPI Copolymer	58	1.67	153	11016	276	63
6. P4VP-*g*-FPI Copolymer	8	0.41	37	3922	289	67
7. P4VP-*g*-FPI Copolymer	24	0.83	76	8056	285	63
8. P4VP-*g*-FPI Copolymer	40	1.49	136	14416	281	61
9. P4VP-*g*-FPI Copolymer	56	1.77	162	17172	277	59

[a.] Average degree of graft polymerization $(\overline{DP})$ was estimated from the peroxide concentration of the 5 min ozone-treated FPI and the graft concentration.
[b.] Determined by differential scanning calorimetry (DSC).
[c.] The films were cast from tetrahydrofuran (THF) solutions.

6.1.2.5 Surface Composition of the MF Membranes Prepared from the PAAc-*g*-FPI and P4VP-*g*-FPI Copolymers

After the PAAc-*g*-FPI and P4VP-*g*-FPI MF membranes had been fabricated by phase inversion in water (pH=6.4) and at room temperature from 10 wt% NMP solutions of the respective copolymers, the surface composition and morphology of the membranes were investigated by XPS.

Figure 6.4 shows the respective C 1s and N 1s core-level spectra of the pristine FPI membrane surface (part (a)), the PAAc-*g*-FPI membrane surfaces with bulk graft concentration of 0.68 and 1.67 (part (b) and part (c), respectively), and the P4VP-*g*-FPI membrane surfaces with bulk graft concentration of 0.83 and 1.49 (part (d) and part (e), respectively) . The C 1s core-level spectrum of the pristine FPI membrane can be curved-fitted with five peak components, having binding energies (BE's) at 284.6 eV for the C-H species, at 285.8 eV for the C-O and C-N species, at 288.4 eV for the $N(C=O)_2$ species, at 291.1 eV for the π-π^* shakeup satellite, and at 292.8 eV for the CF_3 species (Beamson and Briggs, 1992). The O-C=O species of the grafted PAAc polymer chains have a C 1s peak component BE at about 288.5 eV. The BE's of the O-C=O species and the imide –N-$(C=O)_2$ species cannot be resolved clearly. The two species are represented by a single peak component at the BE of about 288.4 eV. The increase in AAc polymer graft concentration with the AAc to FPI molar feed ratio is readily indicated by the steady increase in the intensity ratio of the O-C=O species to the CF_3 species.

The N 1s core-level spectrum of the pristine FPI membrane shows only one peak component at the BE of 400.5 eV, attributable to the $-N(C=O)_2$ (imide) species. The presence of the grafted 4VP polymer on FPI can be deduced from the N 1s peak

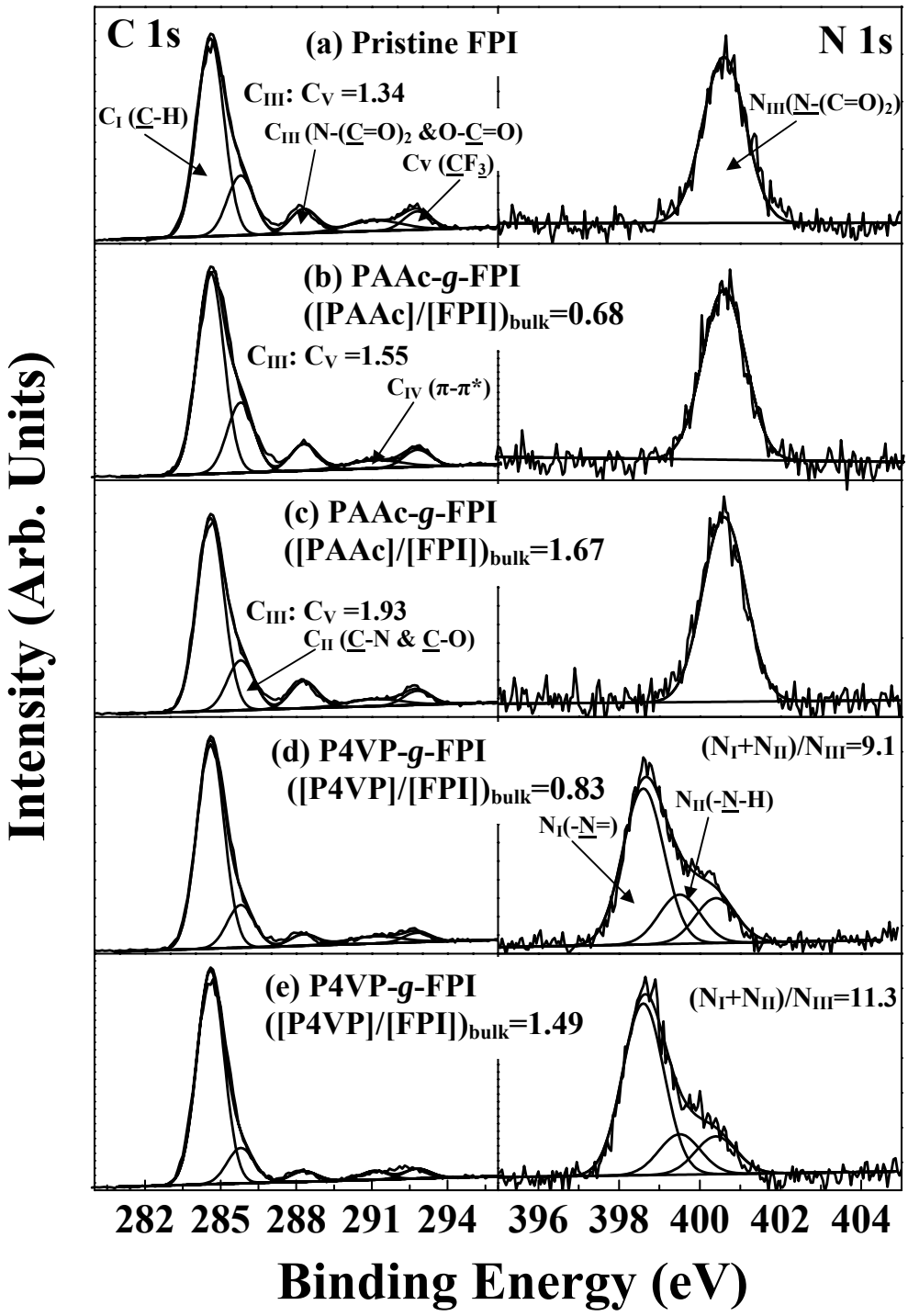

Figure 6.4 XPS C 1s and N 1s core-level spectra of (a) the pristine FPI membrane, the PAAc-*g*-FPI membranes with bulk graft concentrations of (b) 0.68 and (c) 1.67, and the P4VP-*g*-FPI membranes with bulk graft concentrations of (d) 0.83 and (e) 1.49 (Membranes cast by phase inversion in water (pH=6.4) at 25°C from 10 wt% NMP solutions).

component at the BE of 398.5 eV, attributable to the imine species (=N-) of the 4VP polymer (Zhang et al., 2001b). An additional peak component appears at the BE of about 399.5 eV, which may be attributed to the partially protonated or hydrogen-bonded nitrogen in the 4VP polymer. The formation of hydrogen bonding between poly(vinylpyridine)s and other polymers has been reported (Ruokolainen et al., 1998). The increase in graft concentration with the 4VP to FPI molar feed ratio is readily indicated by the steady increase in the ratio of the =N- and –N-H species to the –$N(C=O)_2$ species. Thus, the XPS results are in good agreement with those obtained from the elemental analysis and FTIR spectroscopy.

The surface graft concentrations of the PAAc-*g*-FPI and P4VP-*g*-FPI MF membranes were determined from the XPS derived carbon, nitrogen and fluorine atomic ratios. Figure 6.5 shows the dependence of the surface graft concentration of the PAAc-*g*-FPI MF membrane (part (a)) and P4VP-*g*-FPI MF membrane (part (b)) on the respective monomer to FPI molar feed ratio used for graft copolymerization. The surface graft concentration of each copolymer membrane increases almost linearly with the respective monomer to FPI molar feed ratio. Comparing the surface [C]/[N] and [N]/[F] ratios (determined by XPS) in Figure 6.5 with the bulk composition (determined by elemental analysis) in Figure 6.2, it is obvious that the surface [C]/[N] and [N]/[F] ratios, and thus the graft concentrations, are considerably higher than the corresponding bulk ratios. This phenomenon arises mainly from the enrichment of the AAc and 4VP side chains at the outermost surface during the course of membrane formation by phase inversion in the aqueous medium. For multicomponent polymer systems (including copolymers and polymer blends), surface enrichment of the hydrophilic components arising from interaction with the environments occurs readily (Hester et al.,1999; Chen and Hong, 2002).

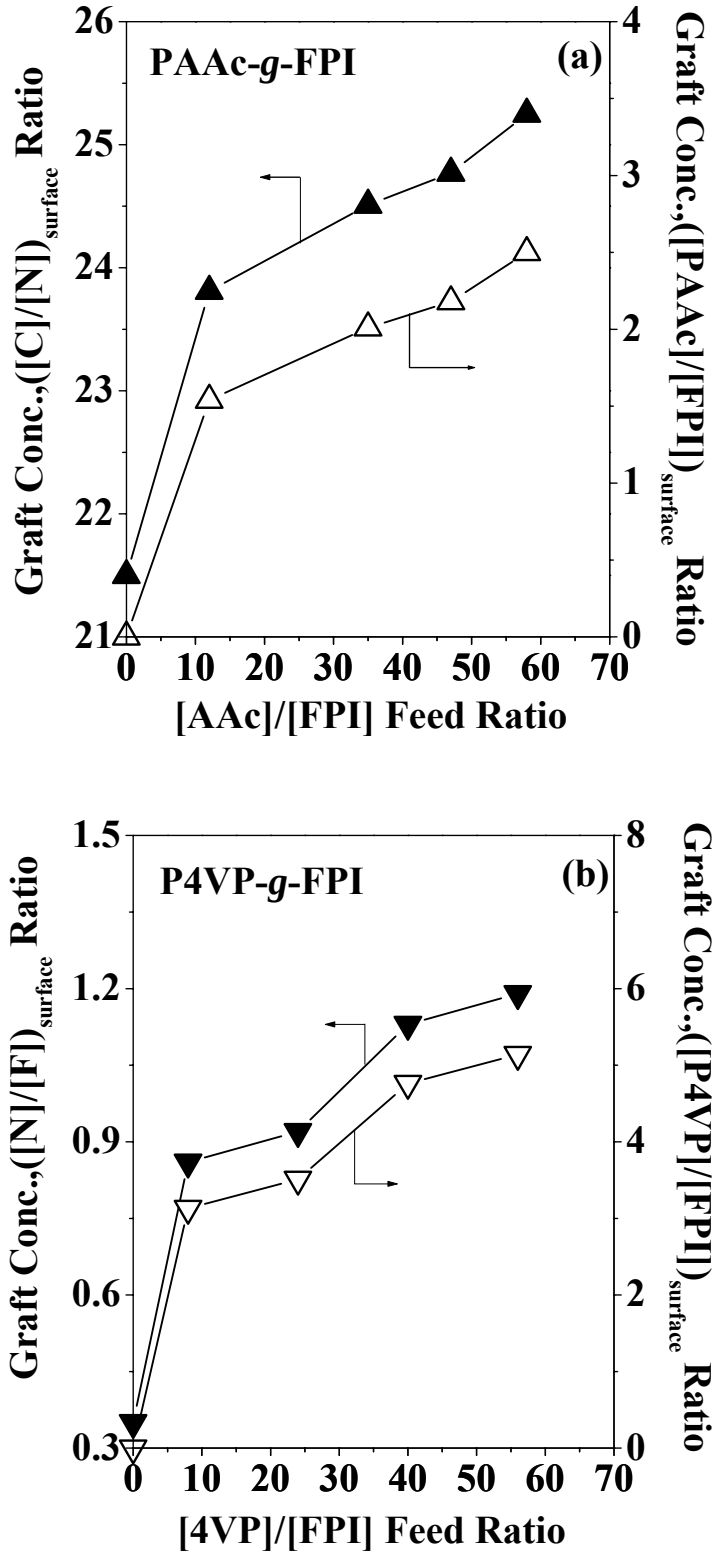

Figure 6.5 Effect of the monomer molar feed ratio on the surface graft concentration of (a) the PAAc-*g*-FPI MF membranes and (b) the P4VP-*g*-FPI MF membranes, cast at 25°C *via* phase inversion in water (pH=6.4) from 10 wt% NMP solutions.

6.1.2.6 Surface Morphology of the PAAc-*g*-FPI and P4VP-*g*-FPI MF Membranes

The surface morphology of the PAAc-*g*-FPI and P4VP-*g*-FPI MF membranes was studied by SEM at a magnification of 2000×. Figure 6.6 shows the SEM images of the respective MF membranes cast by phase inversion at 25°C in water from 10 wt% NMP solutions of the pristine FPI powders, the PAAc-*g*-FPI copolymers with bulk graft concentrations of 0.68, 1.38 and 1.67, and the P4VP-*g*-FPI copolymers with bulk graft concentrations of 0.41 and 1.49. The SEM images reveal that the membranes cast from the NMP solutions of the graft copolymers have a higher porosity than that cast from the pristine FPI, and that the porosity increases with the graft concentration of the AAc or 4VP polymer in the copolymer. In the presence of high concentrations of the hydrophilic AAc or 4VP polymer side chains, surface enrichment of the AAc or 4VP polymer takes place during phase inversion in water to maximize the interfacial interaction between the pore surface and water, resulting in an increase in porosity and pore size of the membrane. Since the interfacial interaction are dictated by the surface graft concentration of the AAc or 4VP polymer side chains, mass migration of the AAc or 4VP polymer side chains in the MF membrane with a high graft concentration readily give rise to larger pores or higher porosity during phase inversion.

6.1.2.7 Pore Sizes of the PAAc-*g*-FPI and P4VP-*g*-FPI MF Membranes

The mean pore size and pore size distributions of various PAAc-*g*-FPI and P4VP-*g*-FPI MF membranes cast from NMP solutions and under different conditions, such as different bulk graft concentrations, different copolymer concentrations of the cast solutions, and different pH values of the casting bath, were measured on the Coulter® Porometer II instrument, using the commercial 'POROFIL' fluid as the wetting agent. The pore size distributions of the PAAc-*g*-FPI and P4VP-*g*-FPI MF membranes cast

under different conditions are shown in Table 6.3. The data indicate that the mean pore size of the MF membrane increases with the graft concentration of the AAc or 4VP side chains in the copolymer.

The dependence of the pore sizes of the PAAc-*g*-FPI and P4VP-g-FPI MF membranes on the pH of the aqueous casting bath is also shown in Table 6.3. The pore size of the PAAc-*g*-FPI MF membrane decreases with the decrease in pH of the casting bath. Thus, a lower proton concentration of the casting bath will lead to a larger pore size. The phenomenon probably arises from the enhanced interaction of the carboxylic acid groups with the aqueous medium at a high pH to give rise to the extensive formation of the carboxylic anions (see below). On the other hand, however, the pore sizes of the P4VP-*g*-FPI MF membrane increase with the decreasing pH of the casting bath. The observation indicates that a high proton concentration in the casting bath will lead to a large pore size. The phenomenon probably arises from the interaction between the pyridine groups on the pore surfaces and the protons in the aqueous solution. The extent of protonation and hydrogen bonding of the pyridine ring is enhanced at a low pH of the casting bath. The pore sizes of the PAAc-*g*-FPI and P4VP-*g*-FPI MF membranes are also dependent on the concentrations of the copolymer in the casting solution, as shown in Table 6.3. The pore sizes decrease drastically with the increase in concentrations of the PAAc-*g*-FPI or P4VP-*g*-FPI copolymer in the casting solution. At low concentration, the extraction of the solvent from the bulk and at the copolymer/non-solvent interface is facilitated. As a result, larger pore sizes are obtained for the resulting MF membranes cast from the copolymer solutions of lower concentrations.

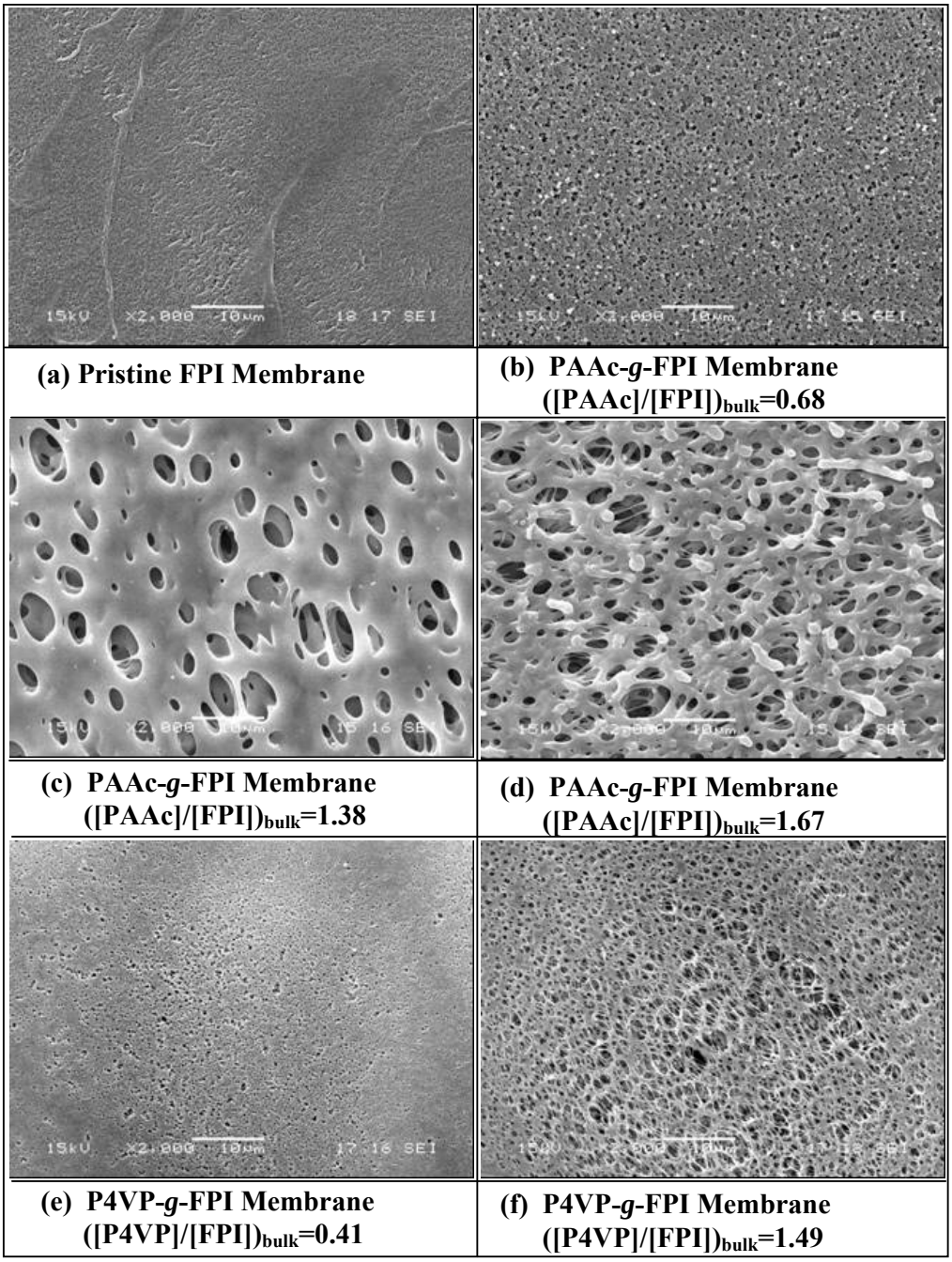

Figure 6.6 SEM images of the MF membranes cast at 25°C by phase inversion in water (pH=6.4) from 10 wt% NMP solutions of (a) the pristine FPI, the PAAc-*g*-FPI copolymers with bulk graft concentrations of (b) 0.68, (c) 1.38, (d) 1.67, and the P4VP-*g*-FPI copolymers with bulk graft concentrations of (e) 0.41 and (f) 1.49.

Table 6.3 Pore Size Distribution [a)] of the PAAc-*g*-FPI and the P4VP-*g*-FPI MF Membranes [b)]

(the data in bold and italic are for the P4VP-g-FPI copolymer)

Molar Feed Ratio	Bulk Graft Conc. of Copolymers	pH Value of Casting Bath	Concentration of Cast Solution (wt%)	Min. Pore Size (μm)	Max. Pore Size (μm)	Mean PoreSize (μm)
(a) Effect of Bulk Graft Conc. on the Pore-Size Distribution						
12/***8***	0.68/***0.41***	6.4	10	0.21/***0.25***	0.38/***0.72***	0.29/***0.29***
35/***24***	0.99/***0.83***	6.4	10	0.22/***0.24***	2.33/***1.98***	0.41/***0.43***
47/***40***	1.38/***1.49***	6.4	10	0.16/***0.29***	3.62/***3.49***	0.45/***0.63***
58/***56***	1.67/***1.77***	6.4	10	0.25/***0.20***	3.18/***4.19***	0.69/***0.82***
(b) Effect of pH Value of the Casting Bath on the Pore-Size Distribution						
35/***56***	0.99/***1.77***	4.9	12	0.31/***0.35***	2.33/***1.04***	0.38/***0.39***
35/***56***	0.99/***1.77***	3.1	12	0.18/***0.41***	0.64/***4.19***	0.28/***0.50***
35/***56***	0.99/***1.77***	2.0	12	0.22/***0.50***	1.72/***2.84***	0.27/***0.64***
35/***56***	0.99/***1.77***	1.0	12	0.18/***0.53***	1.13/***4.33***	0.25/***0.67***
(c) Effect of Solution Conc. on the Pore-Size Distribution						
12/***8***	0.68/***0.41***	6.4	7	0.37/***0.44***	2.17/***3.84***	0.77/***0.93***
12/***8***	0.68/***0.41***	6.4	10	0.21/***0.25***	0.38/***0.72***	0.29/***0.29***
12/***8***	0.68/***0.41***	6.4	15	0.12/***0.12***	0.35/***0.40***	0.16/***0.17***

a. These pore sizes were measured on the Coulter® Porometer II which utilized a liquid displacement technique.

b. Membranes were cast from NMP solutions of the PAAc-*g*-FPI and P4VP-*g*-FPI copolymers at 25°C in aqueous media. Porous membranes cannot be cast from the pristine FPI by the present phase inversion technique.

6.1.2.8 pH-Dependent Flux of Aqueous Solutions Through the PAAc-*g*-FPI and P4VP-*g*-FPI MF Membranes

The pH-dependent flux of aqueous solutions through the pristine FPI, the PAAc-*g*-FPI and the P4VP-*g*-FPI membranes is shown in Figure 6.7. It is clear that the permeability of aqueous solutions through the pristine FPI MF membranes is marginal and pH-independent (Curves 5). The low permeability arises from the low porosity of the membrane. On the other hand, however, the flux of the aqueous solution through the PAAc-*g*-FPI and P4VP-*g*-FPI MF membranes exhibits a pH-dependent behavior, but in an opposite or complementary manner. The permeation rate of the aqueous solution through the PAAc-*g*-FPI membrane decreases with the increase in pH of the solution from 0.5 to 6.4 (Curves 1 and 2), while the permeation rate of the aqueous solution through the P4VP-*g*-FPI membrane increases with the increase in solution pH from 0.5 to 6.4 (Curves 3 and 4), with the most drastic change in permeation rate being observed between pH 1 and 4. Furthermore, the pH-sensitivity of the flux through both types of membranes is enhanced by the increase in graft concentration. The pH-dependent flux of the aqueous solutions through the two types of membranes at pH between 0.5 and 6.4 are completely reversible. These results suggest that both the extent of interaction with the aqueous environment and the conformation of the graft chains vary, reversibly, with the pH of the solution to control the effective pore size of the membrane.

The change in permeability in response to the change in solution pH can be attributed to the change in conformations of the graft chains on the membrane surface, especially on the pore surfaces and in the sub-surface region of the pores. Due to the non-ionizablity of the polymer chains in the pristine FPI membranes, the polymer chain

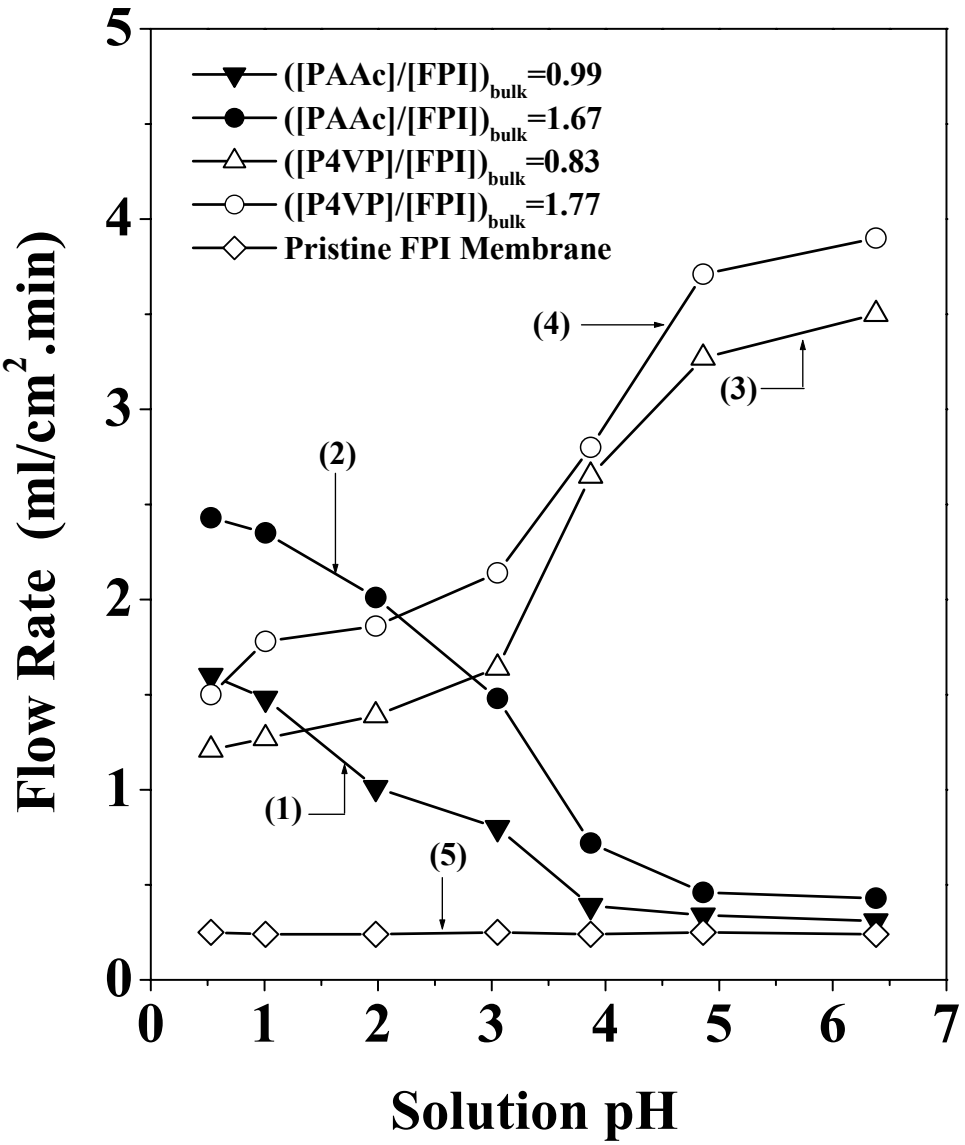

Figure 6.7 pH-dependent permeability of aqueous solutions through the pristine FPI, the PAAc-*g*-FPI and the P4VP-*g*-FPI MF membranes. Curves 1 and 2 are obtained from flux through the PAAc-*g*-FPI MF membranes with graft concentrations or $([PAAc]/[FPI])_{bulk}$=0.99 and 1.67, respectively. Curves 3 and 4 are obtained from flux through the P4VP-*g*-FPI MF membranes with graft concentrations or $([P4VP]/[FPI])_{bulk}$=0.83 and 1.77, respectively. Curve 5 is obtained from the flux through the pristine FPI membrane.

conformation and the membrane pore dimension will remain constant at all pH values. On the other hand, as a weak acid (pKa=4.3), the carboxylic groups of the grafted AAc polymer side chains can be ionized or deprotonated to become negatively charged.

With the increase in pH of the casting solution, most of the carboxylic groups are transformed into carboxylic anions. Strong electrostatic repulsion among the carboxylic anions, together with their strong interaction with the aqueous solution, forces the AAc polymer side chains to adopt a highly extended conformation. The extension of the AAc polymer side chains into the pores and in the sub-surface region of the pores reduces the effective dimension of the pores. As a result, the permeability of the aqueous solution through the MF membrane is reduced. On the other hand, the AAc polymer chains assume a coil or globule conformation under the low-pH conditions. As a result, steric obstruction to the pores of the membrane is substantially reduced and the permeation rate increases. This mechanism is termed the "through-pore mechanism" and has been studied by Israels et al. (Israels et al., 1994), using a two-dimensional self-consistent mean-field (SCF) theory.

On the other hand, as a weak base, the pyridine groups of the grafted 4VP side chains are protonated or become complexed in an acid solution. The resulting ionic character and the electrostatic repulsion among the positively charged pyridinium nitrogen atoms overcome the hydrophobic interactions among the alkyl segments of the chains. The uncoiling of the polymer side chains and their interactions with the aqueous solution at a low pH value lead to an extended conformation in the surface and sub-surface region of the pores. As a result, the effective pore dimension, and thus the permeability of the aqueous solution through the MF membrane, is reduced. The charge transfer interaction of the 4VP polymer with protonic acids has been reported earlier (Liu et al.,

1999). Thus, the P4VP-*g*-FPI MF membranes from the FPI with grafted base polymer side chains complement the PAAc-*g*-FPI MF membranes from the FPI with grafted acid polymer side chains in regulating the flux of the aqueous solutions in the pH range of 0.5 to 6.4.

6.1.3 Conclusion

PAAc-*g*-FPI and P4VP-*g*-FPI copolymers were successfully synthesized through thermally-induced molecular graft copolymerization of the respective AAc and 4VP monomer with the ozone-preactivated FPI backbones in NMP solutions. The MF membranes prepared from the respective PAAc-*g*-FPI and P4VP-*g*-FPI copolymers by phase inversion in water showed enrichment of the AAc and 4VP side chains in the surface region. The mean pore size of both the PAAc-*g*-FPI and P4VP-*g*-FPI MF membranes increased with the increase in graft concentration and the decrease in concentration of the casting solution. The mean pore sizes of the PAAc-*g*-FPI MF membranes also increased with the increase in pH of the casting bath. An opposite behavior was observed for the P4VP-*g*-FPI MF membranes. The flux of aqueous solutions through the PAAc-*g*-FPI and P4VP-*g*-FPI MF membranes exhibited a strong but opposite dependence on the solution pH in the pH range of 0.5 to 6.4. The pH-dependent flux behavior arose from the interaction of the grafted chains on the pore surface and sub-surface region with the aqueous solution.

6.2 Synthesis and Characterization of Fluorinated Polyimide with Grafted Poly(*N*-isopropylacrylamide) Side Chains and the Temperature-sensitive Microfiltration Membranes

6.2.1 Experimental

6.2.1.1 Materials

The fluorinated polyimide (FPI) used in this study was 2,2-bis(3,4-dicarboxyphenyl) hexafluoropropane dianhydride+4,4'-bis(4-aminophenoxy) diphenyl sulfone. The *N*-isopropylacrylamide (NIPAAm) monomer was obtained from Aldrich Chemical Co. The solvent, *N*-methyl-2-pyrrolidone (NMP), was obtained from Merck Chemical Co. The chemical structure of the NIPAAm is shown below.

NIPAAm:

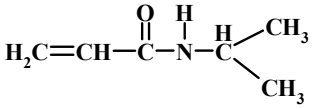

6.2.1.2 Ozone Treatment of FPI

The procedure for ozone treatment of FPI was the same as that described in Section 5.2.1.2. A treatment time of about 5 min was chosen to obtain optimum content of peroxides (Wang et al., 2003). After the ozone treatment, the polymer solution was cooled in an ice bath.

6.2.1.3 Graft Copolymerization of NIPAAm with FPI: the P(NIPAAm)-*g*-FPI Copolymer

The functional copolymer was prepared by thermally-induced molecular graft copolymerization of NIPAAm with the ozone pre-activated FPI in NMP at 60°C for 6 h and under an argon atmosphere. The monomer and about 20 ml of the FPI solution were introduced into a 3-necked round bottom flask equipped with a thermometer, a

condenser, and a gas line. The NIPAAm monomer concentrations were varied from 0.01 g/ml to 0.16 g/ml. The final volume of each reaction mixture was adjusted to 50 ml. The solution was saturated with purified argon for 1 h under stirring. The reactor flask was then placed in a thermostated water bath at 60°C to initiate the graft copolymerization reaction. A constant flow of argon was maintained during the thermal graft copolymerization process. After the reaction time of 6 h, the reactor flask was cooled in an ice bath and the NIPAAm graft-copolymerized FPI (P(NIPAAm)-*g*-FPI) was precipitated in excess amount of doubly distilled water. After filtration, the copolymer was further purified by stirring for 48 h in copious amounts of doubly distilled water at room temperature. The precipitation and exhaustive washing process ensured the complete removal of the residual monomer and homopolymer. The copolymers were then dried by pumping under reduced pressure for subsequent characterization.

6.2.1.4 Preparation of Microfiltration (MF) Membranes

MF membranes were prepared by phase inversion in aqueous media from a NMP solution containing 10 wt% FPI homopolymer or P(NIPAAm)-*g*-FPI copolymer. The polymer or copolymer solution was cast onto a glass plate. After allowing exposure in air for a short time, the glass plate was immersed in a bath of doubly distilled water (non-solvent). The temperature of the water in the casting bath was varied from 4°C to 55°C. Each membrane was left in the bath for 20 min after separation from the glass plate. The purified membranes were dried under reduced pressure for subsequent characterization.

6.2.1.4 Infrared Spectroscopy Measurements

Fourier transform infrared (FTIR) spectra of the FPI and the P(NIPAAm)-*g*-FPI copolymers, dispersed in KBr, were obtained on a Bio-Rad FTIR spectrophotometer (Model FTS135) under ambient conditions. The procedure was the same as that described in Section 6.1.1.7.

6.2.1.5 Thermal Analyses

The thermal properties of the homopolymer and copolymer samples were measured by both thermogravimetric (TG) analysis and differential scanning calorimetry (DSC). The procedures were the same as those described in Section 5.1.1.6.

6.2.1.6 Water Contact Angle Measurements

Static water contact angles of the pristine FPI and the P(NIPAAm)-*g*-FPI films cast from THF solutions were measured at 27°C and 60% relatively humidity by the sessile drop method, using a 3 μL water droplet in a telescopic goniometer (Model 100-00-230, Rame-Hart, Mountain Lakes, NY, USA). The procedures were the same as those described in Section 6.1.1.11.

6.2.1.7 Elemental Analyses

The carbon, nitrogen, hydrogen and fluorine elemental contents of the pristine FPI and the P(NIPAAm)-*g*-FPI copolymer samples were determined using a Perkin-Elmer 2400 element analyzer. The procedures were the same as those described in Section 5.2.1.5.

6.2.1.8 XPS Measurements

The surface composition of the samples was determined by XPS. the procedure was the same as that described in Section 3.1.9.

6.2.1.9 Morphology and Pore Size of the MF Membranes

The surface morphology of the MF membranes was studied by scanning electron microscopy (SEM), using a JEOL 6320 electron microscope. The membranes were mounted on the sample studs by means of double-sided adhesive tapes. A thin layer of gold was sputtered on the sample surface prior to the SEM measurement. The SEM measurements were performed at an accelerating voltage of 15 kV.

The pore sizes of the P(NIPAAm)-*g*-FPI membranes were measured using a Coulter® Porometer II apparatus, manufactured by Coulter Electronics Ltd., UK.

6.2.1.10 Measurements of the Temperature-Dependent Flux Through the MF Membranes

Distilled water and 2-propanol were used to study the dependence of permeation rate on temperature. The NIPAAm-*g*-FPI MF membrane was mounted on the microfiltration cell (Toyo Roshi UHP-25, Tokyo, Japan). The micro-filtration cell containing the permeate solution was kept in a thermostated water bath for at least 20 min before the flow was initiated. The temperature of permeate was checked by a thermometer installed at the outlet of the filtration cell. The flux was calculated from the weight of solution permeated per unit time and per unit area of the membrane surface under a fixed N_2 pressure head of 0.4 kg/cm^2.

6.2.2 Results and Discussion

6.2.2.1 Bulk Graft Concentration of the P(NIPAAm)-*g*-FPI Copolymers

For the graft copolymerization of NIPAAm with FPI in solution, the monomer to polymer feed ratio can be used to regulate the graft concentration of the resulting graft copolymer. The bulk contents of nitrogen and fluorine were determined by elemental analysis. The bulk graft concentration of the copolymers is defined as the number of the NIPAAm repeat units in the graft chains per repeat unit of the FPI main chain. Hence the bulk graft concentration can be calculated from the $([N]/[F])_{bulk}$ molar ratio by taking into account of the nitrogen stoichiometries of the graft and the main chains, and the fluorine to nitrogen ratio of the FPI main chain. Thus, the bulk graft concentration or the $([P(NIPAAm)]/[FPI])_{bulk}$ molar ratio can be calculated from the following relationship:

$$([P(NIPAAm)]/[FPI])_{bulk} = 6([N]-[F]/3)_{bulk}/[F]_{bulk}$$

in which the factor 1/3 accounts for the fact that there are 2 nitrogen atoms and 6 fluorine atoms per repeat unit of the FPI chains.

Figure 6.8 shows the dependence of the bulk graft concentration of the P(NIPAAm)-*g*-FPI copolymer on the NIPAAm to FPI molar feed ratio used for graft copolymerization. Thus, the graft concentration increases with increasing monomer concentration. The average length of the graft chains for each copolymer sample, estimated from the peroxide and graft concentration, is shown in Table 6.4.

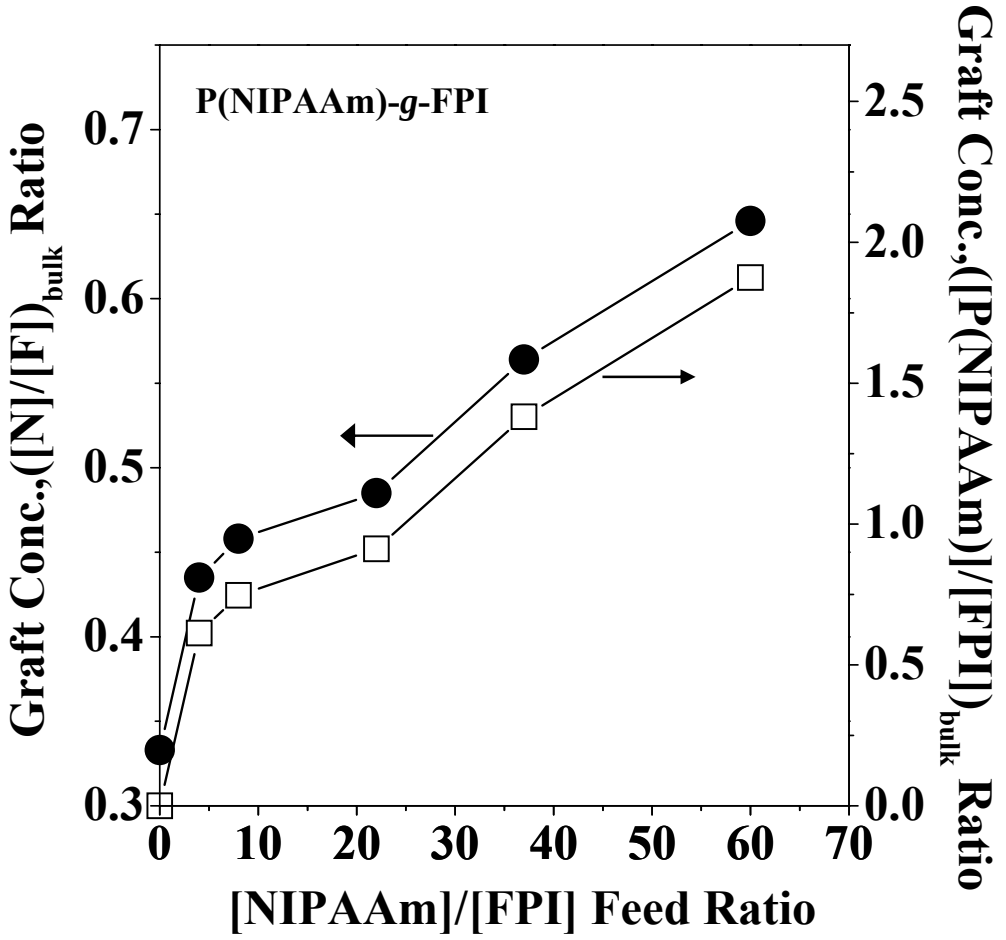

Figure 6.8 Effect of the monomer molar feed ratio on the bulk graft concentration of the P(NIPAAm)-*g*-FPI copolymer.

6.2.2.3 FTIR Spectroscopy of the P(NIPAAm)-*g*-FPI Copolymers

The chemical structures of the FPI and P(NIPAAm)-*g*-FPI copolymers were studied by FTIR spectroscopy. The absorption bands associated with the imide ring and linkage of FPI at 1730 cm^{-1} (symmetrical C=O stretching), 1376 cm^{-1} (C-N stretching), and 1063 cm^{-1} and 744 cm^{-1} (imide ring stretching) are present in all the copolymer samples (Vora et al., 2001). Comparing the FTIR spectra of the P(NIPAAm)-*g*-FPI copolymers with that of the pristine FPI, the absorption band of the copolymer samples at 1645 $cm^{-1}$and 1548 cm^{-1}, attributable, respectively, to the secondary amide C=O stretching and N-H stretching of the amide (O=C-NH) groups of the grafted NIPAAm chains, are present in all the P(NIPAAm)-*g*-FPI samples (Chen et al., 1998). In addition, with the increase in NIPAAm to FPI molar feed ratio, the intensity of the absorption bands at 1645 and 1548 cm^{-1} is enhanced, suggesting an increase in concentration of the grafted NIPAAm side chains. Therefore, the FTIR data suggest that the graft concentration increases with the increase in NIPAAm to FPI molar feed ratio used for graft copolymerization. This result is in good agreement with that obtained from the elemental analysis.

6.2.2.4 Thermogravimetric Analyses of the P(NIPAAm)-*g*-FPI Copolymers

The thermal properties of the graft copolymers were studied by thermogravimetric (TG) analysis. Figure 6.9 shows the TG analysis curves of the pristine FPI (Curve 1), the P(NIPAAm)-*g*-FPI copolymers of different graft concentrations (Curves 2 to 6) and the NIPAAm homopolymer (Curve 7). The P(NIPAAm)-*g*-FPI samples show intermediate weight loss behavior in comparison to that of the pristine FPI and that of the NIPAAm homopolymer. A distinct two-step degradation process is also observed for the copolymers. The onset of the first major weight loss at about 375°C

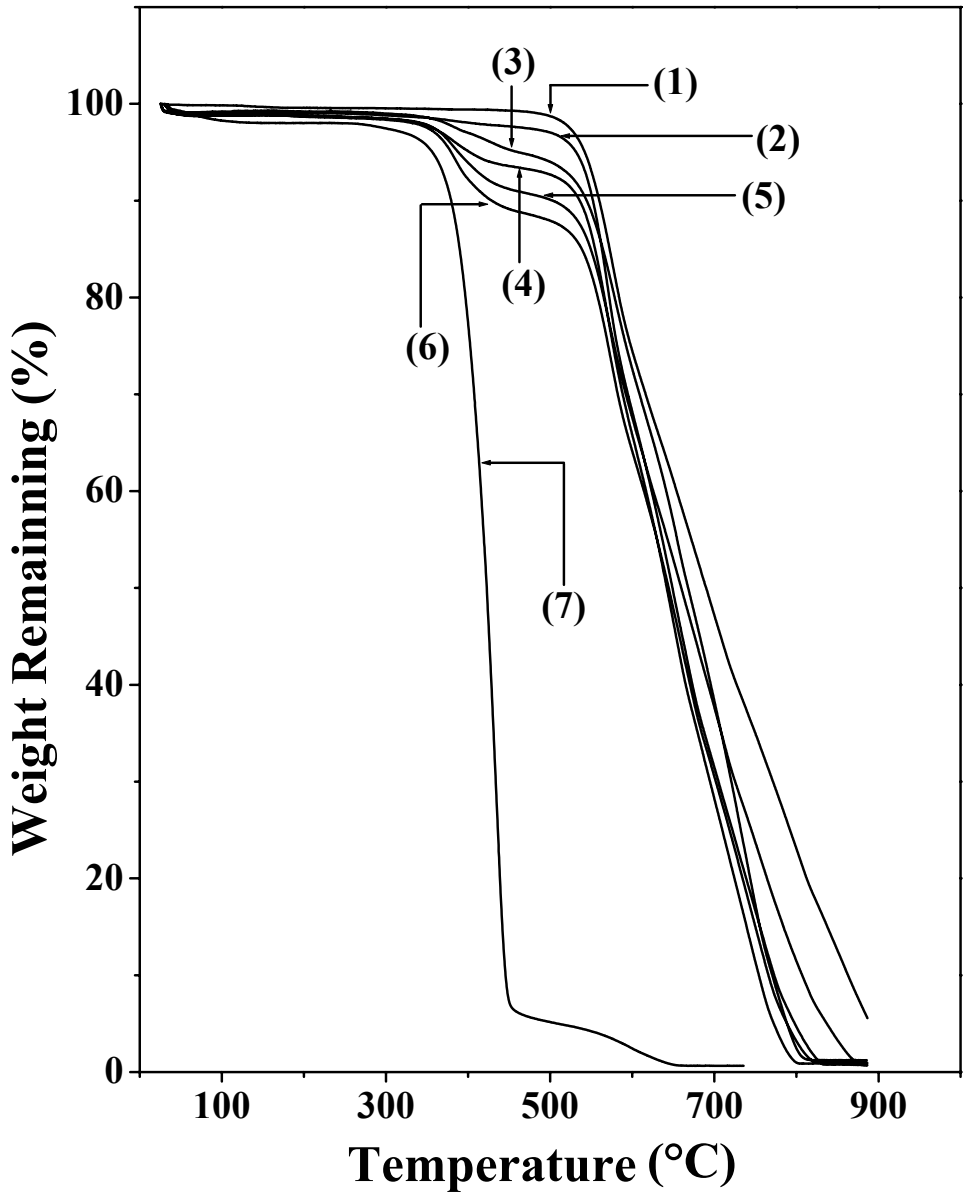

Figure 6.9 TG analysis curves of (1) the FPI homopolymer, the P(NIPAAm)-*g*-FPI copolymers with bulk graft concentrations of (2) 0.61, (3) 0.75, (4) 0.91, (5) 1.38, (6) 1.87, and (7) the NIPAAm homopolymer.

corresponds to the decomposition of the NIPAAm polymer segments. The second major weight loss begins at about 560°C, which coincides with the decomposition temperature of the FPI main chain. The TG analysis curves also indicate that the extent of weight loss in each copolymer during the first stage of thermal decomposition is approximately equal to the NIPAAm polymer content in the graft copolymer.

Table 6.4 shows the glass transition temperature (T_g), obtained from DSC, of the pristine FPI and the P(NIPAAm)-*g*-FPI copolymer of different graft concentrations. A similar trend has been observed as in the case of PAAc-*g*-FPI and P4VP-*g*-FPI, which was shown in Table 6.2. The T_g of the P(NIPAAm)-*g*-FPI copolymer is reduced to about 281°C for copolymers with a bulk graft concentration, or $([P(NIPAAm)]/[FPI])_{bulk}$ ratio, of 1.87 (see Table 1). Graft copolymerization with NIPAAm reduces the structural rigidity of the FPI and increases the molar free volume of the polymer, resulting in the lowering of T_g. It can also be seen from the data in Table 1 that the T_g of the graft copolymer decreases with the increase in graft concentration.

6.2.2.5 Water Contact Angles of the P(NIPAAm)-*g*-FPI Copolymer Films

The pristine FPI film is hydrophobic, with a water contact angle of about 88°. A substantial decrease in water contact angle of the FPI films is achieved through graft copolymerization with NIPAAm. The contact angle is reduced to about 40° for the copolymer film with a bulk graft concentration, $([P(NIPAAm)]/[FPI])_{bulk}$, of 1.87 (Table 1). This phenomenon is attributable to the hydrophilic nature of the grafted NIPAAm polymer side chains below its LCST. Thus, as shown in Table 1, the water contact angle of the P(NIPAAm)-*g*-FPI film decreases with the increase in NIPAAm polymer graft concentration.

Table 6.4 Physicochemical Properties of the FPI and P(NIPAAm)-*g*-FPI Copolymers

FPI Samples	Molar Feed Ratio [NIPAAm]/[FPI]	Graft Concentration $([P(NIPAAm)]/[FPI])_{bulk}$	Graft Chain Length $(\overline{DP})$[a)]	Glass Transition Temperature [b)] (°C)	Water Contact Angle[c)] (± 3°)
1. Pristine FPI	---	----	----	293	88
2. P(NIPAAm)-*g*-FPI Copolymer	4	0.61	56	290	78
3. P(NIPAAm)-*g*-FPI Copolymer	8	0.75	69	289	67
4. P(NIPAAm)-*g*-FPI Copolymer	22	0.91	83	287	61
5. P(NIPAAm)-*g*-FPI Copolymer	37	1.38	126	283	55
6. P(NIPAAm)-*g*-FPI Copolymer	60	1.87	171	281	40

[a.] The average degree of graft polymerization ($\overline{DP}$) and the number of grafts per FPI chain were estimated from the peroxide concentration of the 5-min ozone-treated FPI and the graft concentration. ($\overline{Mn}$ of FPI ~1.56×10^5)

[b.] Determined by differential scanning calorimetry (DSC).

[c.] The films were cast from THF solutions.

6.2.2.6 Surface Composition of the MF Membranes Prepared from the P(NIPAAm)-*g*-FPI Copolymers

Figure 6.10 shows the respective wide scan and N 1s core-level spectra of the membranes prepared from pristine FPI and the P(NIPAAm)-*g*-FPI copolymers of different graft concentrations. All the membranes were cast in doubly distilled water at 27^{o}C. In the case of the pristine FPI, the N1s core level spectrum can be curve-fitted with a single peak component, with binding energy (BE) at 400.5 eV, attributable to the –N(C=O)$_2$- (imide) species (Zhang et al. 2000). The presence of the grafted NIPAAm polymer on FPI can be deduced from the N 1s peak component at the BE of 399.6 eV, attributable to the amide (CONH) species in the NIPAAm polymer (Beamson and Briggs, 1992). The increase in graft concentration with the NIPAAm to FPI molar feed ratio is readily indicated by the steady increase in the ratio of the (CONH) species to the –N(C=O)$_2$ species. It can also be verified from the wide scan spectra that the intensity of the F 1s signal decreases, while that of the N 1s signal increases, with the increase in graft concentration. Thus, the XPS results are in good agreement with those obtained from the FTIR spectroscopy and elemental analysis.

The surface graft concentrations of the P(NIPAAm)-*g*-FPI MF membranes prepared by the phase inversion method are determined from the [N]/[F] ratio (determined by XPS), or the ([N]/[F])$_{surface}$ ratio, and the nitrogen and fluorine stoichiometries of the graft and the main chains. Figure 6.11 shows the dependence of the surface graft concentration of the P(NIPAAm)-*g*-FPI MF membrane, cast at 27^{o}C, on the NIPAAm to FPI molar feed ratio used for the thermally induced graft copolymerization. The surface graft concentration of each copolymer membrane increases almost linearly with the monomer to FPI molar feed ratio. Comparing the surface [N]/[F] ratio

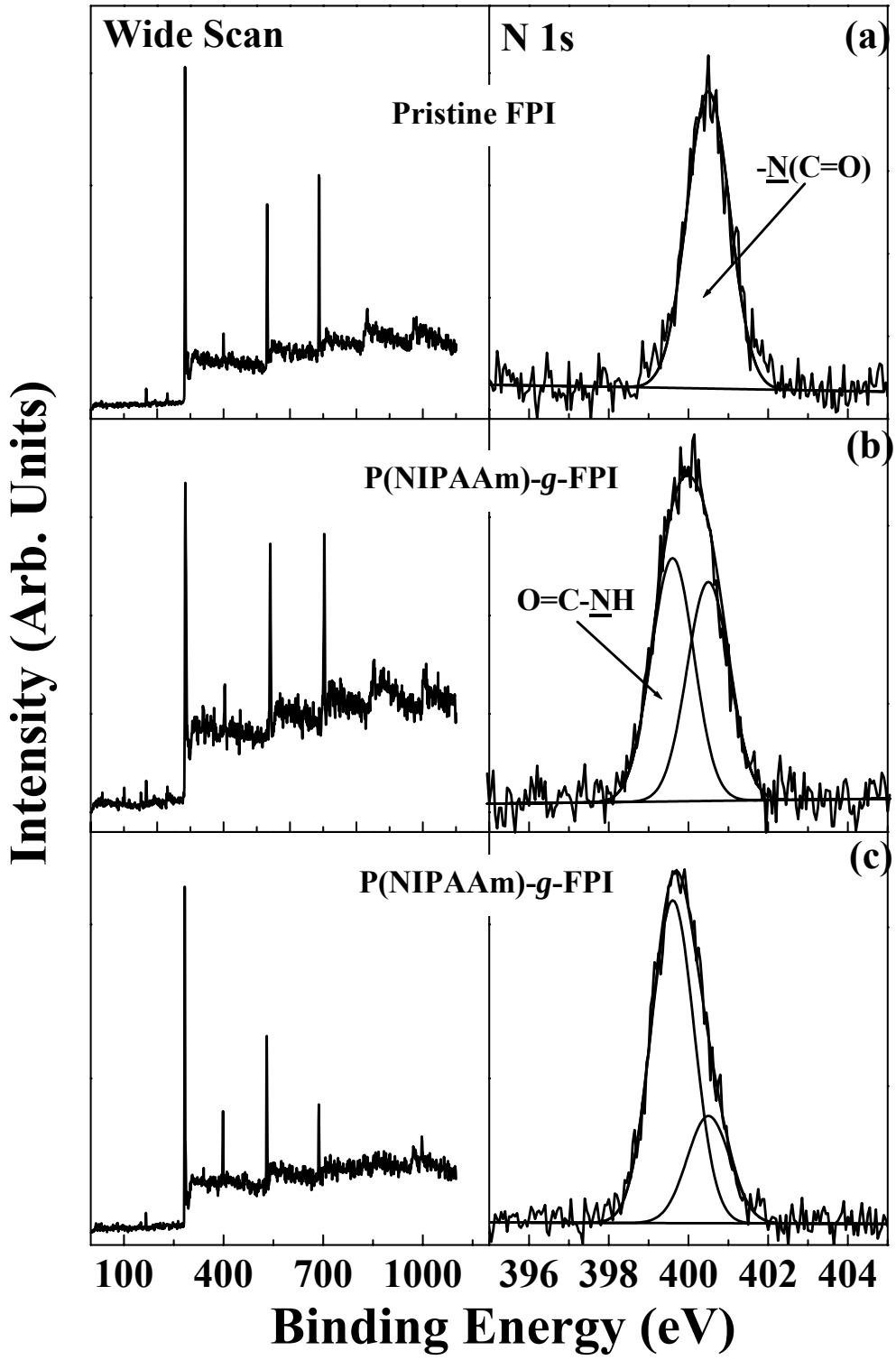

Figure 6.10 XPS wide scan and N 1s core-level spectra of (a) the pristine FPI membrane, and the P(NIPAAm)-*g*-FPI membranes with bulk graft concentrations of (b) 0.61 and (c) 1.38 (Membranes cast by phase inversion in water at 27°C from 10 wt% NMP solutions).

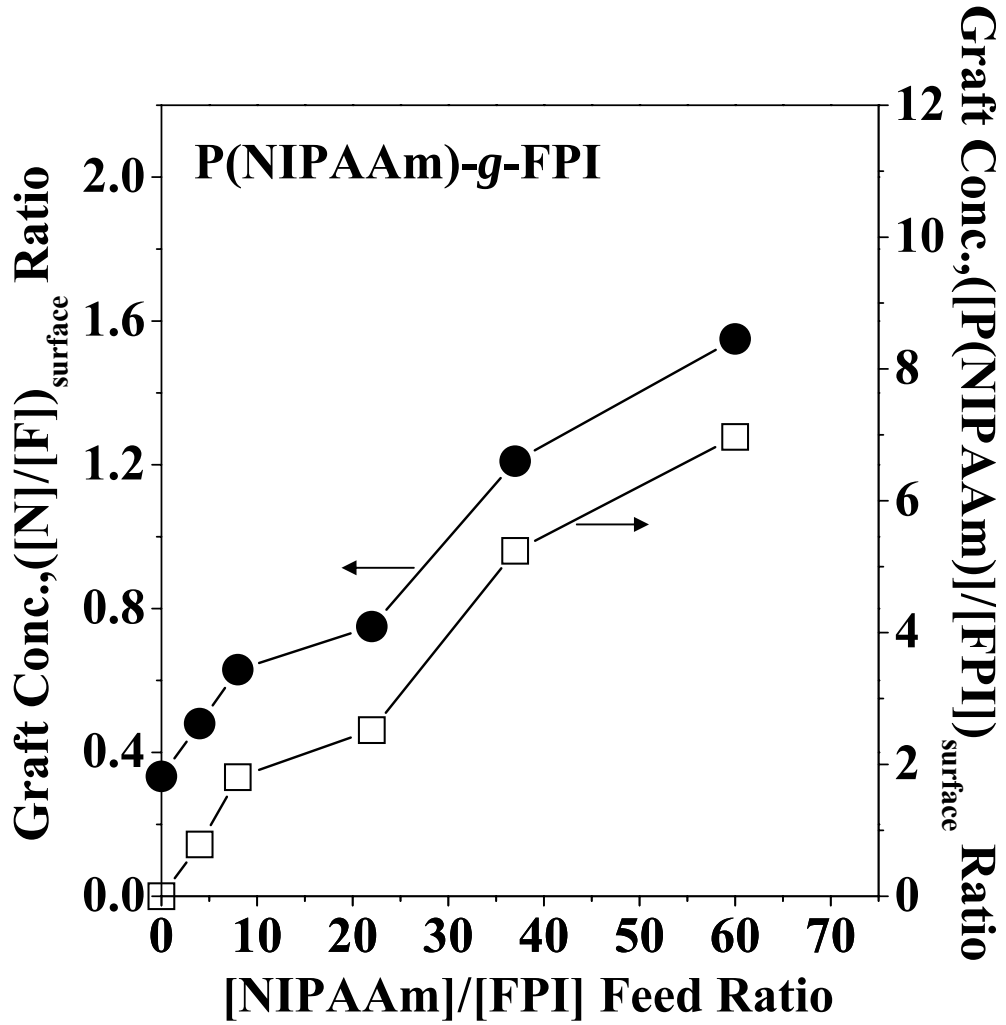

Figure 6.11 Effect of the monomer feed ratio on the surface graft concentration of the P(NIPAAm)-*g*-FPI MF membrane, cast at 27°C *via* phase inversion in water from 10 wt% NMP solutions.

in Figure 6.11 with the corresponding bulk ratio (determined by elemental analysis) in Figure 6.8, it is obvious that the surface [N]/[F] ratio is considerably higher than the corresponding bulk ratio. This phenomenon arises mainly from the enrichment of the NIPAAm side chains at the surface and near-surface region during the course of membrane formation by phase inversion in the aqueous medium. For multicomponent polymer systems (including copolymers and polymer blends), surface enrichment of the hydrophilic components arising from interaction with the environments occurs readily (Hester et al., 1999).

6.2.2.7 Surface Morphology of the P(NIPAAm)-*g*-FPI MF Membranes

The surface morphology of the P(NIPAAm)-*g*-FPI MF membranes was studied by SEM. Figure 6.12 shows the SEM images of the MF membranes cast by phase inversion at 27°C in water from 10 wt% NMP solutions of the pristine FPI powders, and the P(NIPAAm)-*g*-FPI copolymers with bulk graft concentrations of 0.75, 0.91 and 1.38. The SEM images reveal that the membranes cast from the NMP solutions of the graft copolymers have a higher porosity than that cast from the pristine FPI, and that the porosity increases with the graft concentration of the NIPAAm polymer in the copolymer. In the presence of high concentrations of the NIPAAm polymer side chains, surface enrichment of the NIPAAm polymer takes place during phase inversion in water to maximize the interfacial interaction between the pore surface and water, resulting in an increase in porosity and a decrease in pore size of the membrane.

The dependence of the membrane morphology and surface composition on the temperature of the aqueous casting bath is also investigated. The SEM images, obtained at a magnification of ×5000, for MF membranes cast by the phase inversion technique at 4, 27, 32, and 55^{o}C from a 10 wt% NMP solution of the P(NIPAAm)-*g*-

FPI copolymer (bulk graft concentration of 1.38) are shown in Figure 6.13. At casting temperatures below the LCST (~32^{o}C) of the NIPAAm polymer, no obvious difference in pore size distribution and porosity can be observed in the SEM. On the other hand, for membranes cast at temperature above LCST of the NIPAAm polymer, the pore size distribution becomes less uniform. The porosity decreases and the mean pore size increases. As for the surface composition of the membrane, the $([P(NIPAAm)]/[FPI])_{surface}$ ratio, or the $[N]/[F]_{surface}$ ratio, decreases with the increase in the membrane casting temperature, with the most drastic increase being observed at casting temperature near the LCST (Figure 6.14). The phenomena are consistent with the change in chain conformation and orientation at the surface near the LCST of the NIPAAm polymer.

6.2.2.8 Pore Sizes of the P(NIPAAm)-*g*-FPI MF Membranes

The mean pore size and pore size distribution of various P(NIPAAm)-*g*-FPI MF membranes cast from NMP solutions and under different conditions, such as different bulk graft concentrations, different copolymer concentrations of the casting solutions, and different temperatures of the casting bath, were measured on the Coulter® Porometer II instrument. The pore size distributions of the P(NIPAAm)-*g*-FPI MF membranes cast under different conditions are shown in Table 6.5. In agreement with the SEM results for the copolymer membranes, the data in Table 6.5 suggest that the mean pore size of the membrane decreases with the increase in bulk graft concentration of the membrane.

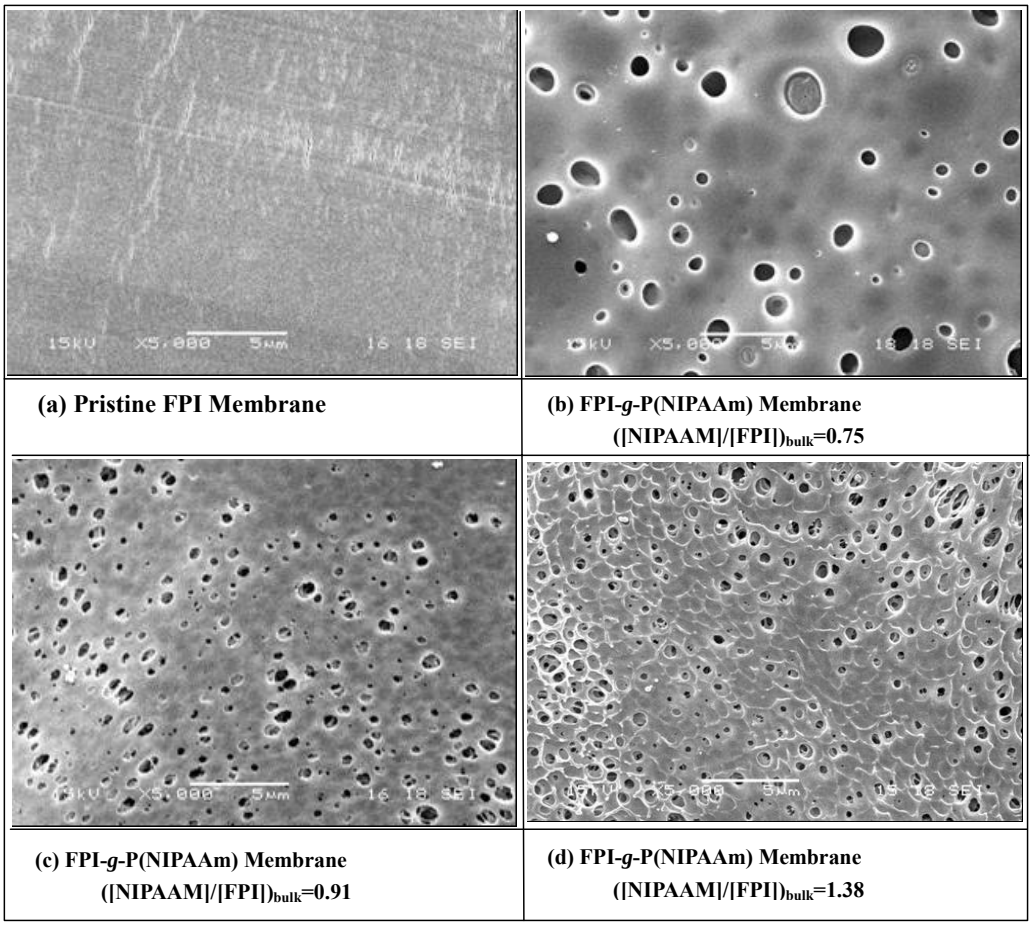

Figure 6.12 SEM images of the MF membranes cast at 27°C *via* phase inversion in water from 10 wt% NMP solutions of (a) the pristine FPI, and the P(NIPAAm)-*g*-FPI copolymers with bulk graft concentrations of (b) 0.75, (c) 0.91, (d) 1.38.

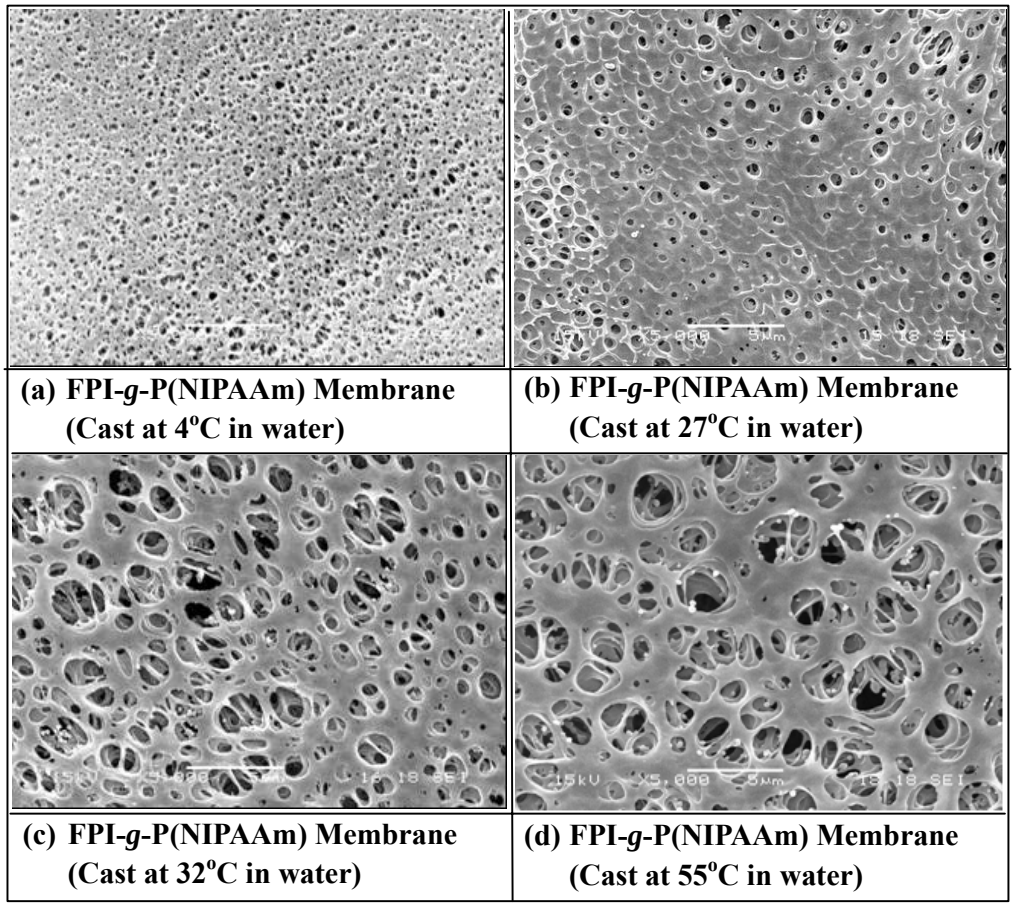

Figure 6.13 SEM images of the P(NIPAAm)-*g*-FPI (bulk graft concentration=1.38) MF membranes cast by phase inversion from 10 wt% NMP solutions at nonsolevent (water) temperatures of (a) 4°C, (b) 27°C, (c) 32°C and (d) 55°C.

Table 6.5 Pore Size Distribution [a)] of the P(NIPAAm)-*g*-FPI MF Membranes [b)]

Molar Feed Ratio	Bulk Graft Conc. of Copolymer	Temperature of Casting Bath (°C)	Concentration of Cast Solution (wt%)	Min. Pore Size (μm)	Max. Pore Size (μm)	Mean PoreSize (μm)
(a) Effect of Bulk Graft Concentration on the Pore-Size Distribution						
4	0.61	27	10	0.11	2.25	0.52
8	0.75	27	10	0.12	2.12	0.51
22	0.91	27	10	0.19	2.10	0.49
37	1.38	27	10	0.20	1.90	0.45
60	1.87	27	10	0.31	1.60	0.41
(b) Effect of the Temperature of Casting Bath on the Pore-Size Distribution						
37	1.38	4	10	0.16	0.87	0.27
37	1.38	20	10	0.17	1.00	0.38
37	1.38	27	10	0.20	1.90	0.45
37	1.38	32	10	0.19	1.92	0.61
37	1.38	55	10	0.21	2.15	0.67
(c) Effect of the Concentration of Casting Solution on the Pore-Size Distribution						
60	1.87	27	7	0.58	2.89	0.55
60	1.87	27	10	0.31	1.60	0.41
60	1.87	27	15	0.22	0.64	0.25

[a.] These pore sizes were measured on the Coulter® Porometer II which utilized a liquid displacement technique.
[b.] Membranes were cast from NMP solutions of the P(NIPAAm)-*g*-FPI copolymers in doubly distilled water.

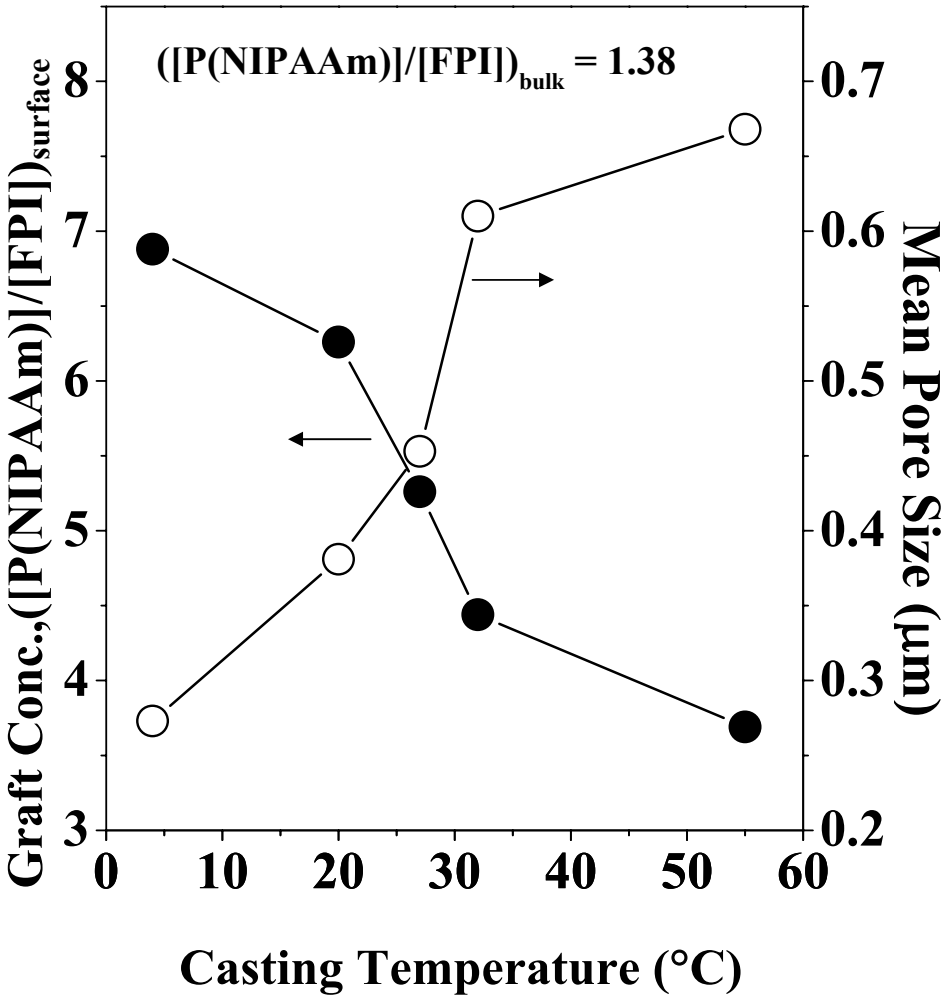

Figure 6.14 Effect of the coagulation water bath temperature on the surface graft concentration and mean pore size of the P(NIPAAm)-*g*-FPI MF membrane. (Bulk graft concentration=1.38, from 10 wt% NMP solutions)

The dependence of membrane pore size distribution on the non-solvent (water) temperature of the casting bath is also shown in Table 6.5. The mean pore size increases with casting temperature. In the vicinity of the LCST (32^{o}C) of the NIPAAm polymer, the most drastic change in mean pore size is observed. The change in mean pore size in response to the change in membrane casting temperature may be attributed to the change in conformation of the NIPAAm polymer side chains on the surface (especially on the pore surfaces) of the P(NIPAAm)-*g*-FPI MF membrane. When the membrane is cast at temperature below the LCST, the NIPAAm polymer side chains are hydrophilic and assume a highly extended conformation. This conformation leads to a delayed demixing between the solvent (NMP) and the water. According to the model given by Smolder et al (Smolders et al., 1992), the loss of solvent is greater than the influx of water. This will lead to a smaller mean pore size of the membrane. On the other hand, when the casting temperature is above the LCST, the NIPAAm polymer side chains associate hydrophobically to form excessively compact molecular structures on the surface, leading to instantaneous demixing. Larger pores are formed due to the diffusional flow which helps to develop a higher solvent concentration in the nuclei of the polymer lean phase present in the proceeding coagulation front (Boom et al., 1992). The data in Figure 6.14 indicate that the surface graft concentration decreases with the increases in the temperature of the casting bath, while the mean pore size increases with the increase in casting temperature. The effect of the temperature of the casting solution on the membrane characteristics is less pronounced when compared to that of the temperature of the coagulation bath, since the volume of the latter is present in large excess. The pore size distribution of the P(NIPAAm)-*g*-FPI membrane can also be manipulated through the changes in solution concentration of the P(NIPAAm)-*g*-FPI copolymer used for casting. The results are also shown in Table

6.5. The membranes were cast from 7, 10 and 15 wt% NMP solutions of the P(NIPAAm)-*g*-FPI copolymer (bulk graft concentration=1.87) at 27^{o}C. With the increase in solution concentration from 7 to 15 wt.%, the mean pore size of the membrane decreases by more than half. The above results suggest that from the regulation of the solution concentration of the copolymer, the graft concentration or the casting temperature, the pore size and porosity of the membranes cast by the phase inversion technique can be controlled to a certain extent. The graft copolymer approach to membrane preparation is thus more versatile than that of modification of the existing membranes by surface graft copolymerization or grafting.

6.2.2.9 Temperature-Dependent Flux of Aqueous Solution through the P(NIPAAm)-*g*-FPI MF Membranes

The temperature-dependent flux of aqueous solutions through the pristine FPI and the P(NIPAAm)-*g*-FPI MF membranes was investigated and the results are shown in Figure 6.15. The permeability of water through the pristine FPI MF membranes was very low and temperature independent (Curve 6). The low permeability is due to the low porosity of the membrane. The permeability of water through the P(NIPAAm)-*g*-FPI MF membranes cast at temperatures above the LCST (Curves 4 and 5) also exhibits a temperature-independent behavior. These copolymer membranes exhibit the same permeation behavior for water as that of the hydrophobic pristine FPI membrane because the NIPAAm side chains associate hydrophobically on the membrane surface (including the pore surfaces). Furthermore, the pore-sizes of these two membranes are probably too large to exhibit any significant sensitivity toward permeate temperature. On the other hand, however, the rate of water flux through the P(NIPAAm)-*g*-FPI MF membranes, cast at temperatures below the LCST, increases with the increase in

permeate temperature from 4°C to 55°C, with the most drastic increase being observed at the permeate temperature around 32°C (Curves 1, 2 and 3).

The temperature-dependent permeation rate results from the change in conformation of the NIPAAm polymer side chains on the surface and sub-surface region of the P(NIPAAm)-*g*-FPI MF membrane. The surface (in particular, the pore surface) of the membrane was enriched with the grafted NIPAAm chains during the phase inversion process. When the NIPAAm polymer side chains are solvated, they do not dissolved into the solution since the NIPAAm chain ends are covalently tethered to the FPI backbone. At permeate temperatures below the LCST of the NIPAAm polymer, the grafted NIPAAm chains extend into the pores and reduce the permeation rate of the aqueous solution. On the other hand, at permeate temperatures above the LCST, the grafted NIPAAm polymer chains shrink and associate hydrophobically on the membranes and pore surfaces, resulting in the opening of the pores of the membrane and, thus, an increase in permeation rate. The temperature-dependent changes in permeation rates are completely reversible at permeate temperatures between 4°C and 55°C. This phenomenon suggests that the conformation of the graft chains and the extent of interaction with the aqueous environment vary reversibly with the permeate temperature to control the effective pore size of the membrane.

For the P(NIPAAm)-*g*-FPI MF membranes cast at temperatures above the LCST of the NIPAAm polymer, the flux of the organic solvent, 2-propanol, also exhibits a temperature-dependent behavior, as shown in Figure 6.16. The temperature-dependent flux of 2-propanol through the P(NIPAAm)-*g*-FPI membrane is also reversible. This phenomenon arises from the dependence of the extent of interaction between the

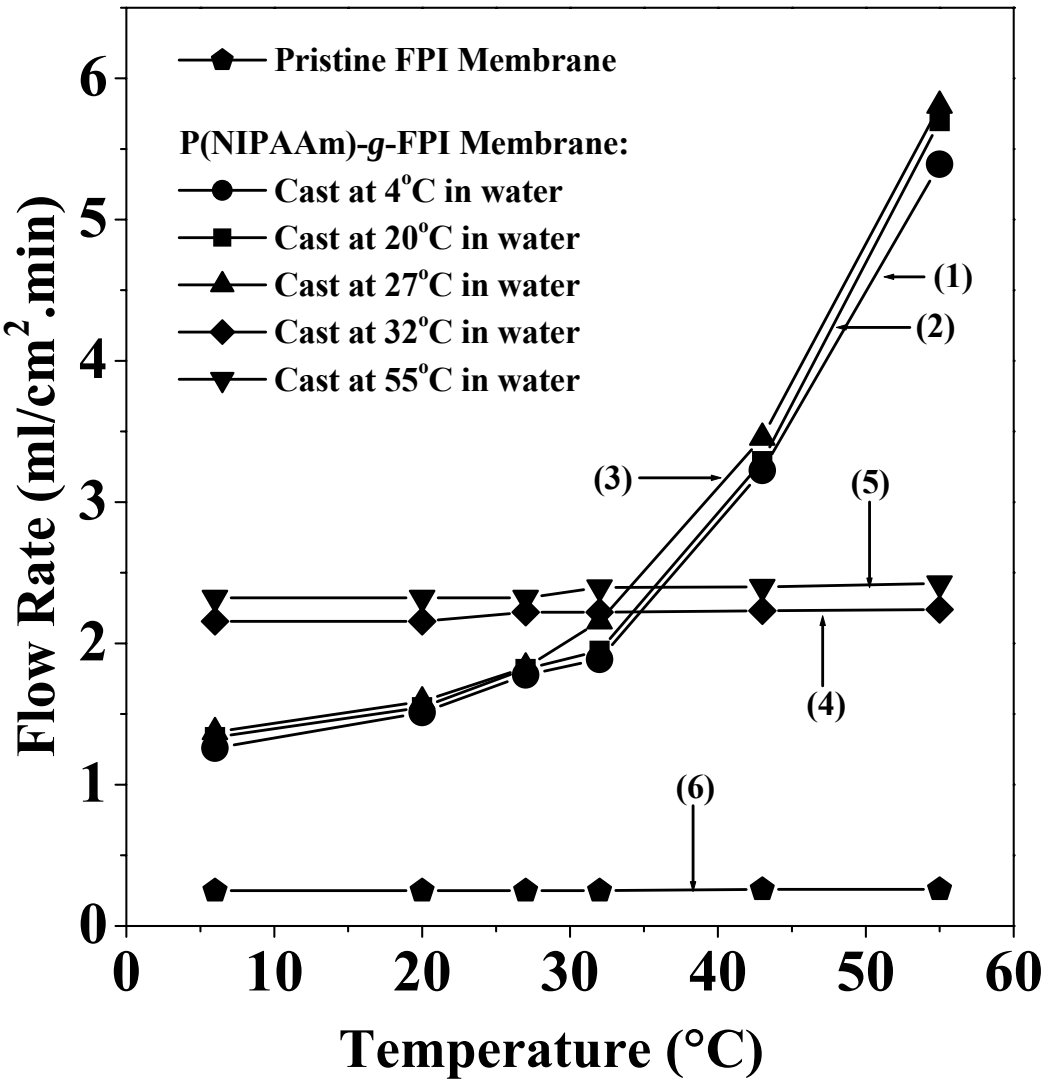

Figure 6.15 Temperature-dependent permeability of water through the P(NIPAAm)-*g*-FPI (bulk graft concentration=1.38) and the pristine FPI membrane. Curve 1 (membrane cast at 4°C), Curve 2 (membrane cast at 20°C) and Curve 3 (membranes cast at 27°C) are obtained from the water fluxes through the three P(NIPAAm)-*g*-FPI MF membranes cast at temperatures below the LCST. Curve 4 (membrane cast at 32°C) and Curve 5 (membrane cast at 55°C) are obtained from the water fluxes through the two copolymer membranes cast at temperatures above the LCST. Curve 6 is obtained from the flux through the pristine FPI membrane. The temperature-dependent flux behaviors (Curves 1, 2 and 3) are completely reversible.

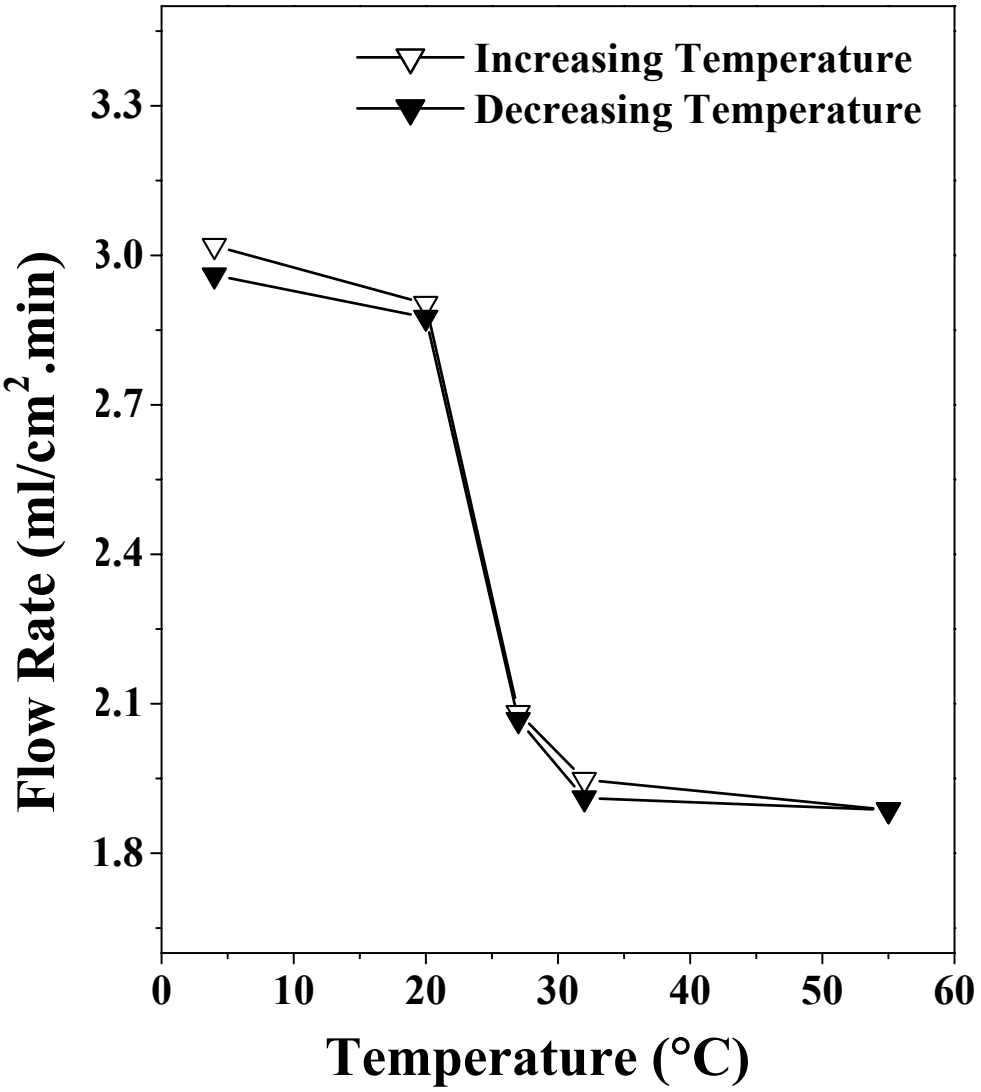

Figure 6.16 Reversible temperature-dependent flux of 2-propanol through the P(NIPAAm)-*g*-FPI MF membrane (bulk graft concentration=1.38) cast at 55^{o}C from a 10 wt% solution.

permeate and the polymer side chains on the permeate temperature. For the membrane cast at a temperature above the LCST, the membrane and pore surfaces are enriched by the hydrophobic conformation of the NIPAAm polymer side chain. During the flux of 2-propanol at temperatures above 32^{o}C, the enriched hydrophobic microstructure of the pore surfaces interacts favorably with the organic solvent. The graft chains are solvated, and the flux through the pores is hindered. At permeate temperatures below 32^{o}C, the change in conformation of the grafted NIPAAm chains and the reduced interaction of 2-propanol with the grafted NIPAAm chains on the pore surfaces result in the opening of the membrane pores. An increase in permeation rate of the organic solvent is observed. Thus, the LCST of the NIPAAm polymer in 2-Propanol appears to be very close to that of the NIPAAm polymer in water. The above results on the temperature-dependent flux of water and 2-isopropanol suggest that the grafted NIPAAm polymer side chains on the membrane pore surface and sub-surface region can act as temperature sensors and valves to regulate the effective pore dimension, and thus the filtration rate, of the membrane for aqueous solutions and certain organic solvents.

6.2.3 Conclusion

P(NIPAAm)-*g*-FPI copolymers were successfully synthesized through the thermally-induced molecular graft copolymerization of NIPAAm monomer with the ozone-preactivated FPI backbones in NMP solutions. The mean pore size of the P(NIPAAm)-*g*-FPI MF membrane increased while the surface graft concentration decreased at higher temperature of the casting bath. The flux of water and 2-isopropanol through the P(NIPAAm)-*g*-FPI MF membrane exhibited a strong dependence on the casting temperature of the membrane and the permeate temperature in the temperature range of 4^{o}C to 55^{o}C. The temperature-dependent flux behavior arose from the interaction of the grafted chains on the pore surface and sub-surface region with the permeate. The present study has shown that molecular functionalization by graft copolymerization prior to membrane fabrication is a relatively simple and effective approach to the preparation of FPI-based MF membranes with well-controlled pore size, uniform surface composition (including the composition of pore surface), and temperature-responsive properties. These physicochemical and morphological characteristics of the pores can be further modified through a simple change in the membrane casting temperature. Thus, the application of fluorinated polyimides as membrane materials has been further extended.

CHAPTER 7

CONCLUSION

Surface graft copolymerization has been shown to be an effective technique for surface functionalization of various substrates relavant to microelectronics. Surface graft copolymerization was successfully carried out *via* (i) the UV-induced graft copolymerization and (ii) plasma-induced graft copolymerization and deposition. In particular, surface modification of Ar plasma-pretreated FPI films was carried out *via* UV-induced graft copolymerization and plasma-induced graft copolymerization with some *N*-containing monomers, such as 1-vinylimidazole (VIDz) and 4-vinylpyridine (4VP). The grafted VIDz or 4VP polymer layer on the PI and FPI surface was used not only as chemisorption sites for the palladium complex during the Sn-free activation process, but also as an adhesion promotion layer for the electrolessly deposited copper on the PI and FPI surfaces. The T-peel adhesion strength for the electrolessly deposited Cu on the graft-modified PI (FPI) surfaces are much higher than that on the pristine and the Ar plasma pre-treated PI (FPI) surfaces. The good adhesion strength is attributable to the synergistic effect of strong interaction between the grafted 4VP and VIDz polymer with the palladium and copper atoms, the spatial distribution of the grafted 4VP and VIDz chains into the metal matrix, and the fact that the graft chains were covalently tethered on the PI (FPI) surface.

Secondly, molecular modification by grafting of thermally labile side chains is a relatively simple and effective in the preparation of nanoporous PI (FPI) films with low dielectric constants and preserved PI backbones. Nanoporous low-κ PI(FPI) films were obtained after thermal imidization of the PAmA with PAAc or P(PEGMA) side chains in an inert atmosphere, followed by thermal decomposition of the side chains in air. The densities of the nanoporous films were 3-14% lower than that of the pristine film. SEM images revealed that the pore sizes were in the order of 30-100 nm. The

dielectric constant of the nanoporous PI(FPI) films decreased with the increase in graft concentration of the side chains, and thus the porosity of the films. Dielectric constant as low as 2.1 and 1.9 were obtained, respectively, for the nanoporous PI and FPI films prepared from this technique.

Finally, molecular functionalization by graft copolymerization was also shown to be an effective approach to prepare "smart" membranes with well-controlled pore size, uniform surface composition (including the composition of pore surface), and pH- or temperature-responsive properties. PAAc-*g*-FPI, P4VP-g-FPI and P(NIPAAm) copolymers were successfully synthesized through thermally-induced molecular graft copolymerization of the respective AAc, 4VP and NIPAAm monomer with the ozone-preactivated FPI backbones in NMP solutions. The MF membranes can be prepared from the respective PAAc-*g*-FPI, P4VP-*g*-FPI and P(NIPAAm) copolymers by phase inversion in water. The MF membranes prepared from the respective copolymers of different graft concentrations showed enrichment of the AAc, 4VP, and NIPAAM functional chains in the surface region. The flux of aqueous solutions through the PAAc-*g*-FPI and P4VP-*g*-FPI MF membranes exhibited a strong but opposite dependence in the pH range of 0.5 to 6.4. On the other hand, the flux of water and 2-isopropanol through the FPI-*g*-P(NIPAAm) MF membrane exhibited a strong dependence on the casting temperature of the membrane and the permeate temperature in the temperature range of 4^{o}C to 55^{o}C. Thus, the application of polyimides as membrane materials has been further extended.

CHAPTER 8

REFERENCES

Alvino, W.M. (ed). Plastics for Electronics: Materials, Properties, and Design Applications. pp. 3-12, New York: McGraw-Hill. 1995.

Alvarez-Lorenzo, C. and A. Concheiro. Reversible Adsorption by a pH- and Temperature-Sensitive Acrylic Hydrogel, J. Control. Release, *80*, pp. 247-257. 2002.

Ang, A.K.S., B.Y. Liaw, D.J. Liaw, E.T. Kang and K.G. Neoh. Low-Temperature Thermal Graft Copolymerization of 1-Vinyl Imidazole on Fluorinated Polyimide Films with Simultaneous Lamination of Copper Foils, J. Appl. Polym. Sci., *74*, pp. 1478-1489. 1999.

Ang, A.K.S., E.T. Kang, K.G. Neoh, K.L. Tan, C.Q. Cui and T.B. Lim. Low-Temperature Thermal Graft Copolymerization of 1-Vinyl Imidazole on Fluorinated Polyimide Films with Simultaneous Lamination to Copper Foils-Effect of Crosslinking Agents, Polymer, *41*, pp. 489-498. 2000.

Auman, B. C. Low Dielectric Constant, Low Moisture Absorption and Low Thermal Expansion Coefficient Polyimides Based on New Rigid Fluorinated Monomers. In Advances in Polyimide Science and Technology, ed by C. Feger, M.M. Khojasteh and M.S. Htoo, P. 15. Lancaster: Technomic Pub. Co. 1993.

Baum, T.H., D.C. Miller and T.R. Otoole. Photoselective Catalysis of Electroless Copper Solution for the Formation of Adherent Copper Films onto Polyimide, Chem. Mater., *3*, pp.714-720. 1991.

Baumgartner, C.E. and L.R. Scott. Development and Thermal Durability of an Interfacial Bond between Electrolessly Deposited Metals and a Fluorinated Polyimide, J. Adhesion Sci. Technol., *9*, pp. 789-799. 1995.

Beamson, G. and Briggs, D.(eds). High Resolution XPS of Organic Polymers: the Scienta ESCA300 Database. P. 214, New York: John Wiley. 1992.

Bogert M.T. and R.R. Renshaw, 4-Amino-*o*-Phthalic Acid and Some of Its Derivatives, J. Am. Chem. Soc., *30*, pp. 1135-1144. 1908.

Bolger, J.C. Polyimide Die Attch Adhesives for LSI Ceramic Packages. In Polyimides: Synthesis, Characterization, and Application, ed by K.L. Mittal, p. 871. New York: Plenum Press. 1984.

Boom, R.M., I.M. Wienk, T. Vandenboomgaard and C.A. Smolders. Microstructures in Phase-Inversion Membranes. 2. The Role of A Polymeric Additive. J. Membrane Sci., *73*, pp. 277-292. 1992.

Boutevin, B., Y. Pietrasanta and J.J. Robin. Synthesis and Application of Graft Poly(vinylidene fluoride) Copolymers .1. Eur. Polym. J., *27*, pp. 815-820. 1991.

Boutevin, B., J.J. Robin and A. Serdani. Synthesis and Applications of Graft-Copolymers from Ozonized Poly(vinylidene fluoride), Eur. Polym. J., *28*, pp.1507-1511. 1992.

Boutevin, B., J.J. Robin, N. Torres and J. Casteil. Graft Copolymerization of Styrene onto Ozonized Polyethylene, Macromol. Chem. Phys., *203*, pp. 245-252. 2002.

Brenner A. and G.E. Riddle. Electrodeless Plating on Metals by Chemical Reduction. In AES Proc. 33, New York, USA, p. 23. 1946.

Briggs, D. (ed). Surface Analysis of Polymers by XPS and Static SIMS, p. 65. New York: Cambridge University Press. 1998.

Brink, L.E.S., S.J.G. Elbers, T. Robbertsen and P. Both. The Anti-Fouling Action of Polymers Preadsorbed on Ultrafiltration and Microfiltration Membranes, J. Membr. Sci., *76*, pp. 281-291. 1993.

Brink, M.H., D.K. Brandom, G.L. Wilkes and J.E. Mcgrath. Synthesis and Characterization of a Novel 3F-Based Fluorinated Monomer for Fluorine-Containing Polyimides, Polymer, *35*, pp. 5018-5023. 1994.

Carter, K.R., R.A. DiPietro, M.I. Sanchez and S.A.Swanson. Nanoporous Polyimides Derived from Highly Fluorinated Polyimide/Poly(propylene oxide) Copolymers, Chem. Mater., *13*, pp. 213-221. 2001.

Chan, C.M., T.M. Ko and H. Hiraoka. Polymer Surface Modification by Plasmas and Photons, Surf. Sci. Rep., *24*, pp. 3-54. 1996.

Charbonnier, M., M. Alami and M. Romand. Plasma Treatment Process for Palladium Chemisorption onto Polymers before Electroless Deposition, J. Electrochem. Soc., *143*, pp. 472-480. 1996.

Charbonnier, M., M. Alami and U. Kogelschatz. New approaches for electroless plating processes by activation of polymer surfaces using low pressure plasma and dielectric-barrier discharge devices. In Metallized Plastics 7: Fundamental and Applied Aspects, ed by K.L. Mittal, pp. 3-26. The Netherlands: VSP. 2001.

Chen, C.W., M.Q. Chen, T. Serizawa and M. Akashi. In-situ Formation of Silver Nanopaticals on Poly(*N*-isopropylacrylamide)-Coated Polystyrene Microspheres, Adv. Mater., *10*, pp.1122-1126. 1998.

Chen, N.P. and L. Hong. Surface Phase Morphology and Composition of the Casting Films of PVDF-PVP Blend, Polymer, *43*, pp. 1429-1436. 2002.

Chou, N.J. and C.H. Tang. Interfacial Reaction during Metallization of Cured Polyimide: An XPS Study, J. Vac. Sci. Technol. A, *2*, p.751.1984.

Chu, L.Y., S.H. Park, T.Yamaguchi and S.I. Nakao. Preparation of Thermo-Responsive Core-Shell Microcapsules With a Porous Membrane and Poly(*N*-isopropylacrylamide) Gates, J. Membr. Sci., *192*, pp. 27-39. 2001.

Chung, J.C., D.J. Gross, J.L. Thomas, D.A. Tirrell and L.R. Opsahl-Ong. pH-Sensitive, Cation-Selective Channels Formed by a Simple Synthetic Polyelectrolyte in Artificial Bilayer Membranes, Macromolecules, *29*, pp. 4636-4641. 1996.

Da, Y.X., H.J. Griesser, A.W.H. Mau, R. Schmidt and J. Liesegang. Surface Modification of Poly(tetrafluoroethylene) by Gas Plasma Treatment, Polymer, *32*, pp. 1126-1130. 1991.

De Souza-Machado, R., S.Y. Wu and D.D. Denton. Dielectric Properties of Polyimides and Factors Influencing Such Properties. In Polyimides: Fundamentals and Applications. Ed by M.K. Ghosh and K.L. Mittal, pp.309-343. New York: Marcel Dekker. 1996.

Dine-Hart, R.A., D.B.V. Parker and W.W. Wright. Br. J. Polymer, *3*, p. 222. 1971.

Dunn, D.S. and J.T. Grant. Infrared Spectroscopic Study of Cr and Cu Metallization of Polyimide, J. Vac. Sci. Technol. A, *7*, pp. 253-255.1989.

Eastmond, G.C., M. Gibas, W.F. Pacynko and J. Paprotny. Grafted and Segmented Hydrophilic Polyimide for Microfiltration Membranes. Part I. Synthesis and Characterization, J. Membrane Sci., *207*, pp. 29-41. 2002.

Ebara, M., T. Aoyagi, K. Sakai and T. Okano. Introducing Reactive Carboxyl Side Chains Retains Phase Transition Temperature Sensitivity in *N*-isopropylacrylamide Copolymer Gels, Macromolecules, *33*, pp. 8312-8316. 2000.

Ebe, A., E. Takahashi, N. Kuratani, S. Nishiyama, O. Imai, K. Ogata, Y. Setsuhara and S. Miyake. Interface Structure between Polyimide Film Substrate and Copper Film Prepared by Ion Beam and Vapor Deposition (IVD) Method, Nucl. Instrum. Meth.B, *121*, pp. 20-2117. 1997.

Ebneth, H. In Metallizing of Plastics: Handbook of Theory and Practice, ed by R. Suchentrunk, Chapt. 3, pp. 35. 30th ASM International, Materials Park, OH. 1993.

Egitto, F.D. and L.J. Matienzo. Plasma Surface Modification and Etching of Polyimides. In Polyimides: Fundamentals and Applications, ed by M.K. Ghosh and K.L. Mittal, pp. 389-453. New York: Marcel Dekker. 1996.

Ektessabi, A.M. and S. Hakamata. XPS Study of Ion Beam Modified Polyimide Films, Thin Solid Films, *377*, pp. 621-625. 2000.

Ellaboudy, A.S., P.J. Oconnor and J.C. Tou. Correlated Electron Spin-Resonance and Infrared Spectroscopic Study of the Postformation Auto-Oxidation Phenomenon in

Plasma-Polymerized 4-Vinyl Pyridine Films, J. Appl. Polym. Sci., *60*, pp.637-647. 1996.

Elmidaoui A., T. Sarraf, C. Gavach and B. Boutevin. Synthesis and Characterization of New Ion-Exchange Membranes, J. Appl. Polym. Sci., *42*, pp. 2551-2561. 1991.

Endrey, A.L. Aromatic Polyimide Particles from Polycyclic Diamines, U. S. Patent 3,179,631. 1965.

Fargere, T., M. Abdennadher, M. Delmas and B. Boutevin. Synthesis of Graft Polymers from an Ozonized Ethylene-Vinyl Acetate Copolymer (EVA). 1. Study of the Radical Polymerization of Styrene Initiated by an Ozonized EVA, J. Polym. Sci. Part A: Polym. Chem., *32*, pp.1377-1384. 1994.

Feger, C. Selection Criteria for Multichip Module Dielectrics. In Multichip Module Technologies and Alternatives: the Basics, ed by D.A. Doane and P.D. Franzon, p.311. New York: Van Nostrand Reinhold. 1993.

Fochler, H., J. Mooney, L. Ball, R. Boyer and J. Grasselli. Spectrochim, Acta, *41A*, p. 271. 1985.

Frerichs, H., J. Stricker, D.A. Wesner and E.W. Kreutz, Laser-Induced Surface Modification and Metallization of Polymers, Appl. Surf. Sci., *86*, pp. 405-410. 1995.

Fujimoto, K., Y. Takebayashi, H. Inoue and Y. Ikada. Ozone-Induced Graft-Polymerization onto Polymer Surface, J. Polym. Sci. Part A: Polym. Chem., *31*, pp.1035-1043. 1993.

Gagliani, J. and D.E. Supkis. Thermally Stable Polyimide Components for Space and Commercial Applications, Adv. Astronaut. Sci., *38*, pp. 193-216. 1979.

Gancarz, I., G. Pozniak, M. Bryjak and A. Frankiewiez. Modification of Polysulfone Membranes. 2. Plasma Grafting and Plasma Polymerization of Acrylic Acid, Acta. Polym., *50*, pp. 317-326. 1999.

Han, L.M., R.B. Timmons, D. Bogdal and J. Pielichowski. Ring Retention *via* Pulsed Plasma Polymreization of Heterocyclic Aromatic Compounds, Chem. Mater., *10*, pp. 1422-1429. 1998.

Hedrick, J.L., C.J. Hawker, R. DiPietro, R. Jerome and Y. Charlier. The Use of Styrenic Copolymers to Generate Polyimide Nanofoams, Polymer, *36*, pp. 4855-4866. 1995a.

Hedrick, J.L., T.P. Russell, J. Labadie, M. Lacus and S.Swanson. High Temperature Nanofoams Derived from Rigid and Semi-Rigid Polyimides, Polymer, *36*, pp.2685-2697. 1995b.

Hedrick, J.L., R.D. Miller, C.J. Hawker, K.R. Carter, W. Volksen, D.Y. Yoon and M. Trollsas. Templating Nanoporosity in Thin-Film Dielectric Insulators, Adv. Mater., *10*, p.1049. 1998a.

Hedrick, J.L., R. DiPietro, Y. Charlier and R. Jerome. Polyimide Nanofoams from Aliphatic Polyester-Based Copolymers, Chem. Mater., *10*, pp.39-49. 1998b.

Heskins, M., J.E. Guillet and E. James. Solution Properties of Poly(*N*-isopropylacrylamide), J. Macromol. Sci. Chem., *A2*, pp. 1441-1455. 1968.

Hester, J.F., P. Banerjee and A.M. Mayes. Preparation of Protein-Resistant Surfaces on Poly(vinylidene fluoride) Membranes *via* Surface Segregation, Macromolecules, *32*, pp. 1643-1650. 1999.

Hirotsu, S., Y. Hirokawa and T. Tanaka. Volume-Phase Transitions of Ionized *N*-isopropylacrylamide Gels, J. Chem. Phys., *2*, pp. 1392-1395. 1987.

Hrubesh, L.W., L.E. Keene and V.R. Latorre. Dielectric-Properties of aerogels, J. Mater. Res., *8*, pp. 1736-1741. 1993.

Huang, X.D., S.H. Goh, S.Y. Lee and C.H.A. Huang. Complexation between Hydrogensulfated Fullerenol and Poly(4-vinylpyridine), Macromol. Chem. Phys., *201*, pp. 281-287. 2000.

Inagaki, N., S. Tasaka and K. Hibi. Surface Modification of Kapton Film by Plasma Treatments, J. Polym. Sci. Part A: Polym. Chem., *30*, pp. 1425-1431. 1992.

Inagaki, N., S. Taska and K. Hibi. Improved Adhesion between Plasma-Treated Polyimide Film and Evaporated Copper, J. Adhesion Sci. Technol., *8*, pp. 395-410. 1994.

Inagaki, N., S. Tasaka and M. Masumoto. Plasma Graft-Polymerization of Vinylimidazole onto Kapton Film Surface for Improvement of Adhesion between Kapton Film and Copper, J. Appl. Polym. Sci., *56*, pp.135-145. 1995.

Inagaki, N., S. Tasaka and M. Masumoto. Improved Adhesion between Kapton Film and Copper Metal by Plasma Graft Polymerization of Vinylimidazole, Macromolecules, *29*, pp. 1642-1648. 1996.

Inagaki, N., S. Tasaka, K. Narushima and K. Mochizuki. Surface Modification of Tetrafluoroethylene-Perfluoroalkyl Vinyl Ether Copolymer (PFA) by Remote Hydrogen Plasma and Surface Metallization with Electroless Plating of Copper Metal, Macromolecules, *32*, pp. 8566-8571. 1999.

Iriyama Y. and H. Yasuda. Fundamental Aspect and Behavior of Saturated Fluorocarbons in Glow-Discharge in Absence of Potential Source of Hydrogen, J. Polym. Sci. Polym. Chem., *30*, pp. 1731-1739. 1992.

Israels, R., D. Gersappe, M. Fasolka, V.A. Roberts and A. Balazs. pH-Controlled Gating in Polymer Brushes, Macromolecules, *27*, pp. 6679-6682. 1994.

Iwata, H., I. Hirata and Y. Ikada. Atomic Force Microscopic Analysis of a Porous Membrane with pH-Sensitive Molecular Valves, Macromolecules, *31*, pp. 3671-3678. 1998.

Jackson, R.L. Pd^{+2}/ Poly(acrylic acid) Thin-Films as Catalysis for Electroless Copper Deposition-Mechanism of Catalyst Formation, J. Electrochem. Soc.**,** *137*, pp. 95-101. 1990.

Jaworek, T., D. Neher, G. Wegner, R.H. Wieringa and A.J. Schouten. Electromechanical Properties of an Ultrathin Layer of Directionally Aligned Helical Polypetides, Science, *279*, pp. 57-60. 1998.

Ju, H.H., S.Y. Kim and Y.M. Lee. pH/Temperature-Responsive Behaviors of Semi-IPN and Comb-Type Graft Hydrogels Composed of Alginate and Poly(*N*-isopropylacrylamide), Polymer, *42*, pp. 6851-6857. 2001.

Kang, E.T. and Y. Zhang. Surface Modification of Fluoropolymers *via* Molecular Design, Adv. Mater., *12,* pp. 1481-1494. 2000.

Karpuzov, D., K.L. Kostov, E. Venkova, P. Kirova, I. Katardjiev and G. Carter. XPS Study of Ion-Beam Irradiation Effects in Polyimide Layers, Nucl. Instrum. Meth.B, *39*, pp. 787-791. 1989.

Katnani, A.D., A.Knoll and M.A. Mycek. Effects of Environment and Heat-Treatment on an Oxygen Plasma-Treated Polyimide Surface and Its Adhesion to a Chromium Overcoat, J. Adhesion Sci. Technol., *3*, pp. 441-453. 1989.

Kesting, R.E. (ed). Materials Science of Synthetic Membranes: A Structural Perspective, Second edition. New York: J. & Sons. 1985.

Kim, D. and Y.R. Shen. Study of Wet Treatment of Polyimide by Sum-Frequency Vibrational Spectroscopy, Appl. Phys. Lett., *74*, pp. 3314-3316. 1999.

Kim, D.W., S.S. Hwang, S.M. Hong, H.O. Yoo and S.P. Hong. Optimization of Foaming Process Using Triblock Polyimides with Thermally Labile Blocks, Polymer, *42*, pp. 83-92. 2001.

Krutchen, C.M. and W.P. Wu. Polymer Foam, Thermoformed Shapes and Methods to Forming It. U.S. Patent 4 535 100. 1985.

Landler, Y. and P. Lebel. Greffage Sur Polychlorure de Vinyle Par Préozonisation, J. Polym. Sci., *48*, pp. 477-489. 1960.

Lankard, J.R. and G. Wolbold. Excimer Laser Ablation of Polyimide in a Manufacturing Facility, Appl. Phys. A, *54*, pp. 355-359. 1992.

Lee, E.H., Y. Lee, W.C. Oliver and L.K. Mansur. Hardness Measurements of Ar^{+}-Beam Treated Polyimide by Depth-Sensing Ultra-Low Load Indentation, J. Mater. Res., *8*, pp. 377-387. 1993.

Lee, E.H. Ion Beam Modification of Polyimides, In Polyimides: Fundamentals and Applications, ed by M.K. Ghosh, K.L. Mittal, pp. 471-505. New York: Marcel Dekker. 1996.

Lee, K.W., S.P. Kowalczyk, J.M. Shaw. Surface Modification of PMDA-ODA Polyimide-Surface-Structure Adhesion Relationship, Macromolecules, *23*, pp. 2097-2100. 1990a.

Lee, K.W., S.P. Kowalczyk. Wet Process Surface Modification of Polyimides: Adhesion Improvement. In Metallization of Polymers, ed by E. sacher, J.J. Pireaux and S.P. Kowalczyk, pp. 179-195. Washington D.C.: ACS Press. 1990b.

Lee, K.W., S.P. Kowalczyk and J.M. Shaw. Surface Modification of BPDA-PDA Polyimide, Langmuir, *7*, pp. 2450-2453. 1991.

Lee, K.W. and A. Viehbeck. Wet-Process Surface Modification of Dielectric Polymers-Adhesion Enhancement and Metallization, IBM J. Res. Develop., *38*, pp. 457-474. 1994.

Lee, K.W. and A. Viehbeck. Wet Chemical Modification of Polyimide Surfaces: Chemistry and Application. In Polyimides: Fundamentals and Applications, Ed by M.K. Ghosh and K.L. Mittal, pp. 505-533. New York: Marcel Dekker. 1996.

Lee, Y.K., S.P. Murarka, S.P. Jeng and B. Auman. In Low-Dielectric Constant Materials-Synthesis and Applications in Microelectronics, ed by T.M. Lu, S.P. Murarka, T.S. Kuan and C. H. Ting, p.31. Pittsburgh: Materials Research Society. 1995.

Lin, V.D., N. B. Colthup, W. G. Fateley and J. G. Grasselli. The Handbook of Infrared and Raman Characteristic Frequencies of Organic Molecules. New York: Academic Press. 1991.

Liu, Y., S. H. Goh, S.Y. Lee and C.H.A. Huan. Miscibility and Interactions in Blends and Complexes of Poly(*N*-acryloyl-*N'*-methylpiperazine) with Poly(*p*-vinylphenol), Macromolecules, *32*, pp. 1967-1971. 1999.

Lyons, A.M., M.J. Vasile, E.M. Pearce and J.V. Waszczak. Copper Chloride Complexes with Poly(2-vinylpyridine)-Preparation and Redox Properties, Macromolecules, *21*, pp. 3125-3134. 1988.

Mack, R.G., E. Grossman and W.N. Unertl. Interaction of Copper with a Vapor-Deposited Polyimide Film, J. Vac. Sci. Technol. A, *8*, pp. 3827-3832. 1990.

Maier, G. Low Dielectric Constant Polymers for Microelectronics. Prog. Polym. Sci., *26*, pp. 3-65. 2001.

Makino D. and Y. Works. Recent Progress of the Application of Polyimides to Microelectronics. In Polymers for Microelectronics, Resists and Dielectrics, ed by L.F. Thompson, C.G. Willson and S. Tagawa, pp.380-402. Washington, D.C.: American Chemical Society. 1994.

Mallory, G.O. and J. Hajdu (ed.). Electroless Plating: Fundamentals and Applications. pp. 75-82, Orlando: American Electroplaters and Surface Finishers Society. 1990.

Marletta, G., S. Pignataro and C. Oliveri. Correlation between the Modification of the Chemical-Structure and the Electrical-Properties of Ar-Ion Bombarded Polyimide, Nucl. Instrum. Meth. B, *39*, pp. 792-795. 1989.

Matienzo, L.J. and W.N. Unertl. Adheion of Metal Films to Polyimides. In Polyimides: Fundamentals and Applications, ed by M. K. Ghosh and K. L. Mittal, pp. 629-696. New York: Marcel Dekker. 1996.

Meek, R.L. A Rutherford Scattering Study of Catalyst Systems for Electroless Cu Plating II. $SnCl_2$ Sensitization and $PdCl_2$ Activation, J. Electrochem. Soc., *122*, p. 1478. 1975.

Misra, A.C., G. Tesoro, G. Hougham and S.M. Pendarkar. Synthesis and Properties of Some New Fluorine-Containing Polyimides, Polymer, *33*, pp. 1078-1082. 1992.

Moharram, M.A., S.M. Rabie and H.M. El-Gendy. Infrared Spectra of Gamma-Irradiated Poly(acrylic acid)-Polyacrylamide Complex, J. Appl. Polym. Sci., *85*, pp. 1619-1623. 2002.

Morgen, M., E.T. Ryan, J.H. Zhao, C. Hu, T. Cho and P.S. Ho. Low Dielectric Constant Materials for ULSI Interconnects, Annu. Rev. Mater. Sci., *30*, pp. 645-680. 2000.

Moulder, J.F., W.F. Stickle, P.E. Sobol and K.D. Bomben. In X-ray Photoelectron Spectroscopy, ed by J. Chastian, p. 41 & p. 85. Perkin-Elmer, Eden Prairie, MN. 1992.

Mulder, M.H.V. Polarization Phenomena and Membrane Fouling. In Basic Principle of Membrane Technology, ed by R.D. Noble and S.A. Stern, pp.121-136. Dordrecht: Kluwer Academic Publishers. 1991.

Muller, G. and D.W. Baudrand. Plating on Plastics: a Practical handbook. Teddington: Robert Draper Ltd. 1971.

Nakamura, Y., Y. Suzuki and Y. Watanabe. Effect of Oxygen Plasma Etching on Adhesion between Polyimide Films and Metal, Thin Solid Films, *291*, pp. 367-369. 1996.

Narcus, H. Practical copper reduction on nonconductors, Metal Finishing, *45*, pp. 64-67.1947.

Narkis, M., M. Paterman, H. Boneh and S. Kenig. Rotational Molding of Thermosetting Three-Phase Syntactic Foams, Polym. Eng. Sci., *22*, pp. 417-421. 1982.

Nonaka, T., S. Matsumura, T. Ogata and S. Kurihara. Synthesis of Amphoteric Polymer Membranes From Epithiopropyl Methacrylate-butylmethacrylate-N,N-dimethylaminopropyl Acrylamide-Methacrylic Acid Copolymers and the Permeation Behavior of Various Solutes through the Membranes, J. Membr. Sci., *212*, pp. 39-53. 2003.

Nunes, S.P., M.L. Sforca and K.V. Peinemann. Dense Hydrophilic Composite Membranes for Ultrafiltration, J. Membr. Sci., *106*, pp. 49-56. 1995.

Pappas, D.L., J.J. Cuomo and K.G. Sachdev, Studies of Adhesion of Metal-Films to Polyimide, J. Vac. Sci. Technol. A, *9*, pp. 2704-2708. 1991.

Park, Y.S., Y. Ito and Y. Imanishi. Permeation Control Through Porous Membranes Immobilized With Thermosensitive Polymer, Langmuir, *14*, pp. 910-914. 1998.

Paunovic, M. and M. Schlesinger. Fundamentals of Electrochemical Deposition. p.133, New York: John Wiley&Sons. 1999.

Peng, T. and Y.L. Cheng. Temperature-Responsive Permeability of Porous PNIPAAM-*g*-PE Membranes, J. Appl. Polym. Sci., *70*, pp. 2133-2142. 1998.

Pearlstein, F. Electroless Nickel Deposition. Activation of Nonmetallic Surfaces. Metal Finishing, *53*, pp.59-61. 1955.

Pertsin, A.J. and Y.M. Pashunin. An XPS Study of In-situ Formation of the Polyimide Copper Surface, Appl. Surf. Sci., *47*, pp. 115-125. 1991.

Pettit, G.H. Laser Ablation of Polyimide. In Polyimides: Fundamentals and Applications, ed by M.K. Ghosh and K.L. Mittal, pp.453-471. New York: Marcel Dekker. 1996.

Pritchart, H.W. The Relationship of the Adhesion of the Deposited Metal to the Intermolecular Interactions, Acta Polym., *34*, p.1132. 1983.

Qin, Z.Y., J. Zhang, H. Zhou, Y.H. Song and T.B. He. Degradation of Polyimide Induced by Nitrogen Laser Irradiation, Nucl. Instrum. Meth. B, *170*, 406 (2000).

Ramos, T., K. Rhoderick, R. Roth, L. Brungardt, S. Wallace, J. Drage, J. Dunne, D. Endisch, R. Katsanes, N. Viernes and D.M. Smith. Nanoporous Silica for Low-*k* Dielectrics, Mater. Res. Soc. Symp. Proc., *511*, pp. 105-110. 1998.

Rozovskis, G., J. Vinkevicius and J. Jacaiauskiene. Plasma Surface Modification of Polyimide for Improving Adhesion to Electroless Copper Coating, J. Adhesion Sci. Technol., *10*, pp. 399-406. 1994.

Ruokolainen, J., J. Tanner, O. Ikkala, G. ten Brinke and E.L. Thomas. Direct Imaging of Self-Organized Comb Copolymer-Like Systems Obtained by Hydrogen Bonding: Poly(4-vinylpyridine)-4-nonadecylphenol, Macromolecules, *31*, pp. 3532-3536. 1998.

Rye, R.R. and A.J. Ricco. High Resolution Metallization of Poly(tetrafluoroethylene). In Metallized Plastics: Fundamentals and Application, ed by K. L. Mittal, pp. 15-27. New York: Marcel Dekker. 1998.

Sarraf, T., B. Boutevin, Y. Pietrasanta and M. Taha. Synthesis of Graft Copolymers From Polyethylene-I., Eur. Polym. J., *20*, pp. 1131-1135. 1984.

Sasaki, S. and S. Nishi. Synthesis of Fluorinated Polyimides. In Polyimides: Fundamentals and Application, ed by M.K. Ghosh and K.L. Mittal, pp. 71-121. New York: Marcel Dekker. 1996.

Sato, K., S. Harada, A. Saiki, T. Kimura, T. Okubo and K. Mukai. Novel Planar Multilevel Interconnection Technology Utilizing Polyimide. Proc. Electron Components Conf., *23*, pp. 15-20. 1973.

Semenova, S.I. Introduction. Trends in Polyimide Membrane Development. In Polyimide Membranes: Applications, Fabrications and Properties, ed by H. Ohya, V.V. Kudryavtsev and S.I. Semenova, Chapt 1, pp.1-8. Japan: Kodansha Ltd. 1996.

Sengupta, K.S. and H.K. Birnbaum. Structural and Chemical Effects of Low-Energy Ion-Boabardment of PMDA-ODA Surfaces, J. Vac. Sci. Technol. A, *9*, pp. 2928-2935. 1991.

Shafeev, G.A.and P. Hoffmann, Light-Enhanced Electroless Cu Deposition on Laser-Treated Polyimide Surface, Appl. Surf. Sci., *139*, pp. 455-460. 1999.

Shimizu, H., H. Kawakami and S. Nagaoka. Membrane Formation Mechanism and Permeation Properties of a Novel Porous Polyimide Membrane, Polym. Advan. Technol., *13*, pp. 370-380. 2002.

Silverman, B.D. and D.E. Platt. Percolation of A Silmulated Metallic Film on a Porous Substrate- the Copper-Polyimide Interface, Phys. Rev. E, *49*, pp. 1028-1039. 1994.

Silverstein, M.S., R. Chen and O. Kesler. Hexafluoropropylene Plasmas: Polymerization Rate-Reaction Parameter Relationships, Polym. Eng. Sci., *36*, pp. 2542-2549. 1996.

Smolders, C.A., A.J. Reuvers, R.M. Boom and I.M. Wienk. Microstructures in Phase-Inversion Membranes. 1. Formation of Macrovoids. J. Membrane Sci. *73*, pp.259-275. 1992.

Sroog, C.E., A.L. Endrey, S.V. Abramo, C.E. Berr, W.M. Edwards and K. L. Olivier. Aromatic Polypyromellitimides From Aromatic Poly(amic acids), J. Polym. Sci. Part A. Polym. Chem., *1*, pp. 1373-1390. 1965.

Sroog, C.E. History of the Invention and Development of the Polyimides. In Polyimides: Fundamentals and Applications. ed by M.K. Ghosh and K.L. Mittal, pp. 1-6. New York: Marcel Dekker. 1996.

Strathmann, H. and K. Kock. The Formation Mechanism of Phase Inversion Membranes, Desalination, *21*, pp.241-255. 1977.

Strathmann, H. Production of Microporous Media by Phase Inversion Processes. In Material Science of Synthetic Membrane, ed by D.R. Lloyd, pp.165-195. Washington, D. C.: American Chemical Society. 1985.

Tan, K.L., L.L. Woon, H.K. Woon, E.T. Kang and K.G. Neoh. Surface Modification of Plasma-Pretreated Poly(tetrafluoroethylene) Films by Graft-Copolymerization, Macromolecules, *26*, pp. 2832-2836. 1993.

Tarducci, C., E.J. Kinmond, J.P.S. Badyal, S.A. Brewer and C. Willis. Epoxide-Functionalized Solid Surfaces, Chem. Mater., *12*, pp. 1884-1889. 2000.

Uchida, E., Y. Uyama and Y. Ikada. Grafting of Water-Soluble Chains onto a Polymer Surface, Langmuir, *10*, pp. 481-485. 1994.

Unertl, W.N. and R.G. Mack. Model Studies of the Interface between Metals and Polyimides. In Metallized Plastics 3: Fundamental and Applied Aspects, ed by K.L. Mittal, pp. 85-108. New York: Plenum Press. 1992.

Van Krevelen, D.W. (ed). Properties of Polymers. third edition. p.321, Amsterdam: Elsevier. 1990.

Viehbeck, A., C.A. Kovac, S.L., Buchwalter, M.J. Goldberg and S.L. Tisdale. Redox Seeding and Electroless Metallization of Polyimides. In Metallization of Polymers, ed by E. Sacher, J.J. Pireaux and S.P. Kowalczyk, p. 394. Washingtion D. C.: ACS Press. 1990.

Vora, R.H., P.S.G. Krishna, S.H.Goh and T.S. Chung. Synthesis and Properties of Designed Low-κ Fluoro-Copolyetherimides. Part 1, Adv. Funct. Mat., *11*, pp. 361-373. 2001.

Vorobyova, T.N. Adhesion Interaction between Electrolessly Deposited Copper Film and Polyimide, J. Adhesion Sci. Technol., *11*, pp. 167-182. 1997.

Walton, H.F. (ed). Principles & Methods of Chemical Analysis. Englewood Cliffs: Prentice-Hall. 1964.

Wang, W.C., R.H. Vora, E.T. Kang, K.G. Neoh and D.J. Liaw. pH-Sensitive Fluorinated Polyimides with Grafted Acid and Base Side Chains, Ind. Eng. Chem. Res., *42*, pp. 784-794. 2003.

Ward, A.J. and R.D. Short. A Tof-SIMS and XPS Investigation of the Structure of Plasma Polymers Prepared from the Methacrylate Series of Monomers, Polymer, *36*, pp. 3439-3450. 1995.

Weichenhain, R., D.A. Wesner, W. Pfleging, H. Horn and E.W. Kreutz. KrF-Excimer Laser Pretreatment and Metallization of Polymers, Appl. Surf. Sci., *110*, pp. 264-269. 1997.

Wilson, D., H.D. Stenzenberger and P.M. Hergenrother (eds.). Polyimide. New York: Chapman & Hall. 1990.

Wu, S.Y., E.T. Kang, K.G. Neoh, H.S. Han and K.L. Tan. Electroless Deposition of Copper on Surface Modified Poly(tetrafluoroethylene) Films from Graft Copolymerization and Silanization, Langmuir, *16*, pp. 5192-5198. 2000.

Wu, S.Y., E.T. Kang, K.G. Neoh and K.L. Tan. Surface Modification of Poly(tetrafluoroethylene) Films by Graft Copolymerization for Adhesion Improvement with Evaporated Copper, Macromolecule, *32*, pp. 186-193. 1999.

Xue, G., Q.P. Dai and S.G. Jiang. Chemical-Reactions of Imidazole with Metallic Silver Studied by the Use of SERS and XPS Techniques, J. Am. Chem. Soc., *110*, pp. 2393-2395. 1988.

Yamamoto, H., Y. Mi and S.A. Stern. Structure Permeability Relationships of Polyimide Membranes, J. Polym. Sci. Part B: Polym. Phys., *28*, pp.2291-2304. 1990.

Yang, G.H., E.T. Kang and K.G. Neoh. Surface Modification of Poly (tetrafluoroethylene) Films by Plasma Polymerization of Glycidyl Methacrylate and Its Relevance to the Electroless Deposition of Copper, J. Polym. Sci. Part A: Polym. Chem., *38*, pp. 3498-3508. 2000.

Yang, G.H., E.T. Kang, K.G. Neoh, Y. Zhang and K.L. Tan. Electroless Deposition of Copper on Polyimide Films Modified by Surface Graft Copolymerization with Nitrogen-containing Vinyl Monomers, Colloid Polym. Sci., *279*, pp. 745-753. 2001.

Yasuda H. and T. Hirotsu. Distribution of Polymer Deposition in Plasma Polymerization. J. Polym. Sci. Part A. Polym. Chem., *16*, pp. 2587-2592. 1978.

Zhang, Y., K.L. Tan, B.Y. Liaw, D.J. Liaw and E.T. Kang. Thermal Imidization of Poly(amic acid) Precusors on Glycidyl Methacrylate (GMA) Graft-Polymerized Si(100) Surface, Thin Solid Films, *374*, pp. 70-79. 2000.

Zhang, Y., K.L. Tan, B.Y. Liaw, D.J. Liaw, E.T. Kang and K.G. Neoh. Thermal Imidization of Fluorinated Poly(amic acid)s on Si(100) Surfaces Modified by Plasma Polymerization and Deposition of Glycidyl Methacrylate, Langmuir, *17*, 2265-2274 2001a.

Zhang, Y., K.L. Tan, G.H. Yang, E.T. Kang and K.G. Neoh. Electroless Plating of Copper and Nickel *via* a Sn-free Process on Polyimide Films Modified by Surface Graft Copolymerization with 1-Vinylimidazole, J. Electrochem. Soc., *148*, pp. C574-C582. 2001b.

Zhou, X., S.H. Goh, S.Y. Lee and K.L. Tan. X-ray Photoelectron Spectroscopic Studies of Interactions between Poly(p-vinylphenol) and Poly(vinylpyridine)s, Appl. Surf. Sci., *119*, pp. 60-66. 1997.

LIST OF PUBLICATIONS

JOUNAL ARTICLES

1. Wang, W.C., R.H. Vora, E.T. Kang, K.G. Neoh, C.K. Ong and L.F. Chen. Nanoporous Ultra-Low-κ Films Prepared from Fluorinated Polyimide with Grafted Poly(acrylic acid) Side Chains, Adv. Mater., 16, pp. 54-57. 2004.

2. Wang, W.C., R.H. Vora, E.T. Kang and K.G. Neoh. Electroless Plating of Copper on Fluorinated Polyimide Films Modified by Surface Graft Copolymerization with 1-Vinylimidazole and 4-Vinylpyridine, Polym. Eng. Sci., 44, pp. 362-375. 2004.

3. Fu, G.D., W.C. Wang, S. Li, E.T. Kang, K.G. Neoh，T.S. Tseng and D.J. Liaw. Nanoporous Low-κ Polyimide Films Prepared from Poly(amic acid)s with Grafted Poly(methylmethacrylate)/Poly(acrylamide) Side Chains, J. Mater. Chem., 13, pp. 2150-2156. 2003.

4. Wang, W.C., G.T. Ong, S.L. Lim, R.H. Vora, E.T. Kang and K.G. Neoh. Synthesis and Characterization of Fluorinated Polyimide with Grafted Poly(N-isopropylacrylamide) Side Chains and the Temperature-Sensitive Microfiltration Membranes, Ind. Eng. Chem. Res., 42, pp. 3740-3749. 2003.

5. Wang, W.C., R.H. Vora, E.T. Kang and K.G. Neoh. Electroless Plating of Copper on Fluorinated Polyimide Films Modified by Plasma Graft Copolymerization and UV-induced Graft Copolymerization with 4-Vinylpyridine, Macromol. Mater. Eng., 288, pp. 152-163. 2003.

6. Wang, W.C., R.H. Vora, E.T. Kang, K.G. Neoh and D.J. Liaw. pH-Sensitive Fluorinated Polyimides with Grafted Acid and Base Side Chains, Ind. Eng. Chem. Res., 42, pp. 784-794. 2003.

7. Wang, W.C., E.T. Kang and K.G. Neoh. Electroless Plating of Copper on Polyimide Films Modified by Plasma Graft Copolymerization with 4-Vinylpyridine, Appl. Surf. Sci., 199, pp. 52-66. 2002.

8. Wang, W.C., Y. Zhang, E.T. Kang and K.G. Neoh. Electroless Deposition of Copper on Poly(tetrafluoroethylene) Films Modified by Plasma-Induced Surface Grafting of Poly(4-vinylpyridine), Plasmas and Polymers, 7, pp. 207-225. 2002.

9. Chen, Y.W., W.C. Wang, W.H. Yu, Z.L. Yuan, E.T. Kang, K.G. Neoh; B. Krauter and A. Greiner. Nanoporous Low-κ Polyimide Films *via* Poly(amic acid)s with Grafted Poly(ethylene glycol) Side Chains from the RAFT-mediated Process, Adv. Funct. Mater., in Press.

10. Chen, Y.W., W.C. Wang, W.H. Yu, E.T. Kang, K.G. Neoh, R.H. Vora, C.K. Ong and L.F. Chen. Ultra-Low-κ Materials Based on Nanoporous Fluorinated Polyimide with Well-defined Pores *via* the RAFT-mediated Graft Polymerization Process, J. Mater. Chem., in Press.

CONFERENCE CONTRIBUTIONS

11. Wang, W.C., E.T. Kang, K.G. Neoh, C.K. Ong and L.F. Chen. Nanoporous Low-κ Polyimide Films Prepared from Poly(amic acid) with Grafted Poly(acrylic acid)- and Poly(ethylene glycol) Side Chains, International Symposium on Thin Film Materials, Processes and Reliability, held at the 203rd Meeting of the Electrochemical Society, April 2003, Paris, France. Electrochemical Society Series 2003, 13, pp. 224-230.

PATENTS：

12. Chen, Y.W., W.C. Wang, G.D. Fu, E.T. Kang and K.G. Neoh. Nanoporous Polymers for Use as Dielectric Materials, U.S. Patent, in Pending.